

Automated Glycan Assembly to Study Carbohydrate Materials

Inaugural-Dissertation

To obtain the academic degree of
Doctor rerum naturalium (Dr. rer. nat.)

submitted to the Department of Biology, Chemistry and Pharmacy
of Freie Universität Berlin

by
Yang Yu
from Anhui/China

2020

This work was performed between November 2016 and September 2019 under the supervision of Dr. Martina Delbianco and Prof. Dr. Peter H. Seeberger in the Department of Biomolecular System, Max Planck Institute of Colloids and Interfaces Potsdam, and the Institute of Chemistry and Biochemistry, Freie Universität Berlin.

1st reviewer: Prof. Peter H. Seeberger

2nd reviewer: Prof. Matthew Hopkinson

Date of oral defense: 27.03.2020

Acknowledgement

First and foremost, I would like to express my deepest gratitude to Dr. Martina Delbianco for the supervision of my PhD study, for her patience in providing me with suggestions on research, and for her continuous support on this thesis.

I would like to thank Prof. Dr. Peter Seeberger for offering the excellent environment and equipment in Department of Biomolecular Systems at the Max-Planck-Institute of Colloids and Interfaces and for reviewing this thesis.

I thank Prof. Dr. Matthew Hopkinson for kindly agreeing to review this thesis.

I would like to thank all the members of *carbohydrate materials* group, Dr. Vittorio Bordoni, Dr. Yuntao Zhu, Dr. Arpita Roychoudhury, Soeun Gim, Theodore Tyrikos-Ergas, Giulio Fittolani, and Zhouxiang Zhao for the insightful and beneficial discussions and the amazing atmosphere in the lab that they create. I would also like to thank all members of *automated glycan assembly* group, Alonso Pardo, Dr. José Angel Danglad-Flores, Dr. Abragam Joseph, Dr. Lemaihoang Kim, Dr. Chandradhish Ghosh, and Dr. Andrew Kononov. I am particularly grateful to Dr. Richard Fair and Heung Sik Hahm for providing me with precious building blocks and to Sabrina Lechnitz for the German translation of the abstract in this thesis.

My sincere thanks also goes to Eva Settels for her help with the HPLC, to Olaf Niemeyer for the maintenance of NMRs, to Heike Runge, Rona Pitschke, Dr. Tobias Heil, Bolortuya Badamdorj and Dr. Nadja Tarakina for the training and measurement on electron microscopes, to Daniel Werner for the training and maintenance of X-ray diffractograms, to Carmen Remde for the instruction on confocal microscope, and to Dr. Oleksandr Savatieiev for the measurement of fluorescence spectrometry.

I thank all members of the Biomolecular Systems Department for the enjoyable working atmosphere, especially Dorothee Böhme, Dacheng Shen, Dr. Eric Sletten, Mara Guidi, Dr. Oren Moscovitz, Dr. Michael Downey, Monica Guberman, Dr. Maria Bräutigam, Jamal Malik, Mauro Sella, Shuo Zhang, Guangzong Tian, Xiaopeng Zou, and Juntao Cai.

My deep gratitude also goes to my family: my parents and Baozheng for supporting me spiritually throughout writing this thesis. Last but not least, I would like to thank Yumei Tang for her love and encouragement that she gives me every day.

Table of Contents

Summary.....	XI
Zusammenfassung.....	XIII
List of Publications.....	XV
List of Abbreviations.....	XVII
1. Introduction.....	1
1.1. Carbohydrates	1
1.1.1. Polysaccharides as materials.....	1
1.1.2. Challenges in polysaccharide materials.....	5
1.2. Synthetic polysaccharides	5
1.2.1. Chemical glycosylation	6
1.2.2. Synthesis of polysaccharides	8
1.2.3. Automated glycan assembly of polysaccharides.....	9
1.2.4. Synthetic carbohydrate materials for structural studies.....	15
1.3. Nanotechnology based on biomolecules	17
1.4. Aims of this thesis.....	18
2. A Capping step during automated glycan assembly enables access to complex glycans in high yield	20
2.1. Introduction.....	20
2.2. Results	22
2.2.1. Pilot synthesizer for capping optimization	22
2.2.2. Optimization of capping condition.....	23
2.2.3. Stability test of common protecting groups under capping condition	24
2.2.4. Application of capping in oligo- and polysaccharide synthesis	25
2.3. Conclusion	29
3. Systematic hydrogen bond manipulations to establish polysaccharide structure-property correlations.....	30
3.1. Introduction.....	30
3.2. Results	33
3.2.1. Synthesis of modified cellulose	33
3.2.2. Conformations of cellulose analogues	38

3.2.3. Aggregation, solubility, and crystallinity study of modified cellulose	39
3.3. Conclusion	41
4. Oligosaccharides self-assemble and show intrinsic optical properties	43
4.1. Introduction.....	43
4.2. Results	45
4.2.1. Self-assembly.....	45
4.2.2. Real-time measurements	49
4.2.3. Photophysical characterization	49
4.3. Conclusion	53
5. Conclusion and outlook.....	54
6. Experimental section	56
6.1. General materials and methods.....	56
6.2. General procedure for automated glycan assembly	56
6.2.1. Preparation of stock solutions.....	57
6.2.2. Modules for automated glycan assembly	57
6.2.3. Post-synthesizer manipulations	60
6.3. Synthesis of building blocks.....	62
6.3.1. Synthesis of building block BB-6a.....	62
6.3.2. Synthesis of building block BB-11 and BB-12	63
6.4. Capping test.....	70
6.4.1. Modification of capping condition	70
6.4.2. Test of stability of Fmoc, Lev and TCA groups.....	74
6.5. Synthesis of oligosaccharides	79
6.5.1. AGA synthesis of 1,6-hexaglucose.....	79
6.5.2. AGA synthesis of 1,4-hexaglucose.....	82
6.5.3. AGA synthesis of Lc4.....	85
6.5.4. AGA synthesis of 50-mer polymannoside	86
6.5.5. AGA synthesis of methylated cellulose hexamers	91
6.5.6. AGA synthesis of methylated cellulose 12-mers	101
6.5.7. Synthesis of partially protected dimers.....	110
6.5.8. Synthesis of fully functionalized dimers.....	119

6.5.9. AGA synthesis of partially deprotected hexamers	121
6.6. Solubility, XRD measurements, and MD simulation of cellulose analogues	126
6.6.1. Solubility measurements	126
6.6.2. XRD Analysis	128
6.6.3. Molecular Dynamics Simulations (selected, by Theodore Tyrikos-Ergas)	130
6.7. Self-assembly of oligosaccharides and characterizations	131
6.7.1. Oligosaccharide self-assembly	131
6.7.2. Characterization of self-assembling samples	135
7. References	143
Appendix 1: NMR spectra	152

Summary

Carbohydrates are ubiquitous in Nature where they play important roles as materials. The structural diversity of carbohydrates results in materials with extremely different properties, from gels to extremely rigid materials. Still, structure-property correlations are hardly established due to the difficulty in obtaining pure molecules and the lack of analytical methods. This lack of knowledge drastically hinders the application of carbohydrate materials in nanotechnology, where, in contrast, DNA and peptide have found great success. In this thesis, automated glycan assembly (AGA) is used as a platform to produce well-defined carbohydrate materials and establish structure-property correlations.

In Chapter 2, the optimization of AGA is discussed. The insertion of a new capping method into the AGA cycle granted access to oligo- and polysaccharides in high yield, minimizing the accumulation of deletion sequences. The use of methanesulfonic acid and acetic anhydride allowed for the fast and quantitative capping of hydroxyl groups that failed to be glycosylated. Commonly used protecting groups in AGA are stable under these capping conditions. Drastically improved overall yields are a consequence of decreased side-products and simplified purifications. Moreover, the building block consumption is reduced. To illustrate the method, the biologically important tetrasaccharide Lc4, as well as a 50-mer polymannoside were prepared.

These optimized AGA conditions provide reliable access to a collection of oligo- and polysaccharides with defined structure, which are ideal for establishing structure-property correlations of natural polysaccharides. Chapter 3 focuses on cellulose, the most abundant polysaccharide in Nature. Well-defined unnatural oligosaccharides including methylated, deoxygenated, deoxyfluorinated, as well as carboxymethylated cellulose and chitin analogues with full control over the degree and pattern of substitution were prepared. Molecular dynamics simulations and crystallographic analysis show how distinct hydrogen-bond modifications drastically affect the solubility, aggregation behavior, and crystallinity of carbohydrate materials.

After proving that oligosaccharides exhibit similar conformational features as their polysaccharide counterparts, the formation of well-defined supramolecular architectures based on simple oligosaccharides was targeted. In Chapter 4, six synthetic oligosaccharides, ranging from dimers to hexamers, are shown to self-assemble into nanostructures of varying morphologies and emit within the visible spectrum in an excitation-dependent manner. Well-defined differences in chain length, monomer modification, and aggregation methods yield glycomaterials with distinct

shapes and properties. The excitation-dependent fluorescence in a broad range within the visible spectrum illustrates their potential for use in optical devices and imaging applications.

The systematic approach presented in this thesis, based on well-defined synthetic oligosaccharides, will create the foundation of our understanding of carbohydrate interactions in Nature.

Zusammenfassung

Kohlenhydrate sind in der Natur allgegenwärtig, wo sie als Materialien eine wichtige Rolle spielen. Die strukturelle Vielfalt von Kohlenhydraten führt zu Materialien mit extrem unterschiedlichen Eigenschaften - von Gelen bis hin zu extrem starren Materialien. Struktur-Eigenschafts-Korrelationen sind immer noch kaum etabliert aufgrund von Schwierigkeiten reine Moleküle zu erhalten und mangels analytischer Methoden. Diese Wissenslücke behindert die Anwendung von Kohlenhydratmaterialien in der Nanotechnologie drastisch, wohingegen DNA und Peptide große Erfolge erzielt haben. In dieser Arbeit wird die automatisierte Festphasensynthese von Glykanen (*Automated Glycan Assembly*, AGA) als Plattform verwendet, um definierte Kohlenhydratmaterialien herzustellen und Korrelationen zwischen Struktur und Eigenschaften herzustellen.

In Kapitel 2 wird die AGA-Optimierung besprochen. Die Einführung einer neuen Capping-Methode in den AGA-Zyklus ermöglichte den Zugang zu Oligo- und Polysacchariden in hoher Ausbeute, durch die Minimierung der Anhäufung von Deletionssequenzen. Die Verwendung von Methansulfonsäure und Essigsäureanhydrid ermöglichte das schnelle und quantitative Capping von Hydroxy-Gruppen, die nicht glykosyliert werden konnten. Häufig in AGA verwendete Schutzgruppen sind stabil unter diesen Bedingungen. Die drastisch verbesserten Gesamtausbeuten sind auf weniger Nebenprodukte und vereinfachte Aufreinigungen zurückzuführen. Darüber hinaus wird der Verbrauch von Monosaccharid-Bausteinen reduziert. Zur Veranschaulichung der Methode wurden das biologisch relevante Tetrasaccharid Lc4 und ein 50-mer-Polymannosid hergestellt.

Diese optimierten AGA-Bedingungen bieten zuverlässigen Zugang zu einer Sammlung von Oligo- und Polysacchariden mit definierter Struktur, die sich ideal für die Herstellung von Struktur-Eigenschafts-Korrelationen von natürlichen Polysacchariden eignen. Kapitel 3 befasst sich mit Cellulose - dem am häufigsten vorkommenden Polysaccharid in der Natur. Es wurden genau definierte unnatürliche Oligosaccharide mit vollständiger Kontrolle über den Substitutionsgrad und das Substitutionsmuster hergestellt, darunter methylierte, desoxygenierte, desoxyfluorierte sowie carboxymethylierte Cellulose- und Chitinanaloga. Molekulardynamik-Simulationen und kristallographische Analysen zeigen, wie drastisch unterschiedliche Wasserstoffbrücken-Modifikationen die Löslichkeit, das Aggregationsverhalten und die Kristallinität von Kohlenhydratmaterialien beeinflussen.

Nachdem bewiesen wurde, dass Oligosaccharide ähnliche Konformationsmerkmale aufweisen, wie ihre Polysaccharid-Gegenstücke, wurde die Bildung wohldefinierter supramolekularer Architekturen basierend auf einfachen Oligosacchariden angestrebt. In Kapitel 4 wird gezeigt, dass sich sechs synthetische Oligosaccharide, die von Dimeren bis hin zu Hexameren reichen, zu Nanostrukturen unterschiedlicher Morphologie zusammenlagern und anregungsabhängig im sichtbaren Spektrum emittieren. Ausschlaggebende Unterschiede in der Kettenlänge, der Monomer-Modifikation und den Aggregationsmethoden ergeben Kohlenhydratmaterialien mit unterschiedlichen Formen und Eigenschaften. Die anregungsabhängige Fluoreszenz in einem breiten Bereich innerhalb des sichtbaren Spektrums zeigt ihr Potenzial für den Einsatz in optischen Geräten und bildgebenden Anwendungen.

Der in dieser Arbeit vorgestellte systematische Ansatz, der auf genau definierten synthetischen Oligosacchariden basiert, wird die Basis für unser Verständnis der Wechselwirkungen von Kohlenhydraten in der Natur bilden.

List of Publications

Scientific Publications and Reviews

1. **Y. Yu**,* T. Tyrikos-Ergas,* Y. Zhu, G. Fittolani, V. Bordoni, A. Singhal, R. J. Fair, A. Grafmüller, P. H. Seeberger, M. Delbianco, Systematic Hydrogen Bond Manipulations to Establish Polysaccharide Structure-Property Correlations. *Angew. Chem. Int. Ed.* **2019**, 131, 13261.
2. **Y. Yu**,* S. Gim,* D. Kim, Z. A. Arnon, E. Gazit, P. H. Seeberger, M. Delbianco, Oligosaccharides Self-Assemble and Show Intrinsic Optical Properties. *J. Am. Chem. Soc.* **2019**, 141, 4833.
3. **Y. Yu**, M. Delbianco, Synthetic Polysaccharides in Recent Trends in Carbohydrate Chemistry. Amsterdam: Elsevier. (in press)
4. K. L. M. Hoang, A. Pardo-Vargas, Y. Zhu, **Y. Yu**, M. Loria, M. Delbianco, P. H. Seeberger, Traceless Photolabile Linker Expedites Chemical Synthesis of Complex Oligosaccharides by Automated Glycan Assembly. *J. Am. Chem. Soc.* **2019**, 141, 9079.
5. M. Delbianco, A. Kononov, A. Poveda, **Y. Yu**, T. Diercks, J. Jiménez-Barbero, P. H. Seeberger, Well-Defined Oligo- and Polysaccharides as Ideal Probes for Structural Studies. *J. Am. Chem. Soc.* **2018**, 140, 5421.
6. **Y. Yu**, A. Kononov, M. Delbianco, P. H. Seeberger, A Capping Step During Automated Glycan Assembly Enables Access to Complex Glycans in High Yield. *Chem. Eur. J.* **2018**, 24, 6075.

* equal contribution.

Scientific Conferences and Symposia Presentations:

1. October 2018, 2nd JCF Potsdam PhD symposium, Potsdam (Germany), oral presentation
2. September 2018, Young Scientists Workshop, Potsdam (Germany), oral presentation
3. July 2018, 29th ICS, Lisbon (Portugal), poster

4. September 2017, Chemical Biology of Disease Meeting, Crete (Greece), oral presentation

List of Abbreviations

Ac	acetyl
ACN	acetonitrile
Ar	aryl
aq.	aqueous
BB	building block
Bn	benzyl
BTA	benzene-1,3,5-tricarboxamide
Bz	benzoyl
Cbz	carboxylbenzyl
CMC	carboxymethyl cellulose
CNCs	cellulose nanocrystals
Cryo-SEM	cryogenic scanning electron microscopy
DBU	1,8-diazabicyclo[5.4.0]undec-7-ene
DCE	dichloroethane
DCM	dichloromethane
DDQ	dichlorodicyanobenzoquinone
DMAc	dimethylacetamide
DMAP	<i>N,N</i> -dimethylaminopyridine
DMF	dimethylformamid
DP	degree of polymerization
ESI	electrospray ionization
Et	ethyl
EtOAc	ethyl acetate
Fmoc	fluorenylmethoxycarbonyl
FTIR	fourier transform infrared
Hex	hexane
HFIP	hexafluoroisopropanol
HPLC	high performance liquid chromatography
HRMS	high resolution mass spectrometry
HSQC	heteronuclear single quantum coherence spectroscopy
<i>i</i> PrOH	isopropanol
Lev	levulinoyl
LevOH	levulinic acid
LG	leaving group
MALDI-TOF	matrix-assisted laser desorption/ionization-time of flight
MC	methylcellulose
MD	molecular dynamics
Me	methyl
MS	mass spectrometry
MsOH	methanesulfonic acid

NIS	<i>N-iodosuccinimide</i>
NMR	nuclear magnetic resonance
NP	normal phase
PA	peptide amphiphile
PG	protecting group
Ph	phenyl
PNA	peptide nucleic acid
<i>p</i> TsOH	<i>p</i> -toluenesulfonic acid
REES	red edge excitation shift
RP	reversed phase
rt	room temperature
sat.	saturated
SEM	scanning electron microscope
Sp1	<i>Streptococcus pneumoniae</i> serotype 1
TCA	trichloroacetyl
TEM	transmission electron microscope
TFA	trifluoroacetic acid
TfOH	trifluoromethanesulfonic acid
THF	tetrahydrofurane
TMS	trimethylsilyl
TMSOTf	trimethylsilyl trifluoromethanesulfonate
Tol	toluene
tPG	temperary protecting group
UV	ultraviolet
XRD	X-ray powder diffraction

1. Introduction

This chapter has been modified in part from the following articles:

Y. Yu,* T. Tyrikos-Ergas,* Y. Zhu, G. Fittolani, V. Bordoni, A. Singhal, R. J. Fair, A. Grafmüller, P. H. Seeberger, M. Delbianco, Systematic Hydrogen Bond Manipulations to Establish Polysaccharide Structure-Property Correlations. *Angew. Chem. Int. Ed.* **2019**, 131, 13261. <https://doi.org/10.1002/anie.201906577>

Y. Yu,* S. Gim,* D. Kim, Z. A. Arnon, E. Gazit, P. H. Seeberger, M. Delbianco, Oligosaccharides Self-Assemble and Show Intrinsic Optical Properties. *J. Am. Chem. Soc.* **2019**, 141, 4833. <https://doi.org/10.1021/jacs.8b11882>

Y. Yu, A. Kononov, M. Delbianco, P. H. Seeberger, A Capping Step During Automated Glycan Assembly Enables Access to Complex Glycans in High Yield. *Chem. Eur. J.* **2018**, 24, 6075. <https://doi.org/10.1002/chem.201801023>

* equal contribution.

1.1. Carbohydrates

Carbohydrates are the most abundant organic compounds in Nature, with comprehensive existence in all the living things. Even though composed mainly of only four elements: carbon (C), hydrogen (H), oxygen (O), and nitrogen (N), they are the most diversified class of molecules in Nature. Carbohydrates are involved in a wide variety of physiological and pathological processes,¹⁻² including cell-cell recognition,³ blood-group classification,⁴ and oncogenic transformation⁵. In addition, the large abundance of carbohydrates in Nature makes them important candidates in materials science.

1.1.1. Polysaccharides as materials

Carbohydrates are also referred to as saccharides. As a rule of thumb, saccharides can be divided into monosaccharides (one unit), disaccharides (two units), oligosaccharides (three to ten units), and polysaccharides (more than ten units). Polysaccharides serve as important biomaterials in Nature. The striking abundance makes carbohydrates an attractive resource of raw material for textile, food, paper, and pharmaceutical industries.

Polysaccharides consisting of one or multiple kinds of monosaccharide units are classified as homopolysaccharides and heteropolysaccharides, respectively. Homopolysaccharides account for the majority of polysaccharides in terms of mass.

Based on the type of monosaccharide and the linkage between these units, different homopolysaccharides are defined, with cellulose, chitin, and amylose among the most abundant (**Figure 1-1**).

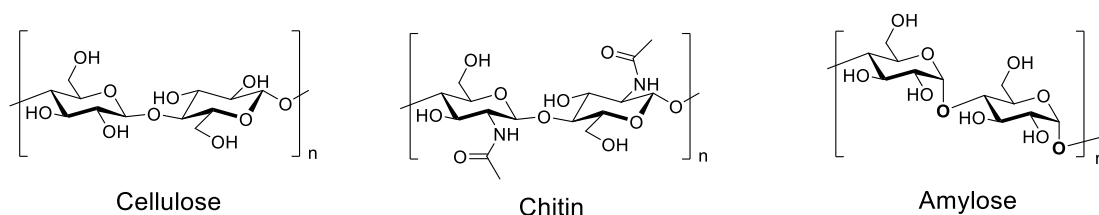


Figure 1-1. Chemical structure of cellulose, chitin, and amylose.

As a polymer, each polysaccharide can be then differentiated by the degree of polymerization (DP). The DP of polysaccharides from different sources varies drastically. Polysaccharides can be also classified as linear or branched, charged or non-charged.

1.1.1.1. Cellulose

Cellulose is the most abundant biomass in Nature, with a wide distribution in the biosphere.⁶ It is one of the major components of the plant cell wall and provides structural support and strength. Cellulose plays also a crucial role in the protective biofilm of some bacteria.⁷

In human society, cellulose has been used since the beginning of civilization in making paper products, clothes, and building materials. Although cellulose cannot be digested by human due to the lack of cellulase, recent discovery in nutriology suggests that taking in cellulose fiber (known as dietary fiber) in diet is beneficial for digestive system.⁸ In addition, cellulose finds broad application in manufacturing scientific devices, such as quantitative filter paper, dialysis membrane, and thin-layer chromatography.

Cellulose is a biopolymer that consists of repeating glucose units, connected through β -1,4-glycosidic bonds (**Figure 1-1**). The β configuration allows for a compact sheet-like secondary structure.⁹ The hydroxyl groups arrange themselves to give a dense H-bonding network (**Figure 1-2A**), which is majorly responsible for the high crystallinity and stiffness of cellulose. While most carbohydrates can hardly be crystallized, the high crystallinity of cellulose allows for substantial structural study with X-ray diffraction.¹⁰ Till now, four types of cellulose crystalline forms based on different H-bonding patterns have been characterized. Cellulose I is the natural form of cellulose. The treatment on cellulose I with alkali irreversibly yields cellulose II, which is lower in free energy than cellulose I. Cellulose III and cellulose IV are less common and can

be also obtained by chemical treatments, but will not be included within the framework of this thesis.

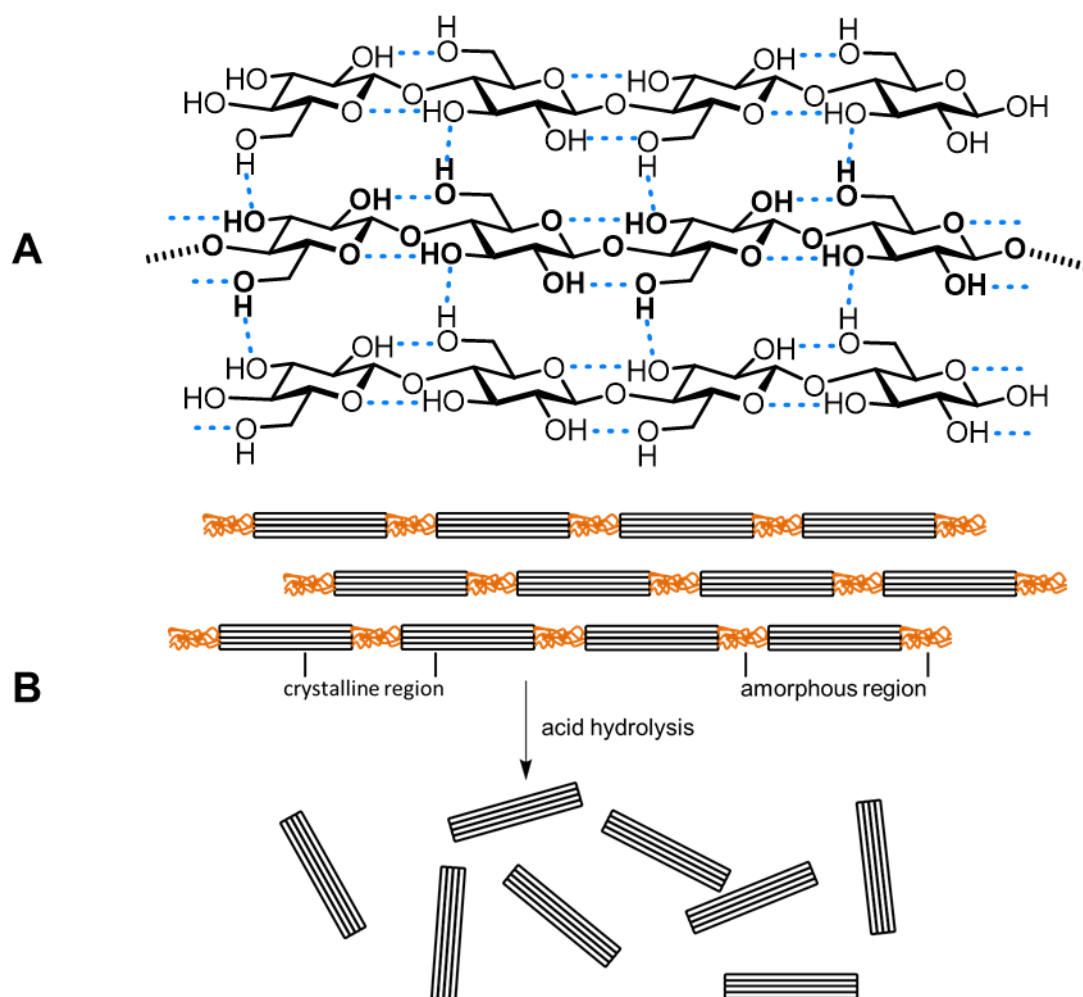


Figure 1-2. Schematic representation of crystalline structure of cellulose (A) and intermittent occurrence of crystalline and amorphous region in cellulose (B).

In the hierarchical structure of cellulose,¹¹ highly ordered crystalline regions are separated by disordered amorphous regions (**Figure 1-2B**).¹² By acid hydrolysis, the crystalline part of cellulose (cellulose nanocrystals, CNCs) can be obtained. Due to their renewable nature, biocompatibility, high stiffness, and low cost, CNCs are gaining popularity in materials engineering.¹³ Important examples of applications of CNCs in material science include the formation of cross-linked hydrogels¹⁴ and hierarchical architectures with interesting optical behavior¹⁵.

Chemical modifications drastically change the properties of cellulose and chemically modified cellulose has found broad application in industry.

Methylation is one of the most common methods for cellulose modification.¹⁶ Methylcellulose (MC) (**Figure 1-3**) is broadly applied as bulk forming laxative pharmaceutical, thickener in food, and additive in construction materials. In addition, methylation gives cellulose a temperature-dependent gelation property¹⁷⁻¹⁸ which has aroused a lot of interests in material sciences.

The introduction of polar carboxymethyl group into cellulose increases the water solubility. Carboxymethyl cellulose (CMC, **Figure 1-3**) is used, in its sodium salt form, as tackifier, lubricant, and thickening agent.¹⁹⁻²⁰ Its properties are largely affected by the degree of substitution.



R = -H or -CH₃: Methylcellulose

R = -H, -CH₂COOH, or -CH₂COONa: Carboxymethyl cellulose

Phosphoethanolamine cellulose

Figure 1-3. Chemical structure of methylcellulose, carboxymethyl cellulose, and phosphoethanolamine cellulose.

In 2018, Thongsomboon et al. reported the first discovery of naturally modified cellulose.²¹ Solid-state NMR analysis confirmed that some bacteria produce modified cellulose which contains a phosphoethanolamine modification at the 6-OH of every second glucose unit (**Figure 1-3**). This modification was then proved to play a crucial role in adjusting the macroscopic morphology of biofilm to better protect the bacteria against harsh conditions.

1.1.1.2. Chitin and amylose

Next to cellulose, chitin is the second most abundant polysaccharide found as the major component of the exoskeletons of crustaceans and insects.²² The chemical structure of chitin is closely related to cellulose. The two polysaccharides share the same structural scaffold and only differs in the substitution at 2-C (**Figure 1-1**). The acetyl amino group of chitin allows for stronger H-bonding compared with the hydroxyl group of cellulose, thus gives chitin higher mechanical strength.

Amylose is one of the major components of starch and an important energy resource for humans.²³⁻²⁴ Amylose shares the same monomeric unit of cellulose but with α -1,4- instead of β -1,4-glycosidic linkage (**Figure 1-1**). This relatively small difference results in an entirely different enzymatic reactivity, which makes starch easily digested by the

enzymes in the mouth, stomach and small intestine of human, while cellulose remains stable during the digestion process. Additionally, the difference in the configuration of the glycosidic bonds drastically affects the secondary structure, with amylose chain adopting an amorphous or helical conformation, with much lower crystallinity than the linear cellulose.

1.1.2. Challenges in polysaccharide materials

Although it is well-known that the properties of polysaccharides are strongly affected by their chemical structure,²⁵ a detailed structure-property correlation is missing, largely due to the lack of pure molecules and effective analytic methods.

To achieve solid characterization and establish structure-property correlations, pure compounds are necessary. However, polysaccharides extracted from natural sources are generally heterogeneous. Due to the structural complexity, large molecular size, and low solubility of natural polysaccharides, purification is often inapplicable. In most cases, chemical synthesis remains the only access to pure samples.²⁶ However, synthesis of carbohydrate is challenging and laborious due to the intrinsic complexity of glycans and the lack of a universal synthetic approach.

The lack of reliable characterizing methods also limits the understanding of carbohydrate materials. Most carbohydrates only consist of four basic elements (C, H, O, N) and do not contain a chromophore. Therefore, very few analytical methods are available for the structural characterization of carbohydrates at the molecular level.²⁷⁻²⁸ In addition, such methods are generally challenging and require expertise. Molecular dynamics simulations have also been applied to assist the structural study of polysaccharides,²⁹⁻³⁰ but remain limited by the lack of validating standards.

1.2. Synthetic polysaccharides

In comparison with DNA and peptide synthesis, the synthesis of polysaccharides is more challenging due to the structural diversity. Polysaccharides can form branched structures, requiring multiple temporary protecting groups (tPGs) for synthesis. In addition, attention should be paid to the stereochemistry of the glycosidic bond (**Figure 1-4**).

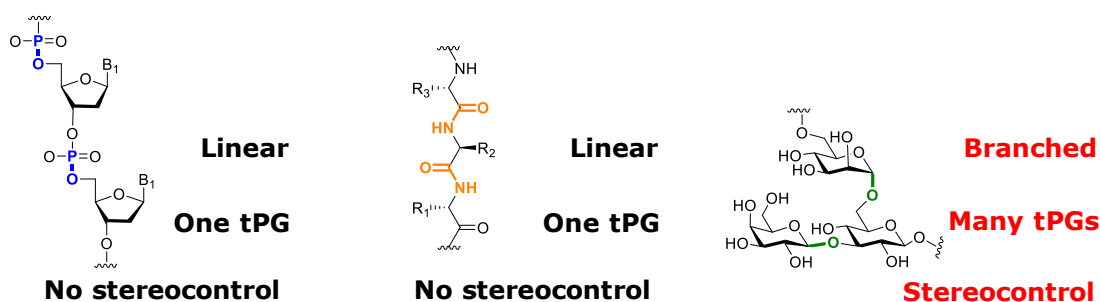


Figure 1-4. Comparison of DNA, peptide, and carbohydrate synthesis.

1.2.1. Chemical glycosylation

A glycosylation reaction forms a glycosidic bond between the glycosyl donor and a hydroxyl group on the glycosyl acceptor. Glycosylation can be catalyzed enzymatically or chemically. In this thesis, only chemical glycosylation is discussed.

The first step of a chemical glycosylation involves the activation of the glycosyl donor with a suitable activator. This results in the departure of the leaving group (LG) with consequent formation of an oxocarbenium ion. Nucleophilic attack by the hydroxyl group on the glycosyl acceptor yields the product (**Figure 1-5A**). The instability and water sensitivity of the intermediates are the major reasons why low temperature and anhydrous condition (usually achieved by molecular sieve) are necessary during the glycosylation process.

When the glycosyl acceptor is itself a sugar, several hydroxyl groups can potentially react (**Figure 1-5B**). Regioselectivity is therefore necessary to obtain the desired product. Protecting groups (PGs) are employed to block the undesired reactive sites and leave only the desired hydroxyl available for coupling (**Figure 1-5B**). The formation of the glycosidic bond generates a new stereogenic center. The glycosyl acceptor can attack from both sides of the oxocarbenium intermediate, resulting in a mixture of products (α and β anomers). Therefore, stereoselectivity should be ensured so that only one anomer is obtained as major product (**Figure 1-5C**). The use of particular PGs is often exploited to control the stereoselectivity by neighboring group participation. This is generally an ester group that, upon activation of the glycosyl donor, can stabilize the oxocarbenium ion and form an acetoxonium ion, which blocks the α face of the activated donor, so that only 1,2-trans linkage is formed (**Figure 1-5C**).

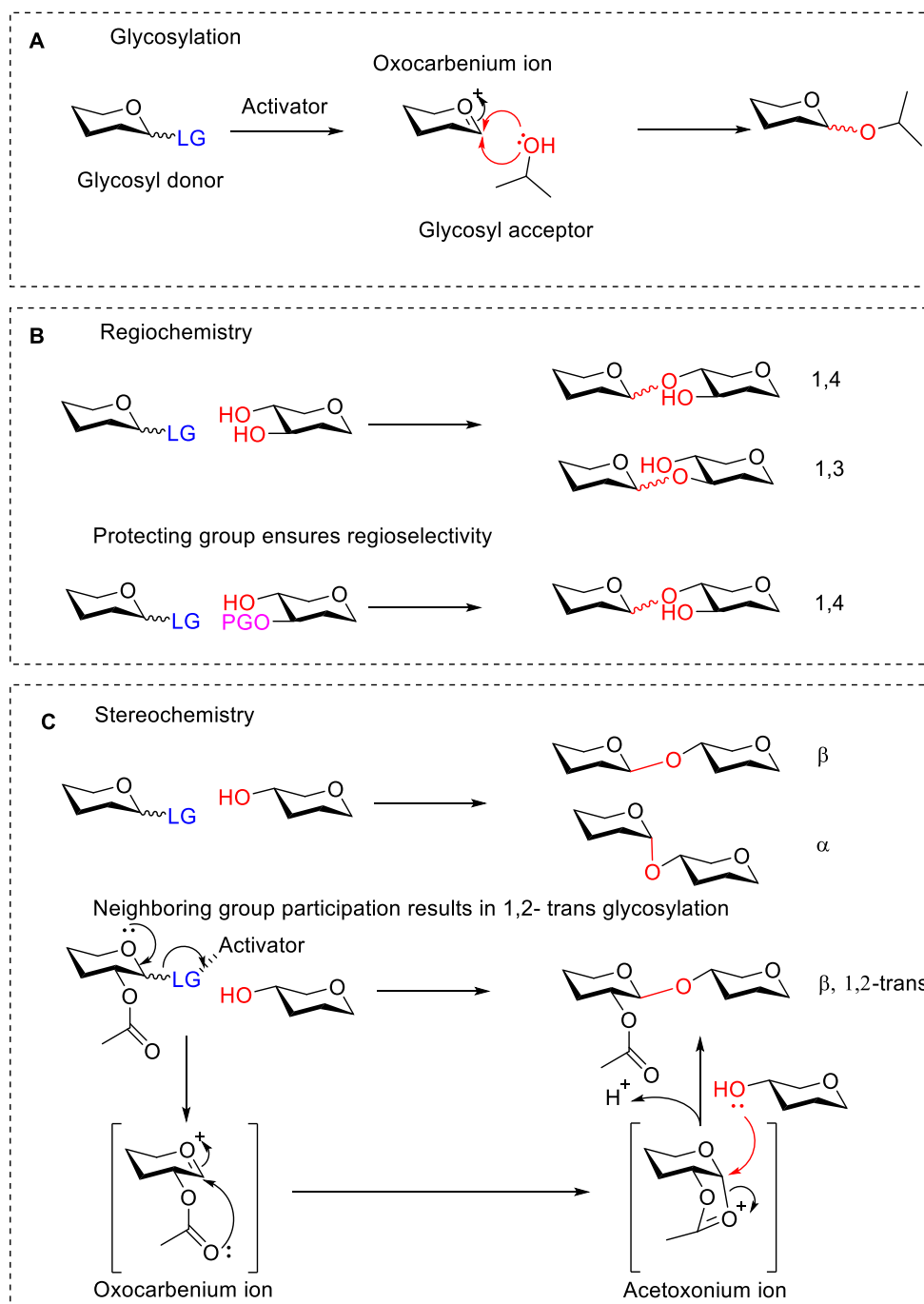


Figure 1-5. General mechanism of glycosylation and regio- and stereochemistry control by protecting groups and neighboring group participation.

The installation and removal of protecting groups result in extra synthetic workload. In addition, some glycosidic bonds are still difficult to construct, such as the 1,2-cis linkage and the ketosidic bond of sialic acid. Many special glycosylation strategies have been developed, such as remote participation,³¹⁻³² or conformational constraint.³³ Nevertheless, the choice of synthetic method for carbohydrates has always been case-dependent.

1.2.2. Synthesis of polysaccharides

In the last decades, many elegant works have been reported that allowed for the access to defined and complex oligosaccharides. Nevertheless, such protocols are still considerably challenging when applied to big polysaccharides, often requiring huge chemical efforts and synthetic steps. Depending on the target molecules, different strategies were employed to minimize the manual work (**Figure 1-6**).

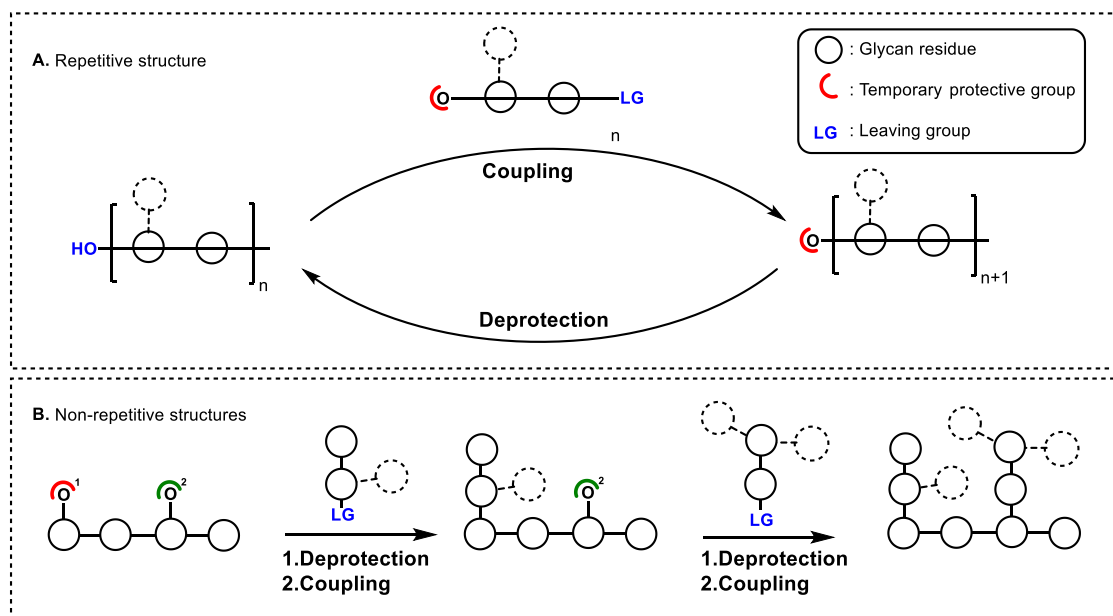


Figure 1-6. General scheme of well-defined polysaccharide synthesis.

Most natural polysaccharides are based on repetitive structures with a repeating unit consisting of one or multiple (linear or branched) glycosidic residues. To synthesize repetitive polysaccharides, a building block representing the repeating unit needs to be obtained and used iteratively (**Figure 1-6A**). A careful protecting group strategy is always employed to assure the desired regio- and stereochemistry.

When the repeating unit consists of a branched structure, the retro-synthesis becomes more complex. As common strategy, a linear multi-ol acceptor is firstly synthesized and the ensuing multi-glycosylation inserts all the branches in one single step.

The synthetic strategy for non-repetitive polysaccharides highly depends on the structures of the target molecule (**Figure 1-6B**). In 2017, an impressive total synthesis of mycobacterial arabinogalactan with 92 monosaccharide units was reported (**Figure 1-7**, $m = 13$, $n = 9$), resulting in the biggest well-defined polysaccharide ever synthesized in solution phase.³⁴ The key glycosylation step was a [31+31+30] coupling, promoted by benzenesulfinyl morpholine/triflic anhydride. A preactivation-based

glycosylation strategy was adopted during the assembly to decrease the need of protecting group manipulation.

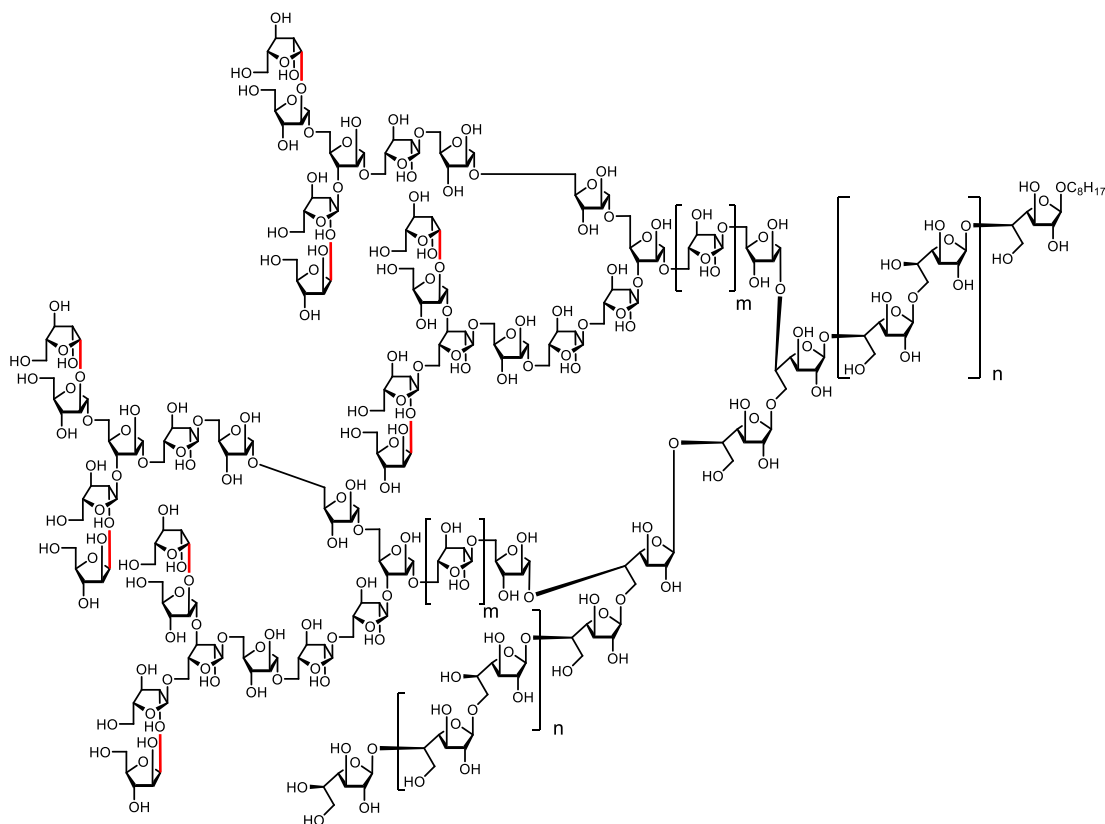


Figure 1-7. Structure of mycobacterial arabinogalactan with highlighted β -arabinofuran linkages (red).

1.2.3. Automated glycan assembly of polysaccharides

Several automated synthetic platforms have been developed to reduce the manual work required by classical solution phase synthesis and to improve the process efficiency. Youshida et al. reported the automated synthesis of hexa-*N*-acetylglucosamine based on electrochemical oxidation.³⁵ Using fluororous tag-assisted automated synthesis, Pohl et al. synthesized trimannoside in solution phase.³⁶ Demchenko et al. reported the automated oligosaccharide synthesis in adapted HPLC.³⁷ Nevertheless, none of the automated synthetic platforms reaches the length beyond hexasaccharide, except for automated glycan assembly.

1.2.3.1. Automated glycan assembly (AGA)

In 1971, Schuerch et al. reported the first solid phase glycan synthesis.³⁸ Since then, much advancement has been made to optimize this method. In parallel, automated synthesis of peptides and oligonucleotides found great success in commercialization.³⁹⁻⁴¹ Automated solid phase glycan synthesis was not achieved until

2001, when Seeberger et al. reported the first fully automated glycan synthesis.⁴² In the ensuing two decades, different linkers and building blocks have been tested and applied in order to enrich the synthesis ability.⁴³⁻⁴⁵

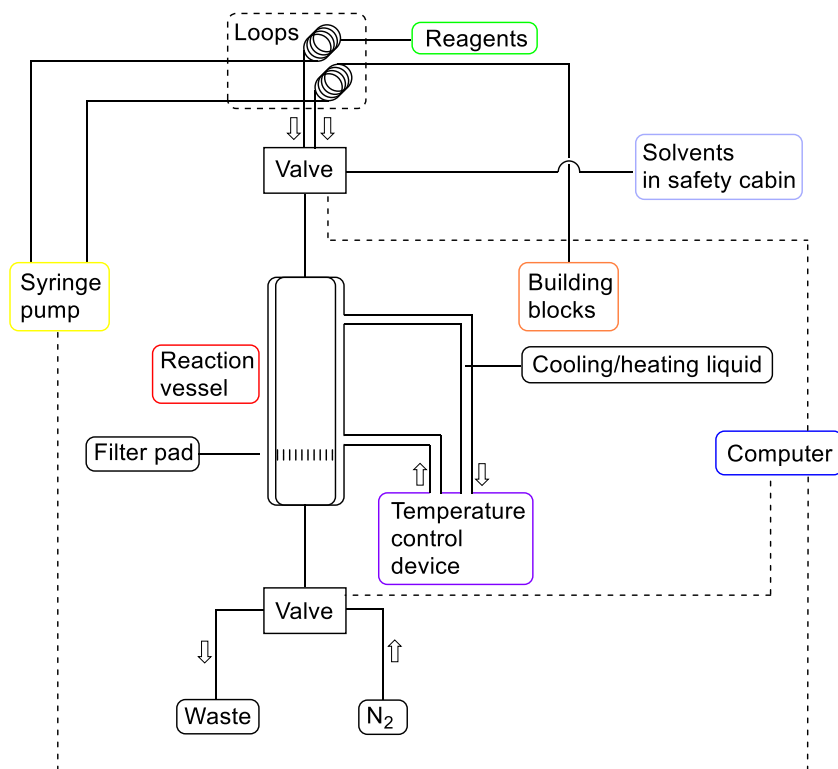


Figure 1-8. Photo and schematic diagram of automated glycan assembly with essential components in colored boxes.

The resin is manually added to the chilled reaction vessel (red box). Reagents (green box) and building blocks (orange box) are delivered from inert-gas-compressed stock glassware to the reaction vessel *via* syringe pumps (yellow box). Solvents (light blue box) are driven to the reaction vessel by compressed argon. A filter pad is fitted at the bottom of the vial to enable a rapid removal of excessive reagents and solvents after each reaction or washing step. The reaction temperature is controlled by a temperature-controlling device (purple box). The operation of the synthesizer is highly programmable and controlled by computer (dark blue box).

All AGA reactions are conducted on solid support. A cleavable linker, containing a free hydroxyl group, is bound to the resin and used as first anchoring point (**Figure 1-9A**). The cleavable part between resin and hydroxyl group enables the release of the synthetic oligosaccharides from the solid support upon completion of AGA. Depending on the cleaving condition, different linkers have been developed, such as metathesis-labile linker, base-labile linker, and photocleavable linker. In this thesis, unless stated otherwise, only the photocleavable linkers are used.

Two types of photocleavable linkers are currently employed. Resin **1** releases the glycan equipped with an aminoalkyl spacer at the reducing end (**Figure 1-9B**), enabling the subsequent attachment of the glycan to a protein or microarray. The recently developed photocleavable linker **2** offers the option of releasing the free reducing end after photocleavage (**Figure 1-9C**).⁴⁵

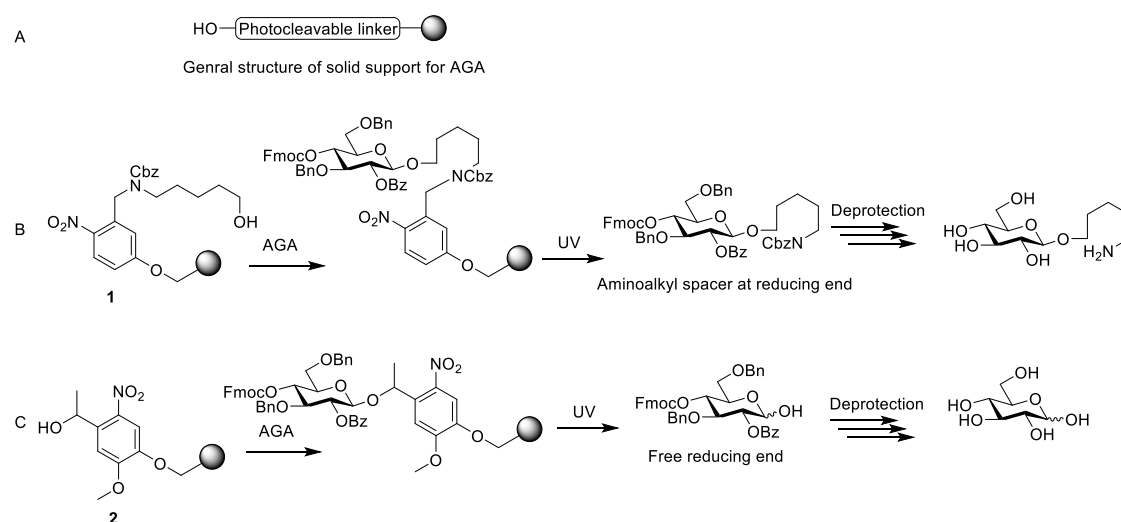


Figure 1-9. Examples of photocleavable linkers currently employed in AGA.

AGA is based on the iterative addition of protected monosaccharides to a growing oligosaccharide chain bound to a solid support (**Figure 1-10**). A sugar building block, equipped with a reactive leaving group, is chemically activated and coupled to the

hydroxyl group of the linker. After glycosylation, the excess building block and reactants are removed by filtration. The BB is equipped with one or multiple temporary protecting groups (generally levuliny group (Lev) or fluorenylmethyloxycarbonyl group (Fmoc)) that permit to release the desired hydroxyl group to be used in the next glycosylation step. All the other BB positions are protected as benzyl ethers or benzoyl esters (permanent protecting groups). The iterative glycosylation and deprotection cycles are programmed and controlled by a computer.

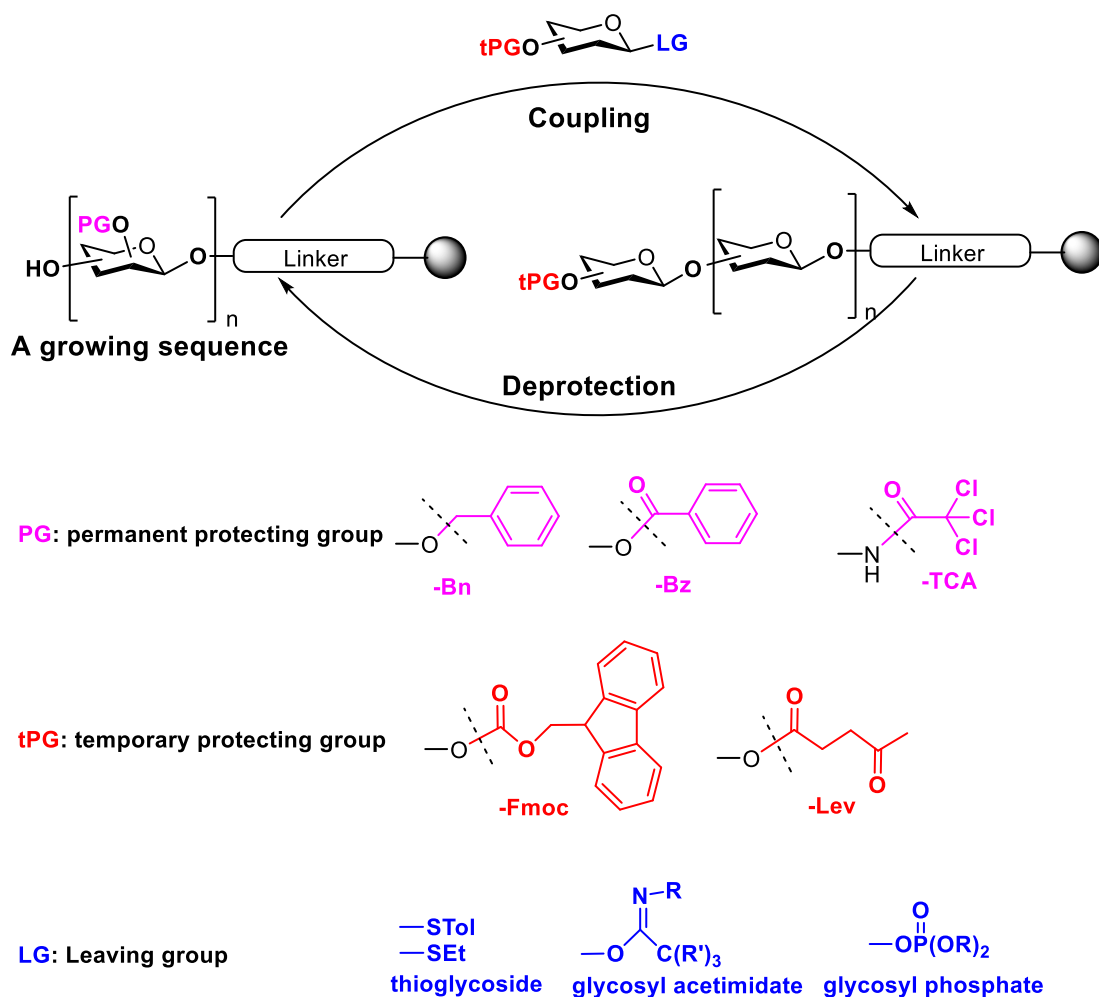


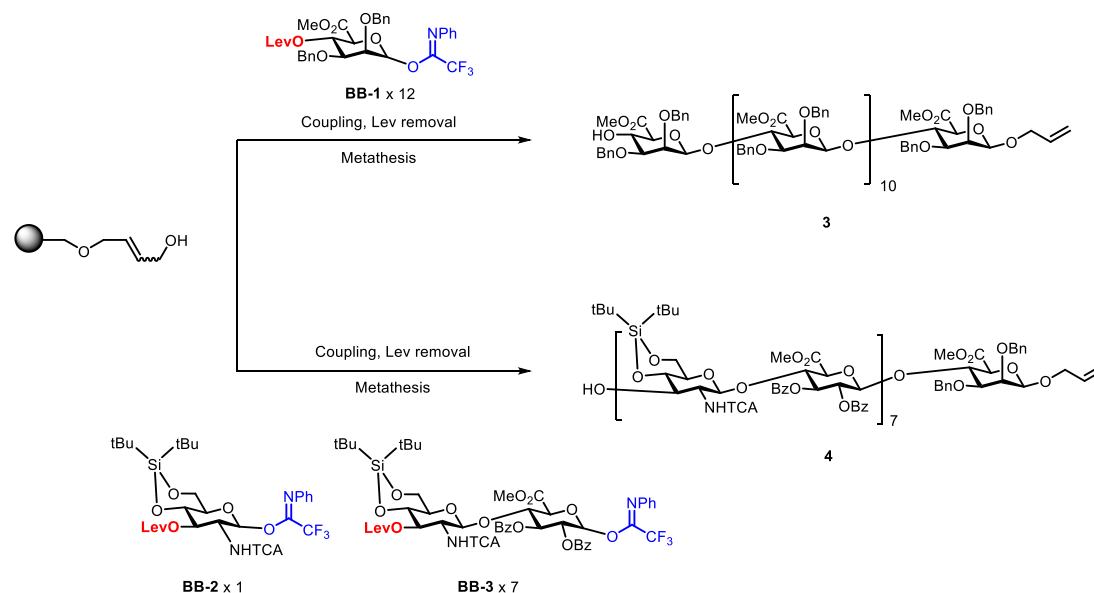
Figure 1-10. Synthetic cycle of automated glycan assembly.

Upon completion of the assembly, the UV light sensitive linker is cleaved from the solid support under the irradiation of a mercury lamp, liberating the desired fully protected polysaccharides. To improve the efficiency of this UV-cleavage, a flow device is employed, which decreases the distance between the light source and the solid support.⁴⁶

Removal of all the protecting groups through methanolysis of the ester-type PGs followed by hydrogenation of the ether PGs affords the target glycan.

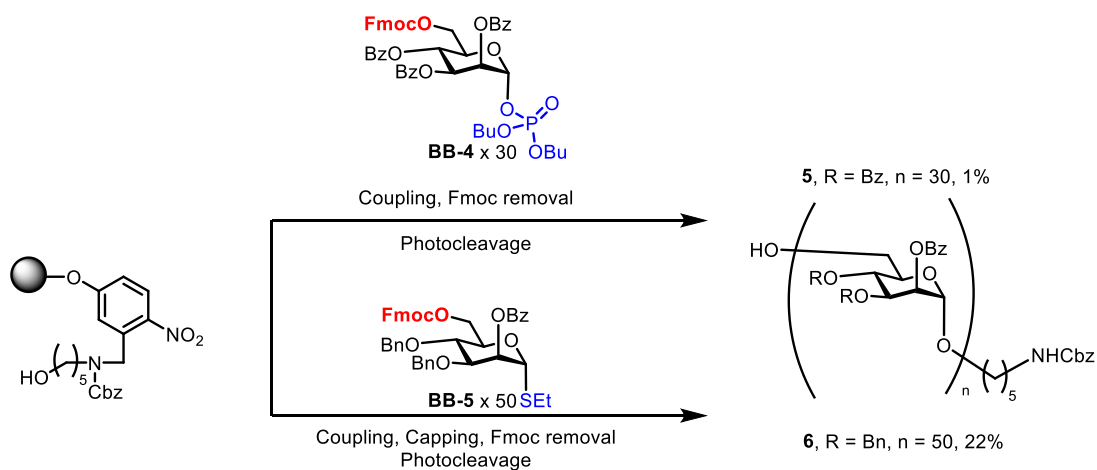
1.2.3.2. Polysaccharide synthesis with AGA

To date, a wide range of glycans have been successfully synthesized with AGA. Still, the synthesis of long polysaccharides remains quite challenging. Here some important achievements are reviewed. In 2012, the 12-mer β -mannuronic acid alginate **3** was synthesized by AGA (**Scheme 1-1**).³² This synthetic route employs Lev as temporary group and trifluoroacetimidate as leaving group. The 12-mer was obtained in a 40% yield, indicating a 90% average coupling efficiency. Similarly, the synthesis of a pentadecasaccharide fragment of hyaluronic acid **4** was reported (**Scheme 1-1**), with 92% average coupling yield. The use of the disaccharide building block **BB-3** permitted to obtain the desired alternated polysaccharides structure. The entire process of eight cycles of automated coupling and deprotection took only 28 hours.



Scheme 1-1. Synthesis of β -mannuronic acid alginate **3** and hyaluronic acid **4**.

In 2013, a 30-mer polymannoside (**5**) was synthesized using a monosaccharide phosphate building block **BB-3** (**Scheme 1-2**).⁴⁷ A "catch-release" strategy was introduced to isolate the desired compound from impurities during the purification process.



Scheme 1-2. Automated glycan assembly of linear polymannosides **5** and **6**.

To push the limit of automated glycan assembly, the 50-mer polymannoside **6** was targeted and synthesized in a 5% yield (**Scheme 1-2**).⁴⁸ This is the longest synthetic oligosaccharide reported directly assembled from monosaccharide building blocks. Notably, an exploratory capping procedure was introduced to reduce the deletion sequences. However, this capping procedure requires 90 minutes and was therefore never implemented in the standard AGA sequence.

Based on the results on polymannosides, AGA was employed for the synthesis of polysaccharides based on different repeating units (**Figure 1-11**). A collection of polysaccharides (homo- and heteropolymers) based on mannose, glucose and glucosamine was synthesized and used for structural studies.⁴⁹ The iterative addition of monomeric BBs permits the introduction of modifications (e.g. a different BB or a labelled unit) in specific positions of the chain. Single site modifications drastically affected the geometry and properties of the final compound, suggesting the potential of AGA for a detailed structure-property study of polysaccharides. Moreover, the insertion of a terminal BB bearing a carboxylic acid introduced a linkage point that was exploited for the block coupling of different oligosaccharides fragments.

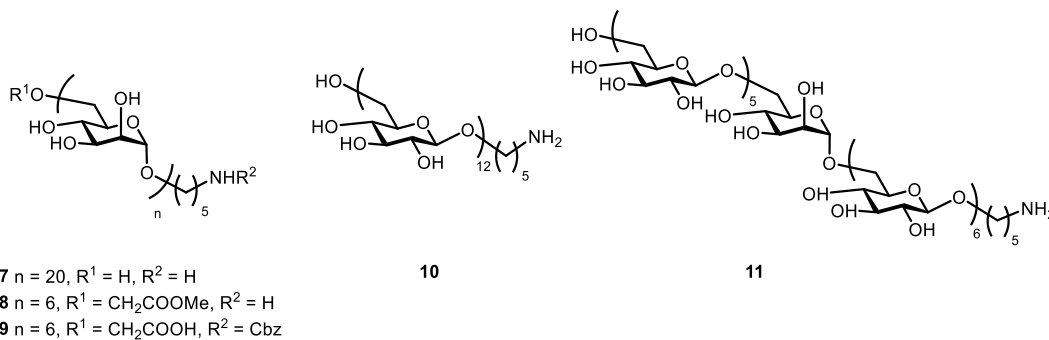


Figure 1-11. Synthetic homo- and hetero-polysaccharides for structural studies and schematic representation of block coupling.

1.2.4. Synthetic carbohydrate materials for structural studies

Large access to well-defined structures allows for detailed structural characterization. Recent years have seen a substantial advancement in the conformational study of carbohydrates based on defined molecules obtained with chemical synthesis.

Carbohydrates had been generally regarded as flexible in aqueous solution, while DNA and peptide have been proved to exhibit well-defined conformations. However, recent research indicates that certain oligosaccharides possess varying degrees of conformational preference in solution state.

In 2018, our group suggested the use of defined oligo- and polysaccharides for structural studies.⁴⁹ Different classes of oligo- and polysaccharides were synthesized and studied with molecular dynamics (MD) simulations and NMR analysis, indicating that each oligomer presents a different geometry and flexibility. For example, in water, a 1,6-oligomannoside **12** adopts a flexible linear structure, while the analogue 1,6-oligoglucoside **10** exists in a more compact helical structure (**Figure 1-12**).

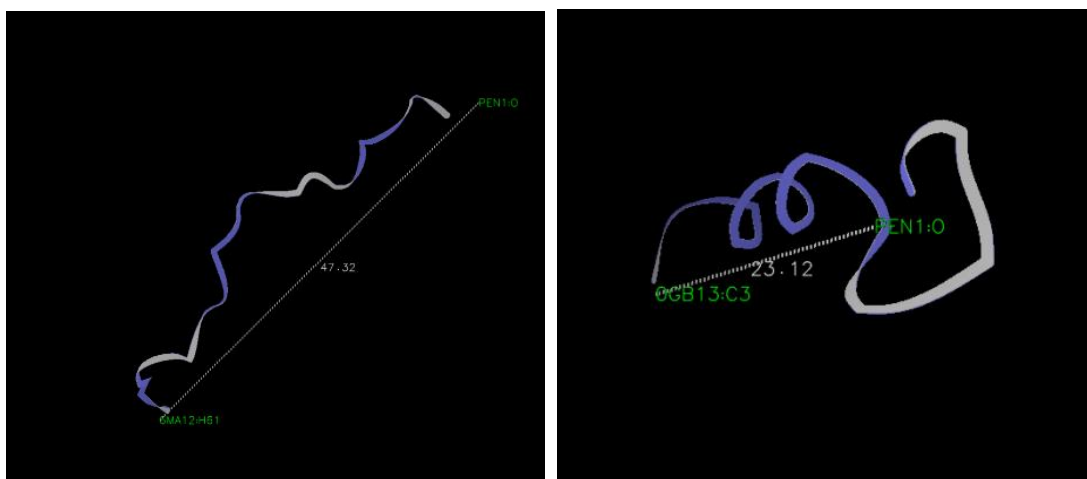
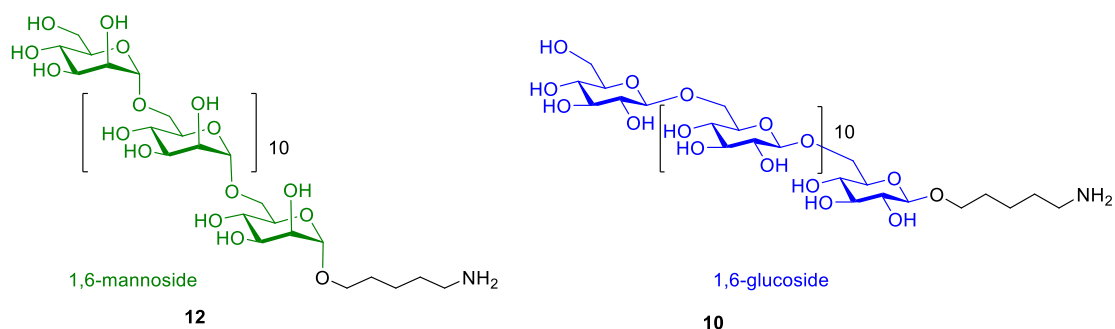


Figure 1-12. Chemical structure and MD simulations of 1,6-mannoside and 1,6-glucoside.

To support the MD model, NMR analysis was employed. NMR is a powerful tool for the structural study of polysaccharides in solution.⁵⁰ However, detailed structural information at monosaccharide level is difficult to obtain, largely due to the chemical shift degeneracy which results in signal overlap and ambiguity in assignment. To simplify the analysis, a $^{13}\text{C}_6$ -labeled glucose unit was inserted at specific position of the hexasaccharide chain. The labelling broke the chemical shift degeneracy and provided reliable NMR information that confirmed the MD results.

In 2013, Ernst et al. discovered a non-conventional H-bond in Lewis X,⁵¹ which stabilizes the conformation of Gal[Fuca(1–3)] β (1–4)GlcNAc trisaccharide motif. NMR studies and quantum mechanical calculation were employed. In 2015, Freedberg et al. further confirmed the existence of this non-conventional H-bond by a temperature-dependent NMR study and molecular dynamics simulations.⁵²

In 2019, Codée et al. synthesized a series of zwitterionic *Streptococcus pneumoniae* serotype 1 polysaccharides (Sp1),⁵³ ranging from tri- to dodecasaccharides. MD simulation and NMR studies unraveled a helical structure for the Sp1 chain. To complete one single helical turn, nine glycosidic units are needed. ELISA and STD-

NMR experiments were then performed, which revealed a minimal antibody binding epitope of 7-8 residues of Sp1. The coincidence of the minimal length for one helical turn and antibody binding affinity might indicate the role of carbohydrate conformation in biological events.

1.3. Nanotechnology based on biomolecules

DNA and peptide have found great success in nanotechnology, based on the following two facts:

- Well established synthetic platform enables quick access to pure material
- Their conformation is well studied by reliable analyzing methods

Taking advantage of the well-established synthetic platform and stable double helical structure of DNA, DNA origami has shown that the design of complex nanostructures can be highly rational and programmable. In 2006, Rothemund reported the sophisticated computer-assisted bottom-up design of DNA sequences,⁵⁴ which can self-organize into a bewildering array of defined supramolecular structures. Since then, a variety of DNA nanostructures were created, offering nanometer control on the supramolecular architectures and found applications in nanorobot construction, drug delivery, and biosensing.⁵⁵

The bottom-up construction of supramolecular structure has also been achieved with peptide-based material. A representative example is the three-block structure, peptide amphiphile (PA) designed by Stupp et al.⁵⁶ The scaffold of PA contains an H-bonding peptide sequence, which has the tendency to assemble in a β -sheet manner. The N-terminus is linked to a hydrophobic C₁₆ alkyl chain, which guides the assembly into one-dimensional supramolecular structure. Charged amino acid residues are connected at the C-terminus, which further stabilize the assembled structure by improving the water solubility. This peptide based self-assembling system is biocompatible, stimuli responsive, self-healable, and biodegradable and has found broad biomedical applications, such as bone regeneration,⁵⁷ smooth muscle preservation,⁵⁸ burn wound healing,⁵⁹ cancer therapy,⁶⁰ and plaque burden reduction in atherosclerosis.⁶¹ Nature has also inspired several synthetic supramolecular architectures. For example, amyloid fibrils in Alzheimer's disease exhibit a defined β -sheet structure, which is responsible for the stability and low solubility of amyloid fibrils and makes it difficult to be removed from human brain.⁶²⁻⁶³ Inspired by the structure of amyloid fibrils, Gazit et al. designed short peptide fragments⁶⁴⁻⁶⁵ (e.g. diphenylalanine⁶⁶) and their analogues (e.g. cyclo-dipeptide,⁶⁷ di-peptide nucleic acid (PNA)⁶⁸), which were shown to exhibit a self-assembly behavior comparable to the natural amyloid

protein. These artificial self-assembled materials exhibit intrinsic fluorescence and unique semiconducting properties.

Carbohydrates are often applied in nanotechnology as adjunct component. In 2017, Stupp et al. introduced sulfated monosaccharide into the PA-based nanostructure to mimic the biological function of natural heparin.⁶⁹ The filamentous glycopeptide was found to exhibit stronger influence on biological signals than its natural counterpart. In 2019, Meijer et al. attached a series of carbohydrate to their renowned benzene-1,3,5-tricarboxamide (BTA) based supramolecular system to mimic the structure and function of the glycocalyx (carbohydrate-enriched coating of many cells).⁷⁰ Still, carbohydrates are rarely used for the creation of the supramolecular architecture, but rather to improve water solubility or as decorating appendances. This is surprisingly considering their ability to engage in hydrogen bonding networks.

As discussed, defined aggregation of carbohydrate is commonly observed in Nature, as with cellulose and chitin, indicating the possibility for carbohydrate-based material to form ordered supramolecular structure. Therefore, carbohydrate-based nanotechnology holds great promise, owing to the biocompatibility, renewability, and high abundance of carbohydrates.

1.4. Aims of this thesis

The general aim of this thesis was the development of an efficient synthetic strategy to produce well-defined oligo- and polysaccharides, as probes to study carbohydrate materials.

The first aim was to improve AGA yields, through the implementation of a capping step into the AGA cycle. The capping method needs to:

- i) be compatible with other AGA reagents and commonly used protecting groups;
- ii) ensure a fast synthesis;
- iii) avoid expensive and toxic materials;
- iv) be able to improve the yield in real synthesis of biologically important oligosaccharides and long polysaccharides;
- v) simplify the purification of long polysaccharides.

The second aim of the thesis was to use AGA to produce a collection of well-defined probes to establish structure-property correlation of oligo- and polysaccharides. This task can be separated into following steps:

- i) A collection of building blocks bearing unnatural modifications (e.g. a methyl group) needs to be synthesized.
- ii) A collection of cellulose analogues with specific modification patterns should be prepared.
- iii) This collection needs to be analyzed in terms of solubility and crystallinity (XRD), with particular attention to the difference between cellulose analogues with and without modifications.
- iv) MD simulations were planned to study the conformation and aggregation of cellulose analogues.

The third aim of this thesis was the study of the self-assembly of oligosaccharides. To this end:

- i) A collection of oligosaccharides has to be designed.
- ii) Suitable self-assembly conditions for carbohydrates needs to be probed.
- iii) Microscopic observations needs to be performed to study the morphology of self-assembled samples.
- iv) Photophysical characterizations should be conducted on the self-assembled samples.

2. A Capping step during automated glycan assembly enables access to complex glycans in high yield

This chapter has been modified in part from the following article:

Y. Yu, A. Kononov, M. Delbianco, P. H. Seeberger, A Capping Step During Automated Glycan Assembly Enables Access to Complex Glycans in High Yield. *Chem. Eur. J.* **2018**, 24, 6075. <https://doi.org/10.1002/chem.201801023>

2.1. Introduction

AGA provides rapid access to different classes of structurally defined glycans. Due to the nature of solid-phase synthesis, excess reagents and building blocks, used to ensure high coupling yields, can be simply removed by washing and filtration from the solid support to accelerate oligosaccharide synthesis. Crucial for a successful AGA is the completion of each glycosylation reaction. In ideal conditions, all hydroxyl groups exposed on molecules attached to the solid support should be glycosylated such that, after removal of the temporary protecting groups (Fmoc and Lev etc.), the next glycosylation cycle can take place only on the freshly released hydroxyl groups. Even in automated peptide and oligonucleotide assembly, where coupling yields commonly exceed 99.9%, a capping step is inserted to minimize the accumulation of n-1 deletion sequences and to maximize the overall yield.⁷¹ Because of the intrinsic structural complexity of carbohydrates, the yields of the glycosylation reaction vary significantly. Incomplete glycosylations can result in deletion sequences that render the final purification challenging. Therefore, excess building block, typically ten equivalents, is added to drive the glycosylation to completion.

Taking an AGA of a trisaccharide as an example (**Figure 2-1**), ideally only the desired trimer should be obtained. In reality, the glycosylation reactions sometimes do not reach completion. This results in free not-glycosylated OH groups on the n-1 glycan sequence. This uncoupled OH group can further participate in the ensuing glycosylation reactions and a mixture of side products is eventually generated, making final purification more difficult. For a trimer synthesis, theoretically, seven different deletion sequences can be generated (**Figure 2-1A**). Additionally, the side reactions consume building block, decreasing the amount of building block available for the glycosylation of the desired sequence.

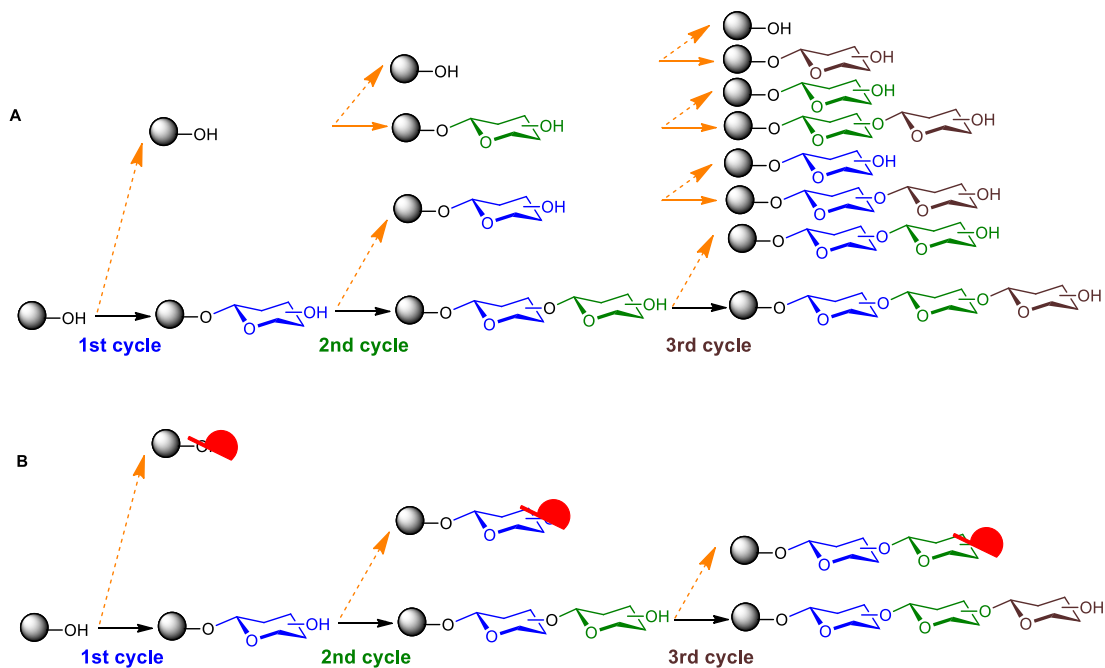


Figure 2-1. Conceived synthesis of a trisaccharide with possible side products without (A) and with capping (B).

Incorporation of a capping step to block the unreacted hydroxyl groups after each glycosylation prevents any undesired chains from growing (**Figure 2-1B**). Efficient capping would help expand the use of AGA to create more complex oligosaccharides in higher yields.

A procedure based on the standard capping conditions used in automated oligonucleotide synthesis using a pyridine-acetic anhydride (Ac_2O) mixture was sometimes implemented in AGA. However, several issues had limited the implementation of this capping step in the standard AGA cycle. Unlike oligonucleotide synthesis, where very limited kinds of building blocks are used, AGA employs a large pool of building blocks and thus the reactivity of hydroxyl group varies much more dramatically. In addition, acetylation with the pyridine- Ac_2O method proved to be quite slow, requiring at least 90 min to reach completion.⁴⁸ No strong nucleophiles (e.g. DMAP) could be utilized to improve the capping rate, as the base-labile 9-fluorenylmethoxycarbonyl (Fmoc) temporary protecting group, commonly used in AGA, is not compatible with strong bases. Herein, an acid-catalyzed capping method to improve the efficiency of AGA is described (**Figure 2-2**) as illustrated in the context of the syntheses of biologically important tetrasaccharide Lc4, as well as a 50-mer polymannose.

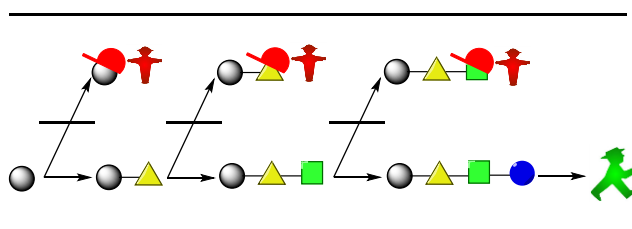


Figure 2-2. Schematic overview of the capping principle used for AGA.

2.2. Results

2.2.1. Pilot synthesizer for capping optimization

For the development of new capping conditions, different solvents and reagents need to be screened. Some of them have never been used in AGA and may potentially contaminate the delivery system of AGA (tubings, syringe pumps, and valves etc.). Therefore, a pilot synthesizer (**Figure 2-3**) was designed and used for capping optimization.

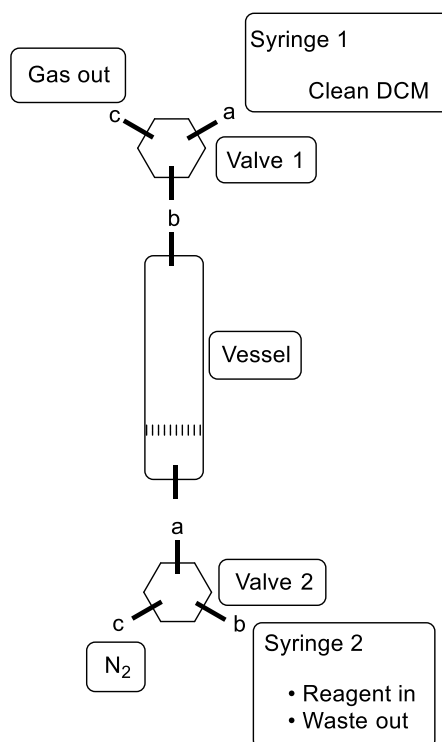
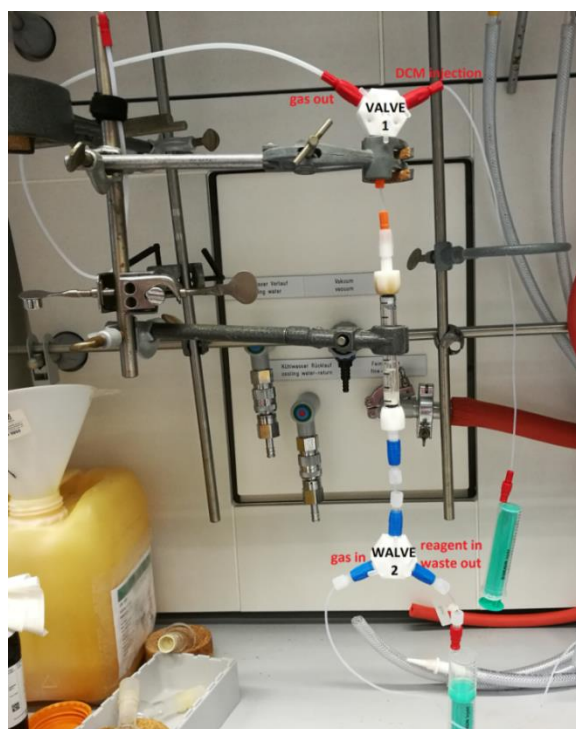


Figure 2-3. Photo and schematic diagram of the pilot synthesizer for capping optimization.

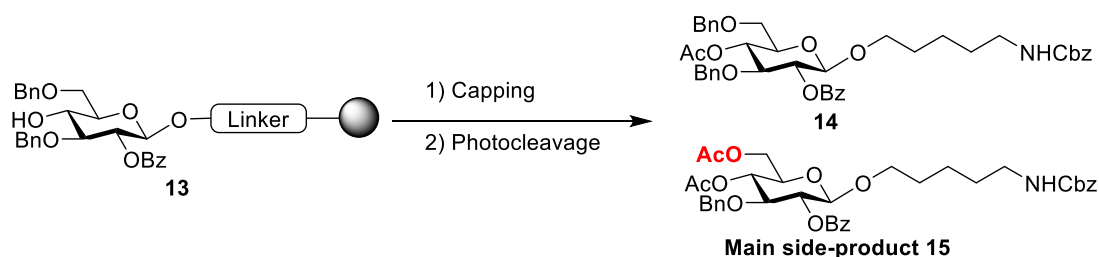
This device consists of a reaction vessel, two valves, and tubings. The reaction vessel is 5 mL in volume and equipped with a filter pad at the bottom. The reaction temperature can be controlled by placing the reaction vessel inside an ice or heating bath.

Valve 1 assures a way out for gas (b → c) or the delivery of fresh DCM from syringe 1 (b → a). Valve 2 enables the connection to compressed N₂ for bubbling (c → a) or to syringe 2 for the injection of capping reagent (b → a) or the removal of waste (a → b). By manual valve-syringe operations, basic functions of the real synthesizer can be replicated with different modules (See in 6.4.1.2).

2.2.2. Optimization of capping condition

Reaction conditions for capping were explored using glycosylated resin **13** (See in 6.4.1.1). Inglis et al. reported a solution-phase acetylation method for alcohols catalyzed by Lewis acid, which only requires 30 seconds for completion.⁷²

Table 2-1. Optimization of the capping conditions.



Entry	Capping conditions ^a	Time (min)	Completion ^b	Formation of 15 ^c
1	0.1% Ac ₂ O, 0.01% TMSOTf	5	Y	N
2	0.1% Ac ₂ O, 0.01% TMSOTf	5 x 6	Y	Y
3	0.1% Ac ₂ O, 0.01% TfOH	5	Y	N
4	0.1% Ac ₂ O, 0.01% TfOH	5 x 6	Y	Y
5	10% Bz ₂ O, 1% TfOH	20	N	N
6	10% Bz ₂ O, 0.1% TfOH	20	N	N
7	10% BzCl in Py	20	N	N
8	10% Ac ₂ O, 1% TFA	20	N	N
9	1% Ac ₂ O, 0.1% MsOH	20	N	N
10	10% Ac ₂ O, 2% MsOH	20	Y ^d	N
11	10% Ac ₂ O, 2% MsOH	20 x 6	Y	N ^d

^aAll reactions were conducted in anhydrous DCM unless otherwise mentioned.

^bMonitored by LC-MS, Y: Capping complete; N: Capping incomplete. ^cMonitored by LC-MS, Y: 6-OBn unstable; N: 6-OBn stable. ^dConfirmed by HPLC (**Method A0**).

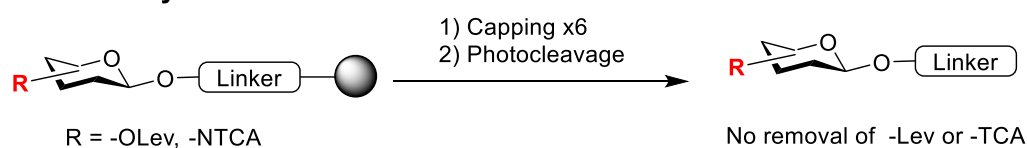
Therefore, acid catalyzed acetylation was selected as capping strategy. After treatment of glycosylated resin **13** with a solution of Ac₂O and different acids in dichloromethane (DCM), the products were cleaved from the solid support and analyzed by LC-MC and/or HPLC (**Table 2-1**).

With a solution of 0.01% TMSOTf and 0.1% Ac₂O in DCM, the acetylation went to completion within five min, but the C6 benzyl ether protecting group was partially cleaved and the resulting hydroxyl group was acetylated to give side-product **15** (**Table 2-1**, entry 1 and 2). This undesired C6-OBn replacement was again observed when trifluoromethanesulfonic acid (TfOH) was used as catalyst (**Table 2-1**, entry 3 and 4). Unsatisfying results were obtained when Ac₂O was replaced by Bz₂O or BzCl. The reaction proved to be much slower, so this option was abandoned. (**Table 2-1**, entry 5, 6, and 7). Milder acids such as trifluoroacetic acid (TFA) failed to give any acetylated product **14** after 20 min (**Table 2-1**, entry 8). Treatment of the resin with a solution of methanesulfonic acid (MsOH) and Ac₂O in DCM, resulted in a partial acetylation of the hydroxyl group (**Table 2-1**, entry 9). A more concentrated solution of methanesulfonic acid (2%) and Ac₂O (10%) resulted in complete acetylation and no cleavage of the C6 benzyl even after six capping cycles (**Table 2-1**, entries 10 and 11).

2.2.3. Stability test of common protecting groups under capping condition

The compatibility of the capping procedure with commonly-used protecting groups was tested. The Fmoc and the levulinoyl (Lev) groups are important temporary protecting groups in AGA, and the trichloroacetyl (TCA) group is often employed to protect amino groups in the synthesis of oligosaccharides containing amino-sugars.

A. Direct stability test



B. Indirect stability test

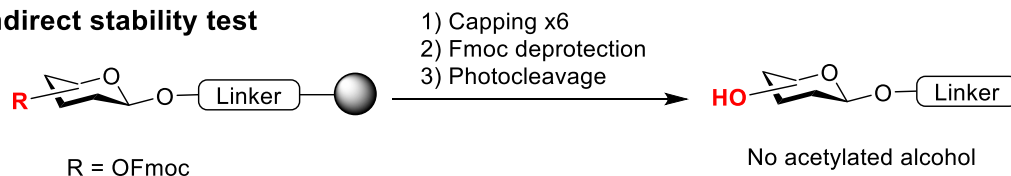


Figure 2-4. Stability test of Lev, TCA, and Fmoc groups.

Glycosylated resins containing these protecting groups (**Figure 2-4**, also see in **6.4.2**) were subjected to six capping cycles and subsequent photocleavage for analysis. No

cleavage or substitution of Lev or TCA group was observed (**Figure 2-4A**). This direct method is not applicable for the Fmoc group that can be partially cleaved during photocleavage. Therefore, an indirect method was adopted, where glycosylated resin containing an Fmoc group was treated with six capping cycles and then subjected to Fmoc deprotection before photocleavage. In the event of Fmoc cleavage during capping, acetylated substrate should be observed. Since no acetylated substrate was observed, Fmoc was proved stable after six capping cycles (**Figure 2-4B**).

2.2.4. Application of capping in oligo- and polysaccharide synthesis

2.2.4.1. Comparative synthesis of 1,6- and 1,4- hexaglucose

The capping procedure was tested for the assembly of various oligosaccharides. AGA syntheses with and without capping were compared to assess the value of a capping step. In order to mimic a particularly bad scenario, the amount of building block used for each coupling was drastically reduced. Since typically ten equivalents of building block are used for AGA, 2.5 equiv./cycle of 1,6-glucose building block **BB-6a** resulted in a moderate yield of the desired hexasaccharide **16a** (14%). The amount of deletion sequences decreased notably when a capping cycle was included (**Figure 2-5**), resulting in a much higher yield for the desired product (30%). The effect of the capping cycle was even more pronounced when 2.5 equiv./cycle of the more sterically hindered 1,4-glucose building block **BB-6b** was used (**Figure 2-5**). Without capping, only trace amounts of the desired hexamer **16b** were observed (1%), while **16b** was obtained as the main product with capping (15%). These comparisons illustrate that capping can render AGA effective even when poor-yielding glycosylations are involved.

Capping blocks the unreacted free hydroxyl groups stopping the deletion sequences from growing. Therefore, less deletion sequences are obtained, leading to easy purification. Secondly, as only the desired sequence participates in the glycosylation without competing hydroxyl groups, no building block donor is “wasted” for the glycosylation of unwanted compounds. These two reasons ensure a better final yield for the desired compound.

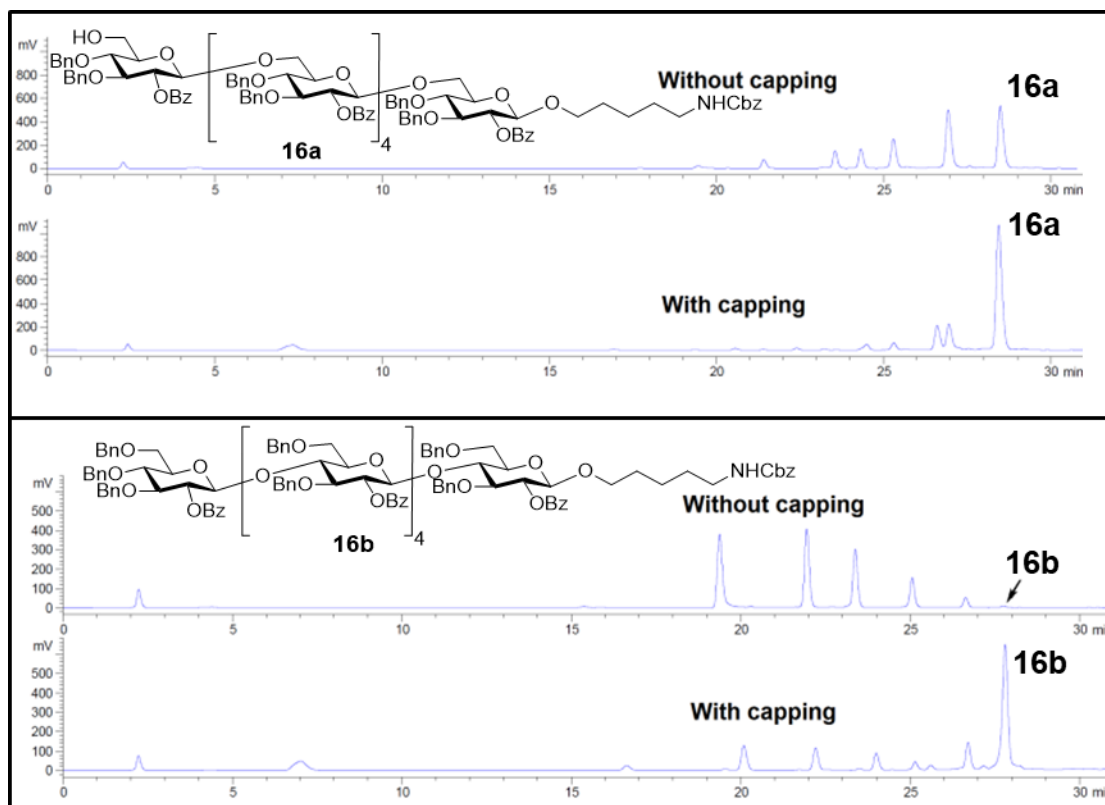
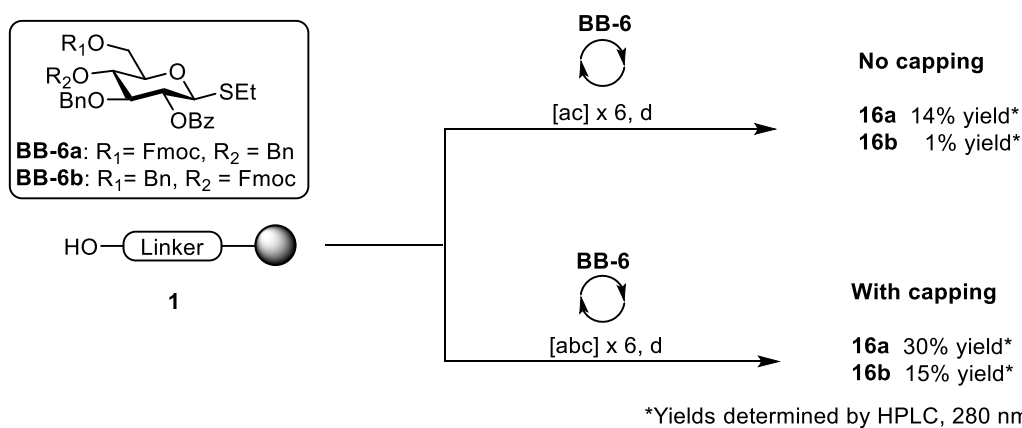


Figure 2-5. Synthesis of 1,6- and 1,4-hexaglycoside 16 with and without capping.

a) Glycosylation conditions: 2.5 equiv. of building block **BB-6**, NIS, TfOH, DCM/dioxane, -20 °C (5 min) → 0 °C (20 min). b) Capping conditions: MsOH (2%) and 10% Ac₂O (10%) in anhydrous DCM, 25 °C for 20 min. c) Fmoc deprotection conditions: piperidine in DMF (20%), 25 °C for 5 min. d) Photocleavage conditions: UV (305 nm, 20 °C). HPLC analysis of the crude products (**Method A0**). ELSD trace is shown in the figure, while the 280 nm channel was used for yield determination (See in **6.5.1.3** and **6.5.2.3**).

2.2.4.2. Implementation of capping for the synthesis of Lc4 and 50mer

Encouraged by the success of the hexasaccharide, AGA including a capping step was tested for the synthesis of the biologically important lactotetraosyl (Lc4) (**Figure 2-6A**). Lc4 is the backbone of the lacto subfamily of glycosphingolipids, which serves various roles in the control of physiological processes including cell growth, motility, and signal transduction.⁷³⁻⁷⁵ Previously, a 41% yield for the AGA of tetrasaccharide **17** using building blocks **BB-7**, **BB-8**, and **BB-9** was reported without capping.⁷⁶ To enhance yields, two cycles of glycosylation were needed for each synthetic step, thus using a total of ten equivalents of building block for each elongation. Using the newly-developed capping cycle, tetrasaccharide Lc4 was obtained in 67% yield even though only one cycle of 6.5 equiv. of building block was used for each glycosylation step. The HPLC of the crude product (**Figure 2-6A**) showed high purity which permitted easy purification.

The novel AGA procedure was tested for the synthesis of a 50-mer oligomannoside (**Figure 2-6B**). Our recent synthesis of this oligosaccharide yielded 50-mer polymannoside **6** in just 5% yield, using a basic capping method.⁴⁸ This synthesis of the longest synthetic oligosaccharide directly assembled from monosaccharide building blocks required ten days for completion (without capping: 2 hours/cycle; with capping: 4 hours/cycle). Using the new capping method and optimized synthesis parameters, the coupling cycle for the incorporation of each building block was shortened to 90 minutes, such that the 50-mer was obtained within four days and in drastically improved yield (22%) using building block **BB-5**. In addition to the 50-mer, the 49-mer in both uncapped (**18**) and capped (**19**) form were synthesized to serve as controls in assessing the resolution power of the HPLC in the separation of longer polysaccharides. Uncapped 50-mer **6**, that represents the desired final product of AGA, and the potential deletion sequence, the uncapped 49-mer **18**, are eluted with virtually the same retention time. In contrast, capped 49-mer **19** is eluted more than one minute earlier than the desired compound and can be readily separated from the final product. This finding demonstrates that capping not only improves the yield, but also generates more readily separable side-products, even when polysaccharides are prepared.

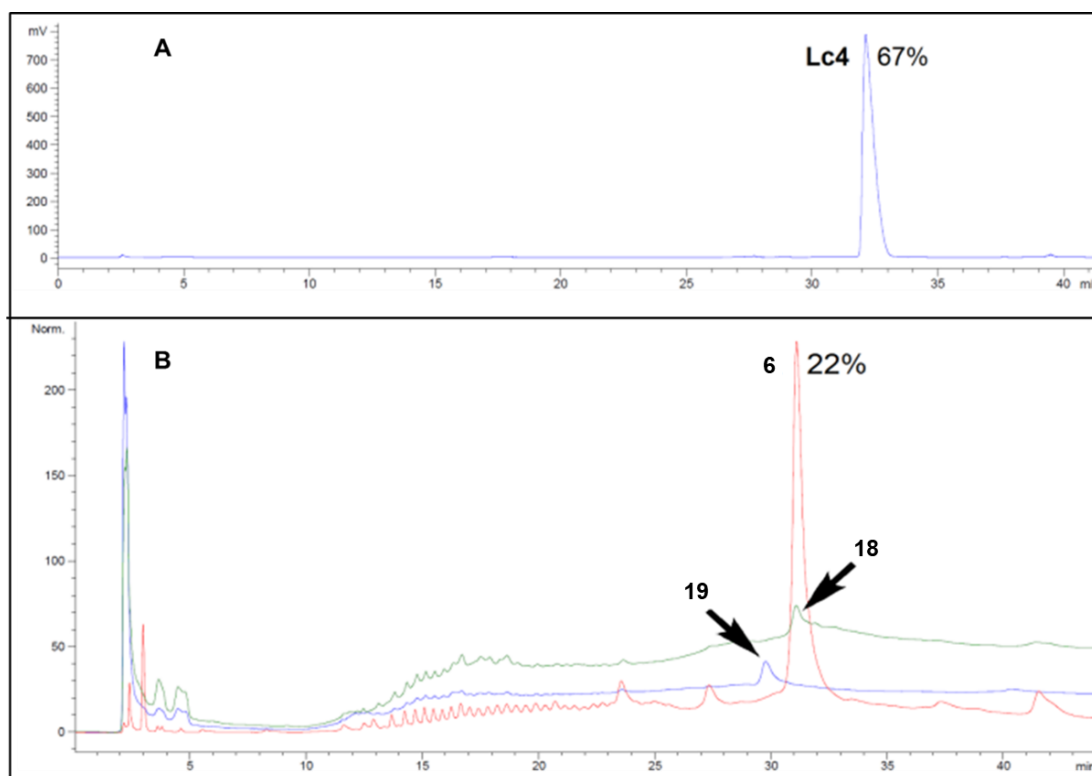
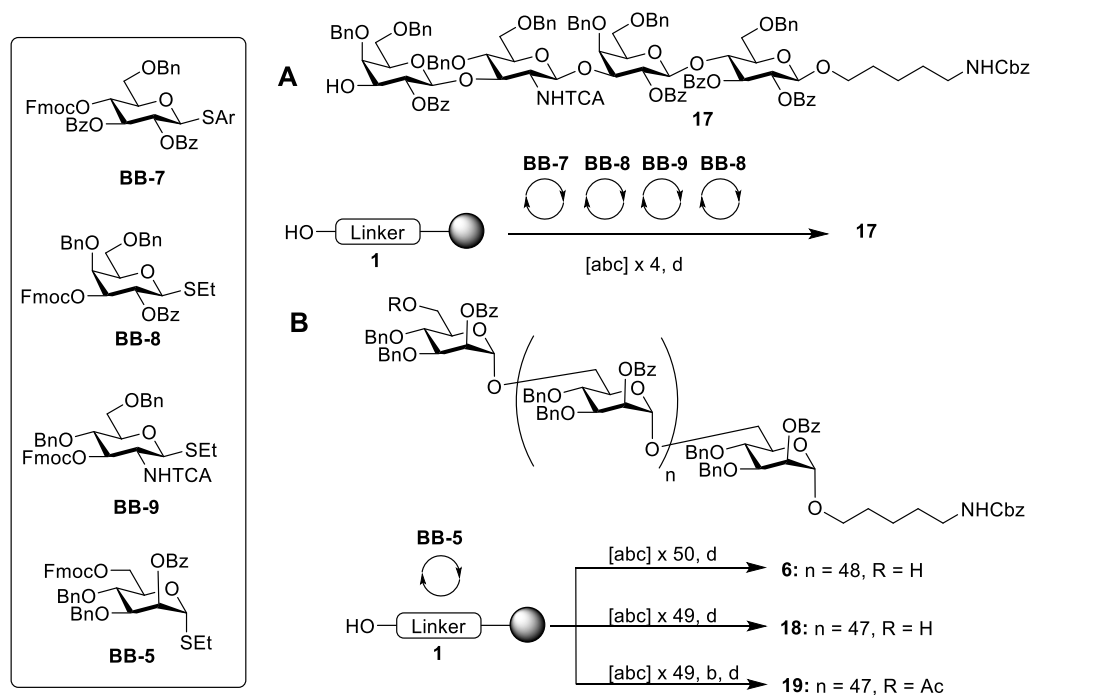


Figure 2-6. Implementation of capping to the synthesis of tetrasaccharide Lc4 (A) and a 50-mer (B) oligomannose. a) Glycosylation conditions: building block (2.5 equiv), NIS, TfOH, DCM/dioxane, $-20\text{ }^{\circ}\text{C}$ (5 min) \rightarrow $0\text{ }^{\circ}\text{C}$ (20 min). b) Capping conditions: MsOH (2%) and Ac₂O (10%) in anhydrous DCM, $25\text{ }^{\circ}\text{C}$ for 20 min. c) Fmoc deprotection conditions: piperidine in DMF (20%), $25\text{ }^{\circ}\text{C}$ for 5 min. d) Photocleavage

conditions: UV (305 nm, 20 °C). HPLC analysis of the crude products is shown (**Lc4**: 280 nm, **Method A0**; **6**: ELSD trace, **Method A50**).

2.3. Conclusion

In conclusion, the incorporation of a 20 minute capping step into the coupling cycle mildly and efficiently blocks the unreacted hydroxyl groups after each glycosylation. The efficiency of AGA was significantly improved as illustrated by the comparison of syntheses with and without capping. Overall yields improved by decreasing the formation of side-products while lowering the amount of building block used by 33%. The purification of the desired product was greatly facilitated as demonstrated in the synthesis of a 50-mer. The capping procedure described here is now incorporated in all AGA syntheses since it improves yields and decrease building block consumption during oligosaccharide assembly.

3. Systematic hydrogen bond manipulations to establish polysaccharide structure-property correlations

This chapter has been modified in part from the following article:

Y. Yu,* T. Tyrikos-Ergas,* Y. Zhu, G. Fittolani, V. Bordoni, A. Singhal, R. J. Fair, A. Grafmüller, P. H. Seeberger, M. Delbianco, Systematic Hydrogen Bond Manipulations to Establish Polysaccharide Structure-Property Correlations. *Angew. Chem. Int. Ed.* **2019**, 131, 13261. <https://doi.org/10.1002/anie.201906577>

* equal contribution.

3.1. Introduction

The new capping method described in Chapter 2 improves the efficiency of AGA, allowing for quick access to pure and well-defined polysaccharides for the study of polysaccharides structure and property. Cellulose is the most abundant polysaccharide on earth and, because of its well-studied supramolecular organization, was selected as model system. The stability, crystallinity, and poor water solubility of cellulose are the result of a dense network of inter- and intramolecular hydrogen bonds that create allomorphs with different properties (See in 1.1.1.1).⁷⁷⁻⁷⁸ In particular, the hydrogen bond between the OH(3) and the O(5) of the ring stabilizes the cellobiose repeating unit, with additional stabilization gained from intra- and intermolecular interactions (chain stacking) involving OH(6), OH(3), and OH(2) (**Figure 3-1**).^{9, 79-80}

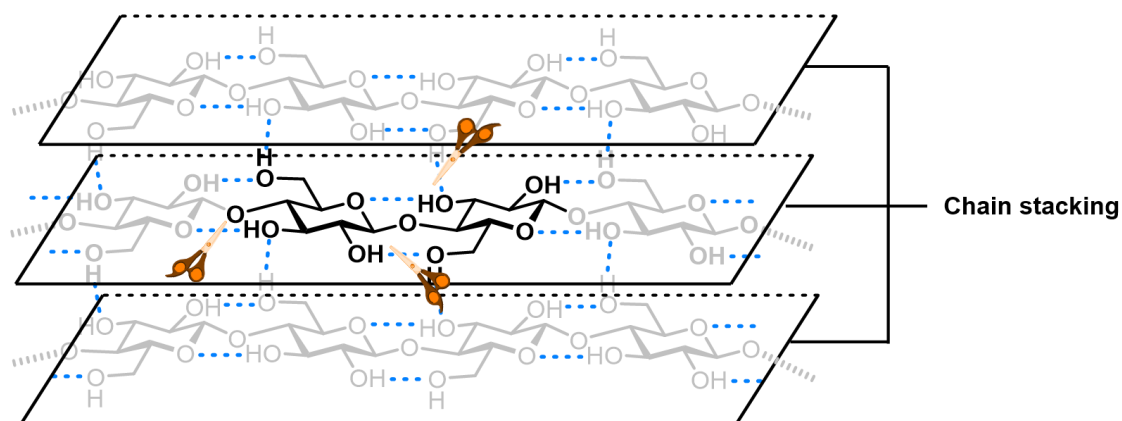


Figure 3-1. Cellulose hydrogen bond network with cellobiose repeating unit highlighted. Chemical modification (symbolized by scissors) can be used to manipulate the hydrogen bond network.

Chemical modifications are commonly used to block cellulose H-bonds and alter the organization of cellulose, creating new materials with enhanced water solubility or ionic character (See in 1.1.1.1).^{21, 81-83} Non-regioselective derivatization results in polydisperse materials with respect to length and modification patterns that do not allow for proper structure-function correlations. The lack of standards and experimental data also hampered *in silico* modelling. Molecular dynamics (MD) simulations capture some structural changes,⁸⁴⁻⁸⁷ but a detailed structural description is often lacking due to carbohydrate flexibility.

Carbohydrate Materials

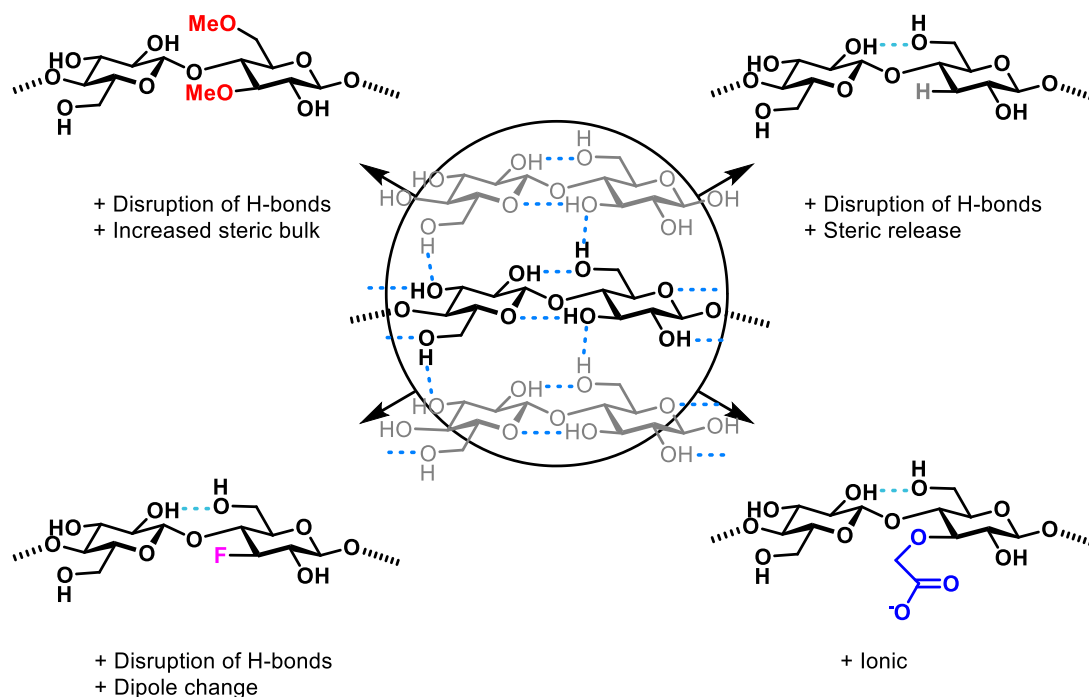


Figure 3-2. Systematic approach to study structure-property correlations in carbohydrate materials.

This project was a cooperative effort of several scientists (**Table 3-1**), in this chapter the major focus will be given to my contribution. Tailor-made cellulose derivatives were designed to selectively disrupt H-bond networks and/or alter the electronic properties in order to establish structure-property correlations (**Figure 3-2**). Methylated, carboxymethylated, deoxygenated, and deoxyfluorinated cellulose, as well as chitin analogues, are prepared with full control over the length, pattern and degree of substitution. MD simulations guided the synthesis, by correlating the disruption of the H-bond network with the increased flexibility of the modified oligosaccharides.

Table 3-1. Contribution table.

Contribution	Name
Synthesis of methylated cellulose, solubility test, XRD measurements	Yang Yu
MD simulations	Theodore Tyrikos-Ergas
Synthesis of deoxygenated and carboxymethyl cellulose	Dr. Yuntao Zhu

3.2. Results

3.2.1. Synthesis of modified cellulose

3.2.1.1. Synthesis of linker-free oligosaccharides

To mimic natural cellulose, glycans with the free reducing end are required. The standard functionalized solid support for AGA **1** (**Figure 3-3**) liberates the glycan bearing an alkylamino linker for further conjugation to proteins or surfaces. For this particular project, this unnatural “tail” is undesirable since it could interfere with the structural analysis (**Figure 3-3A**). Therefore, the UV-labile linker **2** (**Figure 3-3**) was designed to release the free reducing end upon photocleavage.⁸⁸ To our surprise, the ensuing methanolysis of the ester protecting groups in strong basic condition (NaOMe) results in glycan decomposition (peeling) and a mixture of shorter oligosaccharides (penta-, tetra-, and trisaccharides) was obtained (**Figure 3-3B**). This peeling reaction is not observed when the reducing end is protected with a linker (**Figure 3-3A**), indicating that the free reducing end is base-labile and responsible for the glycan peeling.

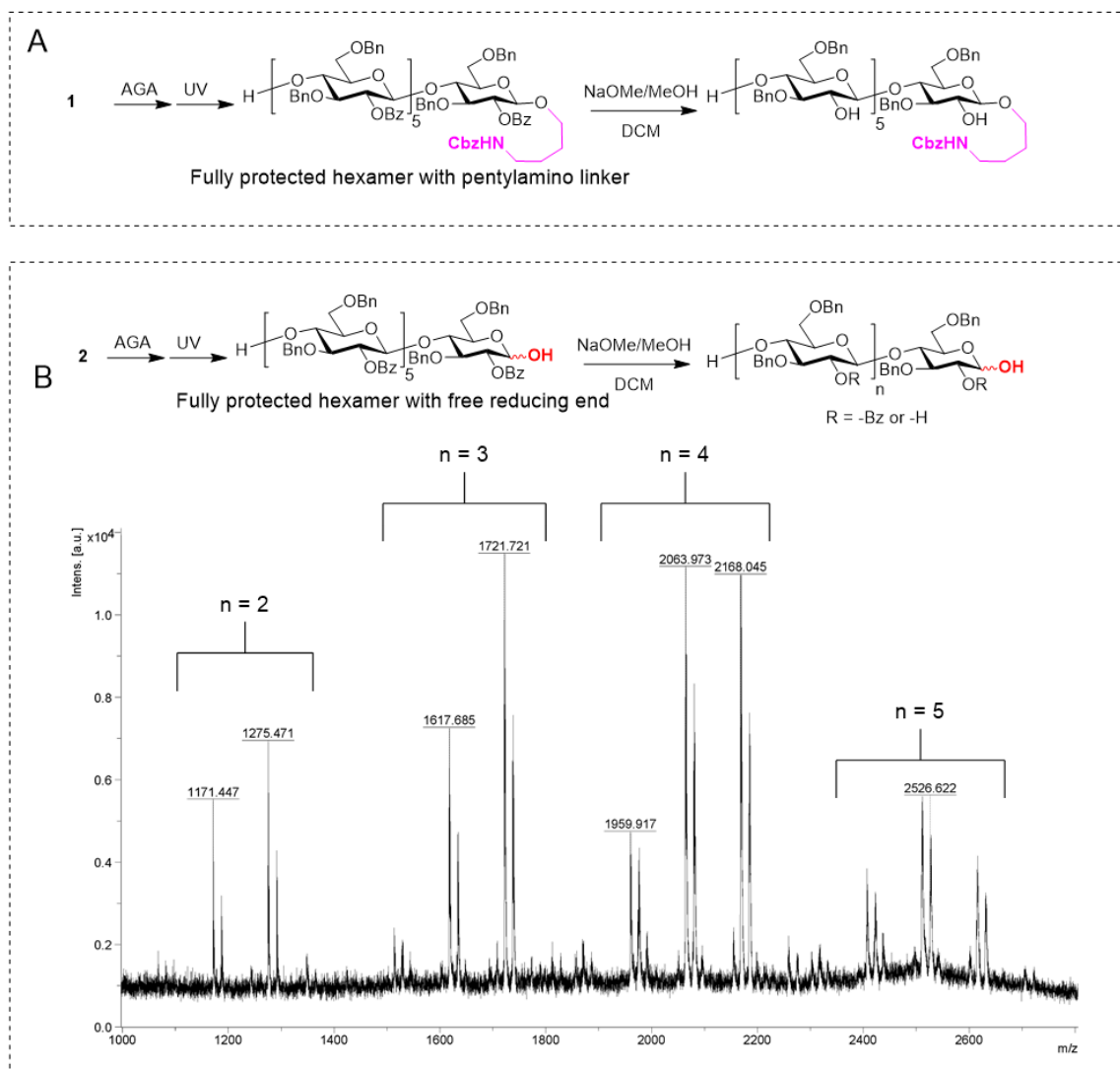
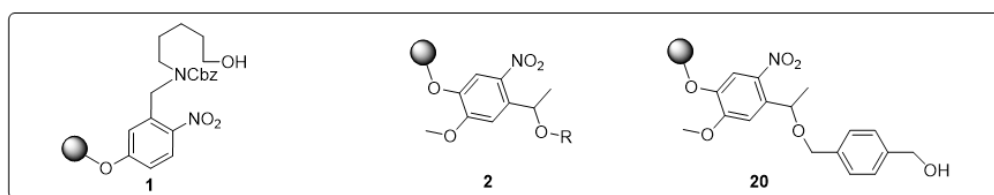


Figure 3-3. Linkers and deprotection process. (A) AGA with resin **1** affords the pentylamino linker functionalized glycan. (B) Peeling of hexasaccharide with free reducing end is observed in basic condition.

To avoid glycan decomposition, one option is to perform methanolysis on solid support (resin **21**, **Figure 3-4**) so that the hydroxyl group at the reducing end is protected with the linker. Upon complete hydrolysis of ester protecting groups, glycan **23** can be released from the solid support (resin **22**).

Standard solution-phase methanolysis conditions (1:10 mixture of NaOMe solution (0.5 M in MeOH) and DCM for 24 hours⁴⁹) were not applicable due to the extremely low reaction rate of solid-phase methanolysis (**Figure 3-4**). Increasing the concentration of the NaOMe solution did not accelerate the reaction, presumably due to the low swelling volume of polystyrene in MeOH (1.6 mL/g). The high swelling volume of polystyrene resin in THF (7.5 mL/g) suggested the use of such a solvent. Treatment of the glycosylated resin with a 1:10 mixture of NaOMe solution (0.5 M in MeOH) and THF resulted in complete ester hydrolysis, within four hours. After photocleavage, the partially deprotected oligosaccharide **23** with free reducing end is subjected to hydrogenolysis to afford the linker-free oligosaccharides. Due to the solid phase nature of this approach, the base catalyst is easily removed by filtration and also resulted in faster hydrogenolysis. This solid phase methanolysis (**Module F**, see in **6.2.3**) was adopted for the synthesis of most cellulose analogues in this thesis. This procedure is also applicable to other types of solid supports (i.e. resin **1**).

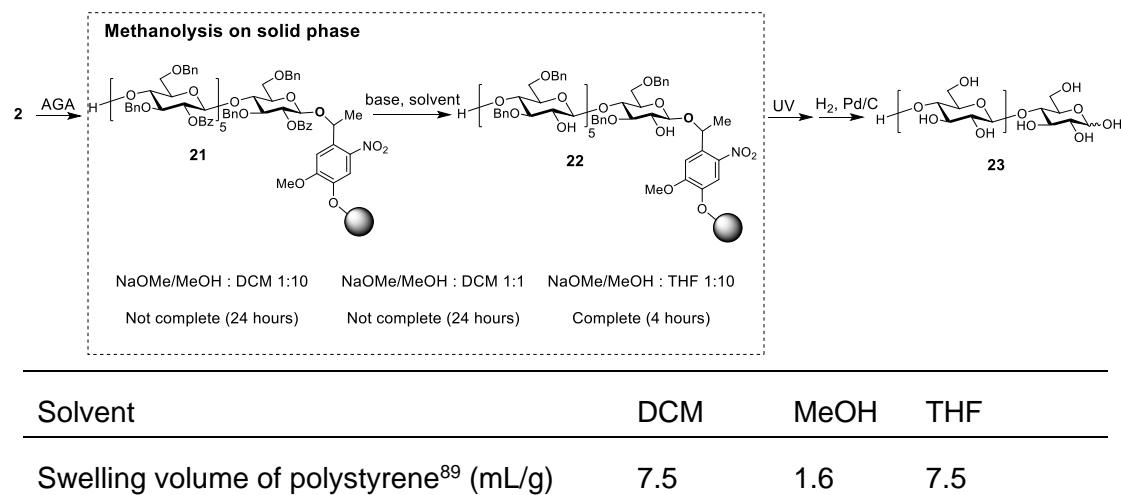


Figure 3-4. Optimization of methanolysis conditions and swelling volume of polystyrene in DCM, MeOH, and THF.

Alternatively, linker **20** (**Figure 3-3**, developed by Dr. Yuntao Zhu⁸⁸) liberates the desired glycan protected with a 4-hydroxymethyl-benzyl group at the reducing end, allowing for solution-phase methanolysis, and subsequent cleavage, during hydrogenolysis.

To monitor the methanolysis on solid phase, a micro-cleavage method was developed (**Figure 3-5A**, see in **6.2.3**). Approximately 20 beads of resin are taken from the reaction and irradiated by UV light (366 nm) for ten minutes. The cleaved compounds are analyzed by MALDI, which proved to give identical signals with UV-cleavage with

full batch (**Figure 3-5B**). This method is now a common strategy to monitor the reaction status not only during methanolysis, but also during AGA.

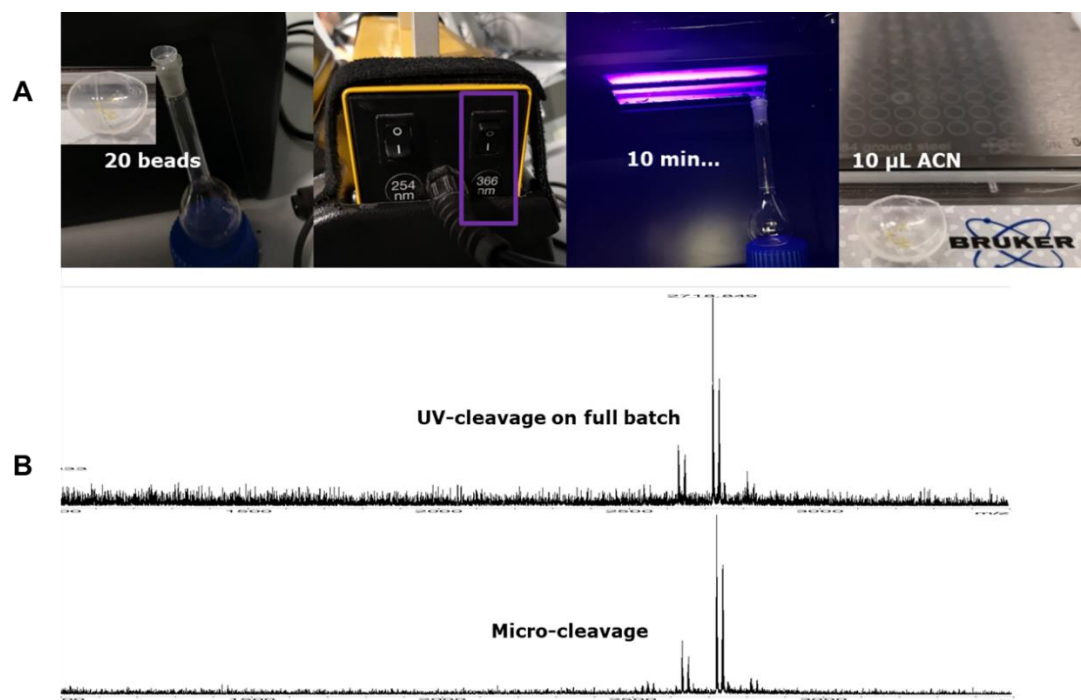


Figure 3-5. Micro-cleavage for monitoring solid phase reaction. (A) Experimental set-ups of micro-cleavage. **(B)** Comparison of MALDI signals from the same batch of AGA synthesis by full batch UV-cleavage (up) and micro-cleavage (down).

3.2.1.2. Synthesis of modified cellulose

A collection of well-defined cellulose derivatives was prepared using AGA (**Figure 3-6, Table 3-1**). Two natural cellulose oligomers (hexamer A_6 and dodecamer A_{12}) and one chitin analogue (N_6) served as standards for the structural analysis. Unnatural analogues with defined substitution patterns were prepared to tune the conformation and properties of the material. Regioselective functionalization was achieved with five “unnatural” monosaccharide building blocks **BB-11 - BB-15** (**Figure 3-6**). Global deprotection afforded oligosaccharide derivatives with complete control over the length, pattern, and degree of functionalization. This thesis emphasizes the synthesis of methylated analogues.

Methylation effectively alters the solubility and gelation properties of cellulose by influencing intra- and intermolecular hydrogen bonding. The resulting methylcellulose is widely used in the food and pharmaceutical industries (See in 1.1.1.). Six hexa- and four dodecamers, with different methylation patterns, were synthesized using **BB-11** and **BB-12**, that contain 3-methyl and 3,6-dimethyl motifs (**Figure 3-6**). The position of the substituents was chosen to selectively disrupt H-bonds that play a fundamental

role in cellulose rigidity. Methylation of OH(3) impedes the H-bond between O(5) and OH(3), while 6-methylation hinders the inter- and intra-chain stabilization offered by OH(6). Structures with a regular methylation pattern (e.g. **(AB)₃**), di-block analogues (e.g. **A₃B₃**), as well as irregularly functionalized structures (e.g. **(ABA)₂**) were assembled to assess the effect of methylation patterns on the overall cellulose conformation. Similar considerations were followed for the synthesis of 3-deoxyfluorinated and 3-deoxygenated cellulose analogues (**Figure 3-6, Table 3-1**). Such modifications, in addition to selectively disrupting H-bonds, are expected to modulate the steric hindrance and dipole orientation within the sugar unit. Additionally, carboxymethylation is introduced to assess the effect of charges on the overall structure.

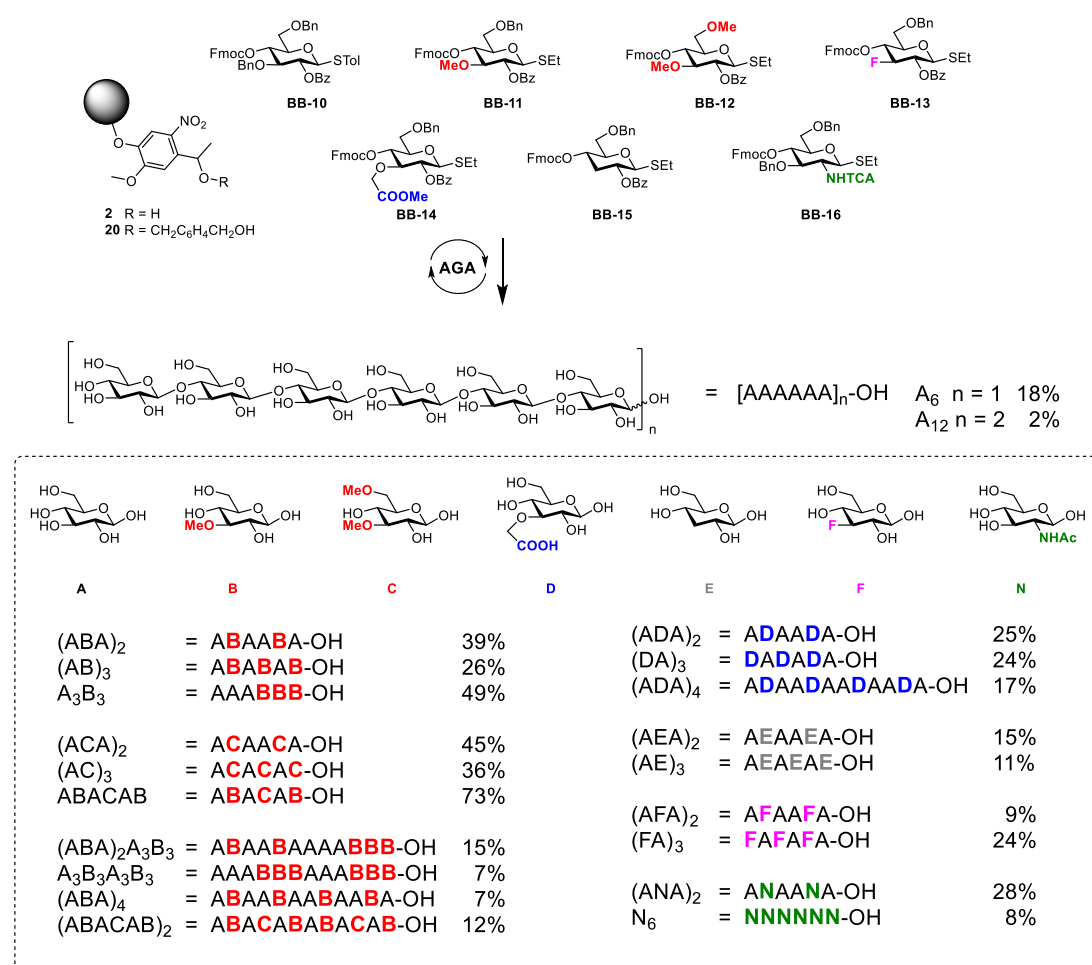


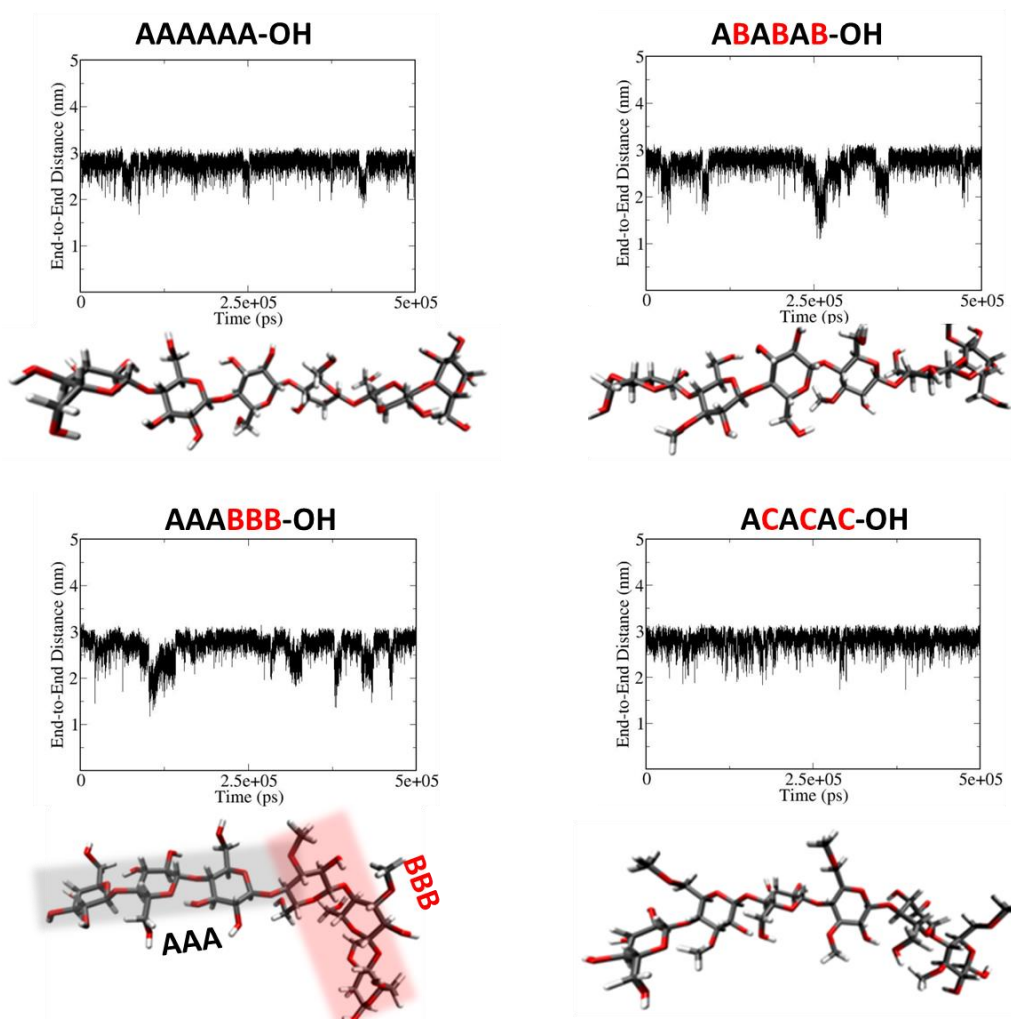
Figure 3-6. AGA synthesis and nomenclature of tailor-made cellulose oligosaccharides.

The synthesis of **A₆** was low yielding (18%) due to the low solubility of the oligosaccharide product. Methylation drastically improved product solubility, that is reflected in much better yields for the unnatural hexasaccharide analogues (24%-72%

overall yield). Similar results were observed for the 12-mer syntheses (**Figure 3-6**), that benefitted from the insertion of **BB-11**, **BB-12** and **BB-14** with drastically better yields than for **A₁₂** (2% overall yield).

3.2.2. Conformations of cellulose analogues

The perturbation of the 3D-shape of oligosaccharides as a result of single-site substitutions was modelled using MD simulations, employing a modified version of the GLYCAM06 carbohydrate force field (performed by Theodore Tyrikos-Ergas).⁹⁰⁻⁹¹



Hexamer	AAAAAA-OH	ABABAB-OH	AAABBB-OH	ACACAC-OH
Average distance (nm)	2.76	2.71	2.65	2.80
Standard deviation	0.17	0.25	0.26	0.17

Figure 3-7. End-to-end distances as a function of MD time, representative conformations as obtained by MD simulations, and average end-to-end distance (displayed as a table).

Cellulose **A₆** revealed a fairly rigid backbone core with low conformational variability (average end-to-end distance 2.76 ± 0.17 nm for **A₆**) (**Figure 3-7**). The structure tends to adopt an extended helical conformation. Large fluctuations are observed for methylated analogues, indicating that these molecules are more flexible. Deoxyfluorination, carboxymethylation and deoxygenation also result in more flexible systems (See in **6.6.3** and publication⁹²).

To examine how specific modifications affect such organized structures, two methylated analogues were studied. A regular alternated substitution pattern, as in the case of **(AB)₃**, revealed an increased distance between OMe(3) and O(5) due to the decreased tendency to form hydrogen bonds and the increased steric bulk. The same degree of methylation but with a di-block distribution, as in the case of **A₃B₃**, resulted in dramatic changes. A significantly more flexible bent shape (**Figure 3-7**) with an end-to-end distance of 2.65 ± 0.26 nm was observed for most of the simulation time. Surprisingly, the OH(3)···O(5) hydrogen bond between the first two glucose monomers was detected for most of the simulation time, suggesting the coexistence of a rigid rod block (**A₃**, marked in gray in **Figure 3-7**) and a very flexible counterpart (**B₃**, marked in red in **Figure 3-7**). Methylation at the 3 and 6 positions (**C**), disrupts the “standard” dihedral values, resulting in a completely new geometry. A similar trend was observed for the dodecamers, with more regular modification patterns exhibiting a higher cellulose character as compared to randomly methylated structures (See in **6.6.3** and publication⁹²).

3.2.3. Aggregation, solubility, and crystallinity study of modified cellulose

Oligosaccharide behavior in a crowded environment was studied and correlated to the material crystallinity and solubility. Long MD simulations (1 μ s production run, by Theodore Tyrikos-Ergas) of concentrated experiments (**Figure 3-8A**) aimed to elucidate molecular interactions. Radial distribution functions (RDFs) (**Figure 3-8B**) were used to characterize the spatial correlations in the systems. The RDF for **A₆** shows three sharp signals at small distances and remains large for distances up to 1.5 nm, indicating high aggregation tendencies of such oligosaccharides. The more soluble methylated analogue **(AB)₃** shows some tendency to aggregate at high concentrations. However, a significantly decreased signal at 0.5 nm indicates the lower probability to find two chains in very close proximity, as compared to cellulose oligomers. RDF peaks are only found at shorter distances, revealing a lower tendency

for cluster formation and a less organized structure, with a homogeneous distribution of molecules beyond the nearest neighbors. No aggregation was detected for A_3B_3 , as expected from the high flexibility of such compound that should prevent chain-stacking.

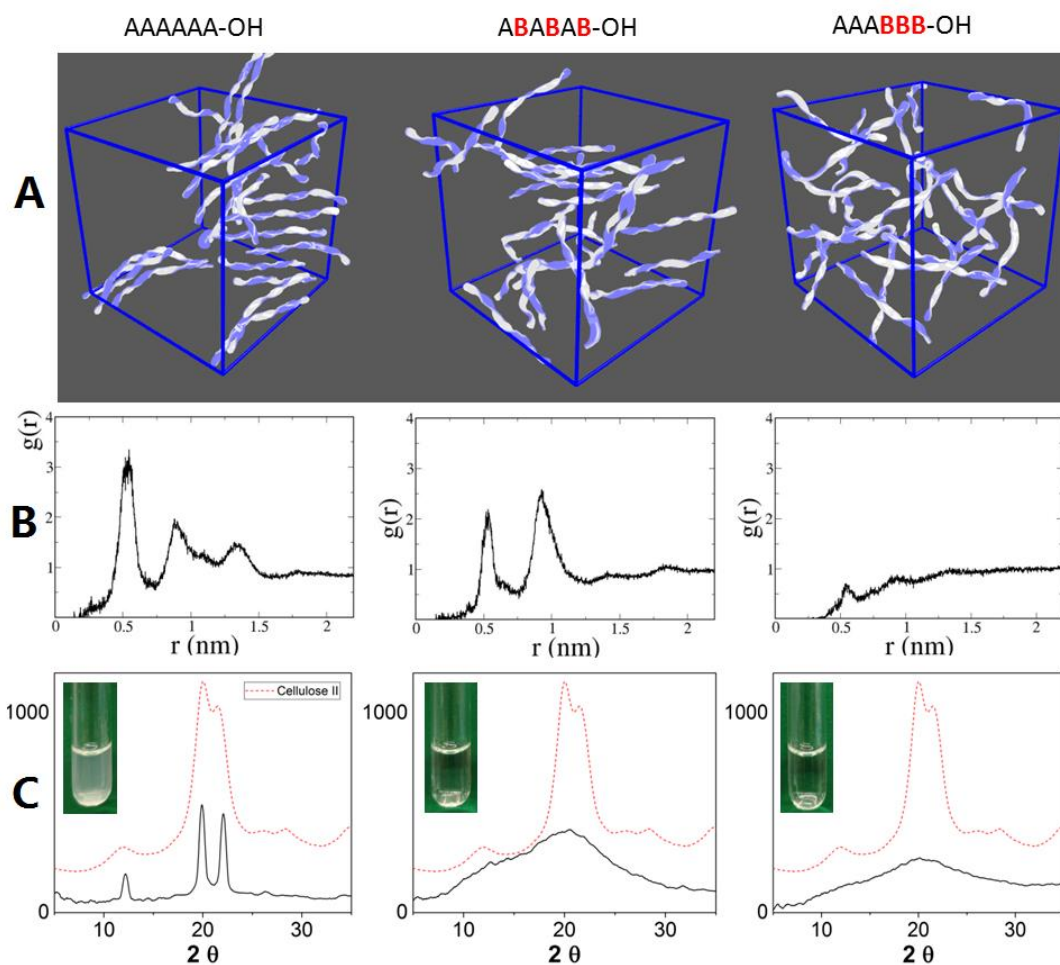


Figure 3-8. Representative snapshots of MD simulations of concentrated solutions (A), RDFs (B), XRD (C), and solubility test (inset).

X-ray diffraction (**Figure 3-8C**, **Figure 3-9** and **6.6.2**) and solubility data (See in **6.6.1**) support the calculations. As anticipated, A_6 and A_{12} are very poorly soluble in water (less than 1 mg/mL), due to the formation of cellulose-like aggregates. Powder XRD measurements of both A_6 and A_{12} gave sharp peaks (**Figure 3-8C** and **Figure 3-9**), that are distinctive for cellulose II, indicating that short oligomers adopt the same aggregation pattern and the same H-bonding arrangement of cellulose. The flat XRD profile of the di-block analogue A_3B_3 indicates the absence of any ordered structural organization, as predicted by the theoretical model (**Figure 3-8**). The alternating methylation pattern of $(AB)_3$, renders the material more sensitive to the X-ray beam angle and, while the XRD peaks are still broad, they resemble the cellulose II structure, as predicted by MD simulations (**Figure 3-8**). This trend is confirmed by the longer

oligomers, where more intense, yet broad, XRD profiles are observed for the regularly substituted analogues (**Figure 3-9**). No cellulose-like character is detected for randomly functionalized structures. Similarly to cellulose, the XRD profile of chitin analogue **N₆** is identical to that of natural chitin (**Figure 3-9**), as it is poorly soluble (13-17 mg/mL) and tends to form gels at higher concentrations. Surprisingly, the hybrid cellulose-chitin (ANA)₂, is much better soluble (> 50 mg/mL) with no ordered supramolecular structure (**Figure 3-9**). All functionalized cellulose analogues are, in contrast to the natural derivatives, highly water soluble (> 50 mg/mL) and form amorphous solids (**Figure 3-9**). Interestingly, while remaining highly water soluble, the deoxy series (**E**) adopts a cellulose-like character in the solid state with two broad, yet noticeable, peaks in the XRD profile (**Figure 3-9**).

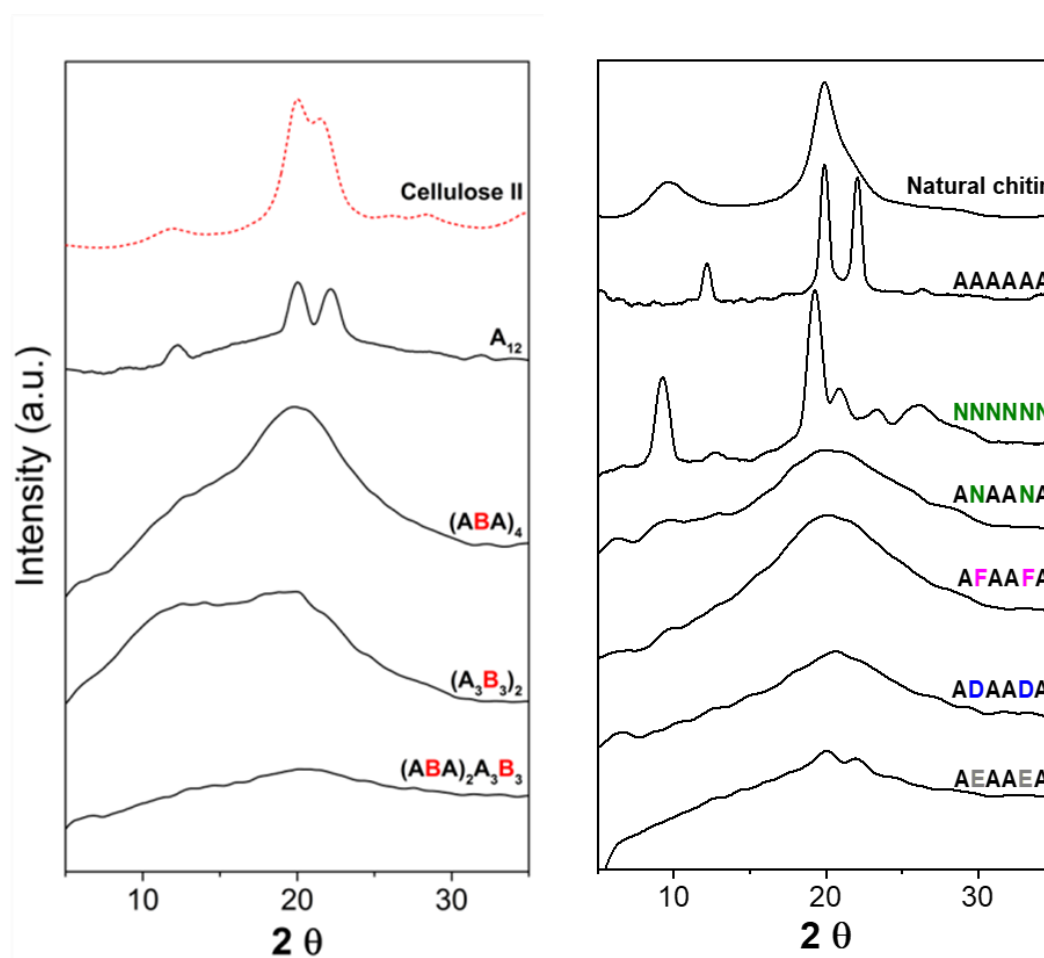


Figure 3-9. Powder XRD analysis of natural oligosaccharides (**A₆**, **A₁₂**, and **N₆**) and selected modified analogues.

3.3. Conclusion

Tailor-made cellulose oligosaccharide analogues, prepared by sequential addition of monomeric BBs using AGA, allow for control over the length and substitution patterns.

Seven BBs bearing unnatural modifications were used to disrupt specific H-bonds and tune the three dimensional shape and properties of the material. Methylation blocked the hydrogen bond between OH(3) and O(5), resulting in an increased flexibility of the chain, as observed by the fluctuation of the end-to-end distance during MD simulations time. Compounds with the same degree of methylation, but different substitution patterns, behave drastically different. Regular substitution patterns result in quasi-linear structures, whereas more bent geometries are observed with a block arrangement. These structural features control the aggregation process that is expressed in high crystallinity for the natural compound and amorphous organization for irregular or block substituted analogues. A more significant disruption of the “standard” dihedral values was observed with methylation at the OH(3) and OH(6) positions. All unnatural analogues are drastically more soluble, due to the more flexible backbone. Novel bio-materials with tuned properties that could be engineered depending on nature and pattern of the substituents can be envisioned. The collection of unnatural compounds will be available to evaluate enzymatic degradation and substrate specificity.

4. Oligosaccharides self-assemble and show intrinsic optical properties

This chapter has been modified in part from the following article:

Y. Yu,* S. Gim,* D. Kim, Z. A. Arnon, E. Gazit, P. H. Seeberger, M. Delbianco, Oligosaccharides Self-Assemble and Show Intrinsic Optical Properties. *J. Am. Chem. Soc.* **2019**, 141, 4833. <https://doi.org/10.1021/jacs.8b11882>

* equal contribution.

4.1. Introduction

Simple peptides^{57, 93-95} and DNA⁹⁶⁻⁹⁸ can spontaneously self-assemble to form defined supramolecular patterns. These supramolecular architectures are the essence of modern bionanotechnology, with implications in the medical⁹⁹⁻¹⁰¹ and energy^{67, 95, 102} fields. The main limitation to the use of these systems is often associated with the modest quantities that can be produced. Polysaccharides are much more abundant, biocompatible, and cheap, but have found much less applications in nanotechnology. This is surprisingly if we consider that some polysaccharides (e.g. cellulose and chitin) can generate highly ordered hierarchical structures, tunable by chemical modifications (see in Chapter 3). To date, natural polysaccharides have found applications in drug delivery¹⁰³ and tissue engineering¹⁰⁴. Still, the use of polysaccharide materials is limited. The extraction, purification and analysis of natural polysaccharides is hindered by the low solubility. Besides, the polydispersity of chain length and modifications results in poor quality control and reproducibility of polysaccharide-based materials.

Chemical synthesis provides an attractive alternative to the modification of natural polysaccharides. Collections of related compounds can be created to study the aggregation tendency of carbohydrate materials. In addition, it was recently shown that, like peptides and DNA, some oligosaccharides can adopt defined conformations in solution.⁴⁹ As peptide and DNA nanotechnologies are heavily based on defined secondary structures, we hypothesized that such conformations could be used for the formation of supramolecular assemblies.

The inspiration came from the problematic deprotection of hexasaccharide **28 (Figure 4-1A)**.⁴⁹ This semi-protected hexasaccharide proved so poorly soluble in most solvents that further chemical manipulations are impossible. A similar compound that carries fewer benzyl ethers (i.e. hexamer **29, Figure 4-2**) showed fewer solubility and reactivity issues. These differences likely are a consequence of the formation of supramolecular

structures due to strong intermolecular interactions, such as hydrogen bonding, together with π - π interactions of the benzyl ether modifications.

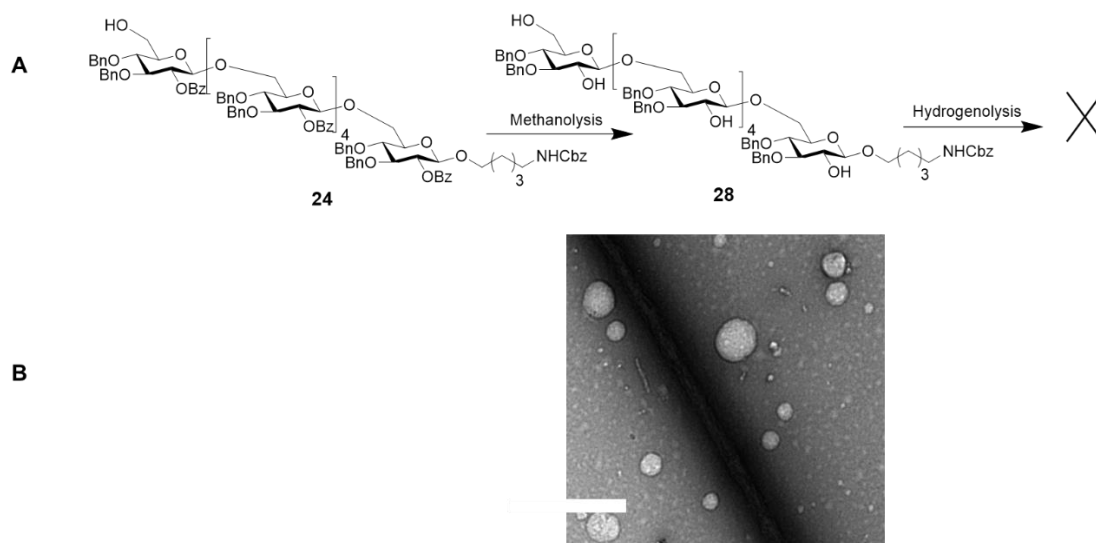


Figure 4-1. Insoluble compound 28 leads to synthetic difficulty (A) and forms nanoparticles upon sonication in water (B, scale bar: 1 μ m). A suspension of compound 28 in water was sonicated for 30 minutes. TEM sample was stained with uranyl acetate (negative staining)

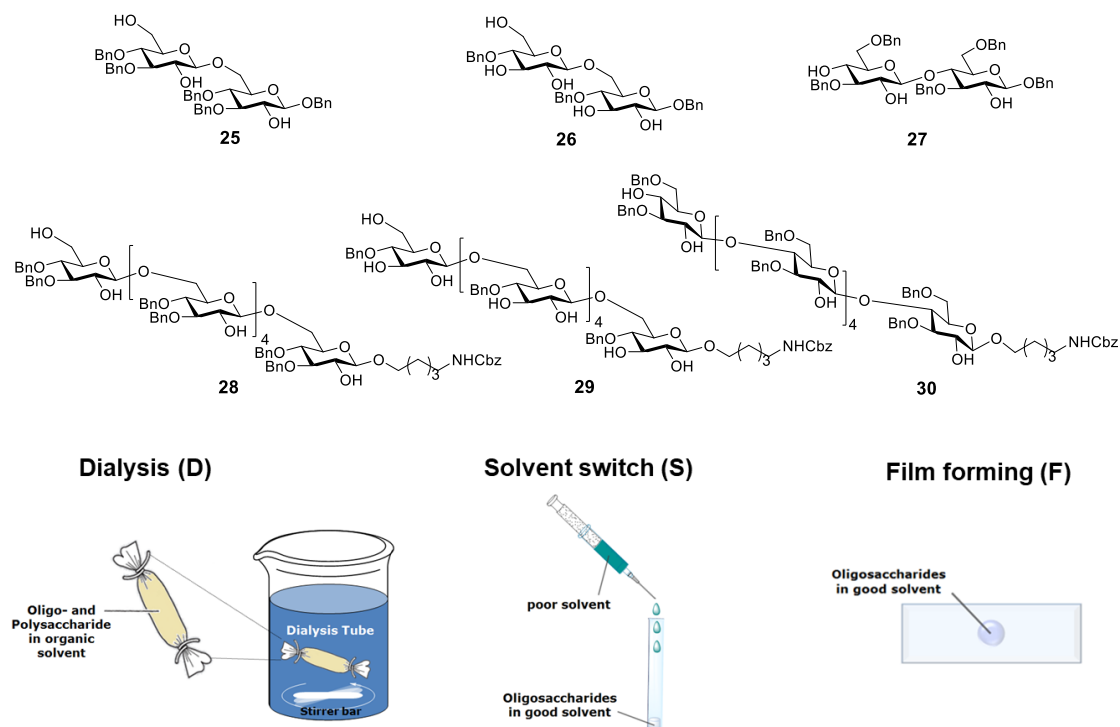


Figure 4-2. Synthetic carbohydrates for self-assembly study.

In this chapter, the systematic study of the self-assembly of synthetic carbohydrates is presented. Three hexasaccharides (**28-30**) as well as three disaccharides (**25-27**) (**Figure 4-2**) were prepared to probe the influence of chain length, linkage, and modification on morphology and property of self-assembled carbohydrate materials. This project was carried out in collaboration with Soeun Gim.

4.2. Results

In preliminary test, we suspended compound **28** in water followed by sufficient sonication. TEM observations (**Figure 4-1B**) suggested the formation of spherical aggregates in water, which motivated us to systematically study the self-assembly behavior of carbohydrates. Due to the lack of literature on oligosaccharides self-assembly, we followed self-assembly methods reported for other biomolecules (i.e. peptides, DNAs, PNAs). Based on the solubility of oligosaccharides **25-30**, we explored dialysis (**D**), solvent-switch (**S**) and film forming (**F**) methods (**Figure 4-2**). Within each method, several parameters can be modulated (e.g. solvent, concentration) to trigger different self-assembling behavior. Beside microscopic observations, photophysical characterization was also conducted to study the property of the self-assembled samples.

4.2.1. Self-assembly

4.2.1.1. Nomenclature for the self-assembled samples

The names of the self-assembled samples indicate the sugar oligomer (e.g. **26**) and the assembly method (**D**, **S**, or **F**). In solvent-switch and film forming methods, different solvents (i.e. hexafluoroisopropanol (HFIP), dimethylacetamide (DMAc), acetone (Ace), and isopropanol (*i*PrOH)) were screened. Therefore, the solvent name is appended for those samples. For example, **26-S-HFIP** means compound **26** prepared by solvent-switch method with HFIP as good solvent. Detailed conditions for the formation of each sample are given in **6.7.1**.

4.2.1.2. Dialysis method

The oligosaccharide was dissolved in a dimethylacetamide (DMAc)/water mixture and dialyzed against water. TEM measurements revealed nanoparticles with diameters of 40-60 nm for all the samples (**Figure 4-3**). These particles exist in solution as confirmed by dynamic light scattering (DLS) measurements (**Figure 4-3**) and cryo-SEM of **26-D** (**Figure 4-3-inset**).

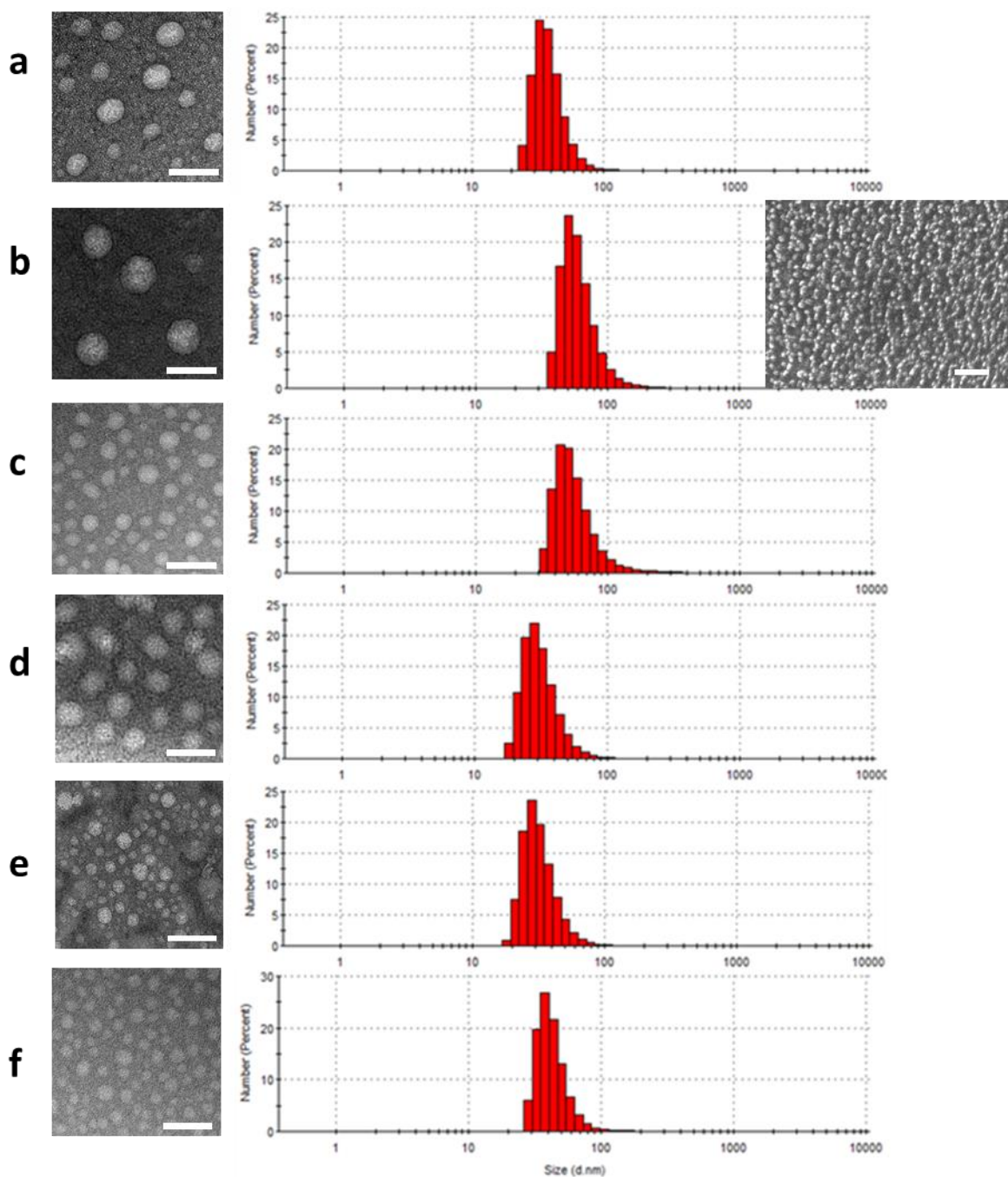


Figure 4-3. TEM images (left, scale bar: 100 nm) and DLS analysis (right) of samples prepared by dialysis method (0.1 mg mL^{-1}). (a) 25-D, (b) 26-D, (c) 27-D, (d) 28-D*, (e) 29-D, and (f) 30-D*. * 0.01 mg mL^{-1} due to poor solubility of the starting material. The cryo-SEM image of **26-D** (inset, scale bar: $1 \mu\text{m}$) confirmed the presence of the particles in solution.

4.2.1.3. Solvent-switch

Direct injection of water into a glycan solution in HFIP (solvent-switch) results in faster mixing, higher oligosaccharide concentration and altered self-assembly behavior

(Figure 4-4). Needle-like structures were found for **26-S-HFIP** (5-10 μm length, 10-50 nm height and 100-500 nm width, Figure 4-4-b) and a spheroidal architecture (1-2 μm diameter) for the hexamer **29-S-HFIP** analogue (Figure 4-4-e). These supramolecular structures were stable for one month at ambient conditions and resisted dilution and sonication (See in 6.7.2). **25-S-HFIP** assembled into a mixture of rods and toroid structures (Figure 4-4-a), while **28-S-DMAc** formed clusters of nanoparticles (Figure 4-4-d). Differences in oligosaccharide structure such as linkage and modification patterns fundamentally affect the material morphology as **27-S-HFIP** (Figure 4-4-c) and **30-S-DMAc** (Figure 4-4-f) aggregated randomly and did not form any ordered supramolecular structure. Compounds **27** and **30** are based on a fairly rigid 1,4 glycosidic linkage (secondary alcohol) and therefore can adopt a limited number of conformations in solution. The flexibility of the 1,6 linkage allows for higher conformational diversity, permitting the formation of fundamentally different nanostructures.

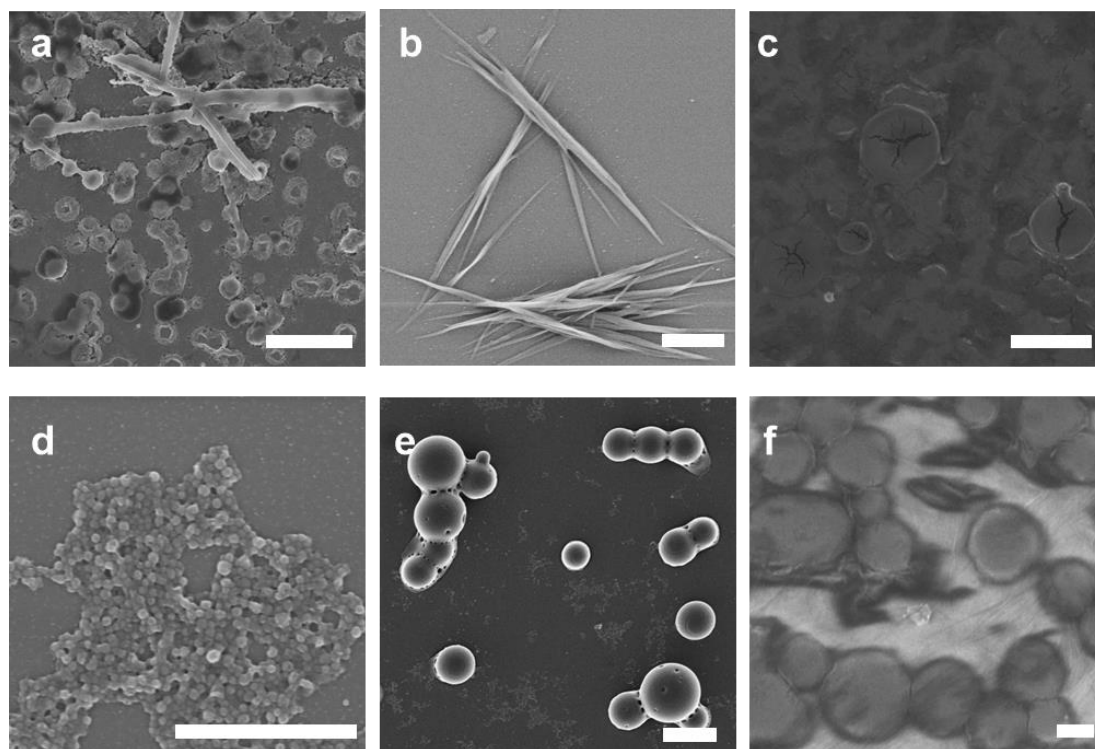


Figure 4-4. SEM images (scale bar: 2 μm) of samples prepared by the solvent-switch method. (a) **25-S-HFIP-low** (0.1 mg mL^{-1}), (b) **26-S-HFIP**, (c) **27-S-HFIP**, (d) **28-S-DMAc**, (e) **29-S-HFIP**, and (f) **30-S-DMAc**. If not mentioned, the standard concentration is 2 mg mL^{-1} and the content of organic solvent is 2%.

4.2.1.4. Screening of conditions for the self-assembly of disaccharide 26

Motivated by the well-defined, disperse, and stable needle-like structures obtained from disaccharide **26** (Figure 4-4), more conditions for the assembly of this compound were screened. Dialysis using a higher concentration of **26** (2 mg mL^{-1}) led to the formation of nanofibers (Figure 4-5-a), likely due to the further association of the spherical particles existing in the diluted solution. The solvent exchange method generated longer needles when a lower concentration of compound **26** was employed (0.1 mg mL^{-1}) (Figure 4-5-b). A higher HFIP content (20%) did not change the shape or length of the supramolecular structures (Figure 4-5-c). In this case, the selective solvation properties of HFIP, in a HFIP–H₂O system, result in a similar local HFIP concentration, limiting aggregation diversity. A similar elongated morphology was obtained when isopropyl alcohol was used instead of HFIP (Figure 4-5-d). When DMAc was used, short and flat bar-like structures were observed. A gel-like microwire material was obtained in acetone (Figure 4-5-f, see in 6.7.2). The diversity observed is ascribed to the different conformations adopted by compound **26**, when solvated by different solvents. In particular, the well-known ability of HFIP to cluster the hydrophobic regions of peptides and affect their folding (HFIP-induced enhancement of the hydrophobic effect)¹⁰⁵⁻¹⁰⁶ is responsible for the dramatic differences of the generated nanostructures.

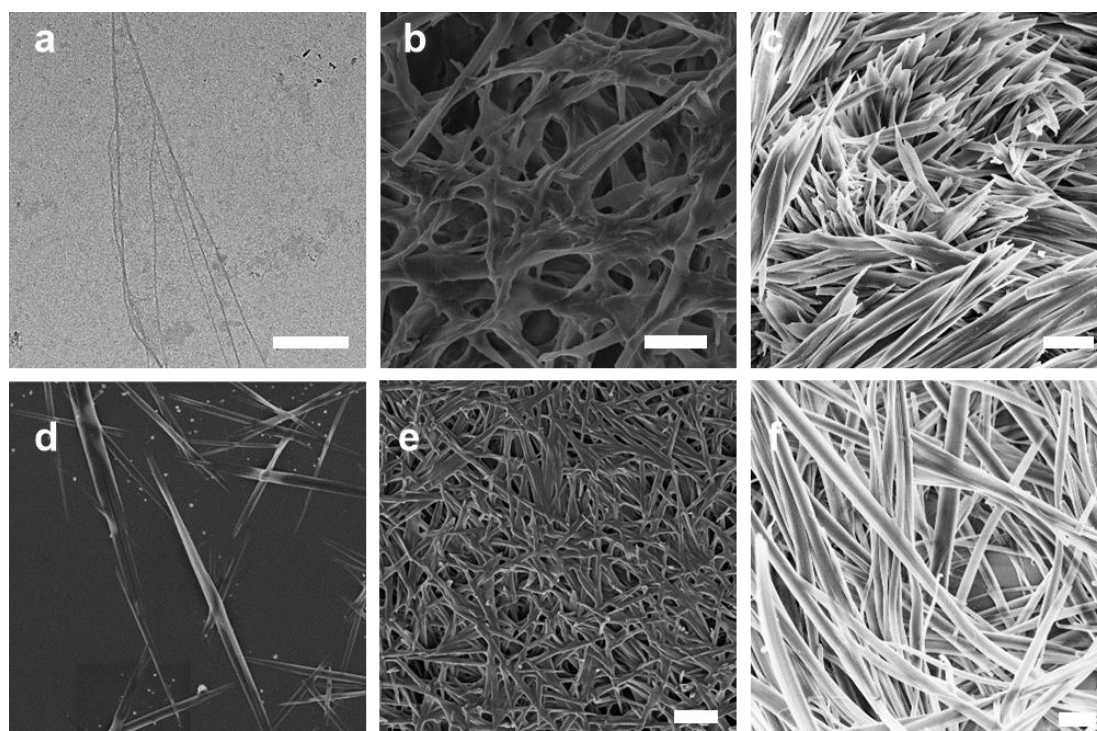


Figure 4-5. Screening of assembly conditions for compound **26**. (a) TEM image (scale bar: 500 nm) for 26-D-high (2 mg mL^{-1}). (b-f) SEM images (scale bar: 2 μm) for (b) 26-S-HFIP-low (0.1 mg mL^{-1}), (c) 26-S-HFIP-20%, (d) 26-S-*i*PrOH-20%, (e)

26-S-DMAc, and (f) 26-S-Ace-20%. If not mentioned, the standard concentration for the solvent-switch method (S) is 2 mg mL⁻¹ and the content of organic solvent is 2%.

4.2.2. Real-time measurements

The self-assembly of **26-S-HFIP** was captured in real-time using bright-field microscopy (**Figure 4-6**) by injecting a freshly-prepared solution into a cell counting slide. Needle-like structures diffuse from the HFIP droplets containing the oligosaccharide into the surrounding water. The contact between the needles and a second HFIP droplet (**Figure 4-6**, time 06:52) disrupt the droplet to release the oligosaccharide and results in further needle growth. Surprisingly, glycan-containing HFIP droplets are intensely fluorescent. We believe that this phenomenon is the result of the formation of supramolecular chromophores within the material, as previously observed for self-assembled peptides, nucleic acids, and amino acids.¹⁰⁷⁻¹¹¹ An extended π -conjugation system and/or charge delocalization through a dense hydrogen-bonding network are generally responsible for this behavior.

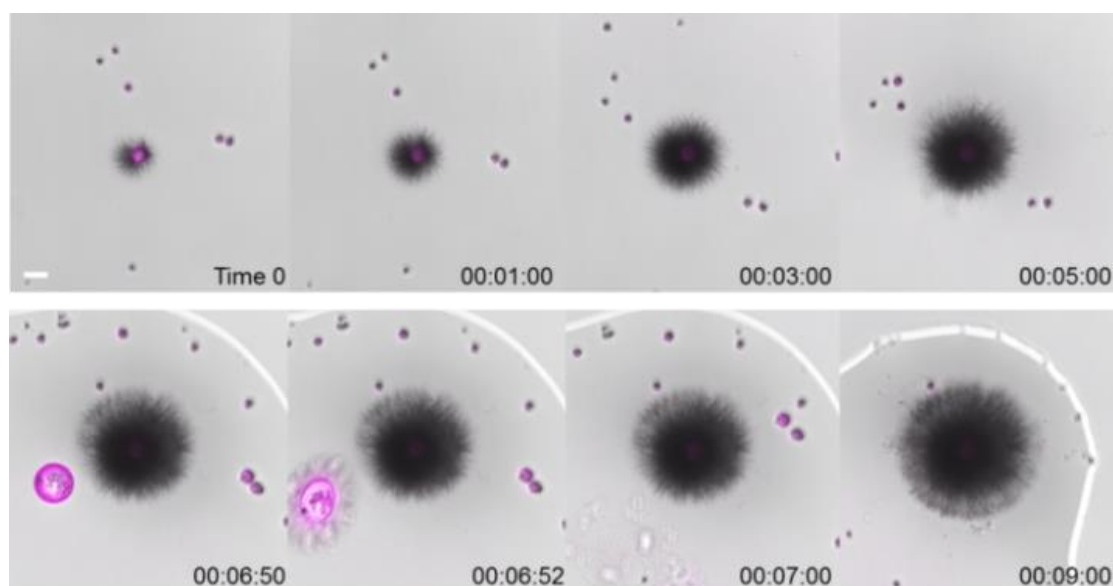


Figure 4-6. Real-time merged bright-field (scale of gray) and fluorescence (magenta) images illustrate the self-assembly process for 26-S-HFIP. Excitation wavelength at 405 nm and detection range 410-676 nm (scale bar: 20 μ m).

4.2.3. Photophysical characterization

4.2.3.1. Polarized optical microscope characterization of 2-S-HFIP

The needle-like structure of **26-S-HFIP** is an indication of highly ordered supramolecular arrangement. Therefore, this sample was visualized with a polarized optical microscope (**Figure 4-7A**), which showed intense birefringence, indicating that

26-S-HFIP exhibits anisotropic property. Moreover, staining with Congo red, a commonly-used dye to detect highly-ordered amyloid fibrils, gave intense gold-green birefringence (**Figure 4-7B**).

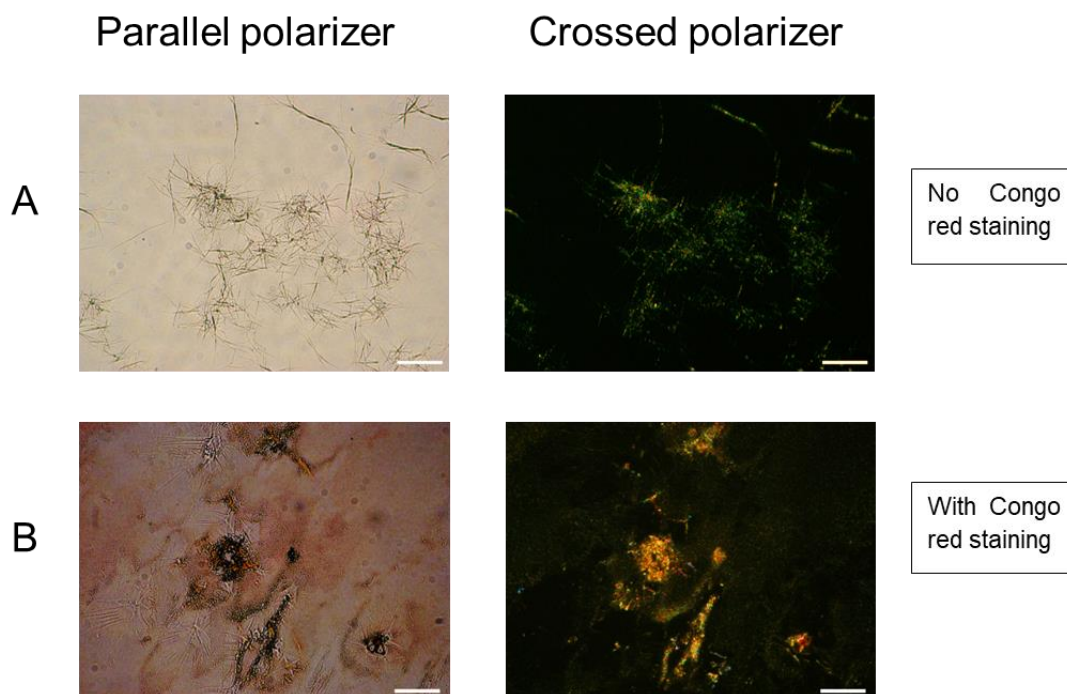


Figure 4-7. Polarized microscopy images of 26-S-HFIP with parallel (left) and perpendicular (right) polarizer, without (A) and with (B) Congo red staining (scale bar: 20 μm). Congo red staining was performed following reported literature.

4.2.3.2. Confocal microscopy and XRD analysis

Confocal microscopy analysis of different morphologies revealed that thin films prepared by direct evaporation of a glycan solution in HFIP on a slide glass (**26-F-HFIP**) emit strongly in four different channels (**Figure 4-8A**) upon visible light irradiation. Films prepared in other organic solvents showed a similar fluorescence behavior (See in 6.7.2). Aggregates obtained *via* the solvent-switch method are only weakly emissive (**Figure 4-8A**). This observation agrees with the supramolecular chromophore hypothesis, since emission intensity is strong in organic solvents, where a dense H-bonding network is favored and quenching occurs when the H-bonding pattern is disrupted by water. The morphology of these materials was further probed with X-ray powder diffraction (XRD) (**Figure 4-8B**). **26-S-HFIP** exhibited sharp peaks, as typical for crystalline structures; in contrast, **26-F-HFIP** shows broad peaks. This confirms the drastic change in morphology upon interaction with water (**26-S-HFIP**). To better evaluate the causes of this phenomenon, compounds (**31-35**) were prepared.

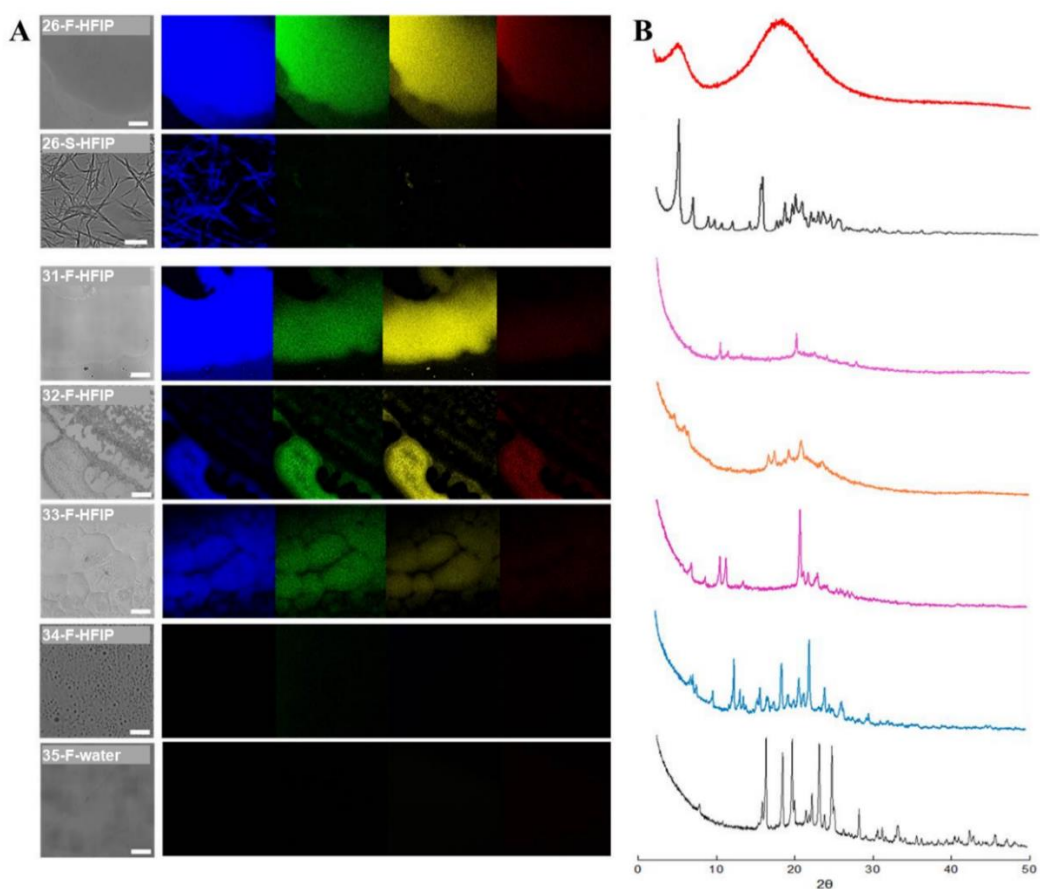
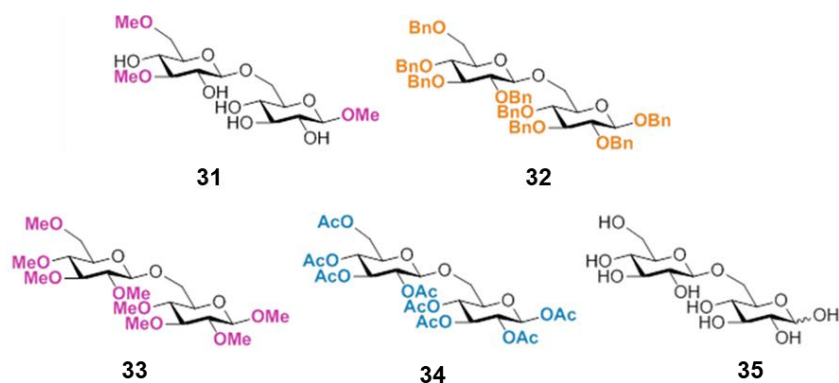


Figure 4-8. (A) Confocal microscopy images of 26 prepared by HFIP film-forming F (scale bar: 100 μm), solvent-switch S (scale bar: 10 μm), and compounds 31-35 prepared by film-forming method (scale bar: 100 μm) in four different channels (blue(ex/em): 405/451 nm, green: 488/529 nm, yellow: 561/597 nm, and red: 633/709 nm). (B) XRD profiles of 26-F-HFIP (red) and 26-S-HFIP (black) and compounds 31-35.

To probe the importance of aromatic groups for the emissive behavior, compound **31** was synthesized. This amphiphilic, partially methylated analogue allows for the formation of a dense hydrogen bonding network, in the absence of aromatic groups.

Upon film formation (**31-F-HFIP**), compound **31** showed a similar optical behavior, confirming that the optical properties are not merely a result of π - π stacking.

Disaccharides **32-34** are fully functionalized, blocking the formation of a dense hydrogen bonding network within the material. Different substituents (Bn vs Me vs Ac) were tested. Surprisingly, confocal microscopy analysis showed emissive behavior for compound **32-F-HFIP** and **33-F-HFIP**. We suspect that such compounds, even in the absence of a strong hydrogen bonding network, maintain a self-organization tendency. On the other hand, the per-acetylated analogue **34**, as well as the fully deprotected compound **35**, showed no emission. XRD analysis of all the materials suggested a correlation between the broad XRD profile and the emissive behavior. Similarly, the appearance of sharp peaks in the XRD profiles, indicating high crystallinity, is associated with emission quenching.

4.2.3.3. Absorption and emission spectroscopy

Further photophysical characterization showed a broad absorption band for compound **26-F-HFIP**, associated with the formation of new self-assembled entities upon film formation. The broadening of the absorption spectrum is not observed for compound **26** in solution, nor for the low emissive, crystalline sample **26-S-HFIP** (**Figure 4-9A**). Excitation spectra (See in **6.7.2**) confirmed that the emissive species are linked to this spectral region (350 – 500 nm). Emission quantum yield was calculated for **26-F-HFIP** ($\Phi_{(\lambda_{\text{ex}} = 360 \text{ nm})} = 0.85 \pm 0.01\%$). Moreover, unlike commonly-used dyes, where the emission peak position is independent of the excitation wavelength, the emission spectrum of **26-F-HFIP** is drastically affected by the excitation wavelength (**Figure 4-9B**). A broad fluorescence emission profile was observed with maxima shifting from 410 to 490 nm as the excitation is changed from 340 to 410 nm. This red edge excitation shift (REES) is a common phenomenon observed in graphene oxide,¹¹⁰ ionic liquids,¹¹¹ and highly ordered assemblies.¹⁰⁸ A very similar behavior was reported by Gazit et al. for self-assembling PNA dimers (**Figure 4-9C**).

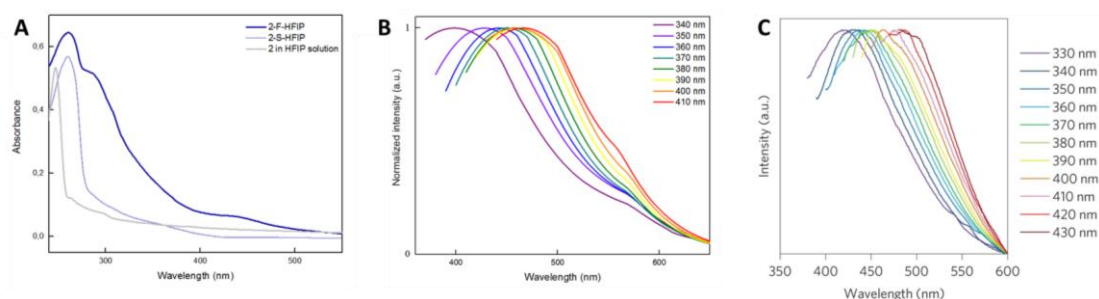


Figure 4-9. Absorption and emission spectroscopy. (A) Absorption spectra of **26-F-HFIP**, **26-S-HFIP** (recorded for the solid samples), and compound **26** in HFIP

solution. (B) Normalized emission spectra of **26-F-HFIP** at excitation wavelengths of 340, 350, 360, 370, 380, 390, 400, 410, 420, and 430 nm, showing the red shifting of the emission maxima. Spectra acquired at r.t. (C) Normalized emission spectra of di-PNA from literature by Gazit et al.¹⁰⁸

4.3. Conclusion

In conclusion, I successfully generated supramolecular structures from fully synthetic well-defined oligosaccharides, and demonstrated that the fine-tuning of the oligosaccharide structure has a tremendous effect on the material morphology. The three dimer and hexamer analogues with different glycosidic linkages and protecting group patterns form similar nanospheres when generated by the slow dialysis method, whereas distinctive microstructures are obtained with the fast solvent-switch method. These compounds show unique optical properties such as broad emission profiles and red edge excitation shift. Further studies to modulate the fluorescent properties of such materials are currently underway, with potential applications for optical devices and nanotechnology. These findings suggest that synthetic oligosaccharides are viable substrates for the fundamental study of the forces that guide the polysaccharide aggregation in Nature. For example, tuning glycomaterial properties through the synthesis of well-defined structures will be relevant for drug delivery systems, where carbohydrate-carbohydrate interactions play a significant role in cellular uptake.

5. Conclusion and outlook

This thesis highlights the use of synthetic tailor-made oligo- and polysaccharides to study carbohydrate materials at different levels: chemical structure, conformation, aggregation tendency, and properties. The ultimate goal of my work is to understand the fundamental principles that guide carbohydrate interactions and provide important information for the rational design and application of carbohydrate materials. Here, the remaining challenges are highlighted. Several aspects of future work can be envisioned:

- 1) Even though the biological roles of carbohydrates have long been appreciated,¹⁻² the correlation between structure and function has not been clarified. Specific chemical modifications permitted a deeper understanding of cellulose structure and properties as shown in Chapter 3. This methodology can be applied to other glycans for studying their conformational preference, physical property, and functions. Such studies will boost a better understanding and utilizing of carbohydrates.¹¹²
- 2) Natural cellulose aggregates into nanocrystals, that is used for applications in nanotechnology and materials science.¹³⁻¹⁵ Short cellulose fragments (i.e. A₆) aggregate with the same packing of natural cellulose as shown in XRD measurement in chapter 3 and are promising candidates for self-assembly studies. Preliminary data showed that A₆ can self-assemble into nanorods (**Figure 5-1**, left) with similar size of natural cellulose nanocrystals (**Figure 5-1**, right). Further study are needed to elucidate the crystallinity of the nanorods. This artificially self-assembled cellulose nanorods are valuable materials for studying the structure and properties of natural CNCs owing to their chemical homogeneity.

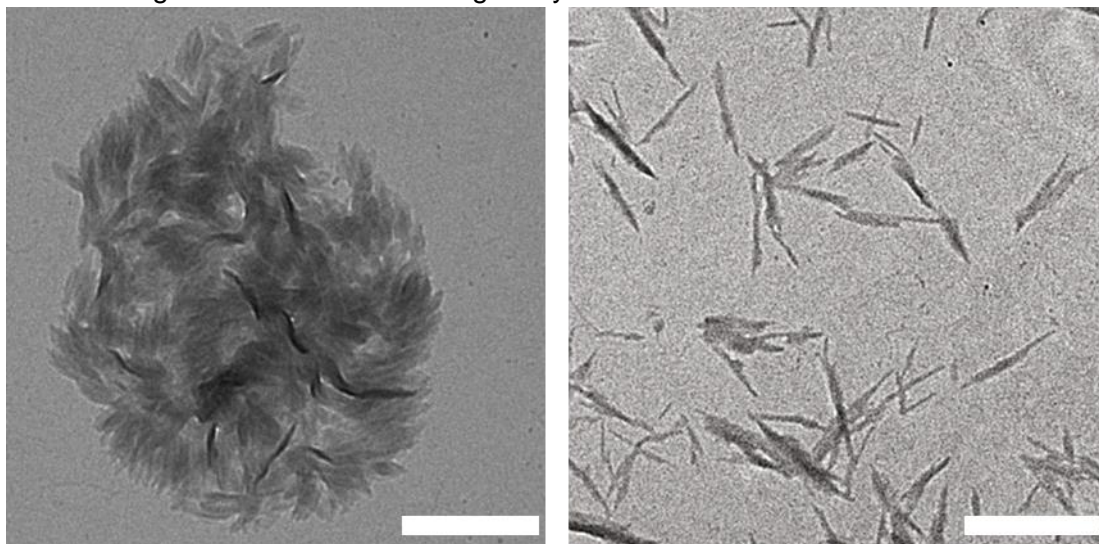


Figure 5-1. TEM images of self-assembling A6 (left) and extracted cellulose nanocrystals (right)¹¹³ (Scale bar: 500 nm).

- 3) The knowledge gained from my thesis work can guide the bottom-up design of cellulose analogues for the construction of supramolecular structures. A cellulose-like

domain (A_n) provides tendency for well-defined aggregation, limiting water solubility. A modified counterpart (X_n) disrupts the regular aggregation of cellulose, improving water solubility. A di-block structure (**Figure 5-2**) is a promising candidate for the construction of ordered supramolecular structures with high stability in water. A similar multi-block approach (i.e. BTA and peptide amphiphiles, **Figure 5-2**, also see in **1.3**) has found great success for the construction of ordered 2D supramolecular architectures, with implications in catalysis,¹¹⁴⁻¹¹⁵ regenerative medicine,⁵⁸ and cancer therapy¹¹⁶.

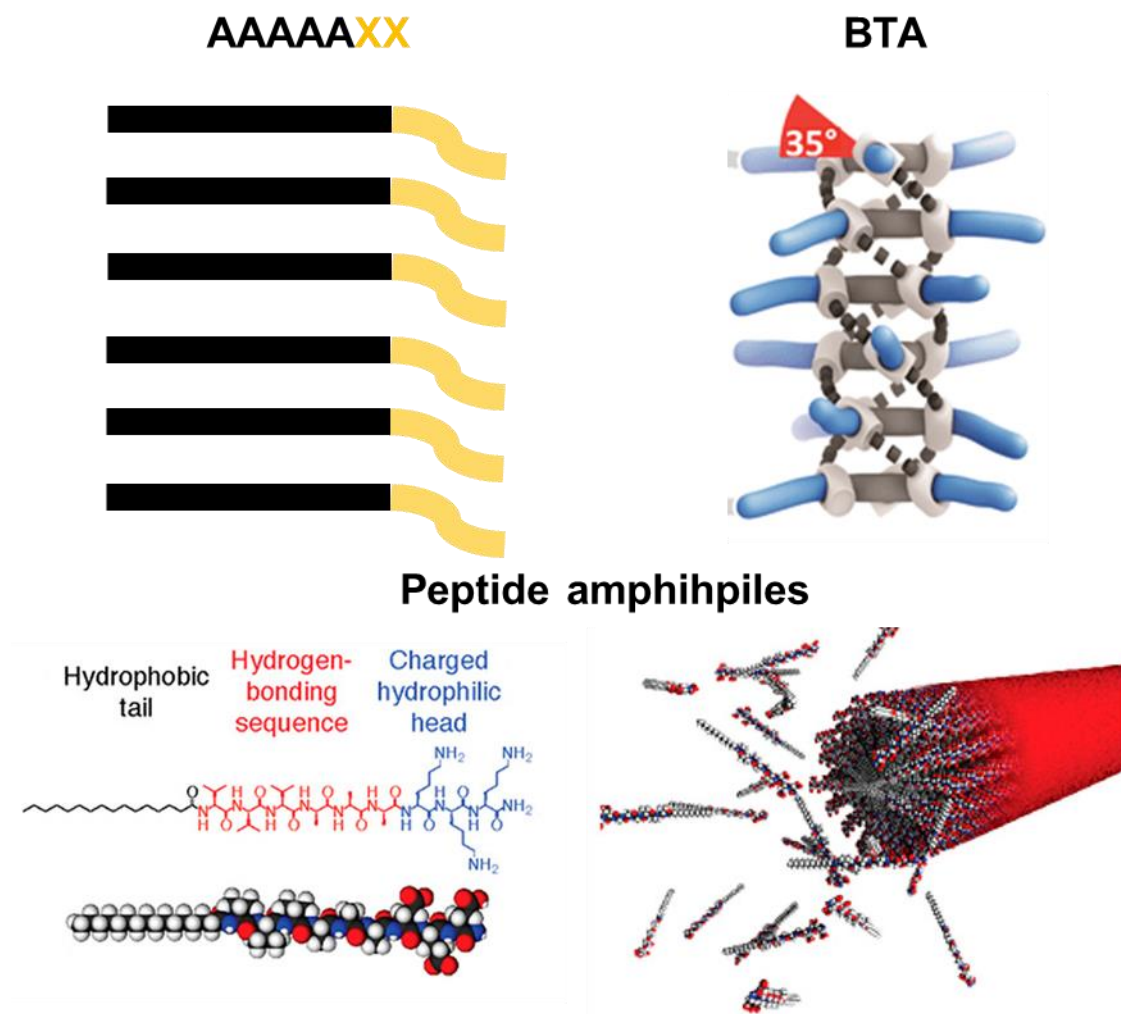


Figure 5-2. Schematic illustration of cellulose derivatives with block structure (top left: A: non-modified cellulose; X: modified cellulose), BTA (top right)⁷⁰, and peptide amphiphiles (bottom)⁵⁶.

6. Experimental section

In this section, only my contributions to each project will be included unless otherwise specified. More experimental data can be found in the publication mentioned at the beginning of each chapter.

6.1. General materials and methods

All chemicals used were reagent grade and used as supplied unless otherwise noted. The automated syntheses were performed on a home-built synthesizer developed at the Max Planck Institute of Colloids and Interfaces. Merrifield resin LL (100-200 mesh, novabiochem™) was modified and used as solid support. Analytical thin-layer chromatography (TLC) was performed on Merck silica gel 60 F254 plates (0.25 mm). Compounds were visualized by UV irradiation or dipping the plate in a p-anisaldehyde (PAA) solution. Flash column chromatography was carried out by using forced flow of the indicated solvent on Fluka Kieselgel 60 M (0.04 – 0.063 mm). Analysis and purification by normal and reverse phase HPLC was performed by using an Agilent 1200 series. Products were lyophilized using a Christ Alpha 2-4 LD plus freeze dryer. ^1H , ^{13}C and HSQC NMR spectra were recorded on a Varian 400-MR (400 MHz), Varian 600-MR (600 MHz), or Bruker Biospin AVANCE700 (700 MHz) spectrometer. Spectra were recorded in CDCl_3 by using the solvent residual peak chemical shift as the internal standard (CDCl_3 : 7.26 ppm ^1H , 77.0 ppm ^{13}C) or in D_2O using the solvent as the internal standard in ^1H NMR (D_2O : 4.79 ppm ^1H). High resolution mass spectra were obtained using a 6210 ESI-TOF mass spectrometer (Agilent) and a MALDI-TOF autoflex™ (Bruker). MALDI and ESI mass spectra were run on IonSpec Ultima instruments. IR spectra were recorded on a Perkin-Elmer 1600 FTIR spectrometer. Optical rotations were measured by using a Perkin-Elmer 241 and Unipol L1000 polarimeter. For XRD measurements, a Bruker D8 Advanced X-ray diffractometer with $\text{Cu K}\alpha$ radiation was used.

6.2. General procedure for automated glycan assembly

Solvents used for dissolving building block and making activator, TMSOTf and capping solutions were taken from an anhydrous solvent system (jcmeyer-solvent systems). Other solvents were HPLC grade. The building blocks were co-evaporated three times with chloroform and dried for 1 h on high vacuum before use. Activator, deprotection, acidic wash, capping and building block solutions were freshly prepared and kept under argon during the automation run. All yields of products obtained by AGA were calculated on the basis of resin loading. Resin loading was determined by performing

one glycosylation (Module C) with 10 equiv of building block followed by DBU promoted Fmoc-cleavage and determination of dibenzofulvene production by measuring its UV absorbance. Unless mentioned otherwise, the conditions and modules of AGA are also applied to other chapters.

6.2.1. Preparation of stock solutions

- **Building block:** building block was dissolved in 1 mL of dichloromethane (DCM).
- **Activator solution:** 1.35 g of recrystallized NIS was dissolved in 40 mL of a 2:1 mixture of anhydrous DCM and anhydrous dioxane. Then triflic acid (55 μ L) was added. The solution is kept at 0°C for the duration of the automation run.
- **Fmoc deprotection solution 1:** A solution of 20% piperidine in dimethylformamide (DMF) (v/v) was prepared.
- **Fmoc deprotection solution 2:** A solution of 20% triethylamine in DMF (v/v) was prepared.
- **TMSOTf Solution:** Trimethylsilyl trifluoromethanesulfonate (TMSOTf) (0.45 mL) was added to DCM (40 mL).
- **Capping solution:** A solution of 10% acetic anhydride (Ac_2O) and 2% methanesulfonic acid (MsOH) in anhydrous DCM (v/v) was prepared.

6.2.2. Modules for automated glycan assembly

Module A: Resin Preparation for Synthesis (20 min)

All automated syntheses were performed on 0.0125 mmol scale. Resin was placed in the reaction vessel and swollen in DCM for 20 min at room temperature prior to synthesis. During this time, all reagent lines needed for the synthesis were washed and primed. Before the first glycosylation, the resin was washed with the DMF, tetrahydrofuran (THF), and DCM (three times each with 2 mL for 25 s). This step is conducted as the first step for every synthesis and test.

Module B: Acidic Wash with TMSOTf Solution (20 min)

The resin was swollen in 2 mL DCM and the temperature of the reaction vessel was adjusted to -20 °C. Upon reaching the low temperature, TMSOTf solution (1 mL) was added drop wise to the reaction vessel. After bubbling for 3 min, the acidic solution was drained and the resin was washed with 2 mL DCM for 25 s.

Action	Cycles	Solution	Amount	T (°C)	Incubation time
Cooling	-	-	-	-20	(15 min)*

Deliver	1	DCM	2 mL	-20	-
Deliver	1	TMSOTf solution	1 mL	-20	3 min
Wash	1	DCM	2 mL	-20	25 s

*Time required to reach the desired temperature.

Module C: Thioglycoside Glycosylation (35 min)

The building block solution (0.08 mmol of BB in 1 mL of DCM per glycosylation) was delivered to the reaction vessel. After the set temperature was reached, the reaction was started by drop wise addition of the activator solution (1.0 mL, excess). The glycosylation conditions are building block dependent (we report the most common set of conditions). After completion of the reaction, the solution is drained and the resin was washed with DCM, DCM:dioxane (1:2, 3 mL for 20 s) and DCM (two times, each with 2 mL for 25 s). The temperature of the reaction vessel is increased to 25 °C for the next module.

Action	Cycles	Solution	Amount	T (°C)	Incubation time
Cooling	-	-	-	-20	-
Deliver	1	BB solution	1 mL	-20	-
Deliver	1	Activator solution	1 mL	-20	-
Reaction time (BB dependent)	1			-20 to 0	5 min 20 min
Wash	1	DCM	2 mL	0	5 s
Wash	1	DCM : Dioxane (1:2)	2 mL	0	20 s
Heating	-	-	-	25	-
Wash	2	DCM	2 mL	> 0	25 s

Module D: Capping (30 min)

The resin was washed with DMF (two times with 2 mL for 25 s) and the temperature of the reaction vessel was adjusted to 25 °C. Pyridine solution (2 mL, 10% in DMF)

was delivered into the reaction vessel. After 1 min, the reaction solution was drained and the resin washed with DCM (three times with 3 mL for 25 s). Capping solution (4 mL) was delivered into the reaction vessel. After 20 min, the reaction solution was drained and the resin washed with DCM (three times with 3 mL for 25 s).

Action	Cycles	Solution	Amount	T (°C)	Incubation time
Heating	-	-	-	25	(5 min)*
Wash	2	DMF	2 mL	25	25 s
Deliver	1	10% Pyridine in DMF	2 mL	25	1 min
Wash	3	DCM	2 mL	25	25 s
Deliver	1	Capping Solution	4 mL	25	20 min
Wash	3	DCM	2 mL	25	25 s

*Time required to reach the desired temperature.

Module E: Fmoc Deprotection (9 min)

The resin was washed with DMF (three times with 2 mL for 25 s) and the temperature of the reaction vessel was adjusted to 25 °C. Fmoc deprotection solution (2 mL) was delivered into the reaction vessel. After 5 min, the reaction solution was drained and the resin washed with DMF (three times with 3 mL for 25 s) and DCM (five times each with 2 mL for 25 s). The temperature of the reaction vessel is decreased to -20 °C for the next module.

Action	Cycles	Solution	Amount	T (°C)	Incubation time
Wash	3	DMF	2 mL	25	25 sec
Deliver	1	Fmoc depr. Solution 1	2 mL	25	5 min
Wash	1	DMF	2 mL		
Cooling	-	-	-	-20	-
Wash	3	DMF	2 mL	< 25	25 sec
Wash	5	DCM	2 mL	< 25	25 sec

Module E*: Fmoc Deprotection with TEA (20 min)

The resin was washed with DMF (three times with 2 mL for 25 s) and the temperature of the reaction vessel was adjusted to 25 °C. Fmoc deprotection solution 2 (2 mL) was delivered to the reaction vessel. After 5 min, the reaction solution was drained. The

deprotection process was repeated for three times. The resin was washed with DMF (three times with 3 mL for 25 s) and DCM (five times each with 2 mL for 25 s). The temperature of the reaction vessel is decreased to -20 °C for the next module.

Action	Cycles	Solution	Amount	T (°C)	Incubation time
Wash	3	DMF	2 mL	25	25 sec
Deliver	3	Fmoc depr. Solution 2	2 mL	25	5 min
Wash	1	DMF	2 mL		
Cooling	-	-	-	-20	-
Wash	3	DMF	2 mL	< 25	25 sec
Wash	5	DCM	2 mL	< 25	25 ec

6.2.3. Post-synthesizer manipulations

Module F: On-resin Methanolysis

The resin was suspended THF (5 mL). 0.5 mL of NaOMe in MeOH (0.5 M) was added and the suspension was gently shaken at room temperature. After micro-cleavage (**Module G1**) indicated the complete removal of benzoyl groups (generally around 4 hours), the resin was repeatedly washed with MeOH (2mL x 3) and DCM (2mL x 3).

Module G: Cleavage from Solid Support

The oligosaccharides were cleaved from the solid support using a continuous-flow photoreactor as described previously.

Module G1: Micro-cleavage from Solid Support

Trace amount of resin (around 20 beads) was dispersed in DCM (0.1 mL) and irradiated with a UV lamp (6 watt, 356 nm) for 10 minutes. ACN (10 µL) was then added to the resin and the resulting solution analyzed by MALDI.

Module H: Solution-phase methanolysis

The protected oligosaccharide was dissolved in MeOH: DCM (1.5 mL, 1:1). NaOMe in MeOH (0.5 M, 3 equiv. per benzoyl ester) was added and the solution was stirred at room temperature for 12 h, neutralized with Amberlite IR-120 (H⁺ form), filtered and concentrated *in vacuo*. The crude compound was used for hydrogenolysis without further purification.

Module H*: Solution-phase methanolysis for 3-O-methoxycarbonyl sugars

The protected oligosaccharide was dissolved in THF (1.5 mL). NaOMe in MeOH (0.5 M, 3 equiv. per benzoyl ester) was added and the solution was stirred at room temperature for 12 h, neutralized with HOAc and concentrated *in vacuo*. The crude compound was used for hydrogenolysis without further purification. These conditions also hydrolyze the methyl esters due to the trace amount of water in the reaction mixture.

Module I: Hydrogenolysis

The crude compound obtained from *Module F or H* was dissolved in 2 mL of EA:*t*BuOH:H₂O (1:0.5:0.5). Palladium on carbon (Pd/C, 10%) was added and the reaction was stirred in H₂ bomb with 60 psi pressure. Generally, the hydrogenolysis is completed within 1 hour. If the reaction does not go to completion after 1 hour, the reaction should be monitored every 30 min and stopped right after completion to prevent the undesired reduction of the free reducing end. Upon completion, the reaction was filtered through celite and washed with DCM, *t*BuOH and H₂O. The filtrates were concentrated *in vacuo*.

Module I*: Hydrogenolysis at ambient pressure

The crude compound obtained from *Module H** was dissolved in 2 mL of EA:*t*BuOH:H₂O (1:0.5:0.5). 100% by weight Pd-C (10%) was added and the reaction was stirred under H₂-atmosphere for 6 h. The reaction was filtered through celite and washed with *t*BuOH and H₂O. The filtrates were concentrated *in vacuo*. For 3-O-methoxycarbonyl sugars, the pH value was adjusted to 2-3 by using formic acid before HPLC purification.

Module J: Purification

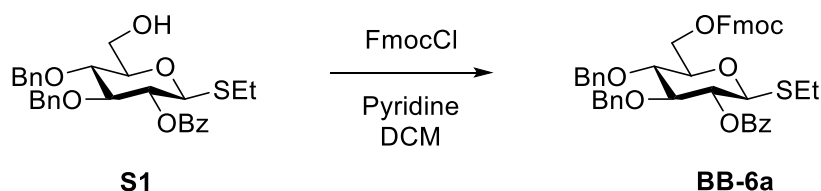
Purification was conducted at different stage of the synthesis as reported for the individual procedures. The crude products were analyzed using analytical HPLC (Agilent 1200 Series spectrometer). The purification was conducted using preparative HPLC (Agilent 1200 Series spectrometer) or C₁₈ reverse phase silica gel column chromatography.

- **Method A:** (YMC-Diol-300 column, 150 x 4.6 mm) flow rate of 1.0 mL / min with Hex – 20% EtOAc as eluent [isocratic 20% EtOAc (5 min), linear gradient to 55% EtOAc (35 min), linear gradient to 100% EtOAc (5 min)].
- **Method A0:** (YMC-Diol-300 column, 150 x 4.6 mm) flow rate of 1.0 mL / min with Hex – 10% EtOAc as eluent [isocratic 10% EtOAc (5 min), linear gradient to 50% EtOAc (20 min), linear gradient to 100% EtOAc (5 min)].

- **Method A50:** (YMC-Diol-300 column, 150 x 4.6 mm) flow rate of 1.0 mL / min with Hex – 20% EtOAc as eluents [isocratic 20% EtOAc (5 min), linear gradient to 40% EtOAc (5 min), linear gradient to 60% EtOAc (30 min), linear gradient to 100% EtOAc (5 min)].
- **Method B:** (YMC-Diol-300 column, 150 x 20 mm) flow rate of 15 mL / min with Hex – 20% EtOAc as eluents [isocratic 20% EtOAc (5 min), linear gradient to 55% EtOAc (35 min), linear gradient to 100%].
- **Method B1:** (YMC-Diol-300 column, 150 x 20 mm) flow rate of 15 mL/min with Heptane/EtOAc as eluent [isocratic 20% EtOAc (5 min), linear gradient to 100% EtOAc].
- **Method B50:** (YMC-Diol-300 column, 150 x 20 mm) flow rate of 15 mL / min with Hex – 20% EtOAc as eluents [isocratic 20% EtOAc (5 min), linear gradient to 50% EtOAc (75 min), linear gradient to 100% EtOAc (10 min)].
- **Method C:** (Synergi Hydro RP18 column, 250 x 4.6 mm) flow rate of 1.0 mL / min with H₂O (0.1% formic acid) as eluents [isocratic (5 min), linear gradient to 30% ACN (30 min), linear gradient to 100% ACN (5 min)].
- **Method D:** (Synergi Hydro RP18 column, 250 x 10 mm) flow rate of 4.0 mL / min with H₂O (0.1% formic acid) as eluents [isocratic (5 min), linear gradient to 30% ACN (30 min), linear gradient to 100% ACN (5 min)].
- **Method E:** (Hypercarb column, 150 x 10 mm) flow rate of 1.3 mL / min with H₂O (0.1% formic acid) as eluents [isocratic (5 min), linear gradient to 30% ACN (30 min), linear gradient to 100% ACN (5 min)].
- **Method M:** (Manual reverse phase C18 silica gel column chromatography): H₂O (10 mL), 5% MeOH (10 mL), 7.5% MeOH (10 mL), 10% MeOH (10 mL), 15% MeOH (10 mL), 20% MeOH (10 mL).
- **Method N:** (Manual normal phase silica gel column chromatography): hexane:EtOAc = 2:1 to 1:2.

6.3. Synthesis of building blocks

6.3.1. Synthesis of building block BB-6a



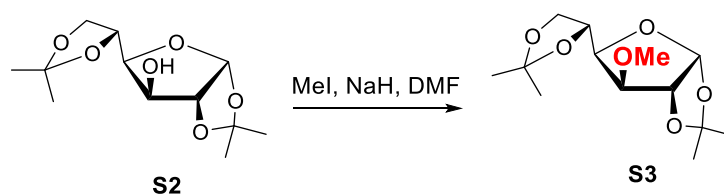
Compound **S1** was prepared according previously reported procedures.¹¹⁷

Monosaccharide **S1** (2.0 g, 3.9 mmol) was dissolved in DCM (20 mL). Pyridine (0.9 mL, 12 mmol) and (9H-fluoren-9-yl)methyl carbonochloridate (2.0 g, 7.9 mmol) were added. The yellow solution was stirred at rt until completion (3 h). The reaction was diluted with DCM and washed with 1 M HCl, then saturated aqueous NaHCO₃ and water. The organic layer was dried over MgSO₄, filtered and evaporated. The resulting yellow oil was purified by column chromatography (hexane:EtOAc = 4:1) to give **BB-6a** as a white solid (2.7 g, 94%).

Analytical data for ethyl 2-O-benzoyl-3,4-di-O-benzyl-6-O-fluorenylmethoxycarbonyl-1-thio- β -D-glucopyranoside **BB-6a**: ¹H NMR (400 MHz, Chloroform-*d*) δ 8.08 – 7.97 (m, 2H), 7.76 (d, *J* = 7.5 Hz, 2H), 7.65 – 7.52 (m, 3H), 7.49 – 7.36 (m, 4H), 7.36 – 7.20 (m, 7H), 7.14 (d, *J* = 1.9 Hz, 5H), 5.33 (t, *J* = 9.5 Hz, 1H), 4.88 (d, *J* = 10.9 Hz, 1H), 4.77 – 4.66 (m, 2H), 4.62 (d, *J* = 11.0 Hz, 1H), 4.56 (d, *J* = 10.0 Hz, 1H), 4.48 (dt, *J* = 11.7, 1.5 Hz, 1H), 4.38 (dd, *J* = 7.8, 2.7 Hz, 2H), 4.33 – 4.22 (m, 2H), 3.88 (t, *J* = 8.7 Hz, 1H), 3.75 – 3.61 (m, 2H), 2.69 (dddd, *J* = 19.8, 12.6, 7.4, 5.2 Hz, 2H), 1.21 (td, *J* = 7.5, 1.1 Hz, 3H); ¹³C NMR (101 MHz, Chloroform-*d*) δ 165.21, 154.92, 143.34, 143.26, 141.26, 141.24, 137.54, 137.48, 133.19, 129.82, 129.75, 128.53, 128.41, 128.29, 128.11, 128.04, 127.98, 127.87, 127.74, 127.17, 125.19, 125.15, 120.02, 84.31, 83.59, 75.37, 75.18, 72.29, 69.99, 66.56, 46.68, 24.03, 14.90; *m/z* (HRMS+) 753.2526 [M + Na]⁺ (C₄₄H₄₂O₈SNa requires 753.2493); [α]_D²⁰ 30.93 (*c* = 1, CHCl₃); IR (neat) ν_{\max} = 1215, 744, 668 cm⁻¹.

6.3.2. Synthesis of building block BB-11 and BB-12

Synthesis of **S3**

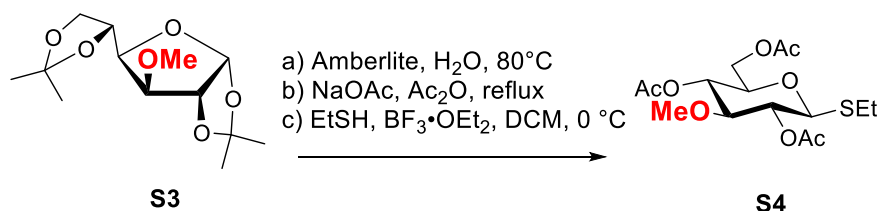


Monosaccharide **S2** (53 g, 204 mmol) was dissolved in anhydrous DMF (1 L). The solution was cooled to 0 °C and NaH (60% by weight in mineral oil, 12.2 g, 305 mmol) was slowly added portion-wise with vigorous stirring. Evolved H₂ was periodically vented during NaH addition. After the NaH addition was complete, the reaction was stirred for 1 h at 0 °C. MeI (25 mL, 407 mmol) was added drop-wise. After MeI addition was complete, the reaction was stirred for 15 min. at 0 °C. The reaction was allowed to warm to rt, during which time a white precipitate formed. The reaction was stirred for 1.5 h at rt and then cooled back to 0 °C. Saturated aq. NH₄Cl was slowly added to quench the reaction. When all H₂ appeared to have been evolved an additional 50 mL

of saturated aq. NH_4Cl was added and the reaction was stirred for additional 15 min. at 0 °C. The reaction was concentrated to < 200 mL under reduced pressure and DCM (1 L) was added. The organic layer was separated and extracted twice with H_2O . The organics were dried over MgSO_4 , filtered, and concentrated to give **S3** as a light yellow oil (56 g, quantitative).

Analytical data for **1,2:5,6-di-O-isopropylidene-3-O-methyl- α -D-glucofuranose, S3**: ^1H NMR (400 MHz, CDCl_3) δ 5.85 (d, $J = 3.7$ Hz, 1H), 4.56 (d, $J = 3.7$ Hz, 1H), 4.31 – 4.25 (m, 1H), 4.11 – 4.04 (m, 2H), 3.99 (dd, $J = 8.6, 5.4$ Hz, 1H), 3.76 (d, $J = 3.0$ Hz, 1H), 3.45 (s, 3H), 1.49 (s, 3H), 1.42 (s, 3H), 1.35 (s, 3H), 1.31 (s, 3H); ^{13}C NMR (101 MHz, CDCl_3) δ 111.88, 109.16, 105.31, 83.83, 82.03, 81.17, 72.53, 67.37, 58.33, 27.01, 26.96, 26.37, 25.54; $[\alpha]_{\text{D}}^{20}$ -100.07 (c 1, CHCl_3); IR (neat) $\nu_{\text{max}} = 1373, 1072$ cm^{-1} ; m/z (HRMS+) 297.1330 $[\text{M} + \text{Na}]^+$ ($\text{C}_{13}\text{H}_{22}\text{O}_6\text{Na}$ requires 297.1309).

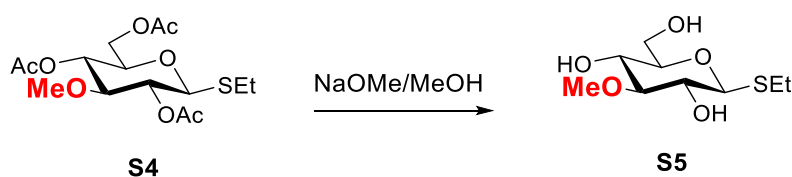
Synthesis of **S4**



Monosaccharide **S3** (56 g, 204 mmol) was suspended in H_2O (400 mL). Amberlite IR-120 (H^+ form, 75 g) was added. The reaction mixture was heated to 80 °C and stirred vigorously for 16 h. The reaction was cooled to rt and the solid material was filtered off. The reaction was concentrated under reduced pressure. The residue was suspended in ACN and then the solvent was removed under reduced pressure to give a pale yellow powder. NaOAc (8.4 g, 102 mmol) was added to the solid sample followed by slow addition of Ac_2O (192 mL, 2.04 mol). The mixture was refluxed for 45 min, during which time it became orange. The reaction was cooled to room temperature, and then quenched with ice. DCM (700 mL) was added and the organic layers were washed twice with H_2O . The organics were dried over MgSO_4 , filtered, and concentrated to give a crude orange oil. This oil was dissolved in DCM (1.3 L). Ethanethiol (38 mL, 510 mmol) was added and the solution was cooled to 0 °C. $\text{BF}_3\cdot\text{OEt}_2$ (39 mL, 306 mmol) was slowly added and the reaction was stirred at 0 °C for 5 h. The pink solution was quenched by slow addition of saturated aq. NaHCO_3 . 700 mL DCM were added and the organic layers washed with saturated aq. NaHCO_3 and H_2O . The organics were dried over MgSO_4 , filtered, and concentrated. The crude product was purified by column chromatography (hexane:EtOAc = 2:1) to give **S4** as a yellow gel (56.7 g, 76%).

Analytical data for **ethyl 2,4,6-tri-O-acetyl-3-O-methyl-1-thio-β-D-glucopyranoside, S4**: ¹H NMR (400 MHz, CDCl₃) δ 5.01 (dd, *J* = 20.2, 10.0 Hz, 2H), 4.39 (d, *J* = 10.0 Hz, 1H), 4.22 – 4.07 (m, 2H), 3.64 – 3.55 (m, 1H), 3.47 (t, *J* = 9.2 Hz, 1H), 3.41 (s, 3H), 2.78 – 2.61 (m, 2H), 2.11 (s, 3H), 2.09 (s, 3H), 2.07 (s, 3H), 1.25 (t, *J* = 7.4 Hz, 3H); ¹³C NMR (101 MHz, CDCl₃) δ 170.88, 169.49, 169.47, 83.84, 82.92, 77.48, 77.16, 76.84, 76.31, 70.83, 69.26, 62.65, 59.32, 24.15, 21.11, 20.95, 20.91, 14.93; [α]_D²⁰ -56.58 (c 1, CHCl₃); IR (neat) ν_{max} = 1743, 1218 cm⁻¹; *m/z* (HRMS+) 387.1093 [M + Na]⁺ (C₁₅H₂₄O₈SNa requires 387.1084).

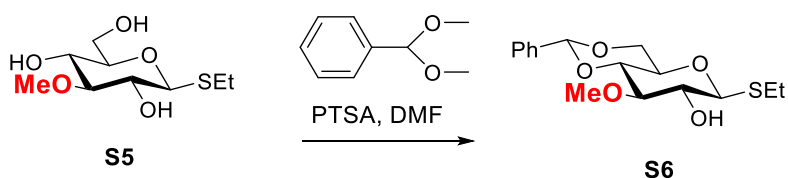
Synthesis of S5



Monosaccharide **S4** (56.7 g, 156 mmol) was dissolved in MeOH (310 mL) and the solution was cooled to 0 °C. NaOMe (840 mg, 15.6 mmol) was added. The reaction was allowed to warm to rt and stirred for 14 h. The reaction was neutralized with Amberlite IR-120 (H⁺ form) and the solid was filtered off. The solvent was removed under reduced pressure to give **S5** as a yellow gel (35.7 g, 96%).

Analytical data for **ethyl 3-O-methyl-1-thio-β-D-glucopyranoside, S5**: ¹H NMR (400 MHz, CD₃OD) δ 4.39 (d, *J* = 9.8 Hz, 1H), 3.86 (dd, *J* = 12.0, 2.2 Hz, 1H), 3.69 – 3.61 (m, 4H), 3.39 – 3.23 (m, 3H), 3.09 (t, *J* = 8.7 Hz, 1H), 2.84 – 2.65 (m, 2H), 1.30 (t, *J* = 7.4 Hz, 3H); ¹³C NMR (101 MHz, CD₃OD) δ 89.42, 86.89, 81.93, 74.17, 71.10, 62.78, 61.28, 24.81, 15.40; [α]_D²⁰ +13.10 (c 1, CHCl₃); IR (neat) ν_{max} = 3389, 1035 cm⁻¹; *m/z* (HRMS+) 261.0791 [M + Na]⁺ (C₉H₁₈O₅SNa requires 261.0767).

Synthesis of S6



Monosaccharide **S5** (35.7 g, 150 mmol) was dissolved in anhydrous DMF (500 mL). *p*-Toluenesulfonic acid (PTSA) (4.3 g, 22.5 mmol) was added and then benzaldehyde dimethyl acetal (45 mL, 300 mmol) was slowly added using a dropping funnel. Following benzaldehyde dimethyl acetal addition the reaction was heated to 45°C and stirred for 18 h. The reaction was cooled to 0°C and quenched by addition of TEA (7

mL). The reaction was concentrated under reduced pressure and the crude product was purified by column chromatography (hexane:EtOAc = 1:1) to give **S6** as a white powder (30.0 g, 61%).

Analytical data for **ethyl 4,6-O-benzylidene-3-O-methyl-1-thio-β-D-glucopyranoside, S6**: ¹H NMR (400 MHz, CDCl₃) δ 7.55 – 7.43 (m, 2H), 7.41 – 7.30 (m, 3H), 5.56 (s, 1H), 4.47 (d, *J* = 9.5 Hz, 1H), 4.35 (dd, *J* = 10.5, 4.9 Hz, 1H), 3.77 (t, *J* = 10.3 Hz, 1H), 3.69 (s, 3H), 3.67 – 3.58 (m, 2H), 3.54 – 3.47 (m, 2H), 3.47 – 3.40 (m, 1H), 2.80 – 2.72 (m, 2H), 1.32 (t, *J* = 7.4 Hz, 3H); ¹³C NMR (101 MHz, CDCl₃) δ 137.30, 134.59, 129.88, 129.15, 128.38, 126.15, 101.40, 86.75, 83.66, 81.49, 72.99, 70.83, 68.77, 61.17, 24.76, 15.39; *m/z* (HRMS+) 349.1106 [M + Na]⁺ (C₁₆H₂₂O₅SNa requires 349.1080).

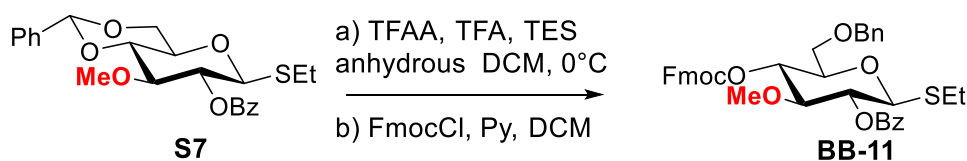
Synthesis of **S7**



Monosaccharide **S6** (30.0 g, 92 mmol) was dissolved in anhydrous DCM (310 mL). The solution was cooled to 0°C and Bz₂O (41.6 g, 184 mmol), 4-Dimethylaminopyridine (DMAP) (5.6 g, 46 mmol), and trimethylamine (TEA) (38 mL, 276 mmol) were successively added. The reaction was allowed to warm to rt and stirred for 12 h, during which time it became yellow and a white precipitate formed. DCM (300 mL) was added and the organic layers were washed with saturated aq. NaHCO₃ and brine. The organics were dried over MgSO₄, filtered, and concentrated. The crude product was purified by column chromatography (7 hexane: 2 EtOAc) to give **S7** as a pale yellow solid (33.1 g, 84%).

Analytical data for **ethyl 2-O-benzoyl-4,6-O-benzylidene-3-O-methyl-1-thio-β-D-glucopyranoside, S7**: ¹H NMR (400 MHz, CDCl₃) δ 8.14 – 8.06 (m, 2H), 7.60 (t, *J* = 7.8 Hz, 1H), 7.53 – 7.44 (m, 4H), 7.41 – 7.33 (m, 3H), 5.60 (s, 1H), 5.27 (t, *J* = 10.2 Hz, 1H), 4.66 (d, *J* = 10.1 Hz, 1H), 4.41 (dd, *J* = 10.5, 4.9 Hz, 1H), 3.82 (t, *J* = 10.3 Hz, 1H), 3.79 – 3.61 (m, 2H), 3.59 (dd, *J* = 9.8, 5.2 Hz, 1H), 3.54 (s, 3H), 2.73 (qd, *J* = 7.4, 3.4 Hz, 2H), 1.24 (t, *J* = 7.5 Hz, 3H); ¹³C NMR (101 MHz, CDCl₃) δ 165.36, 137.27, 133.82, 133.36, 130.31, 130.00, 129.95, 129.17, 128.60, 128.58, 128.39, 126.18, 101.43, 84.47, 82.35, 81.35, 72.18, 70.94, 68.78, 60.90, 24.19, 14.94; [α]_D²⁰ +8.07 (c 1, CHCl₃); IR (neat) ν_{max} = 3442, 1071 cm⁻¹; *m/z* (HRMS+) 431.1529 [M + Na]⁺ (C₂₃H₂₆O₆SNa requires 431.1523).

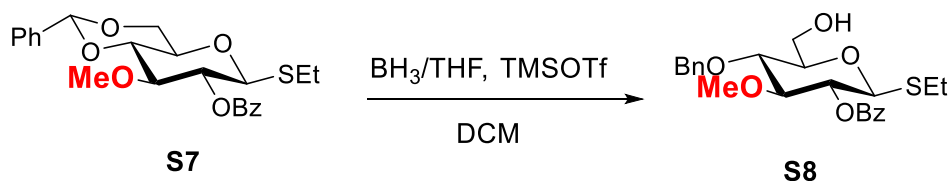
Synthesis of **BB-11**



Monosaccharide **S7** (9.7 g, 22.5 mmol) was dissolved in anhydrous dichloromethane (DCM) (125 mL). Triethylsilane (TES) (21.6 mL, 135 mmol) was added and the solution was cooled to 0°C. Trifluoroacetic acid (TFA) (8.7 mL, 113 mmol) and trifluoroacetic anhydride (TFAA) (1.6 mL, 11.3 mmol) were added sequentially. The solution was stirred at 0°C for 3 hours. The reaction was diluted with DCM (150 mL) and washed with saturated aq. NaHCO₃ (2 x 50 mL) and H₂O (1 x 50 mL). The organics were dried over MgSO₄, filtered, and evaporated. The remaining pale yellow oil was dissolved in pyridine and the solvent was removed under reduced pressure. The crude compound was dissolved in DCM (75 mL). Pyridine (Py) (6.8 mL, 67.6 mmol) was added followed by Fmoc-Cl (11.7 g, 45.1 mmol). The yellow solution was stirred at room temperature under inert Ar atmosphere until completion (3 h). The reaction was diluted with DCM (100 mL) and washed with 1 M HCl (1 x 50 mL), saturated aq. NaHCO₃ (1 x 50 mL), and H₂O (1 x 50 mL). The organics were dried over MgSO₄, filtered, and evaporated. The crude product was purified by column chromatography (hexane : EtOAc = 4:1) to give **BB-11** as a pale yellow solid (9.7 g, 66%).

Analytical data for **ethyl 2-O-benzoyl-6-O-benzyl-4-O-fluorenylcarboxymethyl-3-O-methyl-1-thio-β-D-glucopyranoside, BB-11**: ¹H NMR (400 MHz, CDCl₃) δ 8.09 (d, *J* = 8.0 Hz, 2H), 7.77 (d, *J* = 7.5 Hz, 2H), 7.63 – 7.55 (m, 3H), 7.47 (t, *J* = 7.7 Hz, 2H), 7.41 (t, *J* = 7.5 Hz, 2H), 7.36 – 7.27 (m, 7H), 5.27 (t, *J* = 9.6 Hz, 1H), 4.92 (t, *J* = 9.5 Hz, 1H), 4.58 (d, *J* = 10.0 Hz, 1H), 4.55 (s, 2H), 4.47 (dd, *J* = 10.4, 7.4 Hz, 1H), 4.36 (dd, *J* = 10.4, 6.9 Hz, 1H), 4.21 (t, *J* = 7.1 Hz, 1H), 3.75 (dt, *J* = 11.9, 3.3 Hz, 1H), 3.73 – 3.64 (m, 3H), 3.41 (s, 3H), 2.80 – 2.67 (m, 2H), 1.25 (t, *J* = 7.4 Hz, 3H); ¹³C NMR (101 MHz, CDCl₃) δ 165.14, 154.44, 143.40, 143.26, 141.46, 141.42, 138.01, 133.40, 129.98, 129.84, 128.60, 128.45, 128.03, 127.74, 127.29, 127.27, 125.17, 125.13, 120.20, 83.82, 83.28, 77.36, 75.00, 73.73, 71.89, 70.10, 69.77, 60.17, 46.88, 24.25, 15.02; [α]_D²⁰ +4.60 (c 1, CHCl₃); IR (neat) ν_{max} = 1754, 1729 cm⁻¹; *m/z* (HRMS+) 677.2191 [M + Na]⁺ (C₃₈H₃₈O₈NaS requires 677.2180).

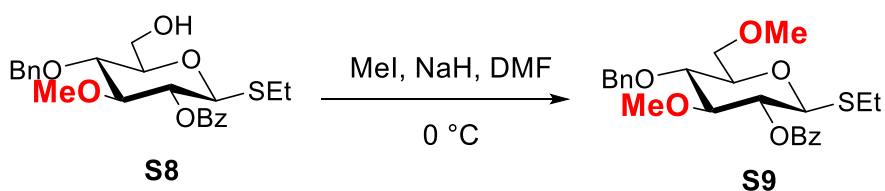
Synthesis of **S8**



Monosaccharide **S7** (19.4 g, 45.1 mmol) was dissolved in anhydrous DCM (78 mL). The solution was cooled to 0°C and a 1 M solution of BH₃ in THF (0.1 M, 180 mL, 180 mmol) was added followed by TMSOTf (4.1 mL, 22.5 mmol). The reaction was allowed to warm to rt and stirred for 4 h. The reaction was then cooled to 0 °C and quenched by addition of saturated aq. NaHCO₃. The reaction was then diluted with DCM and the aqueous layer was separated. The organic layer was extracted with saturated aq. NaHCO₃ and H₂O. The organics were dried over MgSO₄, filtered, and concentrated. The crude product was purified by column chromatography (4 hexane: 1 EtOAc) to give **S8** as a fluffy white solid (16.0 g, 82%).

Analytical data for **ethyl 2-O-benzoyl-4-O-benzyl-3-O-methyl-1-thio-β-D-glucopyranoside, S8**: ¹H NMR (400 MHz, CDCl₃) δ 8.10 (d, *J* = 7.1 Hz, 2H), 7.59 (t, *J* = 7.4 Hz, 1H), 7.47 (t, *J* = 7.7 Hz, 2H), 7.40 – 7.28 (m, 5H), 5.24 – 5.14 (m, 1H), 4.88 (d, *J* = 11.0 Hz, 1H), 4.69 (d, *J* = 11.0 Hz, 1H), 4.58 (d, *J* = 10.1 Hz, 1H), 3.91 (d, *J* = 12.0 Hz, 1H), 3.72 (dd, *J* = 14.0, 7.8 Hz, 1H), 3.65 – 3.59 (m, 2H), 3.53 (s, 3H), 3.50 – 3.41 (m, 1H), 2.71 (qd, *J* = 7.4, 2.4 Hz, 2H), 1.23 (t, *J* = 7.4 Hz, 3H); ¹³C NMR (101 MHz, CDCl₃) δ 165.35, 137.99, 133.33, 129.92, 128.60, 128.56, 128.25, 128.07, 86.55, 83.75, 79.75, 77.25, 75.10, 72.60, 62.15, 60.96, 24.24, 14.98; [α]_D²⁰ +152.44 (c 1, CHCl₃); IR (neat) ν_{max} = 3484, 1725, 1069 cm⁻¹; m/z (HRMS+) 455.1497 [M + Na]⁺ (C₂₃H₂₈O₆SNa requires 455.1499).

Synthesis of **S9**

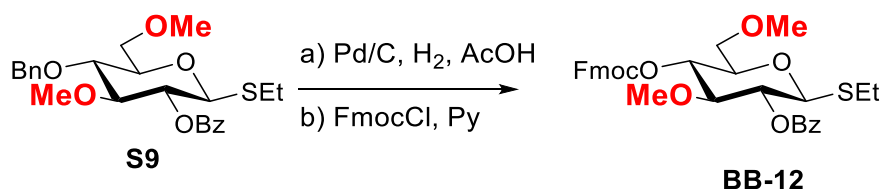


Monosaccharide **S8** (9.25 g, 21.4 mmol) was dissolved in anhydrous DMF (110 mL). The solution was cooled to 0 °C and NaH (60% by weight in mineral oil, 2.14 g, 53.5 mmol) was slowly added. After the NaH addition was complete, the reaction was stirred for 30 min at 0 °C. MeI (4.0 mL, 64.2 mmol) was added drop-wise. The reaction was allowed to warm to rt, during which time a white precipitate formed. The reaction was stirred for 1 hour at rt and then cooled back to 0 °C. Saturated aq. NH₄Cl was slowly added to quench and the reaction. The reaction was concentrated to < 30 mL under

reduced pressure and DCM (200 mL) was added. The organic layer was separated and extracted twice with H₂O. The organics were dried over MgSO₄, filtered, and concentrated to give **S9** as a light yellow gel (9.55 g, quantitative).

Analytical data for **ethyl 2-O-benzoyl-4-O-benzyl-3,6-di-O-methyl-1-thio-β-D-glucopyranoside, S9**: ¹H NMR (400 MHz, CDCl₃) δ 8.09 (d, J = 7.4 Hz, 2H), 7.58 (t, J = 6.8 Hz, 1H), 7.47 (t, J = 7.7 Hz, 2H), 7.37 – 7.28 (m, 5H), 5.20 (t, J = 9.4 Hz, 1H), 4.86 (d, J = 11.1 Hz, 1H), 4.65 (d, J = 11.0 Hz, 1H), 4.50 (d, J = 10.1 Hz, 1H), 3.69 – 3.53 (m, 5H), 3.51 (s, 3H), 3.39 (s, 3H), 2.76 – 2.65 (m, 2H), 1.20 (t, J = 7.5 Hz, 3H); ¹³C NMR (101 MHz, CDCl₃) δ 165.42, 138.28, 133.30, 129.99, 128.62, 128.24, 128.03, 86.74, 83.70, 79.53, 77.48, 75.17, 72.66, 71.51, 60.98, 59.58, 24.11, 14.89; [α]_D²⁰ +11.61 (c 1, CHCl₃); IR (neat) ν_{max} = 1728, 1094, 1071 cm⁻¹; m/z (HRMS+) 469.1666 [M + Na]⁺ (C₂₄H₃₀O₆SNa requires 469.1655).

Synthesis of **BB-12**

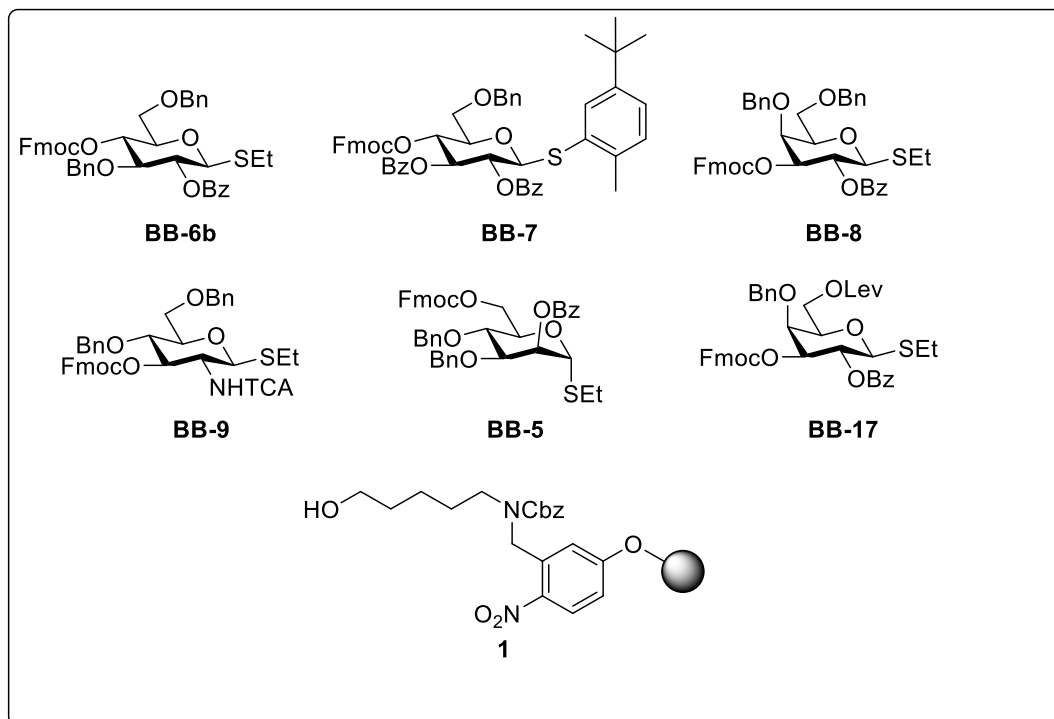


Monosaccharide **S9** (7.36 g, 17.9 mmol) was dissolved in AcOH (40 mL). 3.2 g Pd/C (40% of reactant by weight) was added. The mixture was stirred in H₂ atmosphere at 40 psi for 3 days. The crude material was filtered through celite and the filtrate was concentrated. The crude product was purified by column chromatography (hexane:EtOAc = 3:1 – 1:1) to give a clear gel. The gel was then co-evaporated with pyridine and dissolved in 22 mL of DCM. Pyridine (2 mL, 19.8 mmol) was added followed by Fmoc-Cl (3.45 g, 13.2 mmol). The yellow solution was stirred at rt until completion (3 h). The reaction was diluted with DCM and extracted with 1 M HCl, sat. aq. NaHCO₃, and H₂O. The organics were dried over MgSO₄ and concentrated. The product was purified by column chromatography (4 hexane: 1 EtOAc) to give **BB-12** as a flaky white solid (3.8 g, 40% over two steps).

Analytical data for **ethyl 2-O-benzoyl-4-O-fluorenylcarboxymethyl-3,6-di-O-methyl-1-thio-β-D-glucopyranoside, BB-12**: ¹H NMR (400 MHz, CDCl₃) δ 8.07 (dd, J = 5.1, 3.3 Hz, 2H), 7.77 (d, J = 7.5 Hz, 2H), 7.64 – 7.56 (m, 3H), 7.47 (t, J = 7.7 Hz, 2H), 7.41 (t, J = 7.5 Hz, 2H), 7.31 (tdd, J = 7.5, 2.3, 1.2 Hz, 2H), 5.26 (t, J = 9.6 Hz, 1H), 4.87 (t, J = 9.6 Hz, 1H), 4.58 – 4.43 (m, 3H), 4.28 (t, J = 7.0 Hz, 1H), 3.69 (ddd, J = 12.6, 5.8, 3.0 Hz, 2H), 3.58 – 3.52 (m, 2H), 3.40 (s, 3H), 3.35 (s, 3H), 2.78 – 2.66 (m, 2H), 1.23 (t, J = 7.5 Hz, 3H); ¹³C NMR (101 MHz, CDCl₃) δ 165.18, 154.52, 143.32,

141.47, 133.45, 130.01, 129.81, 128.63, 128.08, 127.32, 125.17, 120.25, 83.82, 83.23, 77.48, 74.81, 71.99, 71.84, 70.19, 60.21, 59.74, 46.90, 24.22, 14.87; $[\alpha]_D^{20} +12.75$ (c 1, CHCl_3); IR (neat) $\nu_{\text{max}} = 1752, 1729, 1247 \text{ cm}^{-1}$; m/z (HRMS+) 601.1870 $[\text{M} + \text{Na}]^+$ ($\text{C}_{32}\text{H}_{34}\text{O}_8\text{SNa}$ requires 601.1867)

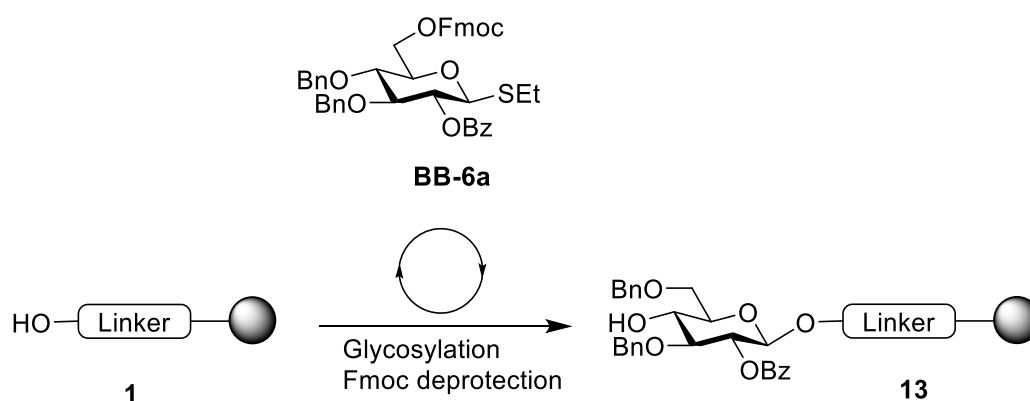
6.4. Capping test



The preparation of linker **1** and building blocks **BB-6b**, **BB-7**, **BB-8**, **BB-9**, **BB-5**, and **BB-17** was conducted according to previously established procedures.^{46, 48, 76, 118}

6.4.1. Modification of capping condition

6.4.1.1. Preparation of resin 13



Module	Conditions
A: Resin Preparation for Synthesis	
B: Acidic Wash with TMSOTf Solution	
C: Thioglycoside Glycosylation	BB-6a 6.5 equiv (-20°C 5 min, 0°C 20 min)
E: Fmoc Deprotection	

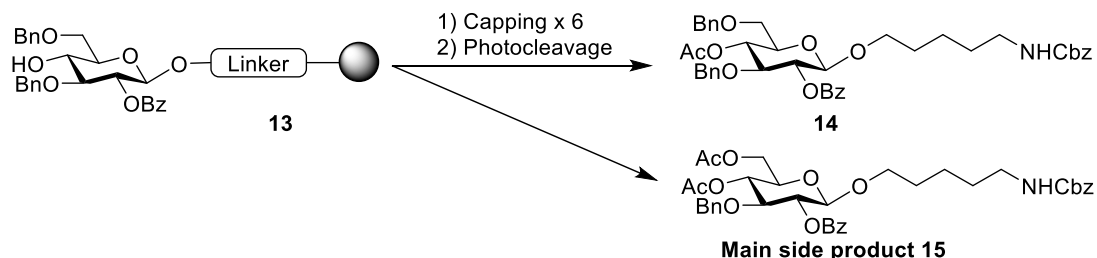
6.4.1.2. Modules for pilot synthesizer

- Module “Inject DCM” :**
 Close Valve 1(a,c), Valve 2(c);
 Open Valve 1(b), Valve 2(a,b);
 Vacuumize Valve 2(b);
 Close Valve 2(b);
 Open Valve 1(a);
 Inject Valve 1(a);
 Close Valve 1(a).
- Module “Waste out”:**
 Close Valve 1(a,c), Valve 2(c);
 Open Valve 1(b), Valve 2(a,b);
 Vacuumize Valve 2(b);
 Close Valve 2(b);
 Open Valve 2(c);
 Close Valve 2(c).
- Module “Inject reagent”:**
 Close Valve 1(a,c), Valve 2(c);
 Open Valve 1(b), Valve 2(a,b);
 Vacuumize Valve 2(b);
 Close Valve 2(b);
 Change syringe 2(b);
 Open Valve 2(b);
 Inject Valve 2(b);
 Close Valve 2(b).
- Module “Bubble”:**
 Close Valve 1(a), Valve 2(b);

Open Valve 1(b,c), Valve 2(a,c);

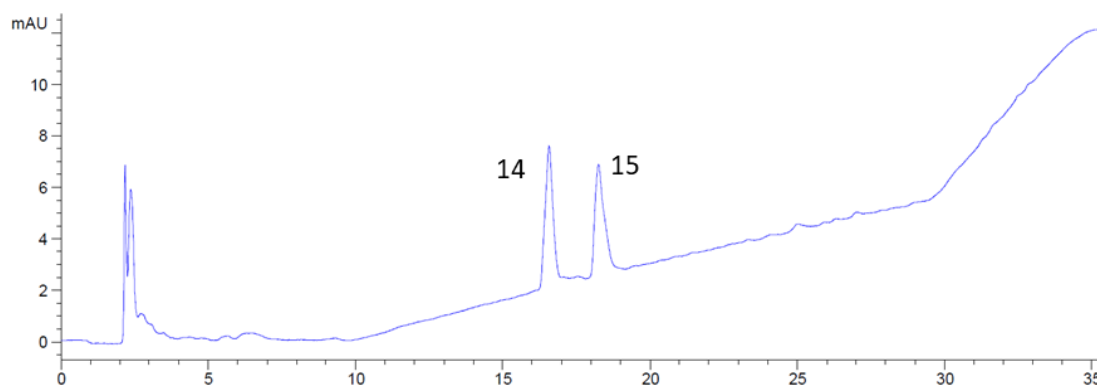
6.4.1.3. Capping with TMSOTf-Ac₂O

This is an example showing the capping test procedure, including capping reaction, photocleavage, and analysis. The other tests in **Table 2-1** were performed following the same strategy.



Resin **13** was treated with 0.1% Ac₂O and 0.01% TMSOTf in DCM for 5 min (Table 1, entry 1, Main Text). Then the solution was drained and the resin was washed with DCM for 3 times (2 mL). This procedure was repeated for six times. Cleavage from the solid support followed by analytical HPLC (**Method A0**) gave two major peaks. Purification using preparative HPLC afforded the desired compound **14** (**Method B**, $t_R = 12.1$ min) and the 6-acetylated compound **15** (**Method B**, $t_R = 14.6$ min).

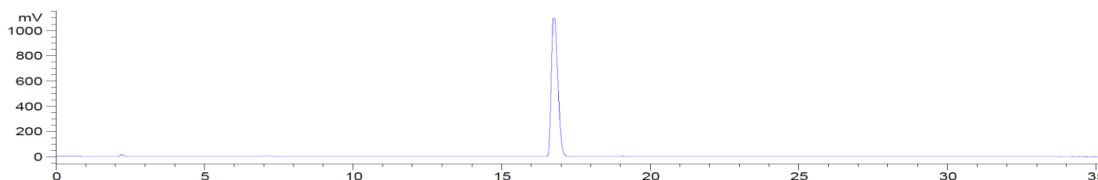
Analytical HPLC (**Method A0**, $\lambda = 280$ nm) of crude products (**14** and **15**).



Analytical data for **N-benzyloxycarbonyl-5-amino-pentyl 4-O-acetyl-2-O-benzoyl-3,6-O-benzyl- β -D-glucopyranoside (14)**: ¹H NMR (400 MHz, CDCl₃) δ 8.05 – 7.97 (m, 2H), 7.60 – 7.51 (m, 1H), 7.43 (t, $J = 7.7$ Hz, 2H), 7.37 – 7.30 (m, 9H), 7.30 – 7.27 (m, 1H), 7.20 – 7.14 (m, 3H), 7.11 (dd, $J = 6.8, 3.0$ Hz, 2H), 5.29 (dd, $J = 9.5, 7.9$ Hz, 1H), 5.11 (t, $J = 9.4$ Hz, 1H), 5.07 (s, 2H), 4.62 – 4.48 (m, 6H), 3.93 – 3.79 (m, 2H), 3.65 (dt, $J = 9.5, 4.6$ Hz, 1H), 3.59 (dd, $J = 4.6, 1.6$ Hz, 2H), 3.43 (q, $J = 7.2$ Hz, 1H), 2.90 (q, $J = 6.7$ Hz, 2H), 1.89 (s, 3H), 1.45 (s, 2H), 1.29 (d, $J = 7.4$ Hz, 2H), 1.18 (q, $J = 7.6$ Hz, 2H); ¹³C NMR (101 MHz, CDCl₃) δ 169.76, 165.06, 156.39, 137.91, 137.74,

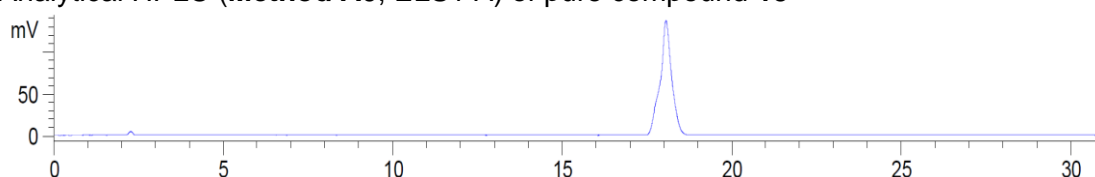
136.79, 133.39, 129.90, 129.85, 128.65, 128.59, 128.52, 128.41, 128.26, 128.21, 128.03, 127.89, 127.82, 101.26, 79.88, 77.48, 77.36, 77.16, 76.84, 73.80, 73.76, 73.46, 71.04, 69.86, 69.81, 66.65, 40.92, 29.50, 29.03, 23.21, 21.00; m/z (HRMS+) 748.3093 [M + Na]⁺ (C₄₂H₄₇NO₁₀Na requires 748.3098).

Analytical HPLC (**Method A0**, ELS1 A) of pure compound **14**

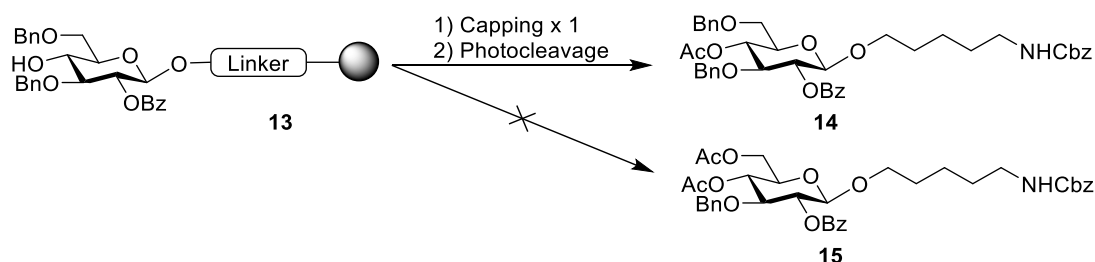


Analytical data for **N-benzyloxycarbonyl-5-amino-pentyl 4,6-di-O-acetyl-2-O-benzoyl-3-O-benzyl-β-D-glucopyranoside (15)**: ¹H NMR (700 MHz, CDCl₃) δ 8.01 (d, *J* = 7.7 Hz, 2H), 7.56 (t, *J* = 7.5 Hz, 1H), 7.43 (t, *J* = 7.6 Hz, 2H), 7.36 (d, *J* = 5.3 Hz, 4H), 7.32 (d, *J* = 6.3 Hz, 1H), 7.17 (d, *J* = 4.9 Hz, 3H), 7.14 – 7.10 (m, 2H), 5.30 (t, *J* = 8.7 Hz, 1H), 5.19 (t, *J* = 9.6 Hz, 1H), 5.07 (s, 2H), 4.60 (d, *J* = 11.3 Hz, 2H), 4.58 – 4.52 (m, 2H), 4.24 (dd, *J* = 12.3, 5.1 Hz, 1H), 4.18 – 4.13 (m, 1H), 3.86 (q, *J* = 9.4, 7.9 Hz, 2H), 3.65 (dd, *J* = 9.2, 4.5 Hz, 1H), 3.43 (d, *J* = 8.8 Hz, 1H), 2.93 (q, *J* = 6.9 Hz, 2H), 2.09 (d, *J* = 1.3 Hz, 3H), 1.98 (s, 3H), 1.52 (s, 2H), 1.47 (d, *J* = 6.3 Hz, 2H), 1.35 – 1.28 (m, 2H); ¹³C NMR (176 MHz, CDCl₃) δ 171.00, 169.51, 165.04, 156.44, 137.70, 136.85, 133.44, 129.91, 129.86, 128.66, 128.63, 128.45, 128.25, 128.22, 128.02, 127.89, 101.39, 79.86, 77.34, 77.16, 76.98, 73.88, 73.47, 72.32, 69.90, 69.86, 66.67, 62.54, 40.96, 29.53, 29.03, 23.21, 20.97, 20.95; m/z (HRMS+) 700.2728 [M + Na]⁺ (C₃₇H₄₃NO₁₁Na requires 700.2734).

Analytical HPLC (**Method A0**, ELS1 A) of pure compound **15**

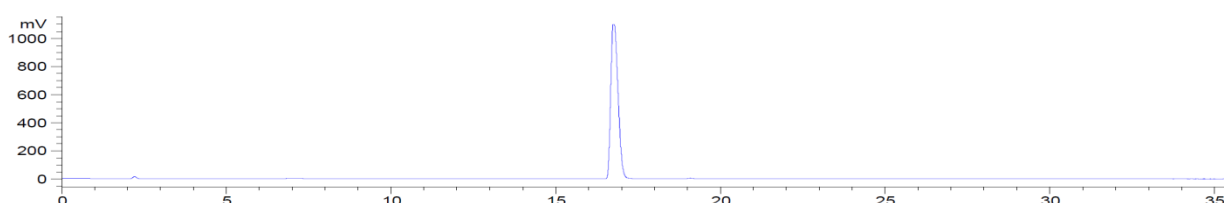


6.4.1.4. Capping with MsOH - Completion test

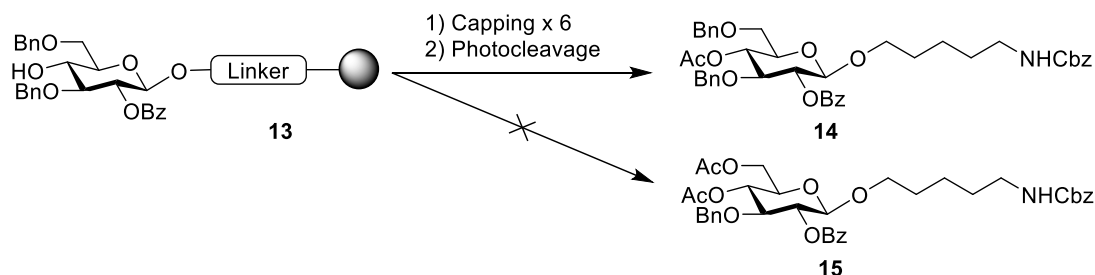


Resin **13** was treated with 10% Ac₂O and 2% MsOH in DCM for 20 min. Then the solution was drained and the resin was washed with DCM for three times (2 mL). Cleavage from the solid support followed by analytical HPLC (**Method A0**) gave one single peak. Purification using preparative HPLC (**Method B**) afforded compound **14**, which indicates the completion of capping after only one cycle of capping.

Analytical HPLC (**Method A0**, ELS1 A) of crude products (**14**)

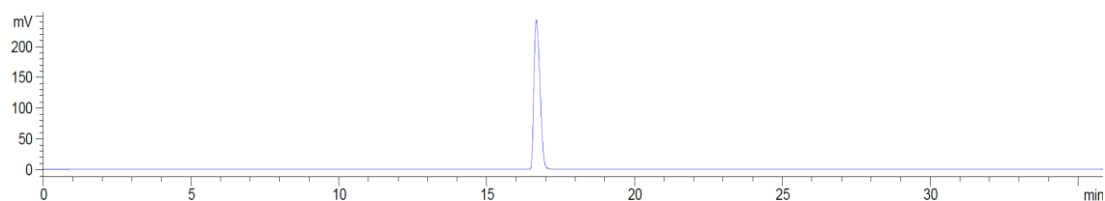


6.4.1.5. Capping with MsOH - Stability test



Resin **13** was treated with 10% Ac₂O and 2% MsOH in DCM for 20 min. Then the solution was drained and the resin was washed with DCM for 3 times (2 mL). This procedure was repeated for six times followed by photocleavage. Cleavage from the solid support followed by analytical HPLC (**Method A0**) gave one single peak. Purification using preparative HPLC (**Method B**) afforded compound **14**, which indicates the stability of 6-Bn even after six cycles of capping.

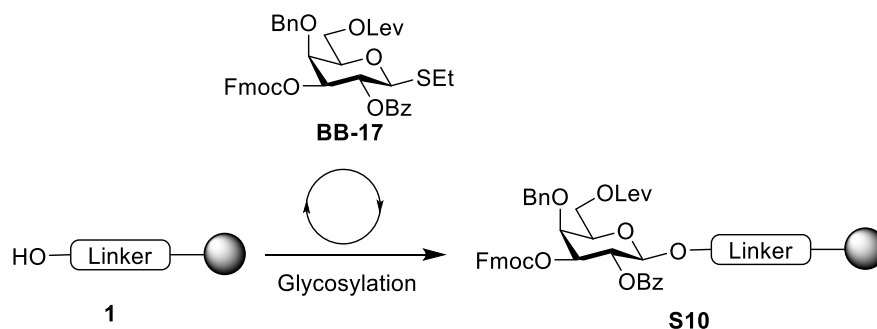
Analytical HPLC (**Method A0**, ELS1 A) of crude products (**14**).



6.4.2. Test of stability of Fmoc, Lev and TCA groups

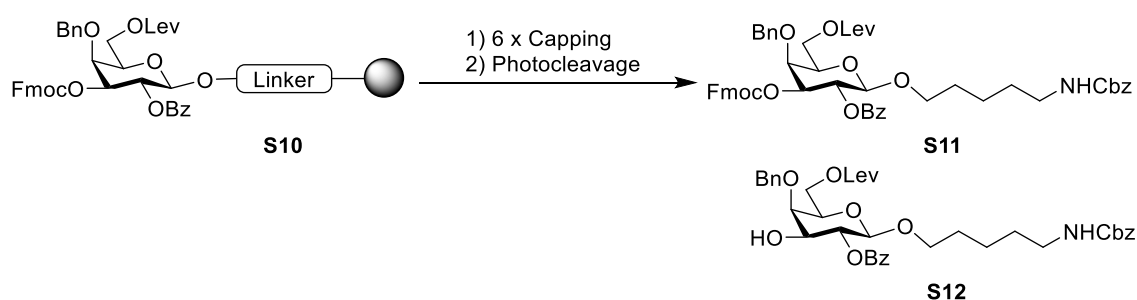
6.4.2.1. Direct stability test for Fmoc and Lev

Preparation of resin S3 containing Lev and Fmoc groups



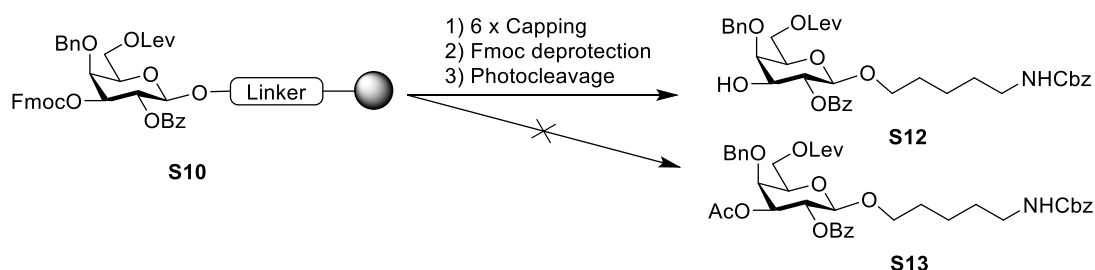
Module	Conditions
A: Resin Preparation for Synthesis	
B: Acidic Wash with TMSOTf Solution	
C: Thioglycoside Glycosylation	BB-17 , 6.5 equiv (-20°C 5 min, 0°C 20 min)

Capping six times followed by photocleavage



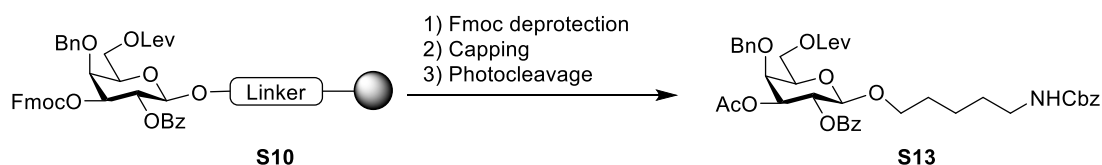
At first, I tried to test the stability of Fmoc group in a direct way. Resin **S3** was capped for six times followed by photocleavage. However, compound **S5** was also obtained. As observed in our laboratory, Fmoc group is not stable during the photocleavage process, which may be the reason of the partial deprotection of Fmoc group. Based on this hypothesis, we tested the stability of Fmoc group again in an indirect way.

6.4.2.2. Indirect stability test for Fmoc



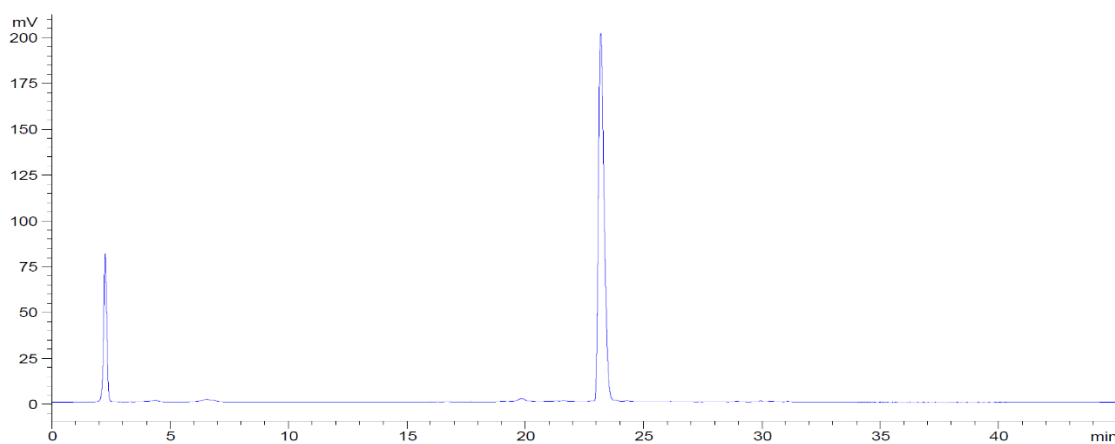
Capping was repeated for six times on resin **S10** before the deprotection of Fmoc group. Cleavage from the solid support followed by analytical HPLC (**Method A0**,

ELS1 A) gave one single peak (See below). Purification using preparative HPLC afforded compound **S12** (**Method B**, $t_R = 24.0$ min) with free 3-hydroxyl group and no 3-acetylated compound **S13** or Lev-protected product were observed. If the Fmoc group was not stable under capping condition and the free hydroxyl group was released during the capping process, theoretically this hydroxyl group should have been capped by the acetyl group giving the corresponding 3-acetylated compound **S13**.



Capping after the deprotection of Fmoc group on resin **S10** was also conducted. Cleavage from the solid support followed by purification using preparative HPLC afforded 3-acetylated compound **S1** (**Method B**, $t_R = 19.3$ min). This result confirms that the hydroxyl group released by the deprotection of Fmoc could be acetylated in capping condition.

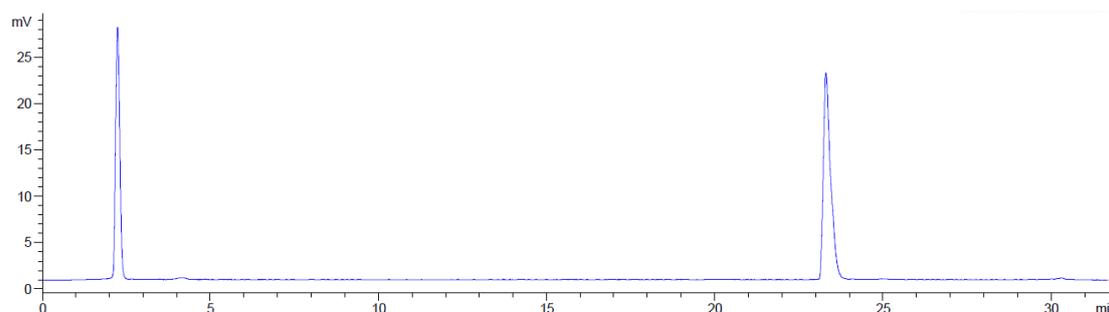
Analytical HPLC (**Method A0**, ELS1 A) of crude products (**S13**)



Analytical data for **N-benzyloxycarbonyl-5-amino-pentyl 2-O-benzoyl-4-O-benzyl-6-O-levulinyl- β -D-galactopyranoside (S12)**: ^1H NMR (700 MHz, CDCl_3) δ 8.04 (d, $J = 7.8$ Hz, 2H), 7.55 (t, $J = 7.5$ Hz, 1H), 7.43 (t, $J = 7.6$ Hz, 2H), 7.40 – 7.33 (m, 7H), 7.32 – 7.28 (m, 3H), 5.27 – 5.22 (m, 1H), 5.10 (s, 1H), 5.06 (s, 1H), 4.80 (q, $J = 11.7$ Hz, 2H), 4.60 (s, 1H), 4.51 (d, $J = 7.8$ Hz, 1H), 4.36 (dd, $J = 11.2, 6.5$ Hz, 1H), 4.19 (dd, $J = 11.2, 6.5$ Hz, 1H), 3.88 (d, $J = 3.5$ Hz, 2H), 3.83 (d, $J = 9.8$ Hz, 1H), 3.73 (t, $J = 6.5$ Hz, 1H), 3.48 (q, $J = 7.2$ Hz, 1H), 2.96 (q, $J = 6.3, 5.8$ Hz, 2H), 2.75 (t, $J = 6.4$ Hz, 2H), 2.58 (s, 1H), 2.55 (t, $J = 6.3$ Hz, 2H), 2.19 (s, 3H), 1.51 – 1.43 (m, 2H), 1.35 (d, $J = 6.9$ Hz, 2H), 1.27 – 1.22 (m, 2H); ^{13}C NMR (176 MHz, CDCl_3) δ 206.58, 172.53,

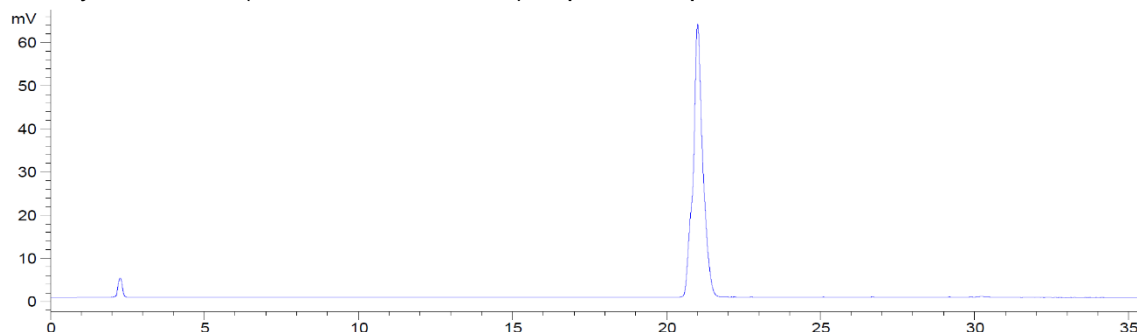
166.98, 156.42, 137.88, 133.48, 129.96, 129.90, 128.75, 128.65, 128.57, 128.35, 128.25, 128.22, 101.19, 77.34, 77.16, 76.98, 75.82, 74.32, 73.61, 72.34, 69.78, 66.66, 62.90, 41.01, 38.05, 29.97, 29.62, 29.14, 27.98, 23.31; m/z (HRMS+) 714.2888 [M + Na]⁺ (C₃₈H₄₅NO₁₁Na requires 714.2890).

Analytical HPLC (**Method A0**, ELS1 A) of pure compound **S12**



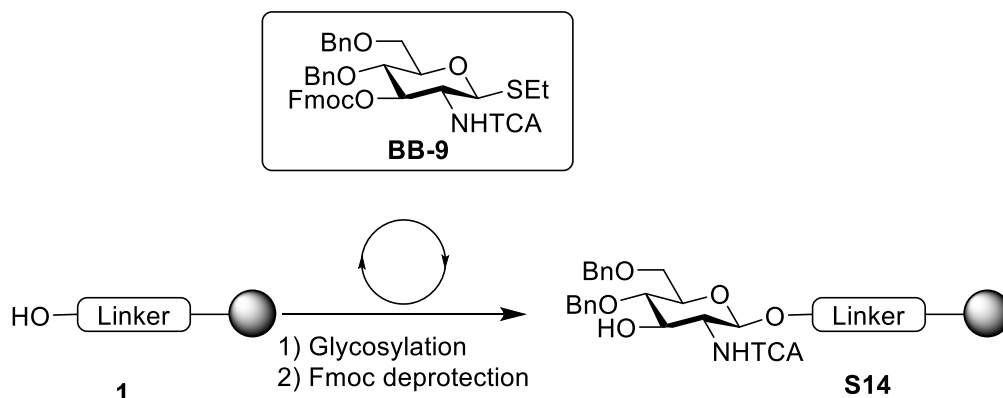
Analytical data for **N-benzyloxycarbonyl-5-amino-pentyl 3-O-acetyl-2-O-benzoyl-4-O-benzyl-6-O-levulinyl-β-D-galactopyranoside (S13)**: ¹H NMR (700 MHz, CDCl₃) δ 8.00 (d, *J* = 7.7 Hz, 2H), 7.55 (t, *J* = 7.4 Hz, 1H), 7.42 (t, *J* = 7.7 Hz, 2H), 7.35 (d, *J* = 3.9 Hz, 8H), 7.30 (dq, *J* = 8.9, 4.5, 3.8 Hz, 2H), 5.61 (dd, *J* = 10.4, 7.9 Hz, 1H), 5.16 (dd, *J* = 10.4, 3.0 Hz, 1H), 5.06 (s, 2H), 4.78 (d, *J* = 11.7 Hz, 1H), 4.59 (d, *J* = 11.6 Hz, 2H), 4.55 (d, *J* = 7.9 Hz, 1H), 4.31 (dd, *J* = 11.1, 6.2 Hz, 1H), 4.15 (dd, *J* = 11.1, 6.6 Hz, 1H), 3.97 (d, *J* = 3.0 Hz, 1H), 3.87 (dt, *J* = 11.3, 5.9 Hz, 1H), 3.78 (t, *J* = 6.5 Hz, 1H), 3.47 – 3.41 (m, 1H), 2.93 (q, *J* = 6.8 Hz, 2H), 2.73 (t, *J* = 6.5 Hz, 2H), 2.52 (t, *J* = 6.4 Hz, 2H), 2.18 (s, 3H), 1.93 (s, 3H), 1.52 (s, 1H), 1.48 – 1.43 (m, 1H), 1.32 (q, *J* = 7.3 Hz, 2H), 1.19 (dt, *J* = 21.7, 6.4 Hz, 2H); ¹³C NMR (176 MHz, CDCl₃) δ 206.55, 172.44, 170.60, 165.34, 137.65, 136.89, 133.40, 129.84, 128.64, 128.60, 128.50, 128.25, 128.19, 128.12, 101.62, 77.34, 77.16, 76.98, 75.15, 73.86, 72.32, 70.36, 69.80, 66.64, 62.63, 40.97, 38.02, 29.97, 29.55, 29.04, 27.92, 23.22, 20.93; m/z (HRMS+) 756.2996 [M + Na]⁺ (C₄₀H₄₇NO₁₂Na requires 756.2997).

Analytical HPLC (**Method A0**, ELS1 A) of pure compound **S13**



6.4.2.3. Stability test of TCA group

Preparation of resin S14 containing TCA group



Module

Conditions

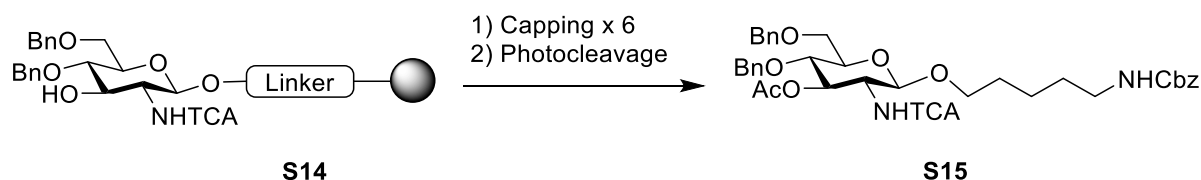
A: Resin Preparation for Synthesis

B: Acidic Wash with TMSOTf Solution

C: Thioglycoside Glycosylation **BB-9**, 6.5 equiv (-20°C 5 min, 0°C 20 min)

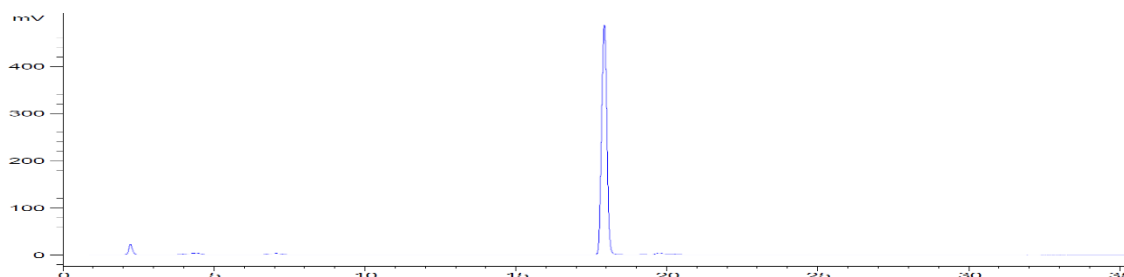
E: Fmoc Deprotection

Capping six times followed by photocleavage



Cleavage from the solid support followed by analytical HPLC (**Method A0**) gave one single peak. Purification using preparative HPLC afforded compound **S15** (**Method B**, $t_R = 14.5$ min), which indicates the stability of TCA group even after 6 cycles of capping.

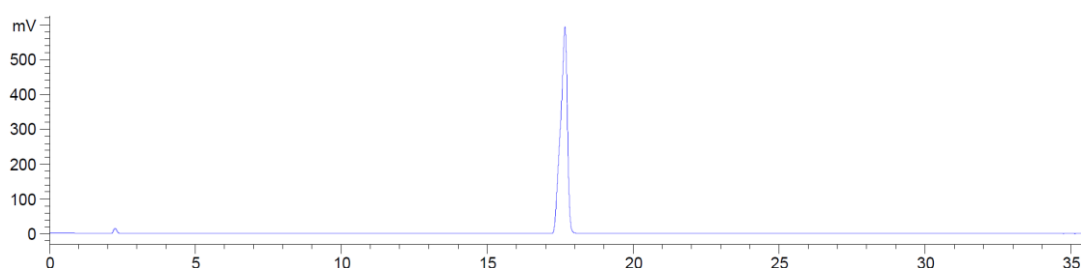
Analytical HPLC (**Method A0**, ELS1 A) of crude products (**S15**)



Analytical data for **N-benzyloxycarbonyl-5-amino-pentyl 3-acetyl-4,6-di-O-benzyl-2-deoxy-2-trichloroacetamido-β-D-glucopyranoside (S15)** ^1H NMR (700 MHz,

CDCl₃) δ 7.37 – 7.33 (m, 8H), 7.30 (tt, *J* = 11.7, 5.3 Hz, 5H), 7.18 – 7.14 (m, 2H), 6.82 (d, *J* = 9.1 Hz, 1H), 5.19 (dd, *J* = 10.7, 9.0 Hz, 1H), 5.09 (s, 2H), 4.81 (s, 1H), 4.65 (d, *J* = 12.1 Hz, 1H), 4.59 – 4.52 (m, 3H), 4.46 (d, *J* = 8.1 Hz, 1H), 3.97 (q, *J* = 9.2 Hz, 1H), 3.89 (dt, *J* = 9.7, 6.1 Hz, 1H), 3.77 (t, *J* = 9.3 Hz, 1H), 3.74 (d, *J* = 3.1 Hz, 2H), 3.53 (dt, *J* = 9.6, 3.2 Hz, 1H), 3.46 – 3.42 (m, 1H), 3.20 – 3.10 (m, *J* = 6.8 Hz, 2H), 1.94 (s, 3H), 1.60 (d, *J* = 7.1 Hz, 1H), 1.48 (q, *J* = 7.3 Hz, 2H), 1.42 – 1.30 (m, 3H); ¹³C NMR (176 MHz, CDCl₃) δ 171.25, 162.06, 156.57, 138.07, 137.80, 136.85, 128.65, 128.63, 128.58, 128.25, 128.19, 128.10, 128.03, 127.95, 127.93, 101.19, 92.61, 77.34, 77.16, 76.98, 75.92, 75.34, 74.87, 74.19, 73.75, 69.70, 68.54, 66.71, 56.18, 41.04, 29.68, 29.08, 23.31, 20.90; *m/z* (HRMS+) 765.2109 [M + Na]⁺ (C₃₇H₄₃Cl₃N₂O₉Na requires 765.2112).

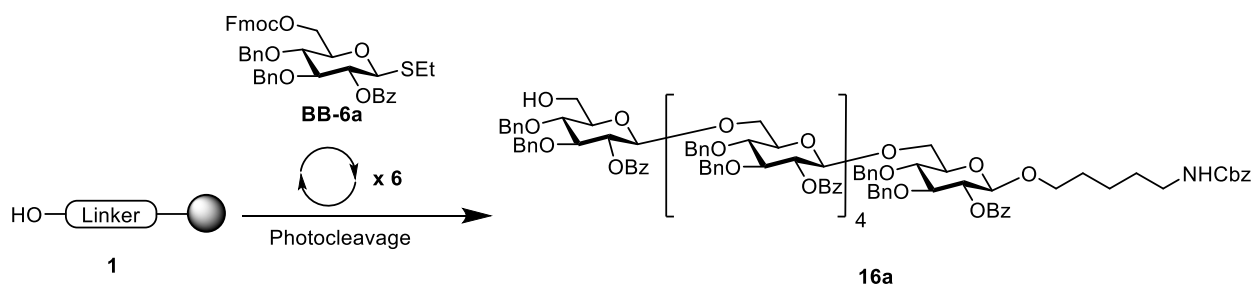
Analytical HPLC (**Method A0**, ELS1 A) of pure compound **S15**



6.5. Synthesis of oligosaccharides

6.5.1. AGA synthesis of 1,6-hexaglucose

6.5.1.1. Synthesis without capping

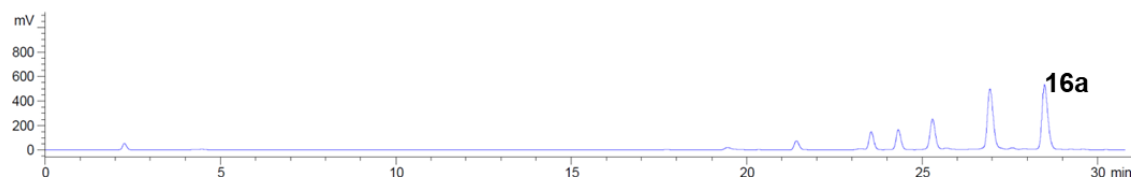


Module	Conditions	
A: Resin Preparation for Synthesis		
6 {	B: Acidic Wash with TMSOTf Solution	
	C: Thioglycoside Glycosylation	BB-6a , 2.5 equiv (-20°C 5 min, 0°C 20 min)
	E: Fmoc Deprotection	

G: Cleavage from Solid Support

Cleavage from the solid support was performed. Yield was calculated by 280 nm signal of analytical HPLC (14%, see below).

Analytical HPLC (**Method A0**, ELS1 A) of crude products (**16a** and deletion sequences)

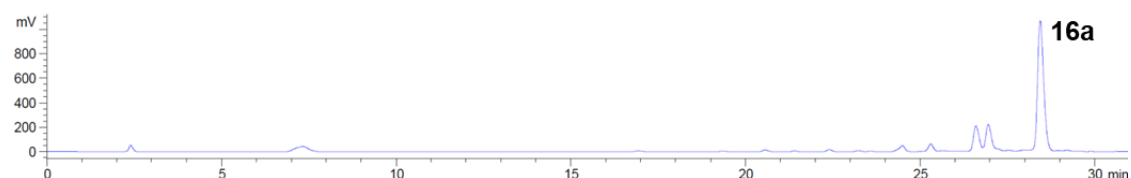


6.5.1.2. Synthesis with capping

Module	Conditions	
A: Resin Preparation for Synthesis		
6 {	B: Acidic Wash with TMSOTf Solution	
	C: Thioglycoside Glycosylation	BB-6a , 2.5 equiv (-20°C 5 min, 0°C 20 min)
	D: Capping	
	E: Fmoc Deprotection	
	G: Cleavage from Solid Support	
J: Purification	Method B	

Cleavage from the solid support followed by purification using preparative HPLC afforded compound **16a** (**Method B**, $t_R = 36.2$ min). Yield was calculated by 280 nm signal of analytical HPLC (30%).

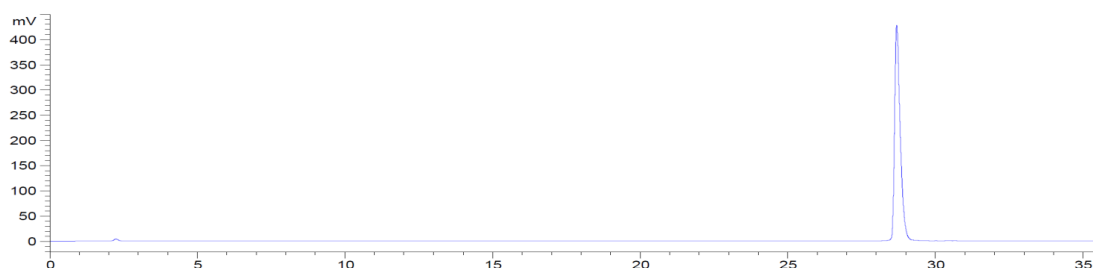
Analytical HPLC (**Method A0**, ELS1 A) of crude products (**16a** and deletion sequences)



Analytical data for 1,6-hexagluose (**16a**): $^1\text{H NMR}$ (700 MHz, CDCl_3) δ 8.24 (d, $J = 7.8$ Hz, 2H), 8.22 – 8.15 (m, 6H), 8.08 (t, $J = 8.4$ Hz, 4H), 7.56 (t, $J = 7.5$ Hz, 2H), 7.44 (ddd, $J = 31.3, 16.2, 7.9$ Hz, 8H), 7.36 – 7.26 (m, 18H), 7.22 (d, $J = 7.4$ Hz, 2H), 7.17 – 7.13 (m, 5H), 7.12 – 7.06 (m, 5H), 7.06 – 6.98 (m, 28H), 6.97 – 6.93 (m, 10H), 6.88

– 6.79 (m, 5H), 5.50 (t, $J = 8.7$ Hz, 1H), 5.43 (p, $J = 9.3$ Hz, 3H), 5.33 (t, $J = 8.7$ Hz, 1H), 5.24 (t, $J = 8.7$ Hz, 1H), 5.12 – 4.99 (m, 2H), 4.85 (t, $J = 9.5$ Hz, 2H), 4.78 (t, $J = 10.1$ Hz, 3H), 4.75 – 4.71 (m, 2H), 4.71 – 4.61 (m, 11H), 4.53 (d, $J = 7.9$ Hz, 1H), 4.51 – 4.44 (m, 3H), 4.39 (ddd, $J = 21.8, 10.3, 5.1$ Hz, 5H), 4.27 (d, $J = 10.0$ Hz, 1H), 4.17 (s, 1H), 4.12 (d, $J = 11.6$ Hz, 1H), 4.09 – 4.01 (m, 4H), 3.97 (t, $J = 9.1$ Hz, 1H), 3.91 (t, $J = 9.0$ Hz, 3H), 3.87 (q, $J = 8.5$ Hz, 4H), 3.80 (q, $J = 9.7, 9.3$ Hz, 2H), 3.75 (dd, $J = 12.1, 7.3$ Hz, 6H), 3.72 – 3.63 (m, 4H), 3.58 (t, $J = 11.0$ Hz, 3H), 3.39 (dtt, $J = 25.8, 17.0, 7.1$ Hz, 6H), 3.30 (t, $J = 9.4$ Hz, 1H), 2.88 (q, $J = 6.7$ Hz, 2H), 1.45 (d, $J = 7.0$ Hz, 1H), 1.37 (dt, $J = 13.3, 7.0$ Hz, 1H), 1.33 – 1.27 (m, 2H), 1.22 (t, $J = 7.2$ Hz, 1H), 1.12 (d, $J = 12.9$ Hz, 1H); ^{13}C NMR (176 MHz, CDCl_3) δ 165.58, 165.52, 165.27, 165.21, 164.90, 164.87, 156.52, 138.38, 138.34, 138.31, 138.17, 138.06, 138.01, 137.91, 137.90, 137.83, 137.74, 137.56, 137.14, 133.45, 133.41, 133.10, 132.89, 132.79, 130.52, 130.49, 130.44, 130.36, 130.33, 130.25, 130.23, 130.19, 130.11, 129.92, 129.90, 128.72, 128.70, 128.66, 128.58, 128.58, 128.48, 128.43, 128.40, 128.37, 128.33, 128.30, 128.25, 128.20, 128.19, 128.16, 128.15, 128.11, 128.05, 128.03, 128.01, 127.99, 127.96, 127.87, 127.85, 127.80, 127.76, 127.73, 127.69, 127.52, 127.49, 127.37, 127.35, 102.83, 102.60, 102.07, 101.91, 101.63, 100.80, 84.28, 84.07, 83.96, 83.48, 82.98, 82.79, 80.18, 79.93, 79.83, 79.77, 79.28, 78.17, 77.34, 77.16, 76.98, 75.85, 75.60, 75.47, 75.43, 75.40, 75.35, 75.26, 75.22, 75.12, 75.05, 74.98, 74.67, 74.60, 74.50, 74.21, 74.19, 74.17, 73.62, 73.40, 70.77, 70.37, 69.52, 66.41, 61.70, 41.11, 29.36, 28.91, 23.27; m/z (HRMS+) 2937.178 $[\text{M} + \text{Na}]^+$ ($\text{C}_{175}\text{H}_{175}\text{NO}_{39}\text{Na}$ requires 2937.164).

Analytical HPLC (**Method A0**, ELS1 A) of pure compound **16a** (8.91 mg in 5.0 mL solvent)

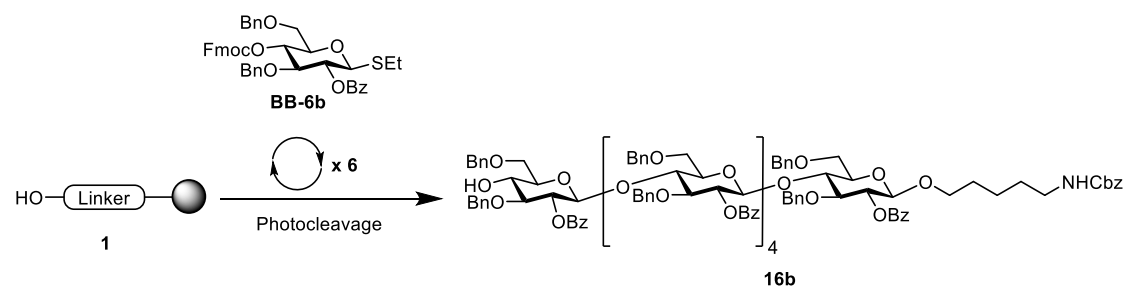


6.5.1.3. Determination of yield using analytical HPLC

Pure compound **16a** (8.91 mg) was dissolved in a 1:1 mixture of hexane and ethyl acetate (5.0 mL). This solution (30 μL) was injected into analytical HPLC (**Method A0**) and the result used as a standard. The yield was calculated by comparison of the area of the product signal (at 280 nm) with the standard.

Sample	Integral area (280 nm)	Yield (%)
8.91 mg pure compound 16a in 5.0 mL	3276	-
Crude product of synthesis 6.5.1.1 in 4.0 mL	2338	14
Crude product of synthesis 6.5.1.2 in 4.0 mL	4978	30

6.5.2. AGA synthesis of 1,4-hexaglucose

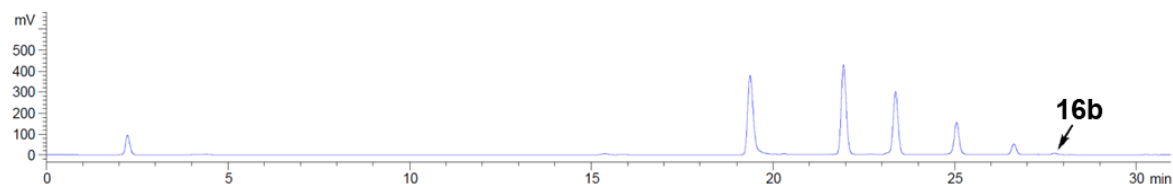


6.5.2.1. Synthesis without capping

Module	Conditions
A: Resin Preparation for Synthesis	
6 {	B: Acidic Wash with TMSOTf Solution
	C: Thioglycoside Glycosylation BB-6b , 2.5 equiv (-20°C 5 min, 0°C 20 min)
	E: Fmoc Deprotection
	G: Cleavage from Solid Support

Cleavage from the solid support was performed. Yield was calculated by 280 nm signal of analytical HPLC (1%).

Analytical HPLC (**Method A0**, ELS1 A) of crude products (**16b** and deletion sequences)

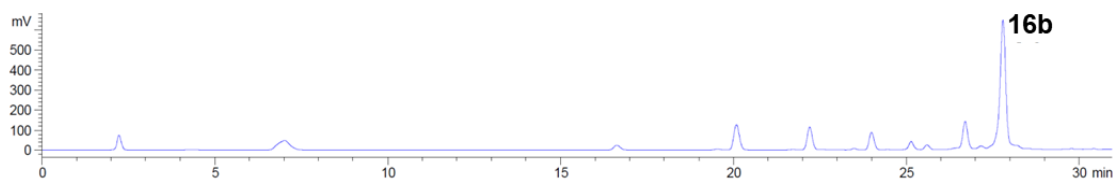


6.5.2.2. Synthesis with capping

Module	Conditions
A: Resin Preparation for Synthesis	
6 {	B: Acidic Wash with TMSOTf Solution
	C: Thioglycoside Glycosylation BB-6b , 2.5 equiv (-20°C 5 min, 0°C 20 min)
	D: Capping
	E: Fmoc Deprotection
	G: Cleavage from Solid Support
J: Purification	Method B

Cleavage from the solid support followed by purification using preparative HPLC afforded compound **16b** (**Method B**, $t_R = 34.8$ min). Yield was calculated by 280 nm signal of analytical HPLC (15%).

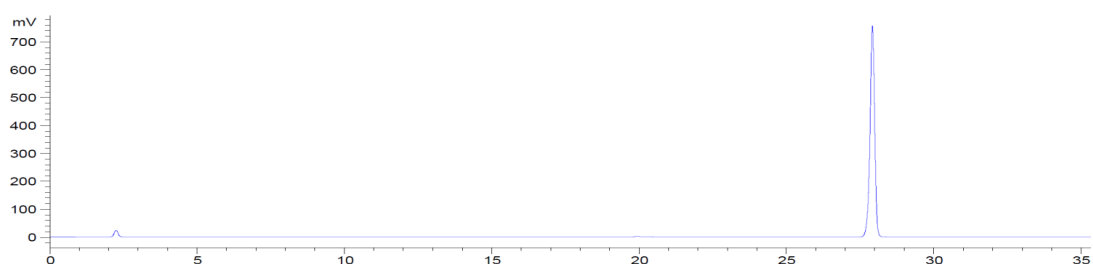
Analytical HPLC (**Method A0**, ELS1 A) of crude products (**16b** and deletion sequences)



Analytical data for 1,4-hexaglucose (**16b**): ^1H NMR (700 MHz, CDCl_3) δ 7.89 (dd, $J = 17.6, 7.7$ Hz, 4H), 7.82 (q, $J = 8.6$ Hz, 8H), 7.59 (dq, $J = 16.0, 7.9$ Hz, 4H), 7.54 (t, $J = 7.5$ Hz, 1H), 7.48 (t, $J = 7.4$ Hz, 1H), 7.47 – 7.43 (m, 4H), 7.43 – 7.37 (m, 6H), 7.33 (p, $J = 7.7$ Hz, 10H), 7.27 (d, $J = 8.7$ Hz, 4H), 7.24 (d, $J = 7.5$ Hz, 3H), 7.18 – 7.01 (m, 38H), 6.99 – 6.86 (m, 12H), 5.23 (t, $J = 8.8$ Hz, 1H), 5.17 (t, $J = 8.8$ Hz, 1H), 5.13 – 5.00 (m, 6H), 4.94 – 4.80 (m, 5H), 4.73 (d, $J = 11.6$ Hz, 1H), 4.67 (d, $J = 11.6$ Hz, 1H), 4.63 (d, $J = 8.1$ Hz, 1H), 4.54 (dtd, $J = 28.5, 16.3, 14.1, 9.6$ Hz, 8H), 4.45 – 4.33 (m, 6H), 4.32 – 4.22 (m, 4H), 4.15 (dd, $J = 19.8, 12.0$ Hz, 2H), 4.08 (t, $J = 9.3$ Hz, 1H), 4.05 – 3.87 (m, 7H), 3.79 (t, $J = 9.1$ Hz, 1H), 3.70 (dd, $J = 10.7, 5.5$ Hz, 1H), 3.63 – 3.55 (m, 2H), 3.55 – 3.46 (m, 5H), 3.46 – 3.38 (m, 4H), 3.31 (ddt, $J = 36.1, 18.2, 9.1$ Hz, 8H), 3.23 (p, $J = 8.1, 7.3$ Hz, 1H), 3.10 (d, $J = 9.7$ Hz, 1H), 3.05 (s, 1H), 2.88 (d, $J = 9.9$ Hz, 1H), 2.84 (d, $J = 6.0$ Hz, 2H), 2.78 (q, $J = 10.4, 9.6$ Hz, 3H), 1.40 (q, $J = 9.1, 7.0$ Hz, 1H), 1.35 – 1.31 (m, 1H), 1.23 – 1.17 (m, 2H), 1.13 – 1.03 (m, 2H); ^{13}C NMR (176 MHz, CDCl_3) δ 165.18, 165.08, 164.98, 164.95, 156.36, 138.97, 138.93, 138.86, 138.79, 138.30, 138.25, 137.88, 137.82, 137.78, 137.67, 136.86, 133.50, 133.34, 133.30,

133.28, 133.13, 133.00, 130.20, 129.94, 129.86, 129.83, 129.81, 129.73, 128.70, 128.68, 128.66, 128.63, 128.53, 128.43, 128.37, 128.35, 128.34, 128.32, 128.30, 128.27, 128.25, 128.21, 128.19, 128.16, 128.06, 128.01, 127.99, 127.98, 127.96, 127.93, 127.91, 127.81, 127.74, 127.21, 127.06, 127.04, 101.27, 100.22, 100.15, 99.98, 99.98, 99.92, 82.00, 80.24, 80.08, 80.05, 77.34, 77.16, 76.98, 76.27, 76.15, 76.04, 74.77, 74.70, 74.65, 74.54, 74.48, 74.46, 74.42, 74.35, 74.19, 73.91, 73.72, 73.62, 73.57, 73.55, 73.49, 73.47, 73.44, 73.23, 73.16, 71.29, 69.48, 67.58, 67.48, 67.19, 66.59, 40.91, 29.45, 28.93, 23.16; m/z (HRMS+) 2937.173 [M + Na]⁺ (C₁₇₅H₁₇₅NO₃₉Na requires 2937.164).

Analytical HPLC (**Method A0**, ELS1 A) of pure compound **16b** (7.13 mg in 5.0 mL solvent)

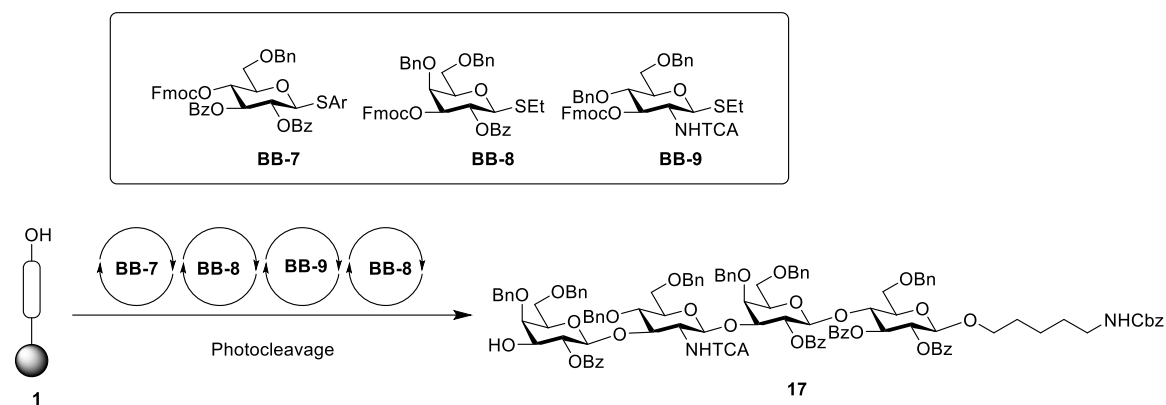


6.5.2.3. Determination of yield using analytical HPLC

Pure compound **16b** (7.13 mg) was dissolved in a 1:1 mixture of hexane and ethyl acetate (5.0 mL). This solution (30 μ L) was injected into analytical HPLC (**Method A0**) and the result used as a standard. The yield was calculated by comparison of the area of the product signal (at 280 nm) with the standard.

Sample	Integral area (280 nm)	Yield (%)
7.13 mg pure compound 16b in 5.0 mL	2503	-
Crude product of synthesis 6.5.2.1 in 4.0 mL	140	1
Crude product of synthesis 6.5.2.2 in 4.0 mL	2371	15

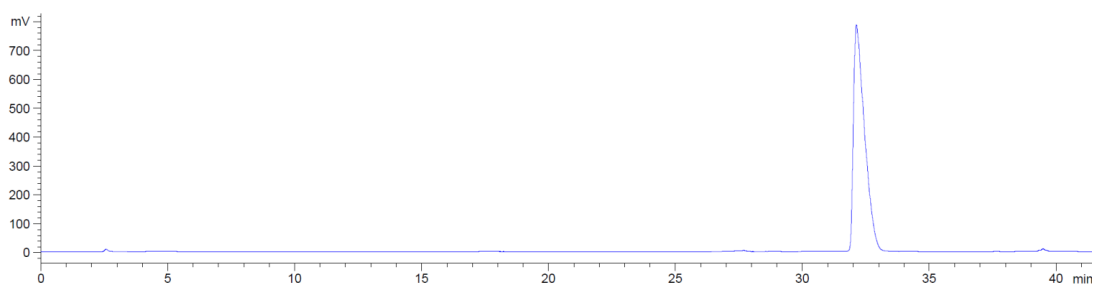
6.5.3. AGA synthesis of Lc4



Module	Conditions
A: Resin Preparation for Synthesis	
B: Acidic Wash with TMSOTf Solution	
C: Thioglycoside Glycosylation	BB-7 , 6.5 equiv (-20°C 5 min, 0°C 5 min)
D: Capping	
E: Fmoc Deprotection	
B: Acidic Wash with TMSOTf Solution	
C: Thioglycoside Glycosylation	BB-8 , 6.5 equiv (-20°C 5 min, 0°C 5 min)
D: Capping	
E: Fmoc Deprotection	
B: Acidic Wash with TMSOTf Solution	
C: Thioglycoside Glycosylation	BB-9 , 6.5 equiv (-20°C 5 min, 0°C 5 min)
D: Capping	
E: Fmoc Deprotection	
B: Acidic Wash with TMSOTf Solution	
C: Thioglycoside Glycosylation	BB-8 , 6.5 equiv (-20°C 5 min, 0°C 5 min)
D: Capping	
E: Fmoc Deprotection	
G: Cleavage from Solid Support	
J: Purification	Method B

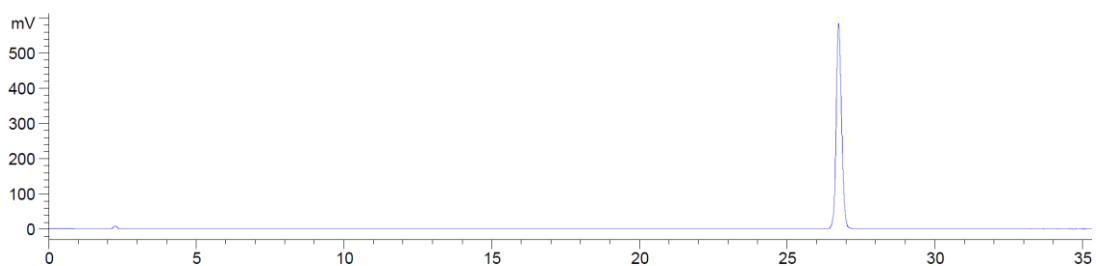
Cleavage from the solid support followed by purification using preparative HPLC (**Method B**, $t_R = 32.4$ min) afforded compound **17** (17.5 mg, 67%).

Analytical HPLC (**Method A0**, ELS1 A) of crude products (**17**)



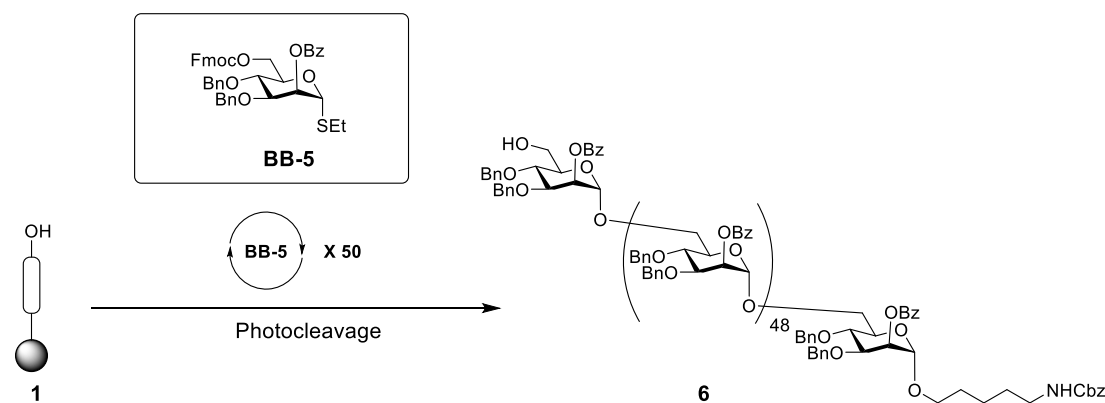
Analytical data for **Lc4 (17)**: $^1\text{H NMR}$ (400 MHz, CDCl_3) δ 8.04 (d, $J = 7.8$ Hz, 2H), 7.90 (d, $J = 7.8$ Hz, 2H), 7.84 (d, $J = 7.8$ Hz, 4H), 7.48 (dt, $J = 16.1, 7.5$ Hz, 4H), 7.35 (td, $J = 13.9, 13.2, 6.8$ Hz, 19H), 7.27 – 7.18 (m, 17H), 7.13 (p, $J = 7.4$ Hz, 12H), 6.63 (d, $J = 7.6$ Hz, 1H), 5.52 (t, $J = 9.4$ Hz, 1H), 5.36 – 5.26 (m, 2H), 5.22 (t, $J = 9.0$ Hz, 1H), 5.05 (s, 2H), 4.90 (d, $J = 10.3$ Hz, 1H), 4.74 (d, $J = 8.3$ Hz, 1H), 4.71 – 4.58 (m, 4H), 4.54 (d, $J = 11.9$ Hz, 2H), 4.47 (d, $J = 8.7$ Hz, 1H), 4.36 (ddt, $J = 30.2, 19.8, 9.5$ Hz, 8H), 4.21 (d, $J = 12.3$ Hz, 1H), 4.04 (q, $J = 11.6$ Hz, 3H), 3.88 (d, $J = 4.7$ Hz, 2H), 3.81 – 3.67 (m, 3H), 3.62 (dd, $J = 10.7, 4.8$ Hz, 2H), 3.52 (dd, $J = 13.8, 6.9$ Hz, 3H), 3.43 (d, $J = 8.6$ Hz, 3H), 3.32 (dd, $J = 14.3, 9.4$ Hz, 4H), 3.07 (q, $J = 8.3$ Hz, 1H), 2.86 (tt, $J = 15.4, 6.4$ Hz, 3H), 2.73 (t, $J = 8.8$ Hz, 1H), 2.40 (d, $J = 10.0$ Hz, 1H), 1.44 (ddq, $J = 20.8, 14.1, 7.0$ Hz, 2H), 1.34 – 1.27 (m, 2H), 1.13 (dt, $J = 14.6, 7.1$ Hz, 2H); m/z (HRMS+) 2092.719 $[\text{M} + \text{NH}_4]^+$ ($\text{C}_{120}\text{H}_{117}\text{Cl}_3\text{N}_3\text{O}_{27}$ requires 2092.725).

Analytical HPLC (**Method A0**, ELS1 A) of pure Lc4 (**17**)



6.5.4. AGA synthesis of 50-mer polymannoside

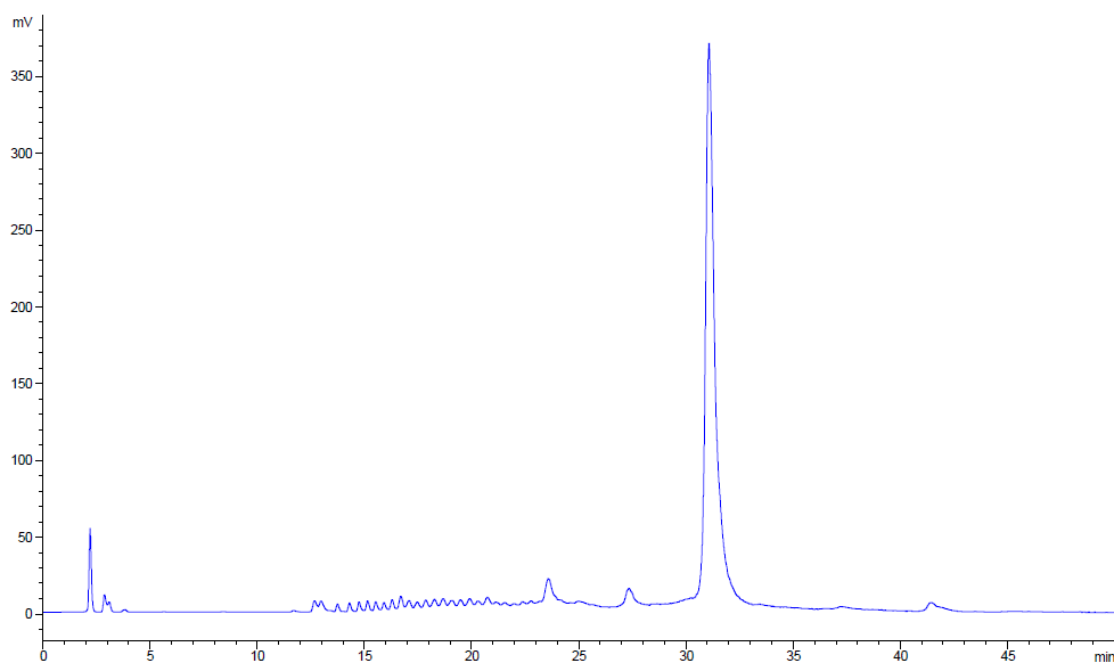
6.5.4.1. Synthesis of 6



Module	Conditions
A: Resin Preparation for Synthesis	
50 {	B: Acidic Wash with TMSOTf Solution
	C: Thioglycoside Glycosylation BB-5 , 6.5 equiv (-20°C 5 min, 0°C 5 min)
	D: Capping
	E: Fmoc Deprotection
G: Cleavage from Solid Support	
J: Purification	Method B50

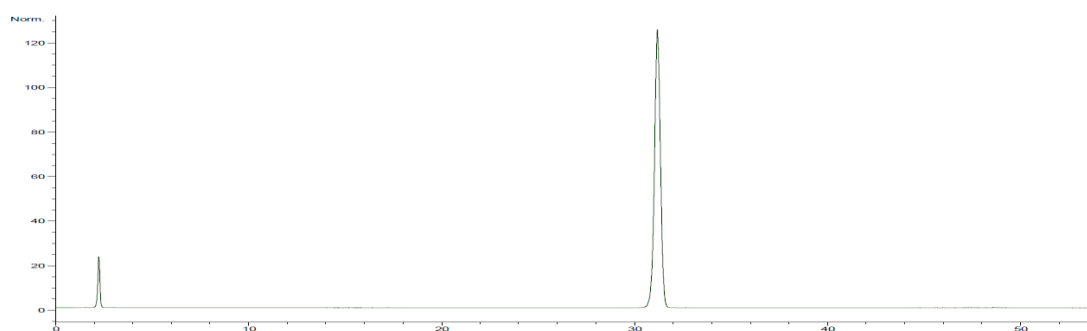
Cleavage from the solid support followed by purification using preparative HPLC (**Method B50**, $t_R = 67.3$ min) afforded desired compound **6** (64 mg, 22%).

Analytical HPLC (**Method A50**, 280 nm) of crude products (**6**).

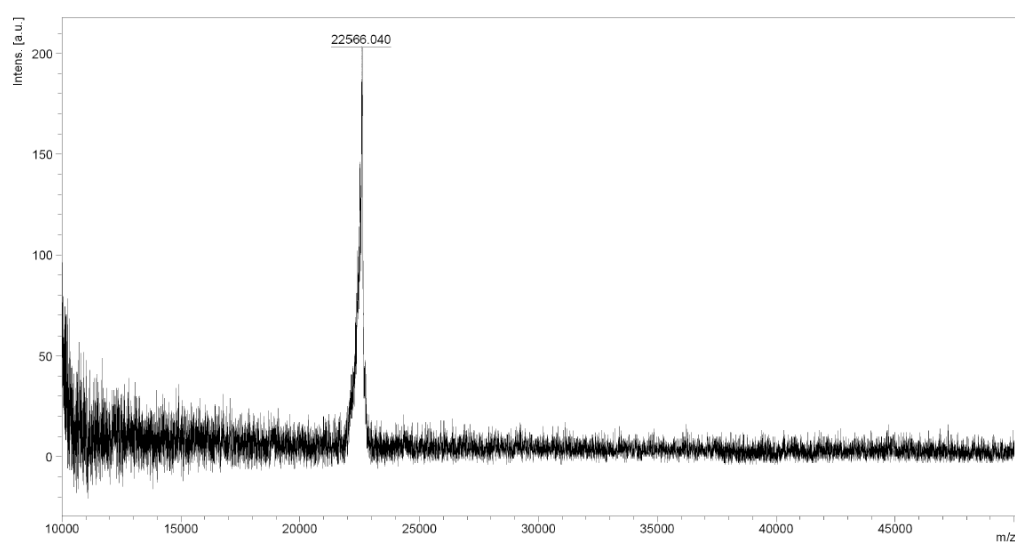


Analytical data for **50-mer polymannose (1→6) (6)**: ^1H NMR (700 MHz, CDCl_3) δ 8.21 – 8.17 (m, 100H), 7.54 – 7.48 (m, 125H), 7.25 – 7.06 (m, 530H), 5.87 – 5.84 (m, 50H), 5.06 (s, 50H), 4.89 (d, $J = 11.5$ Hz, 50H), 4.80 (d, $J = 10.9$ Hz, 50H), 4.44 (d, $J = 10.9$ Hz, 50H), 4.36 (t, $J = 11.2$ Hz, 50H), 4.04 (dd, $J = 9.3, 3.1$ Hz, 50H), 3.99 (t, $J = 9.5$ Hz, 50H), 3.75 (d, $J = 10.6$ Hz, 50H), 3.60 (d, $J = 9.7$ Hz, 50H), 3.45 (d, $J = 11.1$ Hz, 50H), 3.15 – 3.13 (m, 2H), 1.58 – 1.52 (m, 2H), 1.49 (m, 2H), 1.35 – 1.31 (m, 2H); ^{13}C NMR (176 MHz, CDCl_3) δ 165.54, 138.53, 138.48, 137.51, 133.31, 130.01, 129.86, 128.65, 128.49, 128.36, 128.34, 128.14, 128.01, 127.68, 127.64, 127.37, 127.30, 127.24, 127.09, 127.01, 98.55, 78.20, 77.21, 77.02, 76.84, 75.18, 75.00, 73.71, 71.30, 70.90, 68.39, 65.73, 29.72; m/z (MS+) 22566 $[\text{M} + \text{Na}]^+$ ($\text{C}_{1363}\text{H}_{1319}\text{NO}_{303}\text{Na}$ requires 22569).

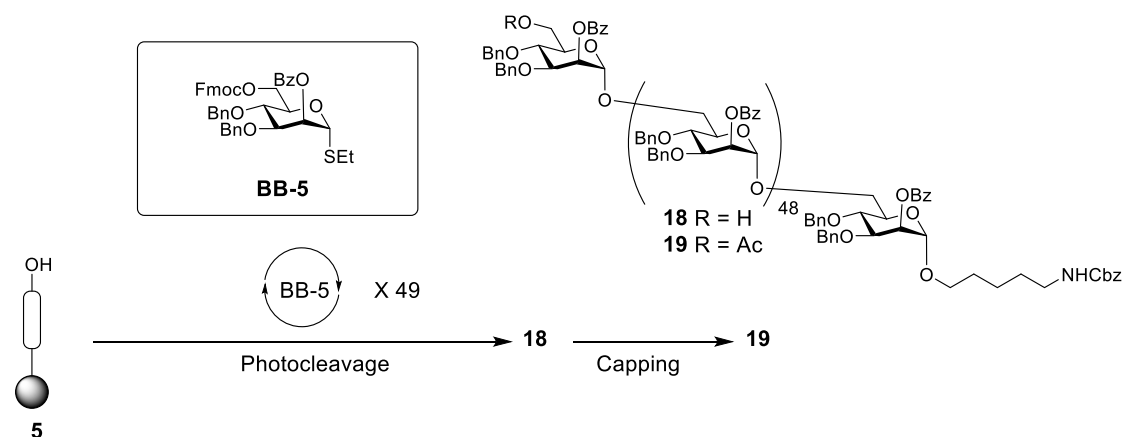
Analytical HPLC (**Method A50**, 280 nm) of pure 50-mer polymannoside (**6**)



MALDI-TOF spectrum of 50-mer polymannoside (**6**)

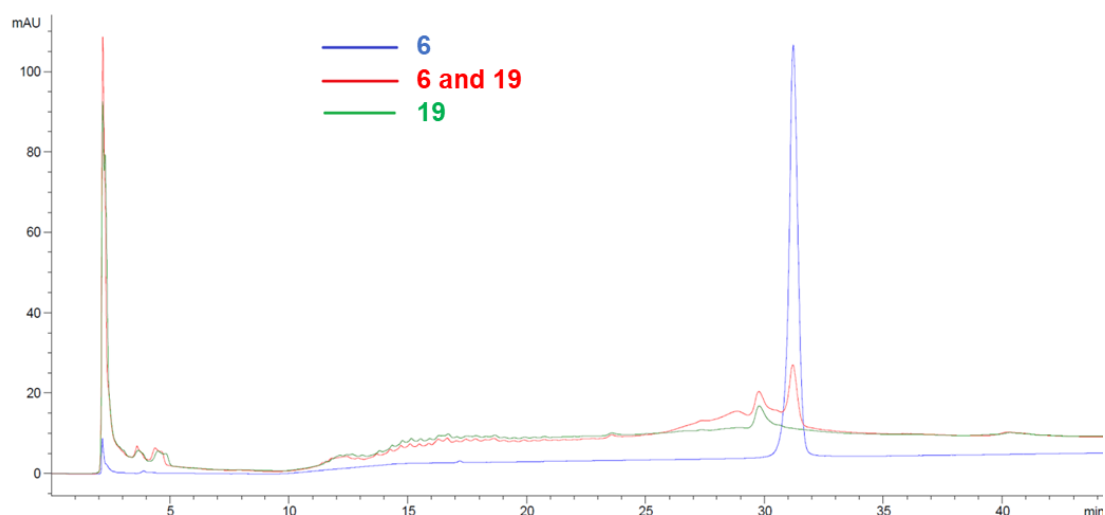


6.5.4.2. Effect of capping on purification

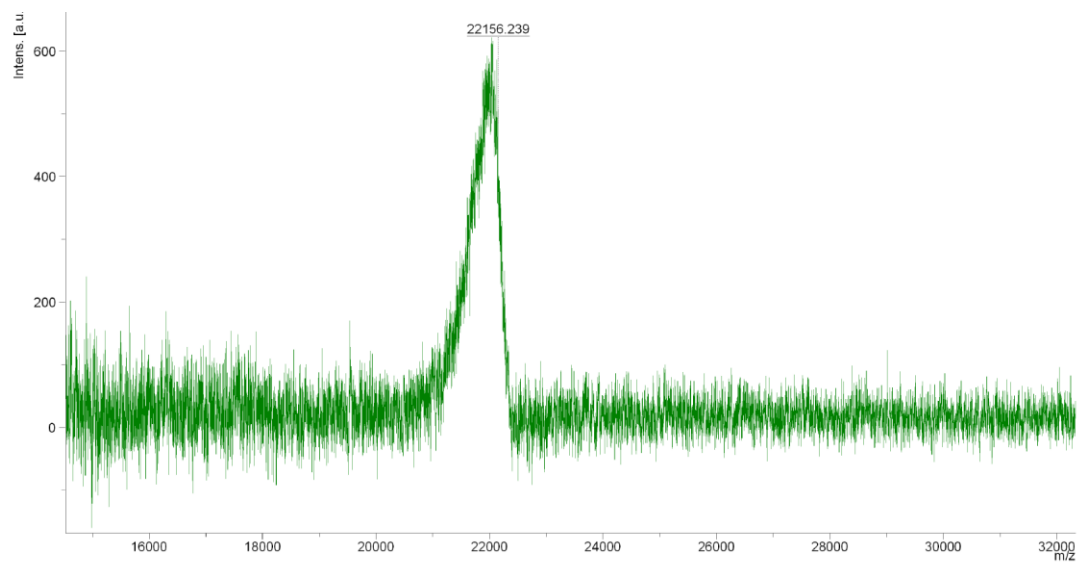


During the synthesis of the synthesis of **6**, after the 49th deprotection of the Fmoc group, trace amounts of resin were taken out of the reaction vessel. Part of this resin was photocleaved to give 49-mer with free hydroxyl group **18**. The rest of the resin was treated with capping condition to afford capped 49-mer **19**. Both crude products were analyzed by analytical HPLC (**Method A50**) and the retention times of **6** and **19** were compared. To give a clearer picture of how capping generates better separation between desired 50-mer and side-product 49-mer, **6** and **19** were mixed and analyzed by analytical HPLC. The peaks of the compounds show baseline separation (See below, red line).

Effect of capping on purification (**Method A50**, 280 nm)



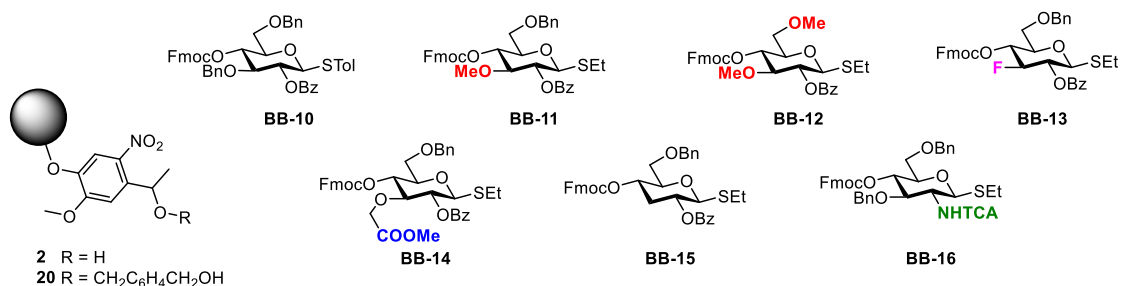
MALDI-TOF spectrum of capped 49-mer polymannose (**19**)



m/z (MS+) 22156 [M + Na]⁺ (C₁₃₃₈H₁₂₉₅NO₂₉₈Na requires 22164).

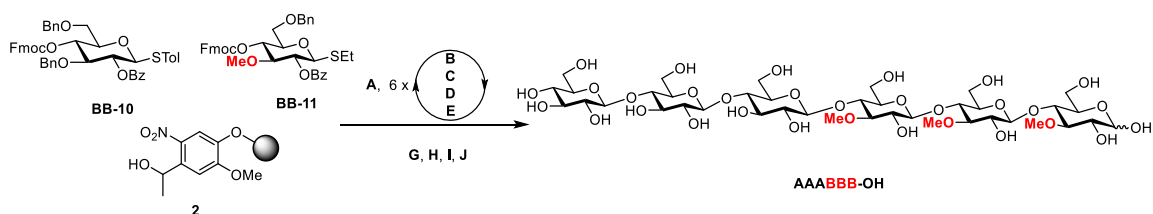
6.5.5. AGA synthesis of methylated cellulose hexamers

Building block **BB-10** and **BB-16** are commercially available. The synthesis of the linkers and other building blocks is the cooperative effort of several scientists (**Table 3-1**). The synthetic details are reported in literature⁹².



The description of general materials, methods and modules for AGA is given in **6.2**. Following final purification, all deprotected products were lyophilized on a Christ Alpha 2-4 LD plus freeze dryer prior to characterization.

6.5.5.1. Synthesis of AAABBB-OH



Module	Conditions
A: Resin Preparation for Synthesis	
3	B: Acidic Wash with TMSOTf Solution
	C: Thioglycoside Glycosylation BB-11, 6.5 equiv. (-20°C 5 min, 0°C 5 min)
	D: Capping
	E: Fmoc Deprotection
3	B: Acidic Wash with TMSOTf Solution
	C: Thioglycoside Glycosylation BB-10, 6.5 equiv. (-20°C 5 min, 0°C 5 min)
	D: Capping
	E: Fmoc Deprotection
F: On-resin Methanolysis	

G: Cleavage from Solid Support

I: Hydrogenolysis

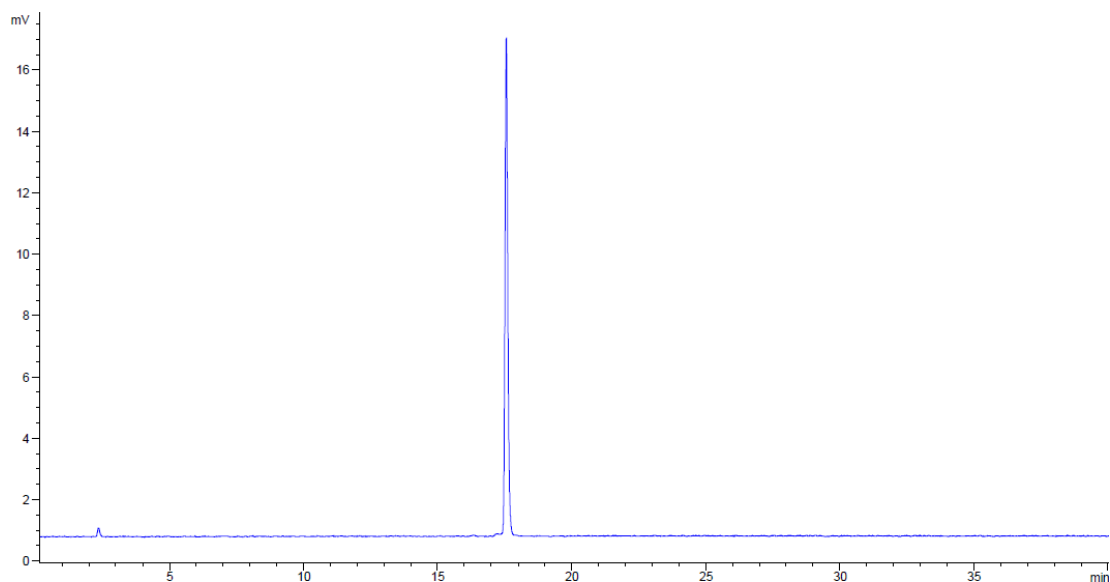
J: Purification

Method M

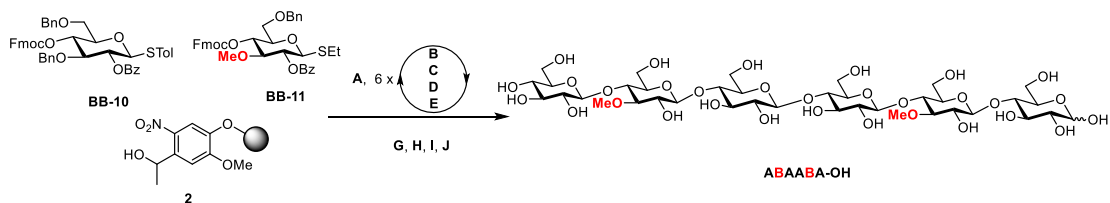
Automated synthesis and global deprotection and purification afforded **AAABBB-OH** as white solid (6.3 mg, 49% overall yield).

Analytical data for **AAABBB-OH**: ^1H NMR (600 MHz, D_2O) δ 5.23 (d, $J = 3.6$ Hz, 0.42 H, $\alpha\text{-H1}$), 4.67 (d, $J = 7.8$ Hz, 0.58 H, $\beta\text{-H1}$), 4.59 – 4.50 (m, 5H), 4.01 (ddt, $J = 12.2, 10.1, 2.2$ Hz, 4H), 3.98 – 3.91 (m, 2H), 3.90 – 3.84 (m, 4H), 3.84 – 3.78 (m, 4H), 3.75 (dd, $J = 12.5, 5.9$ Hz, 1H), 3.68 (td, $J = 8.0, 7.4, 4.1$ Hz, 3H), 3.65 (t, $J = 4.8$ Hz, 2H), 3.62 (s, 3H), 3.62 (s, 6H), 3.60 – 3.51 (m, 5H), 3.51 – 3.44 (m, 5H), 3.44 – 3.40 (m, 2H), 3.40 – 3.30 (m, 4H); ^{13}C NMR (151 MHz, D_2O) δ 102.48, 102.27, 102.22, 102.18, 102.17, 95.72 ($\beta\text{-C1}$), 91.75 ($\alpha\text{-C1}$), 83.51, 83.44, 83.43, 83.39, 80.95, 78.34, 78.32, 75.91, 75.58, 75.49, 75.47, 75.44, 75.40, 74.99, 74.97, 74.96, 74.77, 74.74, 74.12, 73.98, 73.29, 73.18, 73.07, 72.87, 72.69, 72.68, 72.64, 70.69, 70.49, 69.37, 60.49, 59.94, 59.91, 59.87, 59.82, 59.50, 59.11, 59.08, 59.03, 59.00; $[\alpha]_{\text{D}}^{20} +14.62$ (c 0.3, H_2O); IR (neat) $\nu_{\text{max}} = 3340, 2927, 1649, 1032$ cm^{-1} ; m/z (HRMS+) 1055.364 $[\text{M} + \text{Na}]^+$ ($\text{C}_{39}\text{H}_{68}\text{NaO}_{31}$ requires 1055.364).

RP-HPLC of **AAABBB-OH** (ELSD trace, **Method C**, $t_{\text{R}} = 17.6$ min)



6.5.5.2. Synthesis of ABAABA-OH



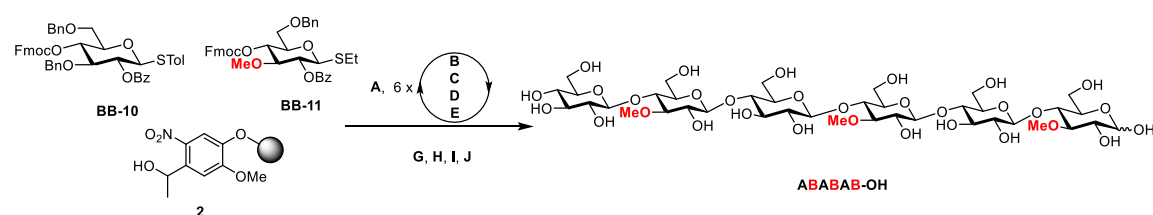
Module	Conditions
A: Resin Preparation for Synthesis	
2	B: Acidic Wash with TMSOTf Solution
	C: Thioglycoside Glycosylation BB-10 , 6.5 equiv. (-20°C 5 min, 0°C 5 min)
	D: Capping
	E: Fmoc Deprotection
2	B: Acidic Wash with TMSOTf Solution
	C: Thioglycoside Glycosylation BB-11 , 6.5 equiv. (-20°C 5 min, 0°C 5 min)
	D: Capping
	E: Fmoc Deprotection
2	B: Acidic Wash with TMSOTf Solution
	C: Thioglycoside Glycosylation BB-10 , 6.5 equiv. (-20°C 5 min, 0°C 5 min)
	D: Capping
	E: Fmoc Deprotection
F: On-resin Methanolysis	
G: Cleavage from Solid Support	
I: Hydrogenolysis	
J: Purification	Method M

Automated synthesis and global deprotection and purification afforded **ABAABA-OH** as white solid (4.9 mg, 39% overall yield).

Analytical data for **ABAABA-OH**: ¹H NMR (600 MHz, D₂O) δ 5.24 (d, *J* = 3.8 Hz, 0.38 H, α-H1), 4.67 (d, *J* = 7.9 Hz, 0.62 H, β-H1), 4.58 – 4.51 (m, 5H), 4.00 (ddt, *J* = 11.7, 6.5, 3.4 Hz, 4H), 3.97 – 3.93 (m, 1H), 3.92 (d, *J* = 1.8 Hz, 1H), 3.89 (d, *J* = 9.1 Hz, 1H), 3.87 – 3.81 (m, 6H), 3.79 (td, *J* = 12.0, 4.8 Hz, 2H), 3.68 (dq, *J* = 12.4, 3.8 Hz, 4H), 3.66 – 3.64 (m, 3H), 3.63 (s, 3H), 3.62 (s, 3H), 3.61 – 3.57 (m, 3H), 3.53 – 3.42 (m,

7H), 3.40 – 3.34 (m, 2H), 3.34 – 3.28 (m, 2H); ¹³C NMR (151 MHz, D₂O) δ 102.32, 102.28, 102.28, 102.25, 102.19, 95.68 (β-C1), 91.74 (α-C1), 83.21, 83.19, 78.55, 78.41, 78.32, 78.20, 75.96, 75.60, 75.41, 75.34, 75.01, 74.97, 74.77, 74.73, 74.71, 74.18, 74.11, 73.94, 73.81, 73.50, 73.26, 72.87, 72.29, 72.24, 71.24, 71.15, 70.03, 69.41, 60.67, 59.96, 59.93, 59.82, 59.76, 59.16, 59.07, 59.02; [α]_D²⁰ +13.27 (c 0.75, H₂O); IR (neat) ν_{max} = 3360, 2876, 1021 cm⁻¹; m/z (HRMS+) 1041.347 [M + Na]⁺ (C₃₈H₆₆NaO₃₁ requires 1041.348).

6.5.5.3. Synthesis of ABABAB-OH



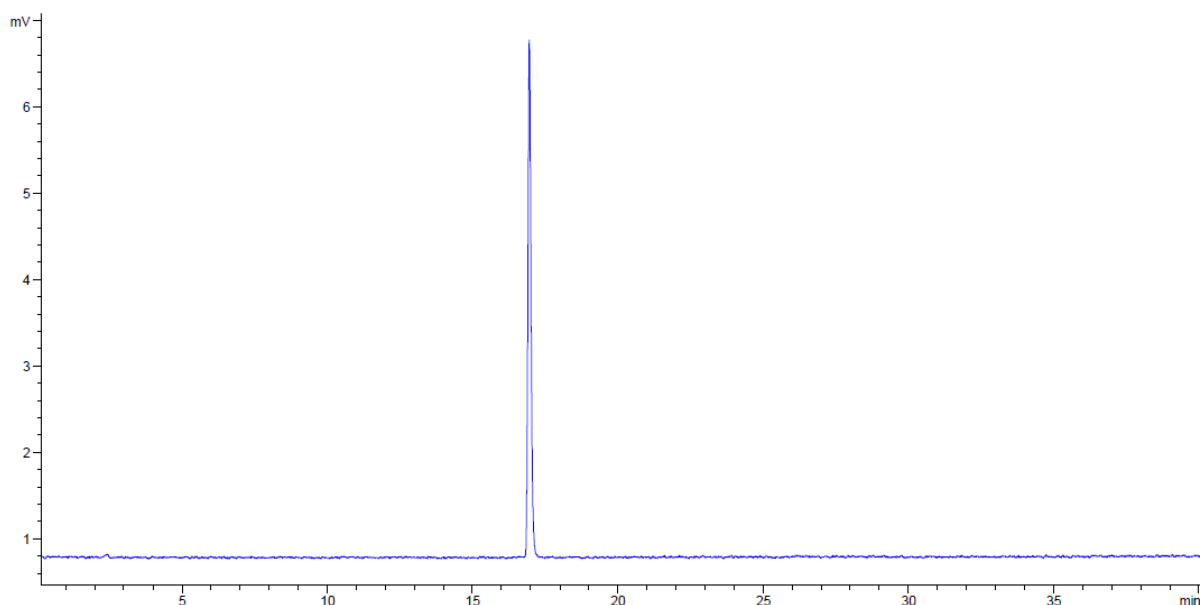
Module	Conditions
A: Resin Preparation for Synthesis	
3 [B: Acidic Wash with TMSOTf Solution	
C: Thioglycoside Glycosylation	BB-11, 6.5 equiv. (-20°C 5 min, 0°C 5 min)
D: Capping	
E: Fmoc Deprotection	
B: Acidic Wash with TMSOTf Solution	
C: Thioglycoside Glycosylation	BB-10, 6.5 equiv. (-20°C 5 min, 0°C 5 min)
D: Capping	
E: Fmoc Deprotection	
F: On-resin Methanolysis	
G: Cleavage from Solid Support	
I: Hydrogenolysis	
J: Purification	Method M

Automated synthesis and global deprotection and purification afforded **ABABAB-OH** as white solid (3.3 mg, 26% overall yield).

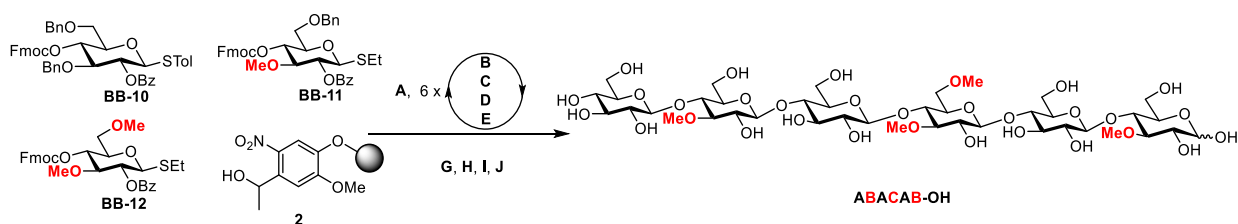
Analytical data for **ABABAB-OH**: ¹H NMR (400 MHz, D₂O) δ 5.14 (d, *J* = 3.3 Hz, 0.45 H, α-H1), 4.59 (d, *J* = 7.8 Hz, 0.55 H, β-H1), 4.51 – 4.41 (m, 5H), 3.93 (d, *J* = 12.3 Hz,

4H), 3.87 (d, $J = 6.9$ Hz, 1H), 3.84 – 3.76 (m, 5H), 3.76 – 3.66 (m, 5H), 3.63 – 3.56 (m, 4H), 3.56 – 3.53 (m, 9H), 3.52 (d, $J = 5.9$ Hz, 5H), 3.46 – 3.39 (m, 3H), 3.39 – 3.32 (m, 5H), 3.32 – 3.20 (m, 4H); ^{13}C NMR (101 MHz, D_2O) δ 102.30, 102.23, 102.19, 102.16, 102.15, 95.65 ($\beta\text{-C1}$), 91.69 ($\alpha\text{-C1}$), 83.39, 83.15, 83.10, 80.86, 78.21, 75.92, 75.82, 75.52, 75.49, 75.35, 75.30, 74.94, 74.72, 74.05, 73.42, 73.24, 73.21, 73.19, 73.08, 72.27, 72.20, 70.62, 70.47, 69.34, 60.59, 59.87, 59.77, 59.66, 59.47, 59.17, 59.07, 59.05, 48.72; $[\alpha]_{\text{D}}^{20} +10.36$ (c 0.2, H_2O); IR (neat) $\nu_{\text{max}} = 3348, 2929, 1651, 1031$ cm^{-1} ; m/z (HRMS+) 1055.361 $[\text{M} + \text{Na}]^+$ ($\text{C}_{39}\text{H}_{68}\text{NaO}_{31}$ requires 1055.364).

RP-HPLC of **ABABAB-OH** (ELSD trace, **Method C**, $t_{\text{R}} = 16.9$ min)



6.5.5.4. Synthesis of ABACAB-OH



Module	Conditions
A: Resin Preparation for Synthesis	
B: Acidic Wash with TMSOTf Solution	
C: Thioglycoside Glycosylation	BB-11 , 6.5 equiv. (-20°C 5 min, 0°C 5 min)

D: Capping

E: Fmoc Deprotection

B: Acidic Wash with TMSOTf Solution

C: Thioglycoside Glycosylation **BB-10**, 6.5 equiv.(-20°C 5 min, 0°C 5 min)

D: Capping

E: Fmoc Deprotection

B: Acidic Wash with TMSOTf Solution

C: Thioglycoside Glycosylation **BB-12**, 6.5 equiv.(-20°C 5 min, 0°C 5 min)

D: Capping

E: Fmoc Deprotection

B: Acidic Wash with TMSOTf Solution

C: Thioglycoside Glycosylation **BB-10**, 6.5 equiv.(-20°C 5 min, 0°C 5 min)

D: Capping

E: Fmoc Deprotection

B: Acidic Wash with TMSOTf Solution

C: Thioglycoside Glycosylation **BB-11**, 6.5 equiv.(-20°C 5 min, 0°C 5 min)

D: Capping

E: Fmoc Deprotection

B: Acidic Wash with TMSOTf Solution

C: Thioglycoside Glycosylation **BB-10**, 6.5 equiv.(-20°C 5 min, 0°C 5 min)

D: Capping

E: Fmoc Deprotection

F: On-resin Methanolysis

G: Cleavage from Solid Support

I: Hydrogenolysis

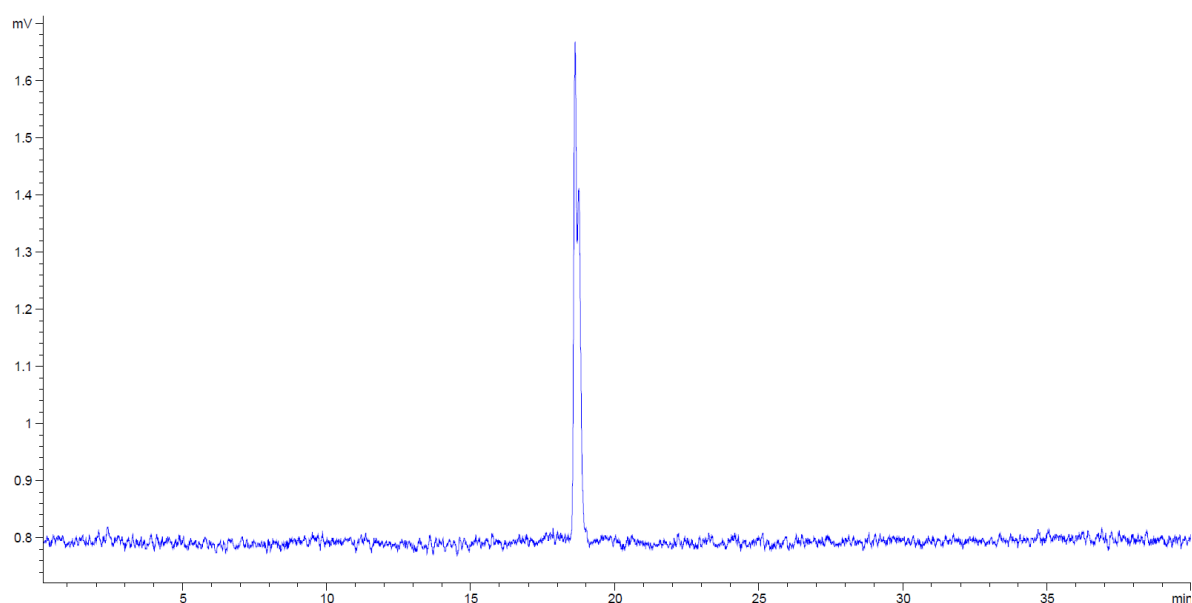
J: Purification

Method M

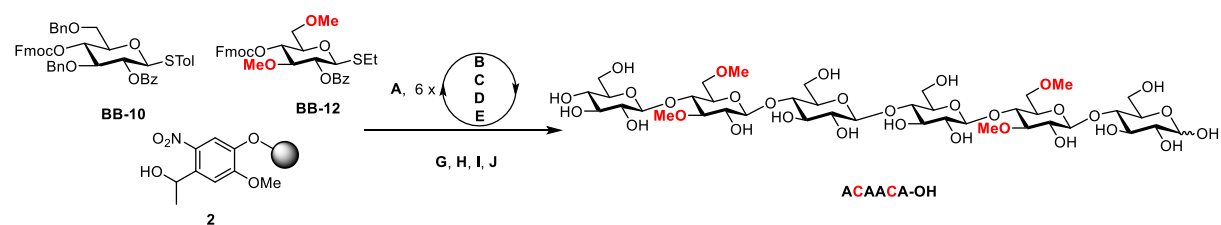
Automated synthesis and global deprotection and purification afforded **ABACAB-OH** as white solid (9.5 mg, 73% overall yield).

Analytical data for **ABACAB-OH**: $^1\text{H NMR}$ (600 MHz, D_2O) δ 5.23 (d, $J = 3.5$ Hz, 0.39 H, $\alpha\text{-H1}$), 4.67 (d, $J = 7.9$ Hz, 0.61H, $\beta\text{-H1}$), 4.58 – 4.51 (m, 4H), 4.46 (d, $J = 7.9$ Hz, 1H), 4.01 (ddd, $J = 12.8, 5.8, 2.8$ Hz, 3H), 3.98 – 3.88 (m, 3H), 3.88 – 3.76 (m, 10H), 3.73 – 3.67 (m, 2H), 3.67 – 3.64 (m, 4H), 3.64 – 3.61 (m, 9H), 3.60 – 3.54 (m, 3H), 3.54 – 3.47 (m, 3H), 3.45 (ddd, $J = 10.6, 5.1, 2.8$ Hz, 4H), 3.42 (s, 3H), 3.40 – 3.35 (m, 3H), 3.34 – 3.30 (m, 1H); $^{13}\text{C NMR}$ (151 MHz, D_2O) δ 102.32, 102.29, 102.23, 102.21, 102.15, 95.71 ($\beta\text{-C1}$), 91.75 ($\alpha\text{-C1}$), 83.45, 83.23, 83.01, 80.90, 78.70, 78.66, 78.37, 75.96, 75.88, 75.60, 75.55, 75.36, 75.31, 75.00, 74.98, 74.80, 74.68, 74.16, 73.50, 73.45, 73.26, 73.23, 73.15, 73.14, 72.31, 72.11, 70.66, 70.52, 69.91, 69.41, 60.67, 59.97, 59.95, 59.87, 59.77, 59.43, 59.17, 59.03, 58.31; $[\alpha]_{\text{D}}^{20} +14.66$ (c 1, H_2O); IR (neat) $\nu_{\text{max}} = 3361, 2953, 1035$ cm^{-1} ; m/z (HRMS+) 1069.379 $[\text{M} + \text{Na}]^+$ ($\text{C}_{40}\text{H}_{70}\text{NaO}_{31}$ requires 1069.379).

RP-HPLC of **ABACAB-OH** (ELSD trace, **Method C**, $t_{\text{R}} = 18.6, 18.7$ min)



6.5.5.5. Synthesis of ACAACA-OH



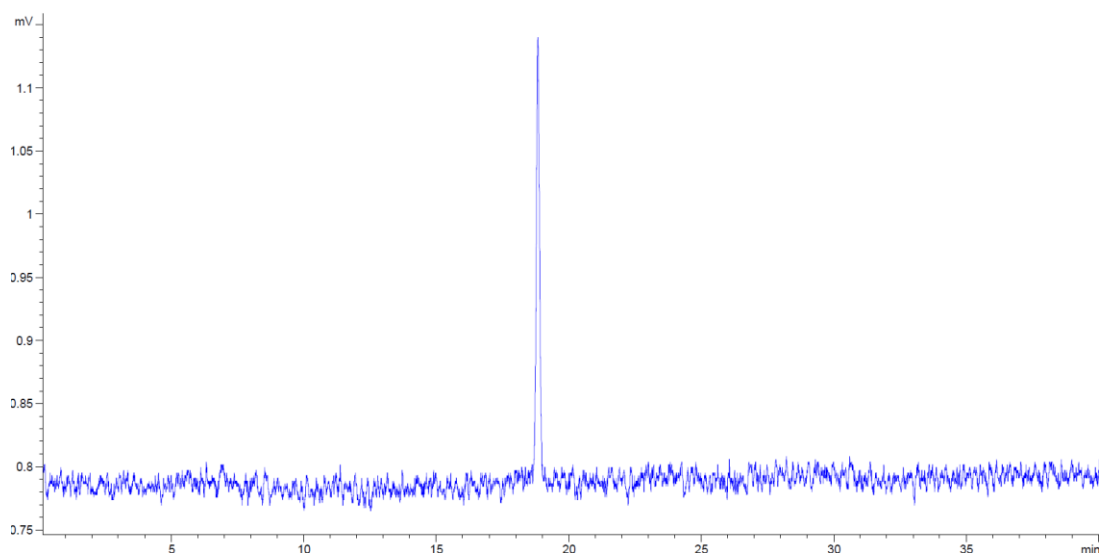
Module	Conditions
A: Resin Preparation for Synthesis	
B: Acidic Wash with TMSOTf Solution	
C: Thioglycoside Glycosylation	BB-10 , 6.5 equiv.(-20°C 5 min, 0°C 5 min)
D: Capping	
E: Fmoc Deprotection	
2	
B: Acidic Wash with TMSOTf Solution	
C: Thioglycoside Glycosylation	BB-12 , 6.5 equiv.(-20°C 5 min, 0°C 5 min)
D: Capping	
E: Fmoc Deprotection	
B: Acidic Wash with TMSOTf Solution	
C: Thioglycoside Glycosylation	BB-10 , 6.5 equiv.(-20°C 5 min, 0°C 5 min)
D: Capping	
E: Fmoc Deprotection	
F: On-resin Methanolysis	
G: Cleavage from Solid Support	
I: Hydrogenolysis	
J: Purification	Method M

Automated synthesis and global deprotection and purification afforded **ACAACA-OH** as white solid (5.9 mg, 45% overall yield).

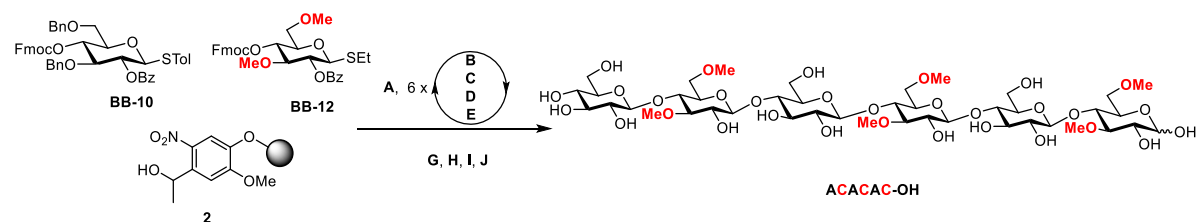
Analytical data for **ACAACA-OH**: ¹H NMR (600 MHz, D₂O) δ 5.24 (d, *J* = 3.8 Hz, 0.39 H, α-H1), 4.67 (d, *J* = 8.0 Hz, 0.61 H, β-H1), 4.55 (dd, *J* = 15.8, 7.7 Hz, 3H), 4.48 – 4.41 (m, 2H), 4.02 – 3.96 (m, 2H), 3.95 (dd, *J* = 6.1, 1.8 Hz, 1H), 3.91 (dd, *J* = 9.5, 1.9 Hz, 1H), 3.90 – 3.86 (m, 2H), 3.86 – 3.82 (m, 3H), 3.82 (t, *J* = 2.1 Hz, 3H), 3.81 – 3.78 (m, 2H), 3.78 – 3.75 (m, 1H), 3.73 – 3.68 (m, 3H), 3.68 – 3.63 (m, 6H), 3.63 – 3.62 (m, 6H), 3.61 – 3.54 (m, 2H), 3.53 – 3.50 (m, 1H), 3.50 – 3.48 (m, 1H), 3.48 – 3.47 (m, 1H), 3.46 – 3.43 (m, 3H), 3.43 – 3.41 (m, 6H), 3.40 – 3.36 (m, 2H), 3.36 – 3.32 (m, 1H), 3.32 – 3.28 (m, 1H); ¹³C NMR (151 MHz, D₂O) δ 102.36, 102.31, 102.31, 102.27, 102.24, 95.67 (β-C1), 91.74 (α-C1), 83.04, 83.01, 78.86, 78.73, 78.52, 78.34, 76.02,

75.64, 75.31, 75.23, 74.81, 74.65, 74.63, 74.22, 74.14, 73.99, 73.76, 73.48, 73.44, 73.40, 73.16, 72.81, 72.16, 72.11, 71.26, 71.10, 69.93, 69.42, 60.66, 59.97, 59.91, 59.83, 59.82, 59.12, 59.02, 58.97, 58.30; $[\alpha]_D^{20} +14.00$ (c 0.8, H₂O); IR (neat) $\nu_{\max} = 3387, 2925, 1650, 1064 \text{ cm}^{-1}$; m/z (HRMS+) 1069.379 [M + Na]⁺ (C₄₀H₇₀NaO₃₁ requires 1069.379).

RP-HPLC of **ACAACA-OH** (ELSD trace, **Method C**, $t_R = 18.8 \text{ min}$)



6.5.5.6. Synthesis of ACACAC-OH



Module	Conditions
A: Resin Preparation for Synthesis	
B: Acidic Wash with TMSOTf Solution	
C: Thioglycoside Glycosylation	BB-12 , 6.5 equiv. (-20°C 5 min, 0°C 5 min)
D: Capping	
E: Fmoc Deprotection	
B: Acidic Wash with TMSOTf Solution	
C: Thioglycoside Glycosylation	BB-10 , 6.5 equiv. (-20°C 5 min, 0°C 5 min)

D: Capping

E: Fmoc Deprotection

F: On-resin Methanolysis

G: Cleavage from Solid Support

I: Hydrogenolysis

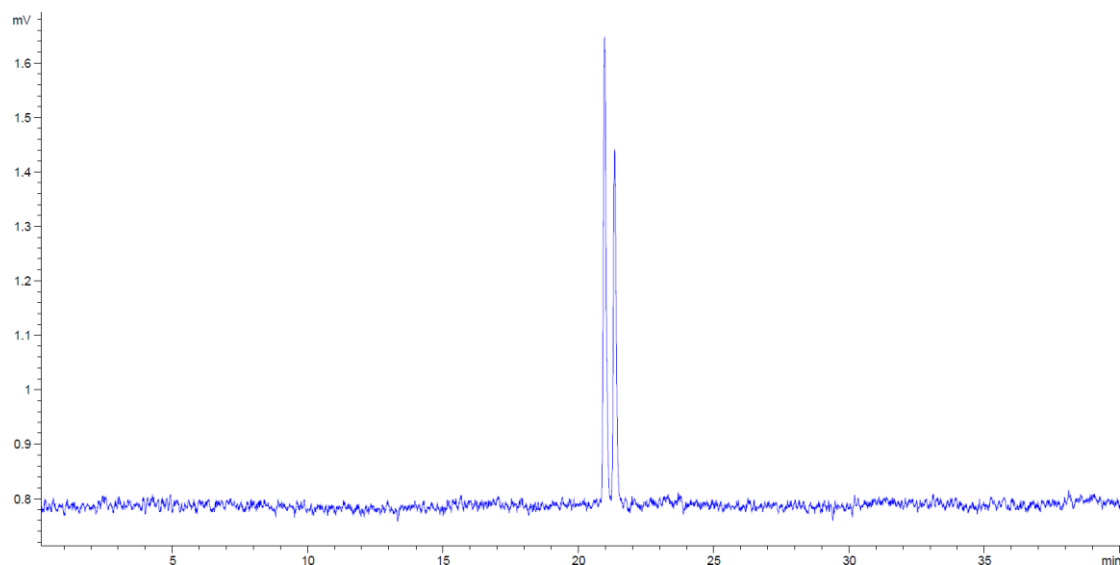
J: Purification

Method M

Automated synthesis and global deprotection and purification afforded **ACACAC-OH** as white solid (4.9 mg, 36% overall yield).

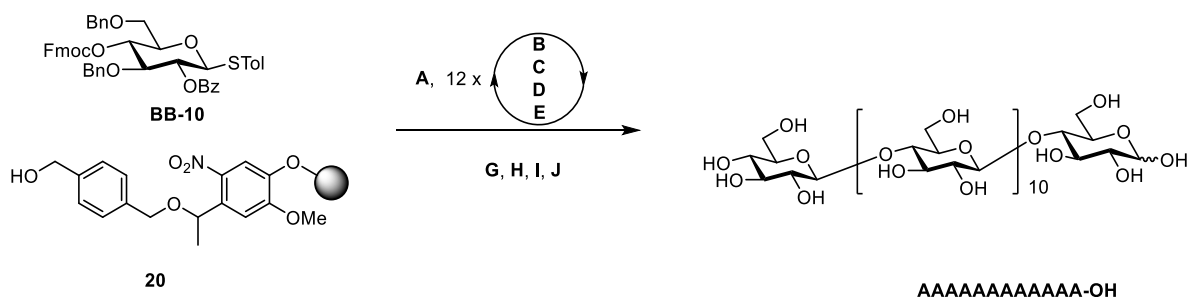
Analytical data for **ACACAC-OH**: ^1H NMR (600 MHz, D_2O) δ 5.21 (d, $J = 3.6$ Hz, 0.43 H, $\alpha\text{-H1}$), 4.66 (d, $J = 7.9$ Hz, 0.57 H, $\beta\text{-H1}$), 4.55 (d, $J = 7.5$ Hz, 2H), 4.47 – 4.41 (m, 3H), 4.06 – 4.02 (m, 1H), 4.00 (dd, $J = 12.4, 2.1$ Hz, 2H), 3.93 (dd, $J = 12.3, 1.5$ Hz, 1H), 3.88 – 3.83 (m, 4H), 3.83 – 3.79 (m, 6H), 3.77 (d, $J = 5.2$ Hz, 1H), 3.71 (ddd, $J = 9.8, 4.4, 2.5$ Hz, 3H), 3.69 – 3.63 (m, 5H), 3.63 – 3.60 (m, 9H), 3.57 (q, $J = 6.1, 5.2$ Hz, 2H), 3.53 – 3.43 (m, 6H), 3.43 – 3.41 (m, 6H), 3.41 (d, $J = 6.2$ Hz, 3H), 3.39 – 3.37 (m, 1H), 3.37 (s, 3H), 3.35 – 3.30 (m, 1H); ^{13}C NMR (151 MHz, D_2O) δ 102.36, 102.34, 102.25, 102.22, 102.18, 95.78 ($\beta\text{-C1}$), 91.72 ($\alpha\text{-C1}$), 83.30, 83.06, 83.01, 80.76, 78.68, 76.02, 75.81, 75.64, 75.41, 75.30, 75.24, 74.73, 74.21, 74.19, 73.62, 73.47, 73.44, 73.40, 73.10, 73.00, 72.18, 72.11, 70.56, 70.03, 69.94, 69.91, 69.42, 69.17, 60.66, 59.96, 59.40, 59.13, 59.03, 58.98, 58.30, 58.20, 58.08; $[\alpha]_{\text{D}}^{20} +19.86$ (c 0.75, H_2O); IR (neat) $\nu_{\text{max}} = 3395, 2928, 1648, 1066$ cm^{-1} ; m/z (HRMS+) 1097.409 $[\text{M} + \text{Na}]^+$ ($\text{C}_{42}\text{H}_{74}\text{NaO}_{31}$ requires 1097.411).

RP-HPLC of **ACACAC-OH** (ELSD trace, **Method C**, $t_{\text{R}} = 21.0, 21.3$ min)



6.5.6. AGA synthesis of methylated cellulose 12-mers

6.5.6.1. Synthesis of AAAAAAAAAAAAA-OH

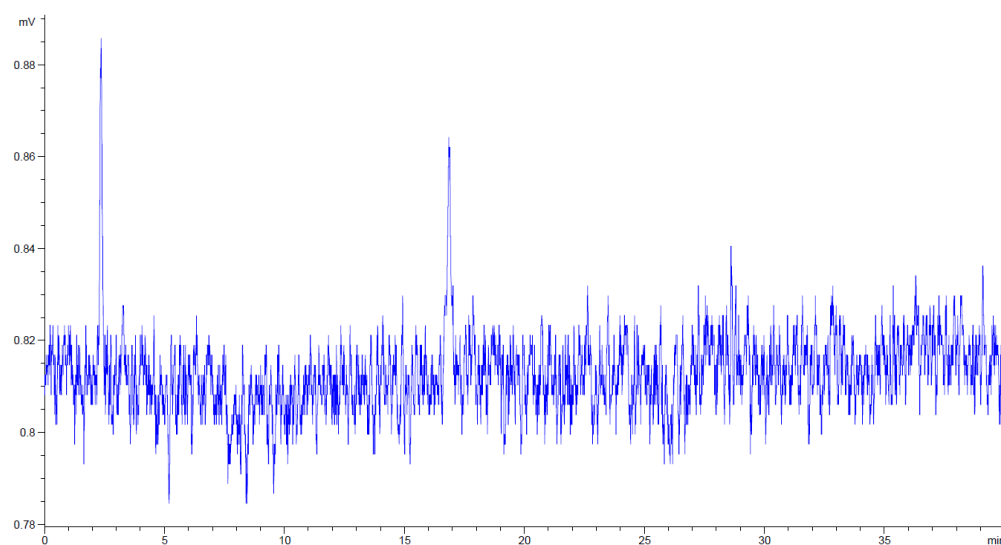


Module	Conditions
A: Resin Preparation for Synthesis	
12	B: Acidic Wash with TMSOTf Solution
	C: Thioglycoside Glycosylation BB-10, 6.0 equiv. (-20°C 5 min, 0°C 5 min)
	D: Capping
	E: Fmoc Deprotection
	F: On-resin Methanolysis
G: Cleavage from Solid Support	
I: Hydrogenolysis	
J: Purification	Method M

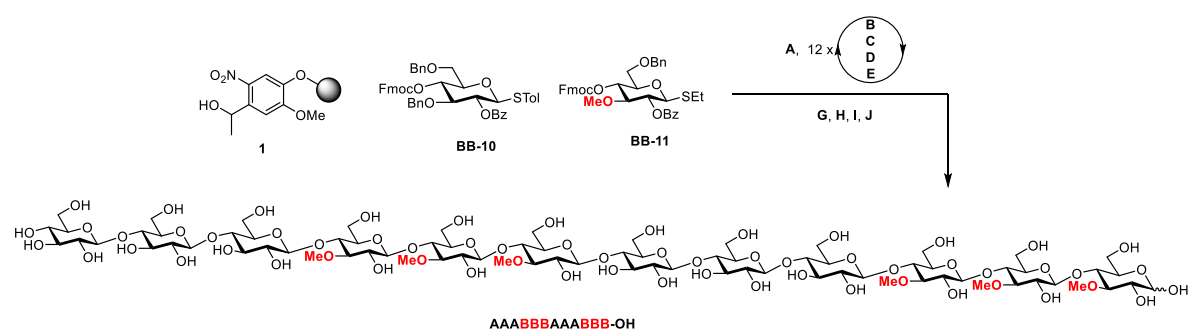
Automated synthesis, global deprotection, and purification afforded **AAAAAAAAAAAA-OH** as white solid (0.6 mg, 2% overall yield).

Analytical data for **AAAAAAAAAAAA-OH**: $^1\text{H NMR}$ (700 MHz, D_2O) δ 5.24 (d, $J = 3.7$ Hz, 0.36 H, $\alpha\text{-H1}$), 4.67 (d, $J = 7.9$ Hz, 0.64 H, $\beta\text{-H1}$), 4.57 – 4.51 (m, 11H), 3.99 (d, $J = 11.9$ Hz, 8H), 3.95 – 3.90 (m, 4H), 3.88 (d, $J = 11.6$ Hz, 2H), 3.84 (dd, $J = 12.9, 4.6$ Hz, 8H), 3.81 (d, $J = 9.3$ Hz, 3H), 3.79 (d, $J = 7.6$ Hz, 1H), 3.76 – 3.73 (m, 1H), 3.69 (q, $J = 9.5$ Hz, 17H), 3.66 – 3.61 (m, 14H), 3.54 – 4.48 (m, 3H), 3.43 (t, $J = 9.4$ Hz, 1H), 3.37 (t, $J = 8.5$ Hz, 8H), 3.31 (dt, $J = 22.7, 8.7$ Hz, 2H); $^{13}\text{C NMR}$ (176 MHz, D_2O) δ 102.34, 78.52, 78.48, 78.35, 78.27, 78.27, 74.82, 74.54, 74.01, 73.15, 73.04, 72.94, 71.32, 60.57, 59.87; solubility not enough for optical rotation measurement; IR (neat) $\nu_{\text{max}} = 3340, 2893, 1644, 1030 \text{ cm}^{-1}$; m/z (HRMS+) 1985.635 $[\text{M} + \text{Na}]^+$ ($\text{C}_{72}\text{H}_{122}\text{NaO}_{61}$ requires 1985.634).

RP-HPLC of AAAAAAAAAA-OH (ELSD trace, Method C, $t_R = 16.9$ min)



6.5.6.2. Synthesis of AAABBBAABB-OH



Module	Conditions
A: Resin Preparation for Synthesis	
3	B: Acidic Wash with TMSOTf Solution
	C: Thioglycoside Glycosylation BB-11 , 6.5 equiv. (-20°C 5 min, 0°C 5 min)
	D: Capping
	E: Fmoc Deprotection
	B: Acidic Wash with TMSOTf Solution
3	B: Acidic Wash with TMSOTf Solution
	C: Thioglycoside Glycosylation BB-10 , 6.5 equiv. (-20°C 5 min, 0°C 5 min)
	D: Capping
	E: Fmoc Deprotection
	B: Acidic Wash with TMSOTf Solution
102	

3 C: Thioglycoside Glycosylation **BB-11**, 6.5 equiv. (-20°C 5 min, 0°C 5 min)
D: Capping
E: Fmoc Deprotection

3 { B: Acidic Wash with TMSOTf Solution
C: Thioglycoside Glycosylation **BB-10**, 6.5 equiv. (-20°C 5 min, 0°C 5 min)
D: Capping
E: Fmoc Deprotection

F: On-resin Methanolysis

G: Cleavage from Solid Support

I: Hydrogenolysis

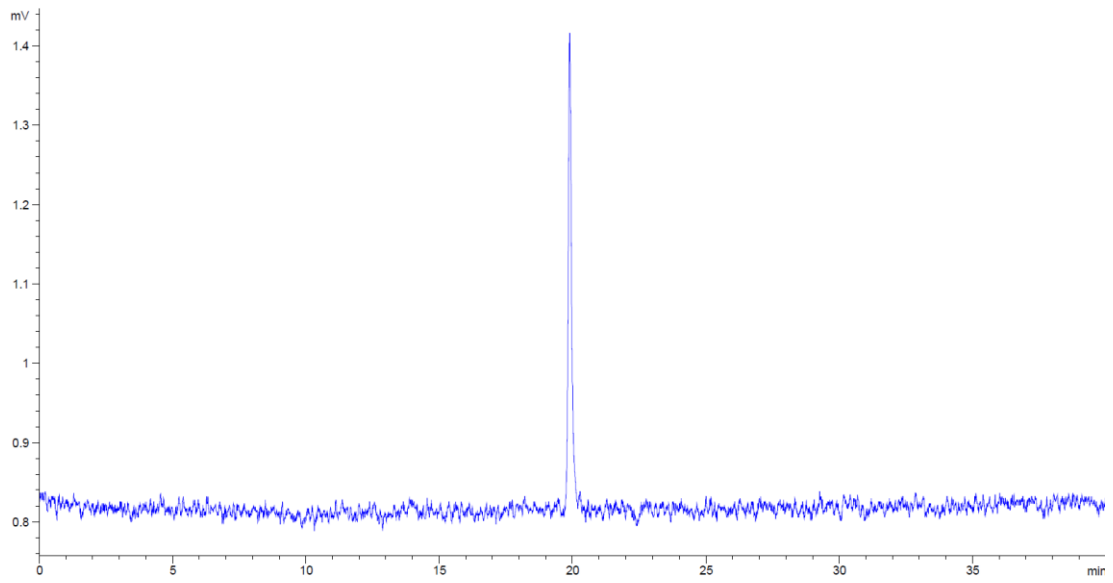
J: Purification

Method M

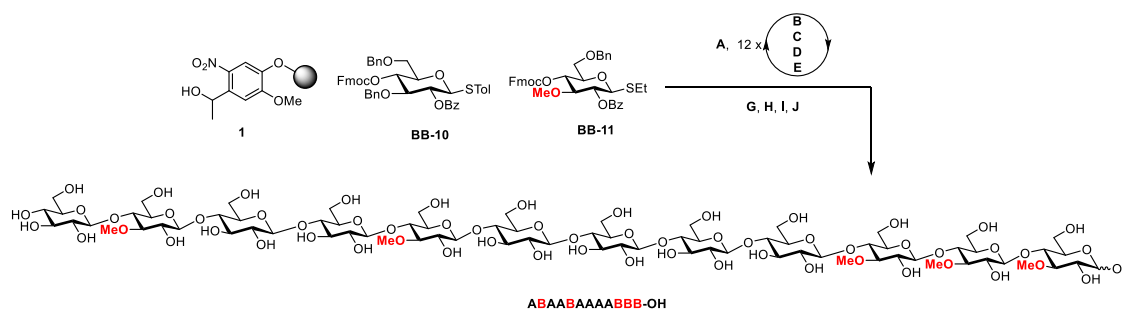
Automated synthesis, global deprotection, and purification afforded **AAABBBAAABBB-OH** as white solid (1.8 mg, 7% overall yield).

Analytical data for **AAABBBAAABBB-OH**: ¹H NMR (600 MHz, D₂O) δ 5.24 (d, *J* = 3.6 Hz, 0.39 H, α-H1), 4.69 (d, *J* = 7.8 Hz, 0.61 H, β-H1), 4.63 – 4.51 (m, 11H), 4.05 – 4.00 (m, 8H), 4.00 – 3.92 (m, 4H), 3.85 (tdd, *J* = 22.6, 12.8, 4.9 Hz, 17H), 3.77 (dd, *J* = 12.6, 5.9 Hz, 2H), 3.73 – 3.65 (m, 13H), 3.65 – 3.62 (m, 18H), 3.59 (td, *J* = 16.7, 14.9, 5.4 Hz, 7H), 3.55 – 3.50 (m, 3H), 3.50 – 3.42 (m, 11H), 3.42 – 3.31 (m, 7H); ¹³C NMR (151 MHz, D₂O) δ 102.49, 102.28, 102.19, 95.72 (β-C1), 91.75 (α-C1), 83.51, 83.45, 83.39, 83.39, 83.23, 78.35, 78.32, 78.18, 75.91, 75.58, 75.45, 75.43, 75.41, 74.99, 74.77, 74.75, 74.12, 73.98, 73.93, 73.30, 73.18, 73.07, 72.87, 72.82, 72.77, 72.71, 72.70, 72.68, 72.65, 72.27, 70.69, 69.38, 60.50, 59.94, 59.90, 59.89, 59.88, 59.82, 59.79, 59.50, 59.15, 59.12, 59.07, 59.03, 59.00; [α]_D²⁰ +10.86 (c 0.2, H₂O); IR (neat) ν_{max} = 3357, 2929, 1647, 1024 cm⁻¹; *m/z* (HRMS+) 2069.728 [M + Na]⁺ (C₇₈H₁₃₄NaO₆₁ requires 2069.728).

RP-HPLC of **AAABBBAAABBB-OH** (ELSD trace, **Method C**, t_R = 19.8 min)



6.5.6.3. Synthesis of ABAABAAAABBB-OH



Module	Conditions
3	B: Acidic Wash with TMSOTf Solution
	C: Thioglycoside Glycosylation BB-11 , 6.5 equiv. (-20°C 5 min, 0°C 5 min)
	D: Capping
	E: Fmoc Deprotection
3	B: Acidic Wash with TMSOTf Solution
	C: Thioglycoside Glycosylation BB-10 , 6.5 equiv. (-20°C 5 min, 0°C 5 min)
	D: Capping
	E: Fmoc Deprotection
2	B: Acidic Wash with TMSOTf Solution
	C: Thioglycoside Glycosylation BB-10 , 6.5 equiv. (-20°C 5 min, 0°C 5 min)
	D: Capping
	E: Fmoc Deprotection
2	B: Acidic Wash with TMSOTf Solution
	C: Thioglycoside Glycosylation BB-10 , 6.5 equiv. (-20°C 5 min, 0°C 5 min)

D: Capping

E: Fmoc Deprotection

F: On-resin Methanolysis

G: Cleavage from Solid Support

I: Hydrogenolysis

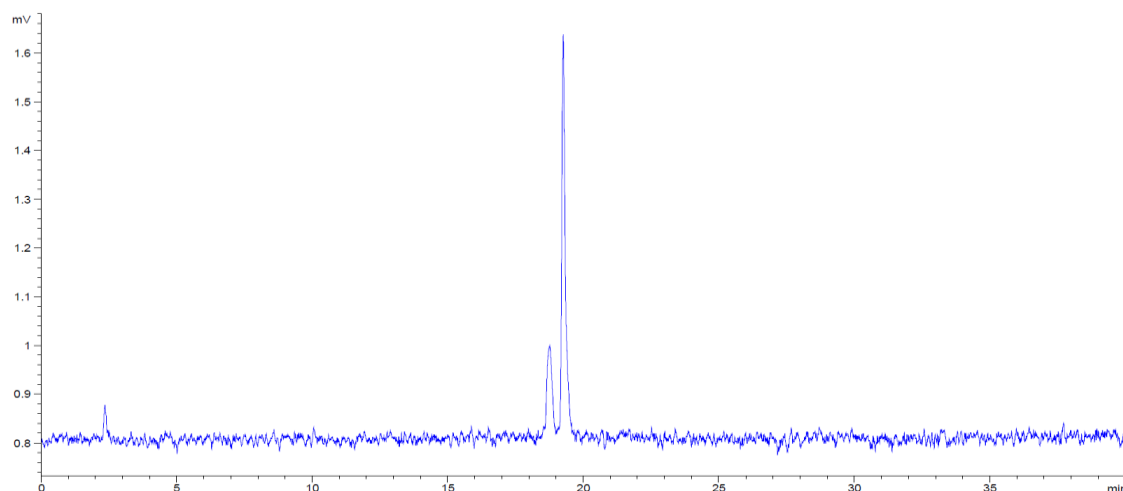
J: Purification

Method M

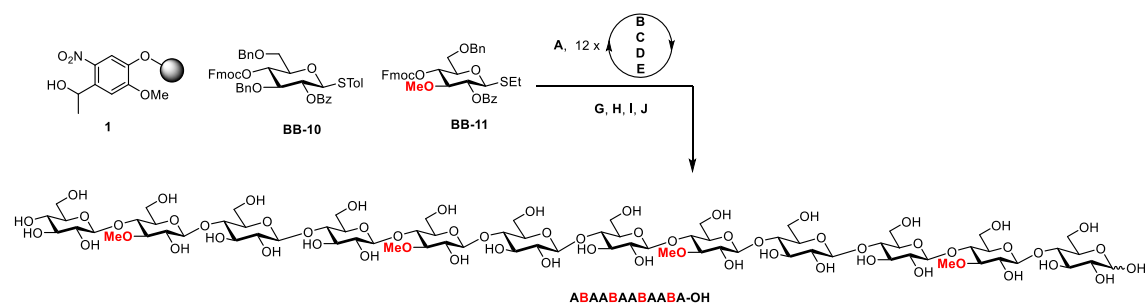
Automated synthesis, global deprotection, and purification afforded **ABAABAAAABBB-OH** as white solid (3.9 mg, 15% overall yield).

Analytical data for **ABAABAAAABBB-OH**: ^1H NMR (600 MHz, D_2O) δ 5.24 (d, $J = 3.5$ Hz, 0.43 H, $\alpha\text{-H1}$), 4.68 (d, $J = 7.8$ Hz, 0.57 H, $\beta\text{-H1}$), 4.60 – 4.52 (m, 11H), 4.01 (d, $J = 11.5$ Hz, 8H), 3.98 – 3.92 (m, 3H), 3.92 – 3.81 (m, 16H), 3.81 – 3.74 (m, 3H), 3.74 – 3.64 (m, 18H), 3.64 – 3.61 (m, 15H), 3.61 – 3.54 (m, 6H), 3.54 – 3.42 (m, 11H), 3.41 – 3.35 (m, 6H), 3.35 – 3.31 (m, 1H); ^{13}C NMR (151 MHz, d_2o) δ 102.35, 102.33, 102.29, 102.24, 102.23, 102.20, 102.19, 95.72 ($\beta\text{-C1}$), 91.76($\alpha\text{-C1}$), 83.52, 83.46, 83.44, 83.43, 83.40, 83.23, 83.18, 83.14, 80.96, 78.36, 78.34, 78.21, 78.21, 75.97, 75.92, 75.91, 75.61, 75.60, 75.48, 75.46, 75.43, 75.42, 75.36, 74.99, 74.76, 74.16, 74.15, 74.13, 73.95, 73.52, 73.31, 73.27, 73.19, 72.87, 72.70, 72.66, 72.31, 60.69, 59.93, 59.92, 59.91, 59.89, 59.82, 59.81, 59.79, 59.50, 59.17, 59.12, 59.08, 59.04, 59.00; $[\alpha]_{\text{D}}^{20} +12.74$ (c 0.2, H_2O); IR (neat) $\nu_{\text{max}} = 3376, 1019 \text{ cm}^{-1}$; m/z (HRMS+) 2055.714 $[\text{M} + \text{Na}]^+$ ($\text{C}_{77}\text{H}_{132}\text{NaO}_{61}$ requires 2055.712).

RP-HPLC of **ABAABAAAABBB-OH** (ELSD trace, **Method C**, $t_{\text{R}} = 18.7, 19.3$ min)



6.5.6.4. Synthesis of ABAABAABAABA-OH



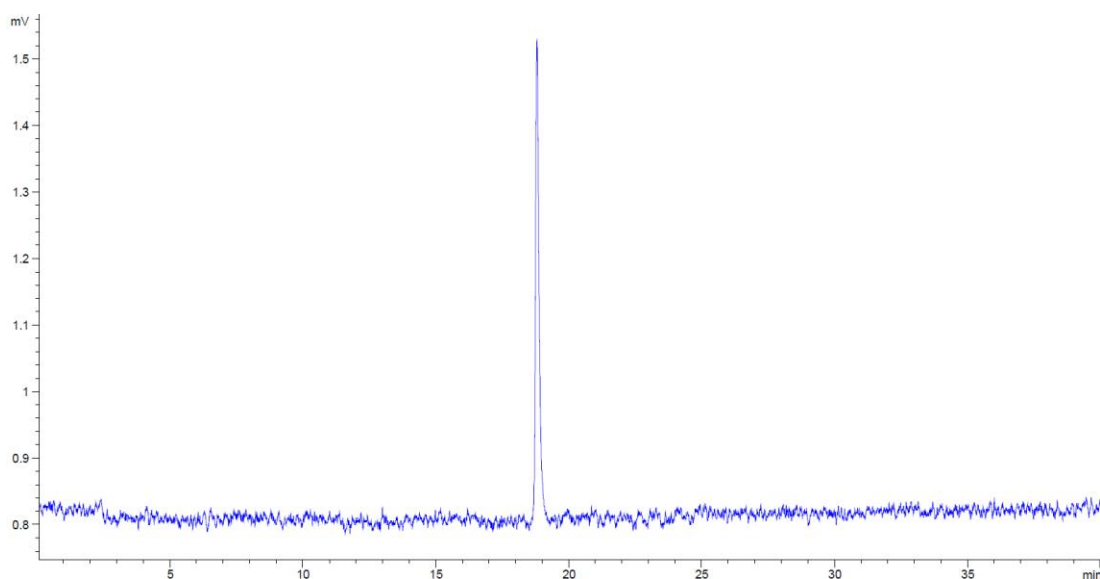
Module	Conditions
A: Resin Preparation for Synthesis	
4	B: Acidic Wash with TMSOTf Solution
	C: Thioglycoside Glycosylation BB-10 , 6.5 equiv. (-20°C 5 min, 0°C 5 min)
	D: Capping
	E: Fmoc Deprotection
	B: Acidic Wash with TMSOTf Solution
	C: Thioglycoside Glycosylation BB-11 , 6.5 equiv. (-20°C 5 min, 0°C 5 min)
	D: Capping
	E: Fmoc Deprotection
	B: Acidic Wash with TMSOTf Solution
	C: Thioglycoside Glycosylation BB-10 , 6.5 equiv. (-20°C 5 min, 0°C 5 min)
	D: Capping
	E: Fmoc Deprotection
F: On-resin Methanolysis	
G: Cleavage from Solid Support	
I: Hydrogenolysis	
J: Purification	Method M

Automated synthesis, global deprotection, and purification afforded **ABAABAABAABA-OH** as white solid (1.8 mg, 7% overall yield).

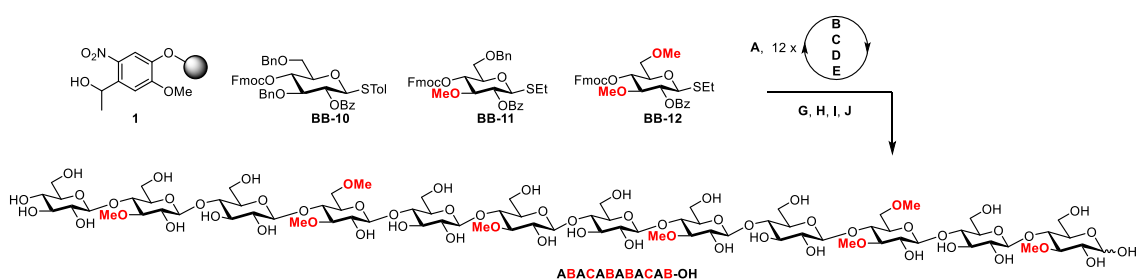
Analytical data for **ABAABAABAABA-OH**: ¹H NMR (700 MHz, D₂O) δ 5.24 (d, *J* = 3.7 Hz, 0.38 H, α-H1), 4.67 (d, *J* = 8.0 Hz, 0.62 H, β-H1), 4.55 (td, *J* = 10.3, 9.0, 4.3 Hz,

11H), 3.96 (dd, $J = 11.7, 5.0$ Hz, 10H), 3.97 – 3.90 (m, 3H), 3.85 (dq, $J = 22.9, 8.5, 6.6$ Hz, 16H), 3.78 (dd, $J = 12.6, 4.4$ Hz, 1H), 3.67 (tt, $J = 10.9, 5.3$ Hz, 17H), 3.62 (s, 12H), 3.60 – 3.55 (m, 5H), 3.53 – 3.41 (m, 11H), 3.37 (q, $J = 8.4$ Hz, 7H), 3.30 (dt, $J = 16.7, 8.6$ Hz, 2H); ^{13}C NMR (176 MHz, D_2O) δ 102.40, 102.36, 102.27, 95.76 ($\beta\text{-C1}$), 91.82 ($\alpha\text{-C1}$), 83.30, 83.25, 78.50, 78.41, 78.28, 76.04, 75.68, 75.49, 75.42, 75.09, 75.05, 74.85, 74.81, 74.27, 74.19, 74.03, 73.90, 73.58, 73.34, 72.95, 72.37, 72.32, 71.32, 71.23, 69.49, 60.75, 60.01, 59.90, 59.84, 59.83, 59.23, 59.14, 59.09; $[\alpha]_{\text{D}}^{20} +11.41$ (c 0.2, H_2O); IR (neat) $\nu_{\text{max}} = 3360, 2926, 1034$ cm^{-1} ; m/z (HRMS+) 2041.697 $[\text{M} + \text{Na}]^+$ ($\text{C}_{76}\text{H}_{130}\text{NaO}_{61}$ requires 2041.696).

RP-HPLC of **ABAABAABAABA-OH** (ELSD trace, **Method C**, $t_{\text{R}} = 18.8$ min)



6.5.6.5. Synthesis of ABACABABACAB-OH



Module	Conditions
A: Resin Preparation for Synthesis	
B: Acidic Wash with TMSOTf Solution	
C: Thioglycoside Glycosylation	BB-11 , 6.5 equiv. (-20°C 5 min, 0°C 5 min)
D: Capping	

E: Fmoc Deprotection

B: Acidic Wash with TMSOTf Solution

C: Thioglycoside Glycosylation **BB-10**, 6.5 equiv.(-20°C 5 min, 0°C 5 min)

D: Capping

E: Fmoc Deprotection

B: Acidic Wash with TMSOTf Solution

C: Thioglycoside Glycosylation **BB-12**, 6.5 equiv.(-20°C 5 min, 0°C 5 min)

D: Capping

E: Fmoc Deprotection

2 B: Acidic Wash with TMSOTf Solution

C: Thioglycoside Glycosylation **BB-10**, 6.5 equiv.(-20°C 5 min, 0°C 5 min)

D: Capping

E: Fmoc Deprotection

B: Acidic Wash with TMSOTf Solution

C: Thioglycoside Glycosylation **BB-11**, 6.5 equiv.(-20°C 5 min, 0°C 5 min)

D: Capping

E: Fmoc Deprotection

B: Acidic Wash with TMSOTf Solution

C: Thioglycoside Glycosylation **BB-10**, 6.5 equiv.(-20°C 5 min, 0°C 5 min)

D: Capping

E: Fmoc Deprotection

F: On-resin Methanolysis

G: Cleavage from Solid Support

I: Hydrogenolysis

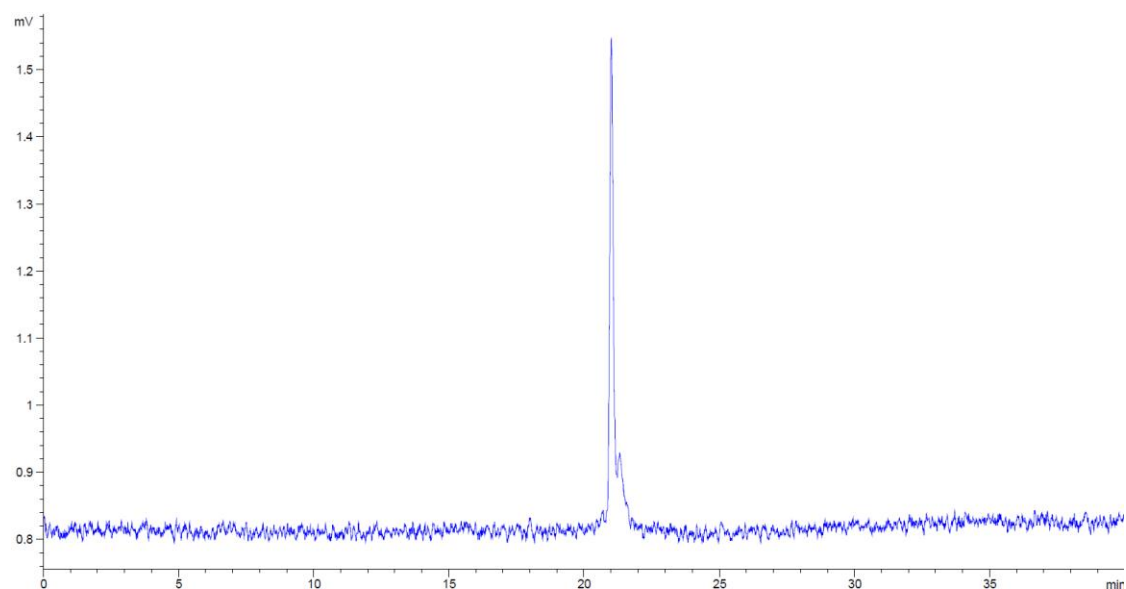
J: Purification

Method M

Automated synthesis, global deprotection, and purification afforded **ABACABABACAB-OH** as white solid (3.2 mg, 12% overall yield).

Analytical data for **ABACABABACAB-OH**: $^1\text{H NMR}$ (600 MHz, D_2O) δ 5.23 (d, $J = 3.5$ Hz, 0.37 H, $\alpha\text{-H1}$), 4.67 (d, $J = 7.9$ Hz, 0.63H, $\beta\text{-H1}$), 4.59 – 4.51 (m, 9H), 4.46 (d, $J = 7.9$ Hz, 2H), 4.01 (d, $J = 11.9$ Hz, 7H), 3.98 – 3.88 (m, 5H), 3.88 – 3.83 (m, 11H), 3.82 (s, 6H), 3.79 – 3.75 (m, 3H), 3.71 (d, $J = 12.7$ Hz, 3H), 3.67 (t, $J = 8.8$ Hz, 10H), 3.64 – 3.60 (m, 18H), 3.59 (d, $J = 11.1$ Hz, 7H), 3.54 – 3.43 (m, 13H), 3.42 (s, 6H), 3.39 – 3.35 (m, 5H), 3.32 (dd, $J = 9.4, 7.9$ Hz, 2H); $^{13}\text{C NMR}$ (151 MHz, d_2o) δ 102.33, 102.30, 102.27, 102.24, 102.24, 102.21, 102.18, 102.18, 95.72, 83.46, 83.24, 83.19, 83.19, 83.02, 82.51, 78.37, 78.35, 75.96, 75.61, 75.43, 75.37, 75.31, 74.99, 74.81, 74.69, 74.17, 73.51, 73.46, 73.27, 73.24, 73.23, 73.21, 73.16, 72.32, 72.26, 72.11, 69.92, 69.42, 60.00, 59.98, 59.97, 59.78, 59.78, 59.76, 59.44, 59.17, 59.07, 59.03, 58.32; $[\alpha]_{\text{D}}^{20} +12.15$ (c 0.2, H_2O); IR (neat) $\nu_{\text{max}} = 3378, 2928, 1066 \text{ cm}^{-1}$; m/z (HRMS+) 2097.759 $[\text{M} + \text{Na}]^+$ ($\text{C}_{80}\text{H}_{138}\text{NaO}_{61}$ requires 2097.759).

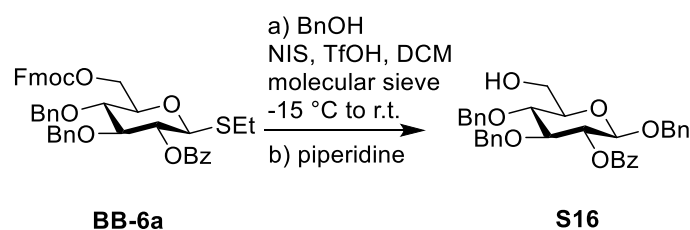
RP-HPLC of **ABACABABACAB-OH** (ELSD trace, **Method C**, $t_{\text{R}} = 21.0, 21.3$ min)



6.5.7. Synthesis of partially protected dimers

6.5.7.1. Synthesis of 25

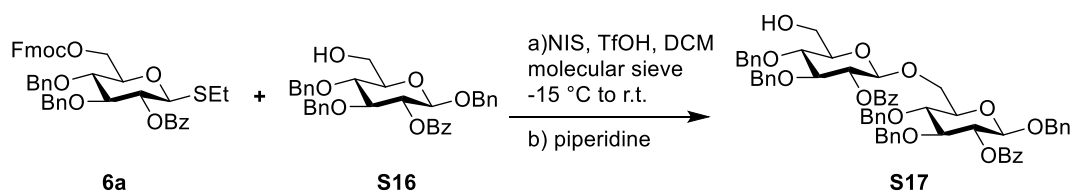
Synthesis of **S16**



Monosaccharide donor **BB-6a** (20.0 mg, 0.027 mmol), *N*-iodosuccinimide (7.4 mg, 0.0239 mmol) and benzyl alcohol (5.9 mg, 0.055 mmol) were dissolved in anhydrous DCM (2 mL). The solution was then stirred with molecular sieve for 1h at room temperature under nitrogen atmosphere and then cooled to -15 °C. A 1% solution of TfOH in DCM (10 μL) was added and the reaction was stirred for 30 min at -15 °C before the removal of cooling bath to raise the temperature to room temperature. After TLC indicated the disappearance of **BB-6a**, piperidine (0.1 mL) was added and the yellow solution was stirred at room temperature for additional 30 min. The reaction was diluted with DCM and washed with H₂O, then saturated aqueous NaCl. The organic layer was dried over Na₂SO₄, filtered and evaporated. The resulting yellow oil was purified by column chromatography (hexane:EtOAc = 3:1) to give **S16** as white solid (13.5 mg, 89%).

Analytical data for **2-O-benzoyl-1,3,4-tri-O-benzyl-β-D-glucopyranose, S16**: ¹H NMR (400 MHz, CDCl₃) δ 8.02 – 7.95 (m, 2H), 7.65 – 7.56 (m, 1H), 7.46 (t, *J* = 7.6 Hz, 2H), 7.41 – 7.27 (m, 5H), 7.24 – 7.10 (m, 10H), 5.39 – 5.30 (m, 1H), 4.86 (dd, *J* = 14.6, 11.8 Hz, 2H), 4.75 (d, *J* = 11.2 Hz, 1H), 4.72 – 4.62 (m, 3H), 4.60 (d, *J* = 8.0 Hz, 1H), 3.92 (dd, *J* = 12.1, 2.5 Hz, 1H), 3.86 – 3.71 (m, 3H), 3.44 (ddd, *J* = 9.6, 4.5, 2.4 Hz, 1H); ¹³C NMR (101 MHz, CDCl₃) δ 165.24, 137.80, 137.71, 137.02, 133.18, 129.89, 129.85, 128.57, 128.39, 128.35, 128.30, 128.13, 128.06, 128.04, 127.79, 127.71, 127.67, 99.69, 82.50, 77.67, 75.40, 75.14, 75.10, 73.70, 70.68, 61.90; *m/z* (HRMS+) 577.2203 [M + Na]⁺ (C₃₄H₃₄O₇Na requires 577.2197).

Synthesis of **S17**

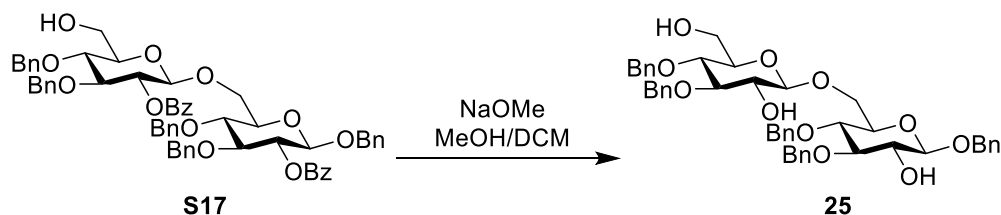


Monosaccharide acceptor **S16** (13.5 mg, 0.0244 mmol), donor **BB-6a** (21.3 mg, 0.0292 mmol) and *N*-iodosuccinimide (6.6 mg, 0.0292 mmol) were dissolved in anhydrous DCM (2 mL). The solution was stirred with molecular sieve for 1h at room temperature under nitrogen atmosphere and then cooled to -15 °C. A 1% solution of TfOH in DCM (10 μL) was added and the reaction was stirred for 30 min at -15 °C before the removal of cooling bath to raise the temperature to room temperature. After TLC indicated the disappearance of **S16**, piperidine (0.1 mL) was added and the yellow solution was stirred at room temperature for additional 30 min. The reaction was diluted with DCM and washed with H₂O, then saturated aqueous NaCl. The organic layer was dried over Na₂SO₄, filtered and evaporated. The resulting yellow oil was purified by

column chromatography (hexane:EtOAc = 3:1) to give **S17** as white solid (20.1 mg, 82%).

Analytical data for **S17**: $^1\text{H NMR}$ (400 MHz, CDCl_3) δ 7.97 (ddd, $J = 16.2, 8.3, 1.4$ Hz, 4H), 7.65 – 7.56 (m, 1H), 7.47 (dt, $J = 16.8, 7.5$ Hz, 3H), 7.41 – 7.29 (m, 10H), 7.25 – 7.01 (m, 17H), 5.36 (dd, $J = 9.3, 7.8$ Hz, 1H), 5.28 (dd, $J = 9.4, 7.9$ Hz, 1H), 4.90 (d, $J = 10.9$ Hz, 1H), 4.79 (d, $J = 11.1$ Hz, 1H), 4.75 – 4.63 (m, 5H), 4.63 – 4.54 (m, 2H), 4.51 (d, $J = 11.1$ Hz, 1H), 4.44 – 4.32 (m, 2H), 4.11 (d, $J = 10.8$ Hz, 1H), 3.98 – 3.84 (m, 2H), 3.84 – 3.62 (m, 4H), 3.62 – 3.52 (m, 1H), 3.49 (dd, $J = 10.1, 5.9$ Hz, 2H); $^{13}\text{C NMR}$ (101 MHz, CDCl_3) δ 165.13, 165.11, 137.82, 137.78, 137.70, 137.67, 136.99, 133.14, 133.08, 129.86, 129.78, 129.72, 128.58, 128.44, 128.41, 128.30, 128.23, 128.21, 128.15, 128.06, 128.02, 127.90, 127.87, 127.75, 127.71, 127.64, 127.58, 101.19, 98.91, 82.64, 82.58, 77.87, 77.67, 75.49, 75.13, 75.12, 74.94, 74.82, 74.71, 73.64, 73.51, 69.75, 68.55, 61.94; m/z (HRMS+) 1023.387 $[\text{M} + \text{Na}]^+$ ($\text{C}_{61}\text{H}_{60}\text{O}_{13}\text{Na}$ requires 1023.393).

Synthesis of **25**

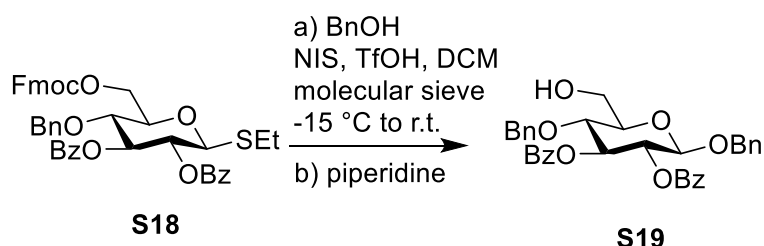


Disaccharide **S17** (20.1 mg, 0.020 mmol) was dissolved in MeOH: DCM (1.5 mL, 1:1). NaOMe in MeOH (0.5 M, 3 equiv. per benzoyl ester) was added and the solution was stirred at room temperature for 12 h, neutralized with Amberlite IR-120 (H^+ form) resin, filtered and concentrated *in vacuo*. The resulting yellow oil was purified by column chromatography (hexane: acetone = 3:1) to give **25** as white solid (13.1 mg, 83%).

Analytical data for **25**: $^1\text{H NMR}$ (400 MHz, CDCl_3) δ 7.43 – 7.27 (m, 25H), 4.95 (ddd, $J = 14.9, 11.4, 3.5$ Hz, 4H), 4.90 – 4.78 (m, 3H), 4.71 – 4.57 (m, 3H), 4.40 (t, $J = 6.5$ Hz, 2H), 4.14 (d, $J = 11.5$ Hz, 1H), 3.87 (d, $J = 11.6$ Hz, 1H), 3.76 (dt, $J = 16.8, 8.4$ Hz, 2H), 3.62 (ddt, $J = 15.7, 12.1, 7.5$ Hz, 7H), 3.39 (d, $J = 5.4$ Hz, 1H); $^{13}\text{C NMR}$ (101 MHz, CDCl_3) δ 138.54, 138.48, 137.97, 137.96, 136.92, 129.95, 128.57, 128.53, 128.51, 128.48, 128.18, 128.11, 128.10, 128.02, 127.99, 127.96, 127.84, 127.77, 103.56, 101.75, 84.39, 84.22, 77.62, 77.26, 75.51, 75.29, 75.15, 75.11, 75.09, 74.83, 74.69, 74.36, 71.36, 68.63, 61.96; m/z (HRMS+) 815.3407 $[\text{M} + \text{Na}]^+$ ($\text{C}_{47}\text{H}_{52}\text{O}_{11}\text{Na}$ requires 815.3402).

6.5.7.2. Synthesis of **26**

Synthesis of **S19**

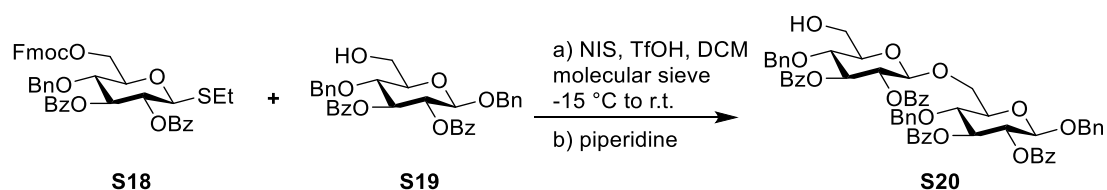


Monosaccharide donor **S18** is purchased from commercial source.

S18 (204 mg, 0.274 mmol), *N*-iodosuccinimide (74 mg, 0.33 mmol) and benzyl alcohol (59.3 mg, 0.055 mmol) were dissolved in anhydrous DCM (2 mL). The solution was then stirred with molecular sieve for 1h at room temperature under nitrogen atmosphere and cooled to $-15\text{ }^{\circ}\text{C}$. A 1% solution of TfOH in DCM (100 μL) was added and the reaction was stirred for 30 min at $-15\text{ }^{\circ}\text{C}$ before the removal of cooling bath to raise the temperature to room temperature. After TLC indicated the disappearance of **S18**, 1 mL piperidine was added and the yellow solution was stirred at room temperature for additional 30 min. The reaction was diluted with DCM and washed with H_2O , then saturated aqueous NaCl. The organic layer was dried over Na_2SO_4 , filtered and evaporated. The resulting yellow oil was purified by column chromatography (hexane:EtOAc = 3:1) to give **S19** as white solid (132 mg, 85%).

Analytical data for **2,3-di-O-benzoyl-1,4-di-O-benzyl- β -D-glucopyranose, S19**: ^1H NMR (400 MHz, CDCl_3) δ 7.89 – 7.80 (m, 4H), 7.44 (q, $J = 7.2$ Hz, 2H), 7.30 (td, $J = 7.7, 3.9$ Hz, 4H), 7.16 – 7.03 (m, 10H), 5.61 (t, $J = 9.6$ Hz, 1H), 5.34 (dd, $J = 9.9, 7.9$ Hz, 1H), 4.80 (d, $J = 12.6$ Hz, 1H), 4.68 (d, $J = 8.0$ Hz, 1H), 4.61 (d, $J = 12.6$ Hz, 1H), 4.52 (s, 2H), 3.95 – 3.82 (m, 2H), 3.74 (ddd, $J = 12.2, 8.4, 3.9$ Hz, 1H), 3.49 (dt, $J = 9.7, 3.2$ Hz, 1H), 1.85 (dd, $J = 8.4, 5.3$ Hz, 1H); ^{13}C NMR (101 MHz, CDCl_3) δ 165.81, 165.45, 137.24, 136.87, 133.34, 133.29, 130.00, 129.89, 129.46, 128.52, 128.50, 128.43, 128.34, 128.13, 128.04, 127.81, 114.22, 99.77, 77.36, 75.61, 75.53, 75.02, 74.94, 72.09, 71.09, 61.73; m/z (HRMS+) 591.1990 $[\text{M} + \text{H}]^+$ ($\text{C}_{34}\text{H}_{32}\text{O}_8\text{Na}$ requires 591.1989);

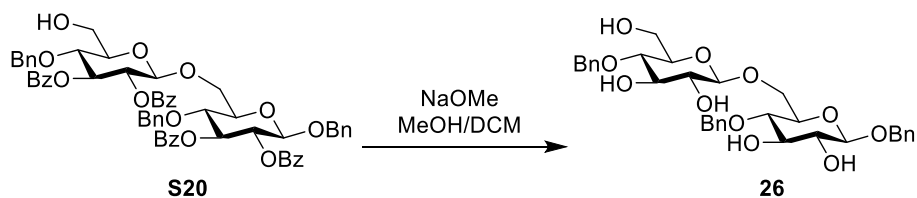
Synthesis of **S20**



Monosaccharide acceptor **S19** (132 mg, 0.232 mmol), donor **S18** (207 mg, 0.278 mmol) and *N*-iodosuccinimide (62.6 mg, 0.278 mmol) were dissolved in anhydrous DCM (2 mL). The solution was then stirred with molecular sieve for 1h at room temperature under nitrogen atmosphere and cooled to -15 °C. A 1% solution of TfOH in DCM (100 μ L) was added and the reaction was stirred for 30 min at -15 °C before the removal of cooling bath to raise the temperature to room temperature. After TLC indicated the disappearance of **S19**, piperidine (1 mL) was added and the yellow solution was stirred at room temperature for additional 30 min. The reaction was diluted with DCM and washed with H₂O, then saturated aqueous NaCl. The organic layer was dried over Na₂SO₄, filtered and evaporated. The resulting yellow oil was purified by column chromatography (hexane:EtOAc = 3:1) to give **S20** as white solid (196 mg, 82%).

Analytical data for **S20**: ¹H NMR (400 MHz, CDCl₃) δ 7.97 – 7.83 (m, 8H), 7.54 – 7.45 (m, 3H), 7.37 (tdt, *J* = 7.5, 5.9, 5.0 Hz, 8H), 7.25 – 7.07 (m, 14H), 7.01 – 6.92 (m, 2H), 5.75 (td, *J* = 9.7, 7.9 Hz, 1H), 5.57 (t, *J* = 9.5 Hz, 1H), 5.47 (dd, *J* = 9.8, 7.8 Hz, 1H), 5.35 (ddd, *J* = 14.6, 9.9, 7.9 Hz, 1H), 4.79 (d, *J* = 7.8 Hz, 1H), 4.73 (d, *J* = 12.7 Hz, 1H), 4.66 – 4.55 (m, 3H), 4.50 (d, *J* = 12.7 Hz, 1H), 4.34 (s, 2H), 4.19 – 4.09 (m, 1H), 4.04 – 3.91 (m, 2H), 3.89 – 3.76 (m, 3H), 3.61 (tdd, *J* = 9.8, 4.5, 2.0 Hz, 2H), 3.52 (s, 1H); ¹³C NMR (101 MHz, CDCl₃) δ 165.74, 165.59, 165.26, 165.24, 137.15, 137.14, 136.74, 133.26, 133.23, 133.19, 133.10, 129.88, 129.85, 129.76, 129.38, 129.32, 129.24, 128.44, 128.43, 128.41, 128.35, 128.33, 128.31, 128.26, 128.03, 127.86, 127.83, 127.77, 101.22, 99.14, 75.99, 75.59, 75.51, 75.09, 74.92, 74.84, 74.69, 74.60, 72.13, 71.86, 70.30, 68.41, 61.66; *m/z* (HRMS+) 1051.345 [M + Na]⁺ (C₆₁H₅₆O₁₅Na requires 1051.351).

Synthesis of **26**

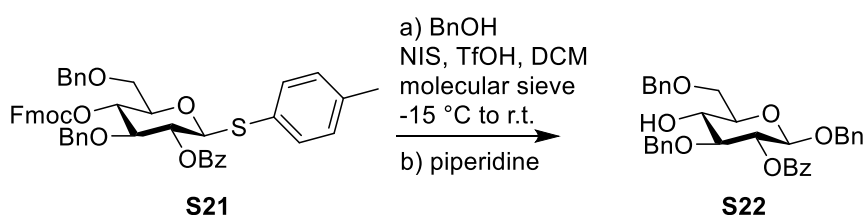


Disaccharide **S20** (196 mg, 0.191 mmol) was dissolved in MeOH: DCM (15 mL, 1:1). NaOMe in MeOH (0.5 M, 3 equiv. per benzoyl ester) was added and the solution was stirred at room temperature for 12 h, neutralized with Amberlite IR-120 (H⁺ form) resin, filtered and concentrated *in vacuo*. The resulting yellow oil was purified by column chromatography (DCM: MeOH = 15:1) to give **26** as white solid (115 mg, 98%).

Analytical data for **26**: ^1H NMR (400 MHz, Methanol- d_4) δ 7.46 – 7.26 (m, 15H), 5.02 – 4.93 (m, 4H), 4.76 – 4.63 (m, 3H), 4.37 (dd, J = 20.3, 7.8 Hz, 2H), 4.17 (dd, J = 11.5, 1.4 Hz, 1H), 3.81 (ddd, J = 21.8, 11.8, 3.3 Hz, 2H), 3.68 (dd, J = 12.0, 4.9 Hz, 1H), 3.61 – 3.47 (m, 4H), 3.43 (t, J = 9.3 Hz, 1H), 3.31 – 3.24 (m, 2H); ^{13}C NMR (101 MHz, Methanol- d_4) δ 138.69, 138.63, 137.69, 127.91, 127.89, 127.76, 127.73, 127.69, 127.29, 127.26, 103.60, 102.00, 77.91, 77.70, 77.10, 76.96, 75.63, 74.75, 74.35, 74.29, 73.95, 73.90, 70.56, 68.13, 60.88; m/z (HRMS+) 635.2457 [$\text{M} + \text{Na}$] $^+$ ($\text{C}_{33}\text{H}_{40}\text{O}_{11}\text{Na}$ requires 635.2462).

6.5.7.3. Synthesis of **27**

Synthesis of **S22**



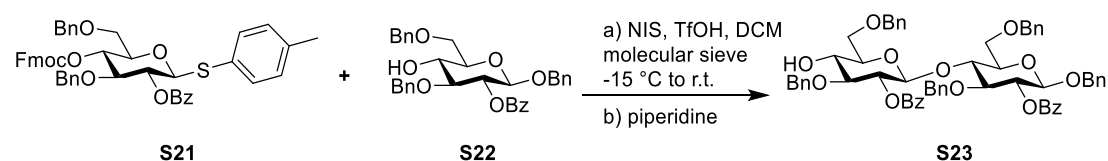
S21 is purchased from commercial source.

Monosaccharide donor **S21** (28.9mg, 0.0274 mmol), *N*-iodosuccinimide (7.4 mg, 0.024 mmol) and benzyl alcohol (5.9 mg, 0.055 mmol) were dissolved in anhydrous DCM (2 mL). The solution was then stirred with molecular sieve for 1h at room temperature under nitrogen atmosphere and cooled to -15 °C. A 1% solution of TfOH in DCM (10 μL) was added and the reaction was stirred for 30 min at -15 °C before the removal of cooling bath to raise the temperature to room temperature. After TLC indicated the disappearance of **S21**, 0.1 mL piperidine was added and the yellow solution was stirred at room temperature for additional 30 min. The reaction was diluted with DCM and washed with H_2O , then saturated aqueous NaCl. The organic layer was dried over Na_2SO_4 , filtered and evaporated. The resulting yellow oil was purified by column chromatography (hexane:EtOAc = 3:1) to give **S22** as white solid (12.3 mg, 81%).

Analytical data for **2-O-benzoyl-1,3,6-tri-O-benzyl- β -D-glucopyranose, S22**: ^1H NMR (400 MHz, CDCl_3) δ 7.96 – 7.86 (m, 2H), 7.57 – 7.48 (m, 1H), 7.41 – 7.35 (m, 2H), 7.32 – 7.21 (m, 5H), 7.18 – 7.02 (m, 10H), 5.32 – 5.21 (m, 1H), 4.78 (d, J = 12.7 Hz, 1H), 4.67 – 4.50 (m, 5H), 4.47 (d, J = 7.9 Hz, 1H), 3.79 – 3.68 (m, 3H), 3.62 – 3.51 (m, 1H), 3.44 (dt, J = 9.5, 4.8 Hz, 1H), 2.66 (s, 1H); ^{13}C NMR (101 MHz, CDCl_3) δ 165.21, 137.93, 137.72, 137.04, 133.15, 129.89, 128.52, 128.42, 128.37, 128.27, 128.09, 128.03, 127.89, 127.81, 127.68, 127.65, 99.39, 82.09, 74.40, 74.08, 73.80,

73.33, 72.21, 70.35, 70.11; m/z (HRMS+) 577.2198 [M + Na]⁺ (C₃₄H₃₄O₇Na requires 577.2197).

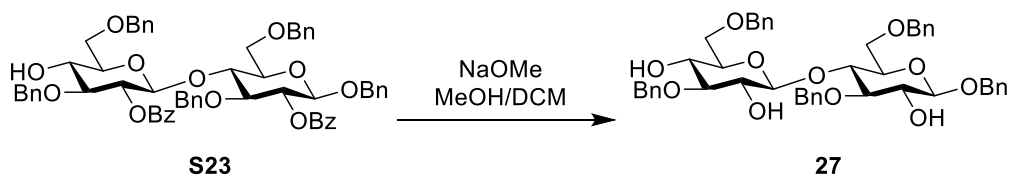
Synthesis of **S23**



Monosaccharide acceptor **S22** (12.3 mg, 0.0222 mmol), donor **S21** (21.1 mg, 0.0266 mmol) and *N*-iodosuccinimide (6.0 mg, 0.027 mmol) were dissolved in anhydrous DCM (2 mL). The solution was then stirred with molecular sieves for 1h at room temperature under nitrogen atmosphere and cooled to -15 °C. A 1% solution of TfOH in DCM (10 μL) was added and the reaction was stirred for 30 min at -15 °C before the removal of cooling bath to raise the temperature to room temperature. After TLC indicated the disappearance of **S22**, piperidine (0.1 mL) was added and the yellow solution was stirred at room temperature for additional 30 min. The reaction was diluted with DCM and washed with H₂O, then saturated aqueous NaCl. The organic layer was dried over Na₂SO₄, filtered and evaporated. The resulting yellow oil was purified by column chromatography (hexane:EtOAc = 3:1) to give **S23** as white solid (18.2 mg, 82%).

Analytical data for **S23**: ¹H NMR (700 MHz, CDCl₃) δ 7.94 (dd, *J* = 22.2, 7.7 Hz, 4H), 7.62 (t, *J* = 7.4 Hz, 1H), 7.58 (q, *J* = 6.8, 6.2 Hz, 1H), 7.47 (t, *J* = 7.6 Hz, 2H), 7.37 (dddd, *J* = 45.9, 30.2, 13.5, 7.5 Hz, 14H), 7.22 – 7.17 (m, 6H), 7.12 (d, *J* = 4.5 Hz, 4H), 7.07 (dt, *J* = 14.2, 6.9 Hz, 3H), 5.30 (t, *J* = 8.6 Hz, 1H), 5.22 (t, *J* = 8.8 Hz, 1H), 4.86 (d, *J* = 11.7 Hz, 1H), 4.81 (d, *J* = 12.7 Hz, 1H), 4.76 (d, *J* = 11.6 Hz, 1H), 4.74 – 4.68 (m, 3H), 4.64 (d, *J* = 11.7 Hz, 1H), 4.53 (d, *J* = 12.7 Hz, 1H), 4.50 – 4.44 (m, 2H), 4.42 (d, *J* = 7.9 Hz, 1H), 4.38 (d, *J* = 12.2 Hz, 1H), 4.12 (t, *J* = 9.2 Hz, 1H), 3.82 (t, *J* = 9.1 Hz, 1H), 3.72 – 3.62 (m, 3H), 3.57 – 3.51 (m, 3H), 3.40 (dt, *J* = 10.2, 5.3 Hz, 1H), 3.24 (dq, *J* = 9.0, 3.6, 3.0 Hz, 1H), 3.09 (s, 1H); ¹³C NMR (176 MHz, CDCl₃) δ 165.12, 164.90, 138.55, 138.13, 138.10, 137.50, 137.11, 133.24, 132.90, 130.02, 129.84, 129.78, 129.68, 128.55, 128.52, 128.49, 128.29, 128.21, 128.19, 128.10, 127.96, 127.94, 127.88, 127.79, 127.71, 127.61, 127.55, 127.10, 100.26, 99.38, 81.82, 80.28, 76.49, 74.77, 74.39, 74.35, 73.95, 73.78, 73.64, 73.59, 73.10, 71.08, 70.01, 67.63; m/z (HRMS+) 1023.391 [M + Na]⁺ (C₆₁H₆₀O₁₃Na requires 1023.393).

Synthesis of **27**

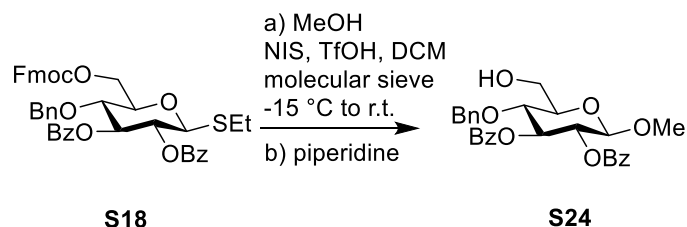


Disaccharide **S23** (18.2 mg, 0.0182 mmol) was dissolved in MeOH: DCM (1.5 mL, 1:1). NaOMe in MeOH (0.5 M, 3eq per benzoyl ester) was added and the solution was stirred at room temperature for 12 h and concentrated *in vacuo*. The resulting yellow oil was purified by column chromatography (hexane: acetone = 3:1) to give **27** as white solid (12.5 mg, 87%).

Analytical data for **27**: ^1H NMR (400 MHz, CDCl_3) δ 7.45 – 7.24 (m, 25H), 5.01 – 4.79 (m, 5H), 4.73 (d, $J = 12.1$ Hz, 1H), 4.67 – 4.53 (m, 3H), 4.45 (s, 2H), 4.38 (d, $J = 7.0$ Hz, 1H), 4.08 – 3.94 (m, 2H), 3.81 (dd, $J = 11.5, 2.2$ Hz, 1H), 3.67 – 3.55 (m, 3H), 3.55 – 3.41 (m, 4H), 3.36 – 3.21 (m, 2H); ^{13}C NMR (101 MHz, CDCl_3) δ 138.95, 138.70, 137.67, 137.53, 137.07, 128.56, 128.53, 128.46, 128.42, 128.33, 128.11, 128.06, 128.03, 127.93, 127.85, 127.77, 127.70, 127.45, 127.30, 103.11, 101.82, 83.55, 83.40, 77.26, 74.88, 74.68, 74.60, 74.57, 74.49, 73.70, 73.65, 73.60, 72.03, 71.10, 70.60, 68.58; m/z (HRMS+) 815.3397 [$\text{M} + \text{Na}$] $^+$ ($\text{C}_{47}\text{H}_{52}\text{O}_{11}\text{Na}$ requires 815.3402).

6.5.7.4. Synthesis of 31

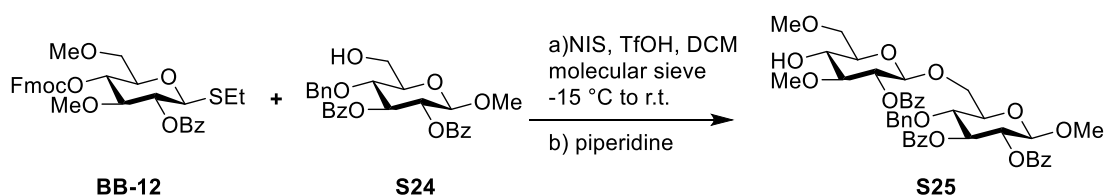
Synthesis of **S24**



Monosaccharide donor **S18** (200 mg, 0.27 mmol), *N*-iodosuccinimide (74.4 mg, 0.239 mmol) and MeOH (18 mg, 0.55 mmol) were dissolved in anhydrous DCM (20 mL). The solution was then stirred with molecular sieve for 1h at room temperature under nitrogen atmosphere and then cooled to -15 $^\circ\text{C}$. A 1% solution of TfOH in DCM (100 μL) was added and the reaction was stirred for 30 min at -15 $^\circ\text{C}$ before the removal of cooling bath to raise the temperature to room temperature. After TLC indicated the disappearance of **S18**, piperidine (1 mL) was added and the yellow solution was stirred at room temperature for additional 30 min. The reaction was diluted with DCM and washed with H_2O , then saturated aqueous NaCl. The organic layer was dried over Na_2SO_4 , filtered and evaporated. The resulting yellow oil was purified by column chromatography (hexane:EtOAc = 2:1) to give **S24** as colorless oil (119 mg, 91%).

Analytical data for **2,3-di-O-benzoyl-4-O-benzyl-1-methyl-β-D-glucopyranose, S24**: ¹H NMR (600 MHz, CDCl₃) δ 7.93 (ddt, *J* = 12.2, 8.3, 1.1 Hz, 4H), 7.52 – 7.46 (m, 2H), 7.36 (td, *J* = 7.7, 3.8 Hz, 4H), 7.22 – 7.06 (m, 5H), 5.74 (t, *J* = 9.6 Hz, 1H), 5.36 – 5.30 (m, 1H), 4.66 – 4.62 (m, 1H), 4.61 (s, 2H), 4.01 – 3.93 (m, 2H), 3.84 (dd, *J* = 12.1, 3.8 Hz, 1H), 3.61 (dt, *J* = 9.7, 3.1 Hz, 1H), 3.52 (s, 3H); ¹³C NMR (151 MHz, cdcl₃) δ 165.84, 165.52, 137.30, 133.31, 133.25, 129.96, 129.86, 129.53, 129.52, 128.52, 128.51, 128.44, 128.34, 128.33, 128.12, 102.21, 75.67, 75.56, 75.11, 74.98, 72.18, 61.68, 57.43; *m/z* (HRMS+) 515.1687 [M + Na]⁺ (C₂₈H₂₈O₈Na requires 515.1676).

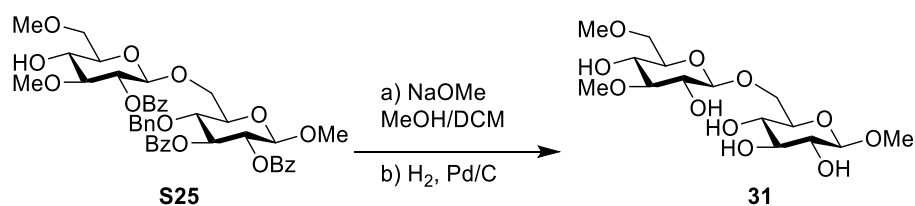
Synthesis of **S25**



Monosaccharide acceptor **S24** (90.0 mg, 0.188 mmol), donor **BB-12** (131.6 mg, 0.226 mmol) and *N*-iodosuccinimide (51.9 mg, 0.226 mmol) were dissolved in anhydrous DCM (20 mL). The solution was stirred with molecular sieve for 1h at room temperature under nitrogen atmosphere and then cooled to -15 °C. A 1% solution of TfOH in DCM (90 μL) was added and the reaction was stirred for 30 min at -15 °C before the removal of the cooling bath to raise the temperature to room temperature. After TLC indicated the disappearance of **S24**, piperidine (1 mL) was added and the yellow solution was stirred at room temperature for additional 30 min. The reaction was diluted with DCM and washed with H₂O, then saturated aqueous NaCl. The organic layer was dried over Na₂SO₄, filtered and evaporated. The resulting yellow oil was purified by column chromatography (hexane:EtOAc = 1:1.5) to give **S25** as white solid (125 mg, 78%).

Analytical data for **25**: ¹H NMR (600 MHz, CDCl₃) δ 7.92 (ddd, *J* = 13.7, 8.3, 1.4 Hz, 4H), 7.71 – 7.65 (m, 2H), 7.48 (ddt, *J* = 7.4, 5.7, 1.7 Hz, 2H), 7.43 – 7.38 (m, 3H), 7.35 (ddd, *J* = 8.2, 4.1, 2.9 Hz, 4H), 7.18 – 7.09 (m, 3H), 7.00 (dd, *J* = 7.8, 1.7 Hz, 2H), 5.93 (d, *J* = 5.2 Hz, 1H), 5.70 – 5.65 (m, 1H), 5.32 (dd, *J* = 9.8, 7.9 Hz, 1H), 4.59 – 4.54 (m, 2H), 4.52 – 4.44 (m, 2H), 3.84 (t, *J* = 9.4 Hz, 1H), 3.77 (dd, *J* = 10.5, 2.0 Hz, 1H), 3.70 (td, *J* = 4.3, 2.8 Hz, 2H), 3.67 – 3.62 (m, 2H), 3.58 (ddd, *J* = 10.0, 7.5, 4.2 Hz, 2H), 3.51 (q, *J* = 1.6 Hz, 1H), 3.50 (s, 3H), 3.49 (s, 3H), 3.39 (s, 3H), 2.75 (s, 1H); ¹³C NMR (151 MHz, cdcl₃) δ 165.79, 165.53, 165.51, 137.24, 136.11, 133.28, 133.18, 129.96, 129.86, 129.85, 129.66, 129.60, 129.54, 128.56, 128.52, 128.51, 128.50, 128.44, 128.41, 128.19, 127.99, 126.39, 120.05, 101.79, 98.28, 81.82, 76.17, 75.80, 75.24, 74.77, 74.16, 72.89, 72.16, 71.26, 68.82, 62.51, 59.63, 58.46, 56.98; *m/z* (HRMS+) 809.2792 [M + Na]⁺ (C₄₃H₄₆O₁₄Na requires 809.2780).

Synthesis of **31**

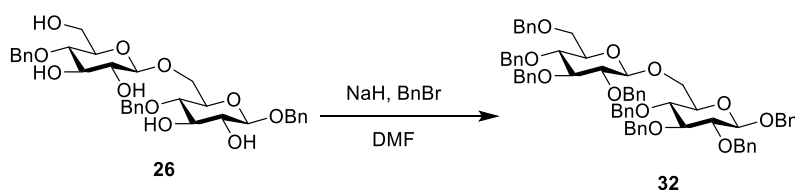


Disaccharide **S25** (125 mg, 0.106 mmol) was dissolved in MeOH: DCM (1.5 mL, 1:1). NaOMe in MeOH (0.5 M, 3 equiv. per benzoyl ester) was added and the solution was stirred at room temperature for 12 h, neutralized with Amberlite IR-120 (H⁺ form) resin, filtered and concentrated *in vacuo*. The crude compound was dissolved in 2 mL of *t*BuOH:H₂O (1:1). 100% by weight Pd-C (10%) was added and the reaction was stirred in H₂ bomb with 60 psi pressure for 10 minutes. The reactions were filtered through celite, washed with MeOH. The filtrates were concentrated *in vacuo*. The resulting yellow oil was purified by C18 silica column chromatography (H₂O: MeOH = 10:1) to give **31** as white solid (45.8 mg, 75%).

Analytical data for **31**: ¹H NMR (400 MHz, Deuterium Oxide) δ 4.34 (d, *J* = 7.8 Hz, 1H), 4.20 (d, *J* = 8.0 Hz, 1H), 4.02 (dd, *J* = 11.7, 2.0 Hz, 1H), 3.68 (dd, *J* = 11.7, 5.8 Hz, 1H), 3.60 (dd, *J* = 11.1, 1.9 Hz, 1H), 3.49 – 3.45 (m, 1H), 3.44 (s, 3H), 3.41 (d, *J* = 1.9 Hz, 1H), 3.39 (s, 3H), 3.37 (d, *J* = 1.8 Hz, 1H), 3.35 – 3.25 (m, 3H), 3.23 (s, 3H), 3.19 (dd, *J* = 10.4, 2.5 Hz, 1H), 3.15 – 3.05 (m, 2H); ¹³C NMR (101 MHz, d₂o) δ 103.23, 102.69, 84.92, 75.53, 74.71, 74.22, 72.91, 72.16, 70.76, 69.27, 68.87, 68.61, 59.58, 58.46, 57.27; *m/z* (HRMS+) 407.1528 [M + Na]⁺ (C₁₅H₂₈O₁₁Na requires 407.1524).

6.5.8. Synthesis of fully functionalized dimers

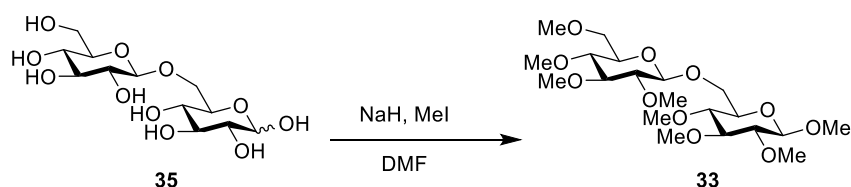
6.5.8.1. Synthesis of **32**



Disaccharide **26** (25.0 mg, 0.0408 mmol) and benzyl bromide (52.0 mg, 0.306 mmol) were dissolved in DMF (2 mL). NaH (7.3 mg, 0.306 mmol) was added and the solution was stirred at room temperature for 12 h. The reaction was then quenched with MeOH (0.1 mL), diluted with DCM and washed with H₂O and saturated aqueous NaCl. The organic layers were dried over Na₂SO₄, filtered and evaporated. The resulting yellow oil was purified by column chromatography (hexane:EtOAc = 4:1) to give **32** as white solid (30.5 mg, 70%).

Analytical data for **32**: ^1H NMR (600 MHz, CDCl_3) δ 7.35 – 7.19 (m, 38H), 7.16 (d, J = 6.9 Hz, 2H), 5.01 (d, J = 11.1 Hz, 1H), 4.96 – 4.88 (m, 3H), 4.86 (d, J = 12.0 Hz, 1H), 4.81 (d, J = 10.8 Hz, 1H), 4.77 (dd, J = 10.9, 6.7 Hz, 4H), 4.70 (d, J = 10.9 Hz, 1H), 4.61 (d, J = 12.2 Hz, 1H), 4.57 – 4.48 (m, 4H), 4.48 – 4.43 (m, 2H), 4.22 (d, J = 11.3 Hz, 1H), 3.70 (ddd, J = 21.0, 11.1, 7.4 Hz, 3H), 3.66 – 3.55 (m, 4H), 3.49 (td, J = 8.4, 3.2 Hz, 2H), 3.44 (t, J = 9.2 Hz, 2H); ^{13}C NMR (151 MHz, cdcl_3) δ 138.56, 138.47, 138.37, 138.17, 138.01, 137.49, 128.40, 128.36, 128.34, 128.32, 128.14, 128.06, 127.92, 127.86, 127.76, 127.70, 127.63, 127.61, 127.59, 127.57, 103.97, 102.59, 84.75, 84.70, 82.30, 82.14, 78.31, 77.82, 75.69, 75.67, 75.16, 74.95, 74.93, 74.87, 74.84, 74.77, 73.51, 71.13, 68.92, 68.62; m/z (HRMS+) 1085.4802 [$\text{M} + \text{Na}$] $^+$ ($\text{C}_{68}\text{H}_{70}\text{O}_{11}\text{Na}$ requires 1085.4810).

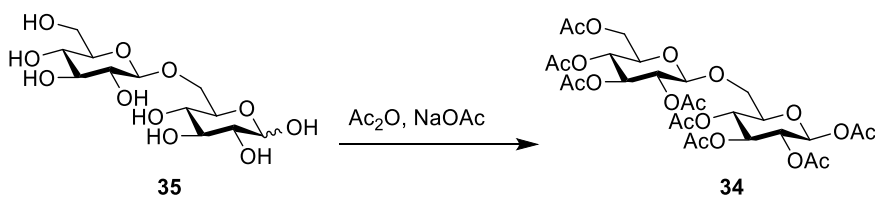
6.5.8.2. Synthesis of **33**



Disaccharide **35** (25.0 mg, 0.0731 mmol) and methyl iodide (125 mg, 0.877 mmol) were dissolved in of DMF (2 mL). NaH (21 mg, 0.877 mmol) was added and the solution was stirred at room temperature for 12 h. The reaction was then quenched by MeOH (0.1 mL), diluted with DCM and washed with H_2O and saturated aqueous NaCl. The organic layers were dried over Na_2SO_4 , filtered and evaporated. The resulting yellow oil was purified by column chromatography (hexane: acetone: DCM = 9:3:1) to give **33** as white solid (10.5 mg, 31%).

Analytical data for **33**: ^1H NMR (600 MHz, CDCl_3) δ 4.31 (d, J = 7.8 Hz, 1H), 4.15 (dd, J = 10.9, 1.9 Hz, 1H), 4.13 (d, J = 7.7 Hz, 1H), 3.65 – 3.62 (m, 2H), 3.62 (s, 3H), 3.61 (s, 3H), 3.57 (s, 3H), 3.56 (s, 3H), 3.56 – 3.53 (m, 1H), 3.52 (s, 6H), 3.51 (s, 3H), 3.40 (s, 3H), 3.36 (ddd, J = 10.0, 6.4, 1.9 Hz, 1H), 3.26 (ddt, J = 7.0, 4.9, 2.2 Hz, 1H), 3.17 (t, J = 8.9 Hz, 1H), 3.13 (dd, J = 6.8, 2.6 Hz, 2H), 3.06 – 3.00 (m, 2H), 2.97 (dd, J = 9.1, 7.7 Hz, 1H); ^{13}C NMR (151 MHz, cdcl_3) δ 104.17, 103.84, 86.59, 86.40, 83.73, 83.59, 79.82, 79.33, 74.60, 74.59, 71.36, 68.72, 60.77, 60.74, 60.43, 60.40, 60.35, 60.30, 59.34, 56.91; m/z (HRMS+) 477.2307 [$\text{M} + \text{Na}$] $^+$ ($\text{C}_{68}\text{H}_{70}\text{O}_{11}\text{Na}$ requires 477.2306).

6.5.8.3. Synthesis of **34**

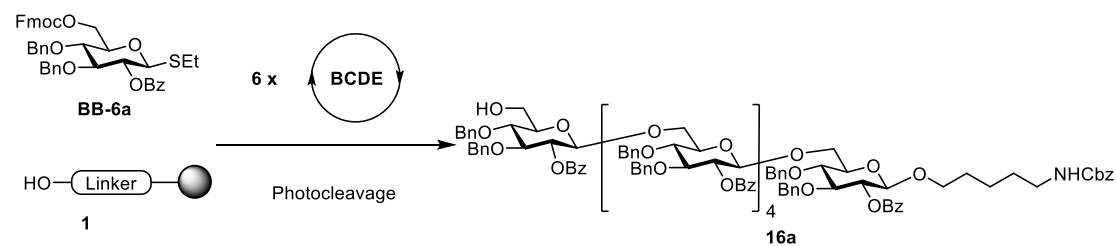


A suspension of **35** (50.0 mg, 0.146 mmol) in acetic anhydride (2 mL) was heated to 90°C. NaOAc (201 mg, 2.33 mmol) was added and the solution was stirred at the same temperature for 12 h. The reaction was then cooled down to room temperature and evaporated. The crude product was suspended in DCM and washed with H₂O and saturated aqueous NaCl. The organic layer was dried over Na₂SO₄, filtered and evaporated. The resulting yellow oil was purified by column chromatography (hexane:EtOAc = 3:1) and recrystallized to give **34** as white solid (45.0 mg, 45%).

Analytical data for **34**: ¹H NMR (400 MHz, CDCl₃) δ 5.67 (d, *J* = 8.2 Hz, 1H), 5.19 (dt, *J* = 15.4, 9.5 Hz, 2H), 5.11 – 4.92 (m, 4H), 4.53 (d, *J* = 7.9 Hz, 1H), 4.24 (dd, *J* = 12.4, 4.7 Hz, 1H), 4.10 (dd, *J* = 12.3, 2.4 Hz, 1H), 3.97 – 3.87 (m, 1H), 3.81 – 3.72 (m, 1H), 3.65 (dt, *J* = 9.6, 3.3 Hz, 1H), 3.55 (dd, *J* = 11.4, 5.8 Hz, 1H), 2.09 (s, 3H), 2.07 (s, 3H), 2.06 (s, 3H), 2.02 (s, 3H), 2.01 (s, 3H), 1.99 (s, 6H); ¹³C NMR (151 MHz, CDCl₃) δ 170.58, 170.17, 170.02, 169.46, 169.34, 169.33, 169.16, 168.75, 100.58, 91.56, 73.85, 72.81, 72.70, 71.87, 70.86, 70.22, 68.39, 68.30, 67.45, 61.80, 20.73, 20.68, 20.55, 20.53, 20.51, 20.49; *m/z* (HRMS+) 701.1893 [M + Na]⁺ (C₆₈H₇₀O₁₁Na requires 701.1899).

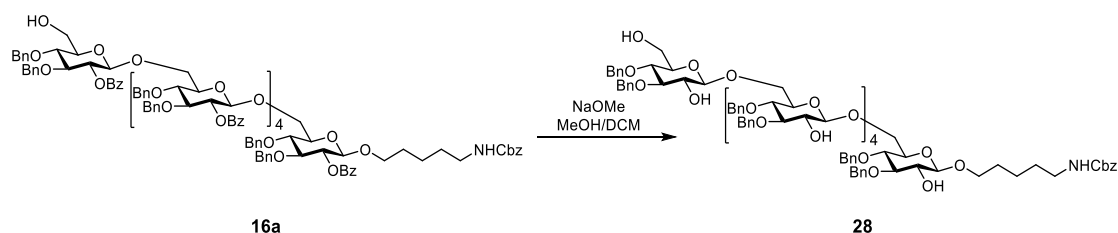
6.5.9. AGA synthesis of partially deprotected hexamers

6.5.9.1. Synthesis of 28



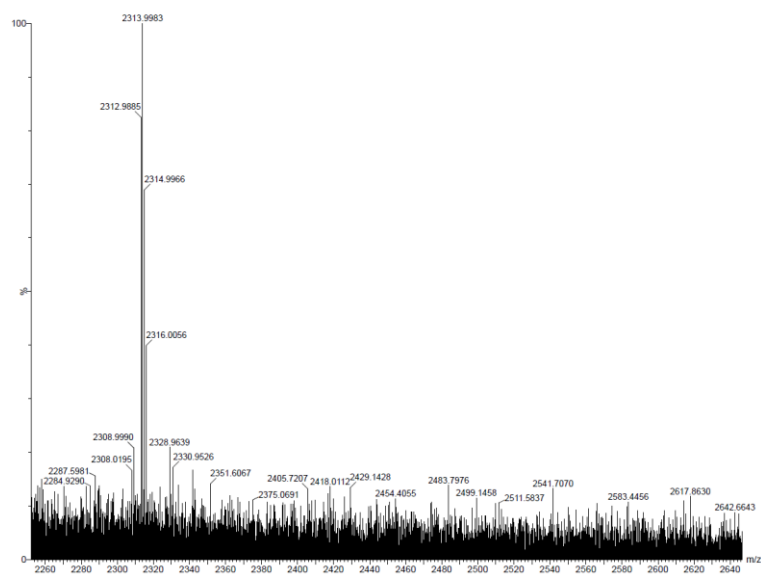
Module	Conditions
A: Resin Preparation for Synthesis	
6	B: Acidic Wash with TMSOTf Solution
	C: Thioglycoside Glycosylation BB-6a , 6.5 equiv. (-20°C 5 min, 0°C 5 min)
	D: Capping
	E: Fmoc Deprotection

Cleavage from the solid support as described in *Post-synthesizer manipulation* followed by purification using preparative HPLC afforded compound **16a** (27.0 mg, 74%).

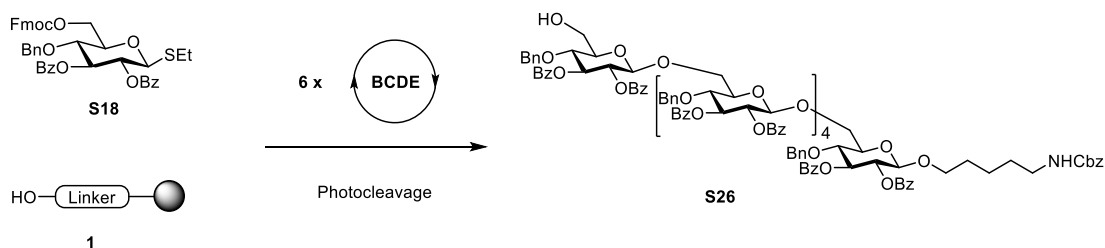


Hexasaccharide **16a** (27.0 mg, 9.27 μmol) was dissolved in MeOH: DCM (1.5 mL, 1:1). NaOMe in MeOH (0.5 M, 3 equiv. per benzoyl ester) was added and the solution was stirred at room temperature for 12 h and then filtered. The resulting solid compound was dispersed in Milli-Q water and sonicated for 1h. The white suspension was then centrifuged at 7000 rcf for 10 min followed by removal of supernatant. The sonication and centrifugation was repeated twice. The solid was then dried *in vacuo* overnight to give **28** as white powder (13.5 mg, 63%); m/z (HRMS+) 2312.999 $[\text{M} + \text{Na}]^+$ ($\text{C}_{133}\text{H}_{151}\text{NO}_{33}\text{Na}$ requires 2313.006); due to the low solubility of compound **28**, no distinguishable NMR spectrum was able to be obtained.

HRMS of **28**



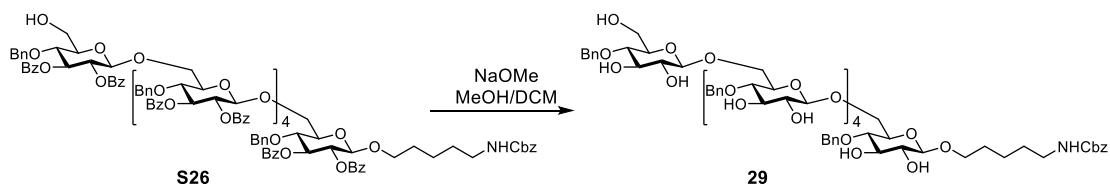
6.5.9.2. Synthesis of **29**



Module	Conditions
A: Resin Preparation for Synthesis	
6	B: Acidic Wash with TMSOTf Solution
	C: Thioglycoside Glycosylation S18 , 6.5 equiv. (-20°C 5 min, 0°C 5 min)
	D: Capping
	E: Fmoc Deprotection

Cleavage from the solid support as described in *Post-synthesizer manipulation* followed by purification using preparative HPLC afforded **S26** (23.0 mg, 61%).

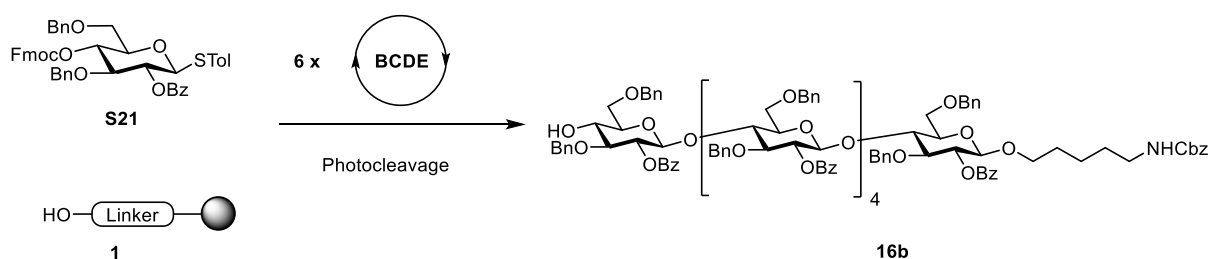
Analytical data for **S26** (1-6): $^1\text{H NMR}$ (600 MHz, CDCl_3) δ 8.29 – 8.22 (m, 6H), 8.20 (d, $J = 7.7$ Hz, 2H), 8.14 – 8.08 (m, 4H), 8.07 (d, $J = 7.9$ Hz, 2H), 8.03 (d, $J = 8.0$ Hz, 1H), 8.01 – 7.92 (m, 6H), 7.90 – 7.86 (m, 2H), 7.53 – 7.43 (m, 4H), 7.42 – 7.20 (m, 22H), 7.20 – 6.99 (m, 21H), 6.99 – 6.94 (m, 2H), 6.93 – 6.85 (m, 5H), 6.85 – 6.73 (m, 4H), 6.73 – 6.64 (m, 5H), 6.61 (t, $J = 7.4$ Hz, 1H), 6.53 (t, $J = 7.5$ Hz, 2H), 6.50 – 6.44 (m, 4H), 6.41 (t, $J = 7.5$ Hz, 2H), 6.02 (t, $J = 9.6$ Hz, 2H), 5.95 (td, $J = 9.6, 7.1$ Hz, 2H), 5.89 – 5.78 (m, 4H), 5.72 – 5.60 (m, 3H), 5.53 – 5.43 (m, 3H), 5.31 (d, $J = 8.0$ Hz, 1H), 5.27 (d, $J = 8.1$ Hz, 1H), 5.11 (t, $J = 10.5$ Hz, 1H), 5.07 – 4.95 (m, 3H), 4.95 – 4.88 (m, 1H), 4.78 (br, 1H), 4.69 – 4.60 (m, 4H), 4.42 – 4.22 (m, 11H), 4.22 – 4.12 (m, 4H), 4.09 – 3.92 (m, 7H), 3.85 – 3.72 (m, 3H), 3.71 – 3.65 (m, 2H), 3.63 (d, $J = 9.6$ Hz, 1H), 3.59 – 3.53 (m, 2H), 3.51 (t, $J = 9.5$ Hz, 1H), 3.28 – 3.24 (m, 1H), 3.21 (dd, $J = 13.4, 2.6$ Hz, 1H), 2.93 (dq, $J = 12.5, 6.3$ Hz, 2H), 1.68 – 1.59 (m, 2H), 1.47 – 1.35 (m, 2H), 1.34 – 1.27 (m, 2H). NMR data were in good agreement with those previously reported.



Hexasaccharide **S26** (23.0 mg, 7.67 μmol) was dissolved in MeOH: DCM (1.5 mL, 1:1). NaOMe in MeOH (0.5 M, 3 equiv. per benzoyl ester) was added and the solution was stirred at room temperature for 12 h, neutralized with Amberlite IR-120 (H^+ form) resin, filtered and concentrated *in vacuo*. The resulting yellow oil was purified by column chromatography (DCM: MeOH = 10:1) to give **29** as white solid (10.2 mg, 76%).

Analytical data for **29**: ^1H NMR (600 MHz, Methanol- d_4) δ 8.01 – 7.96 (m, 2H), 7.55 – 7.51 (m, 1H), 7.42 (t, $J = 7.7$ Hz, 2H), 7.37 (t, $J = 6.6$ Hz, 4H), 7.35 – 7.26 (m, 20H), 7.23 (qt, $J = 7.2, 4.2$ Hz, 6H), 6.88 (dd, $J = 6.9, 4.5$ Hz, 1H), 5.04 (s, 2H), 4.92 (d, $J = 4.6$ Hz, 1H), 4.91 – 4.86 (m, 5H), 4.66 (dd, $J = 11.1, 6.7$ Hz, 2H), 4.60 – 4.54 (m, 4H), 4.34 – 4.30 (m, 2H), 4.29 – 4.26 (m, 1H), 4.22 (d, $J = 7.8$ Hz, 1H), 4.18 (d, $J = 7.9$ Hz, 1H), 4.09 (ddd, $J = 11.9, 7.5, 2.1$ Hz, 2H), 4.04 – 3.94 (m, 3H), 3.86 (dt, $J = 9.7, 6.7$ Hz, 1H), 3.77 – 3.70 (m, 4H), 3.70 – 3.58 (m, 5H), 3.57 – 3.47 (m, 8H), 3.37 (pd, $J = 9.2, 5.6$ Hz, 7H), 3.28 – 3.20 (m, 4H), 3.16 (ddd, $J = 10.1, 4.8, 2.2$ Hz, 1H), 3.10 (q, $J = 6.7$ Hz, 2H), 1.60 (q, $J = 7.7, 7.3$ Hz, 2H), 1.49 (q, $J = 7.3$ Hz, 2H), 1.39 (s, 2H), 1.27 (s, 2H), 0.87 (dt, $J = 18.7, 6.4$ Hz, 2H); ^{13}C NMR (151 MHz, cd_3od) δ 157.46, 138.66, 138.64, 138.62, 131.97, 129.18, 128.03, 127.96, 127.95, 127.92, 127.92, 127.88, 127.85, 127.81, 127.71, 127.66, 127.63, 127.50, 127.37, 127.30, 127.29, 127.25, 127.23, 127.20, 103.81, 103.61, 103.58, 103.52, 103.45, 102.72, 78.44, 78.41, 78.29, 78.07, 77.71, 77.14, 77.09, 77.04, 76.94, 75.57, 74.54, 74.42, 74.38, 74.30, 74.26, 74.13, 74.03, 73.92, 73.84, 73.80, 69.44, 69.05, 68.44, 65.90, 60.88, 48.13, 47.99, 47.84, 47.70, 47.56, 47.42, 47.28, 47.14, 40.38, 29.17, 28.97, 22.88; m/z (HRMS+) 1172.721 $[\text{M} + \text{Na}]^+$ ($\text{C}_{91}\text{H}_{111}\text{NNaO}_{33}\text{Na}$ requires 1772.724).

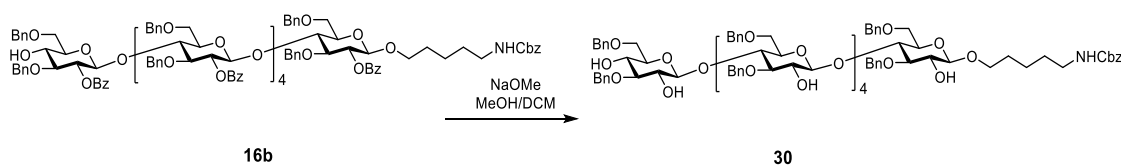
6.5.9.3. Synthesis of 30



Module	Conditions
A: Resin Preparation for Synthesis	
6	B: Acidic Wash with TMSOTf Solution
	C: Thioglycoside Glycosylation S21 , 6.5 equiv. (-20°C 5 min, 0°C 5 min)
	D: Capping

E: Fmoc Deprotection

Post-synthesizer manipulation followed by purification using preparative HPLC afforded compound **16b** (17.0 mg, 47%).



Hexasaccharide **16b** (17.0 mg, 5.83 μmol) was dissolved in MeOH: DCM (1.5 mL, 1:1). NaOMe in MeOH (0.5 M, 3 equiv. per benzoyl ester) was added and the solution was stirred at room temperature for 12 h, neutralized with Amberlite IR-120 (H^+ form) resin, filtered and concentrated *in vacuo*. The resulting yellow oil was purified by column chromatography (hexane: acetone = 3:1) to give **30** as white oil (10.2 mg, 76%).

Analytical data for **30**: ^1H NMR (400 MHz, CDCl_3) δ 7.39 – 7.18 (m, 65H), 5.10 (s, 1H), 4.94 – 4.85 (m, 6H), 4.85 – 4.64 (m, 6H), 4.62 – 4.32 (m, 14H), 4.25 (d, $J = 7.4$ Hz, 1H), 4.01 – 3.83 (m, 6H), 3.78 (d, $J = 10.9$ Hz, 1H), 3.69 – 3.48 (m, 11H), 3.42 (ddd, $J = 21.0, 12.1, 3.4$ Hz, 10H), 3.36 – 3.06 (m, 13H), 1.66 (q, $J = 6.7$ Hz, 4H), 1.59 – 1.52 (m, 4H), 1.43 (t, $J = 7.8$ Hz, 2H); ^{13}C NMR (101 MHz, CDCl_3) δ 156.44, 139.21, 139.19, 139.14, 139.11, 139.00, 138.75, 137.74, 137.44, 137.26, 137.21, 136.56, 128.54, 128.48, 128.41, 128.38, 128.36, 128.29, 128.27, 128.20, 128.15, 128.04, 127.91, 127.88, 127.75, 127.69, 127.38, 127.28, 127.22, 127.09, 126.84, 126.67, 126.57, 126.53, 103.83, 103.79, 103.69, 103.57, 103.35, 102.90, 83.52, 83.47, 83.38, 75.77, 75.51, 75.17, 74.57, 74.38, 74.22, 73.64, 73.60, 73.55, 71.65, 70.44, 69.76, 68.58, 66.64, 40.85, 29.74, 29.58, 29.03, 23.17; m/z (HRMS+) 2328.977 [$\text{M} + \text{K}$] $^+$ ($\text{C}_{133}\text{H}_{151}\text{NO}_{33}\text{K}$ requires 2328.980).

6.6. Solubility, XRD measurements, and MD simulation of cellulose analogues

6.6.1. Solubility measurements

The lyophilized oligomer was weighed in a glass vial and water was injected in portions. After each portion, the mixture was bubbled with N₂ through a syringe for 30 seconds. Upon complete disappearance of insoluble matter, the range of solubility was calculated. The water addition was stopped when the solubility was calculated to be less than 1 mg/mL.

Sample	Mass	Last volume before dissolution (μL)	Volume upon dissolution (μL)	Solubility (mg/mL)
A ₆	1.0 mg	1000	-	<1
A ₃ B ₃	1.0 mg	-	20	>50
(ABA) ₂	1.0 mg	-	20	>50
(AB) ₃	1.0 mg	-	20	>50
ABACAB	1.0 mg	-	20	>50
(ACA) ₂	1.0 mg	-	20	>50
(AC) ₃	1.0 mg	-	20	>50
(AFA) ₂	1.1 mg	-	20	>50
(FA) ₃	1.0 mg	-	20	>50
(ADA) ₂	1.0 mg	-	20	>50
(DA) ₃	1.0 mg	-	20	>50
(AEA) ₂	1.0 mg	-	20	>50
(AE) ₃	1.0 mg	-	20	>50
N ₆	2.6 mg	150	200	13-17
(ANA) ₂	1.0 mg	-	20	>50
A ₁₂	0.6 mg	600	-	<1
A ₃ B ₃ A ₃ B ₃	1.0 mg	-	20	>50
(ABA) ₂ A ₃ B ₃	1.0 mg	-	20	>50

(ABA)₄	1.0 mg	-	20	>50
(ABACAB)₂	1.0 mg	-	20	>50
(ADA)₄	1.0 mg	-	20	>50

6.6.2. XRD Analysis

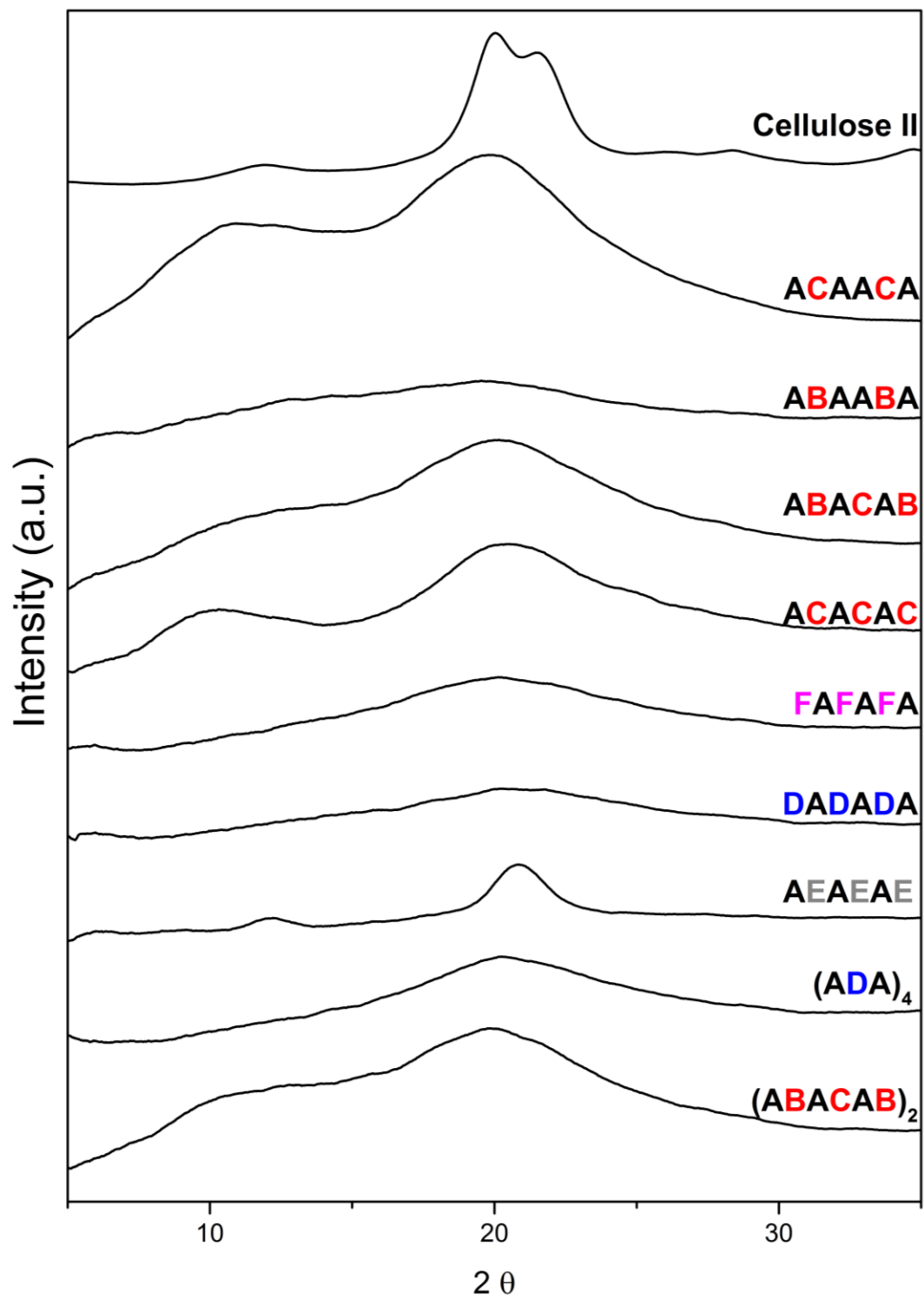


Figure 6-1. XRD data of cellulose analogues.

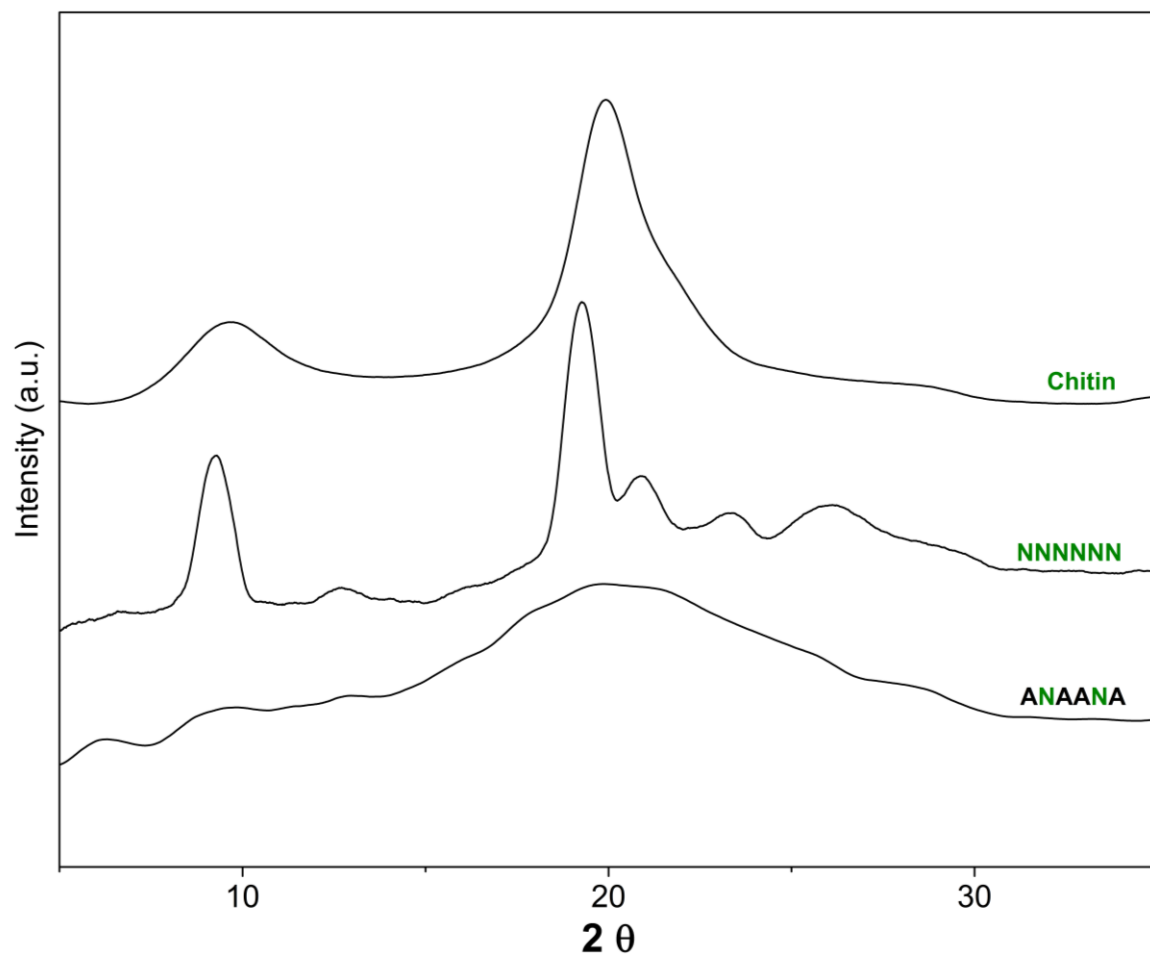


Figure 6-2. Comparison of XRD data of Chitin, NNNNNN, and ANAANA.

6.6.3. Molecular Dynamics Simulations (selected, by Theodore Tyrikos-Ergas)

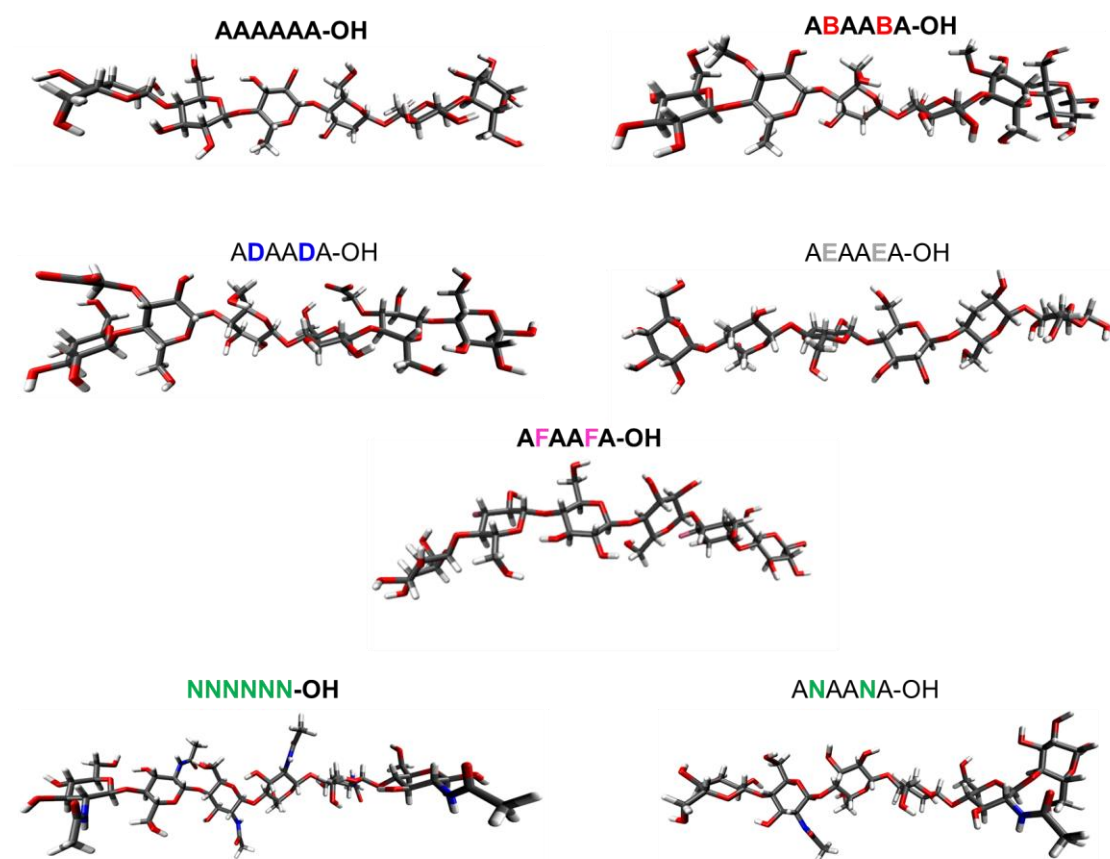


Figure 6-3. Hexasaccharide conformations as obtained by MD simulations (selected).

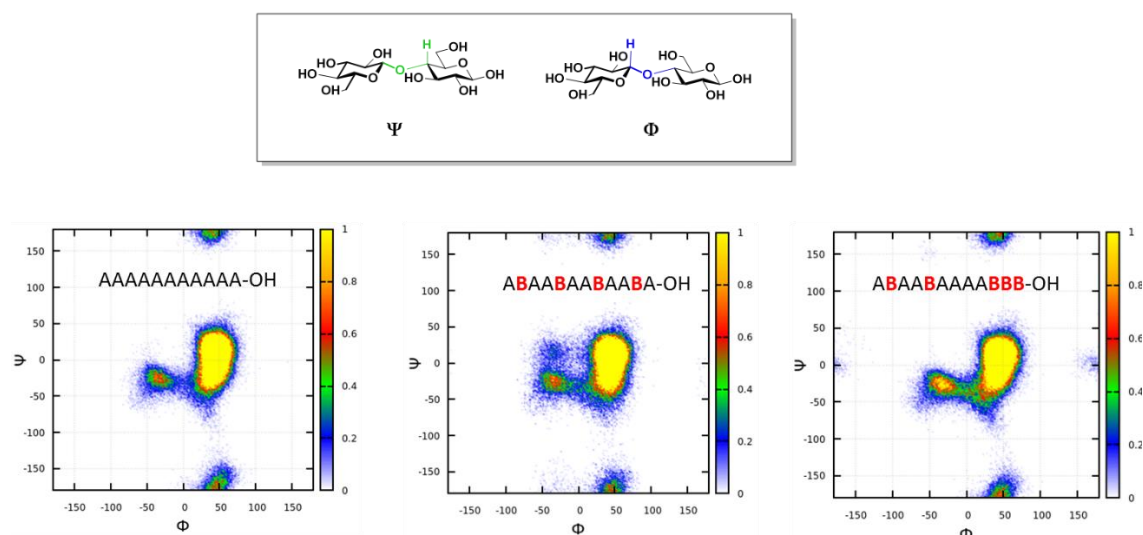


Figure 6-4. Ramachandran plots of dodecamers (selected). A noticeable deviation of the methylated analogues conformations from the main population of A_{12} was observed. An irregular substitution pattern appears to be important to drastically change the cellulose conformation (e.g. $(ABA)_2A_3B_3$). A regular substitution pattern such as $(ABA)_4$ maintains more cellulose character, while improving water solubility. A more detailed analysis of the dihedral angles can be found in reported literature.

6.7. Self-assembly of oligosaccharides and characterizations

6.7.1. Oligosaccharide self-assembly

6.7.1.1. Dialysis method

The oligosaccharide was dissolved in DMAc (1mL) and sonicated for 10 minutes. The mixture was diluted with 1 mL of ultrapure water and sonicated for additional 10 minutes. The final solutions with concentration of 0.01, 0.1 and 2 mg mL⁻¹ were prepared by extensive dialysis (3 days) at room temperature with 500 Da and 1 kDa dialysis tube, for dimers and hexamers, respectively.

Sample	Compound	Concentration (mg mL ⁻¹)
25-D	25	0.1
26-D	26	0.1
26-D-high		2.0
27-D	27	0.1

28-D	28	0.01*
29-D	29	0.1
30-D	30	0.01*

*0.01 mg mL⁻¹ due to poor solubility of the starting material.

6.7.1.2. Solvent-switch method

Stock solutions of the oligosaccharide (5, 10 and 100 mg mL⁻¹) in HFIP, isopropyl alcohol, acetone and DMAc were prepared. Ultrapure water was added at room temperature to give a final concentration of 0.1, 2 and 20 mg mL⁻¹.

Sample	Compound	Solvent	Organic solvent content (%)	Concentration (mg mL ⁻¹)
25-S-HFIP	25	HFIP	2	2.0
25-S-HFIP-low		HFIP	2	0.1
26-S-HFIP	26	HFIP	2	2.0
26-S-HFIP-20%		HFIP	20	
26-S-iPrOH-20%		iPrOH	20	
26-S-Ace-20%		Ace	20	20.0
26-S-Ace-20%-high				
26-S-DMAc		DMAc	2	2.0
27-S-HFIP	27	HFIP	2	
28-S-DMAc	28	DMAc	2	
29-S-HFIP	29	HFIP	2	
30-S-DMAc	30	DMAc	2	

6.7.1.3. Film-forming method

The oligosaccharide was dissolved in a proper solvent (10 mg mL⁻¹) and dried on the slide glass at room temperature.

Sample	Compound	Preparation method	Organic Solvent	Concentration (mg mL ⁻¹)
25-F-HFIP	25	Film-forming	HFIP	10.0
26-F-HFIP	26		HFIP	
26-F-iPrOH			iPrOH	
26-F-Ace			Ace	
26-F-DCM			DCM	
27-F-HFIP			27	
28-F-HFIP	28			
29-F-HFIP	29			
30-F-HFIP	30			
31-F-HFIP	31			
32-F-HFIP	32			
33-F-HFIP	33			
34-F-HFIP	34			
35-F-water	35	water		

6.7.2. Characterization of self-assembling samples

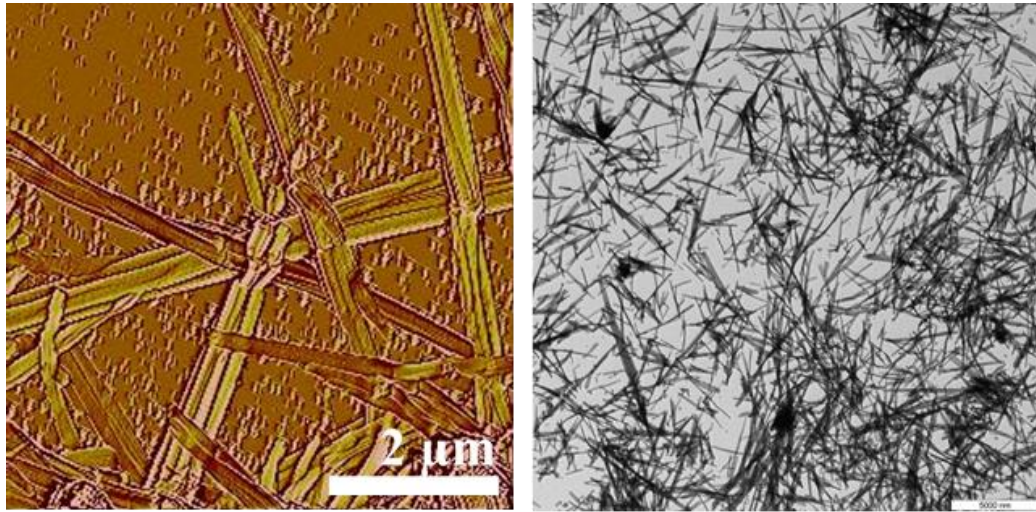


Figure 6-5. AFM (left) and TEM (right) images of 26-S-HFIP.

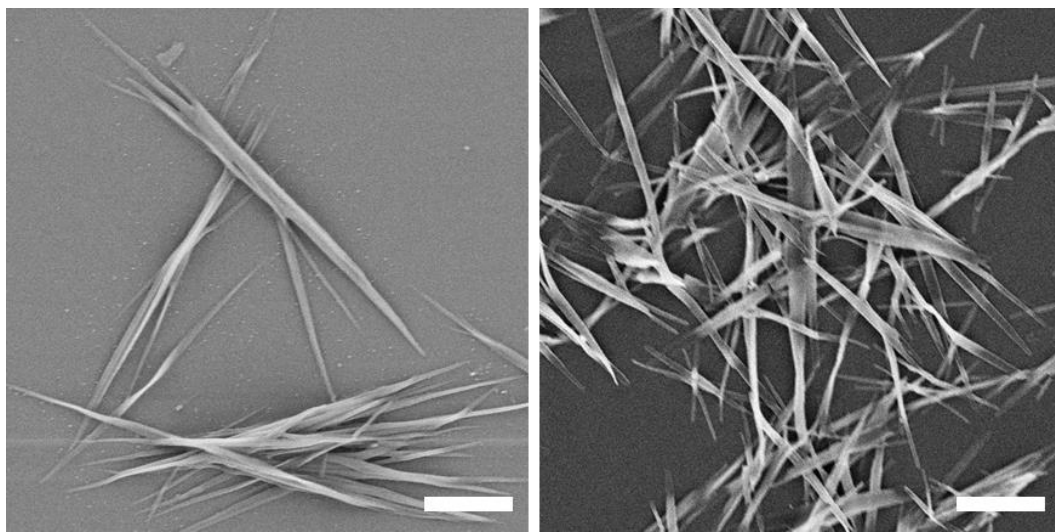


Figure 6-6. SEM images of 26-S-HFIP for time 0 (left) and after one month upon dilution (right) (scale bar: 2 μm).

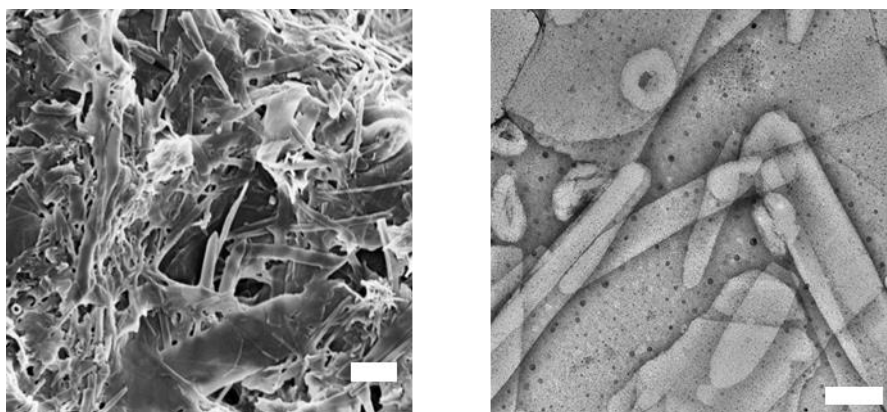


Figure 6-7. SEM (left, scale bar: 2 μm) and TEM (right, scale bar: 200 nm) images of 25-S-HFIP.

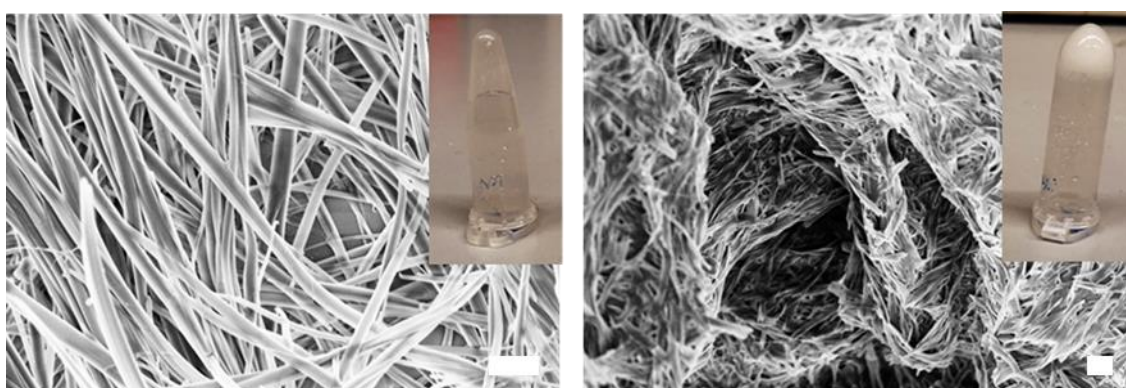


Figure 6-8. SEM images and photographs (inset) of 26-S-Ace-20% with 2 mg mL⁻¹ (left) and 26-S-Ace-20%-high with 20 mg mL⁻¹ (right) (scale bar: 2 μm).

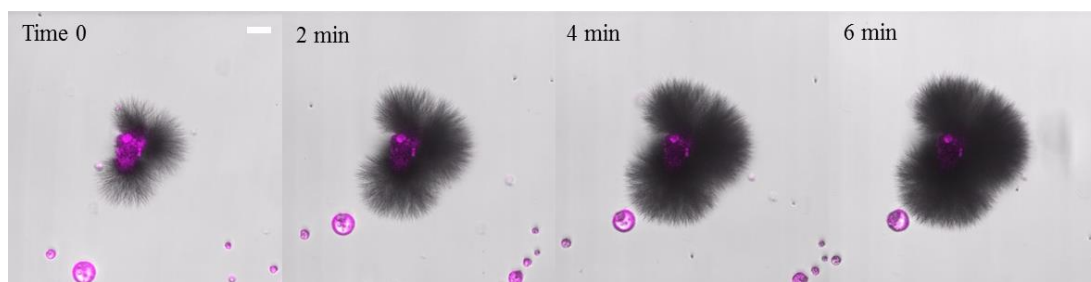


Figure 6-9. Real-time merged bright-field (scale of gray) and fluorescence (magenta) images of self-assembly process for 26-S-HFIP with excitation wavelength at 405 nm and detection range 410-676 nm (scale bar: 20 μm). Compound **26** was dissolved in HFIP with a 100 mg mL^{-1} concentration. After addition of ultrapure water (final concentration of 2 mg mL^{-1}), the solution was transferred to a cell counting slide (EVE™ slide from NanoEnTek) and observed with a confocal microscope.

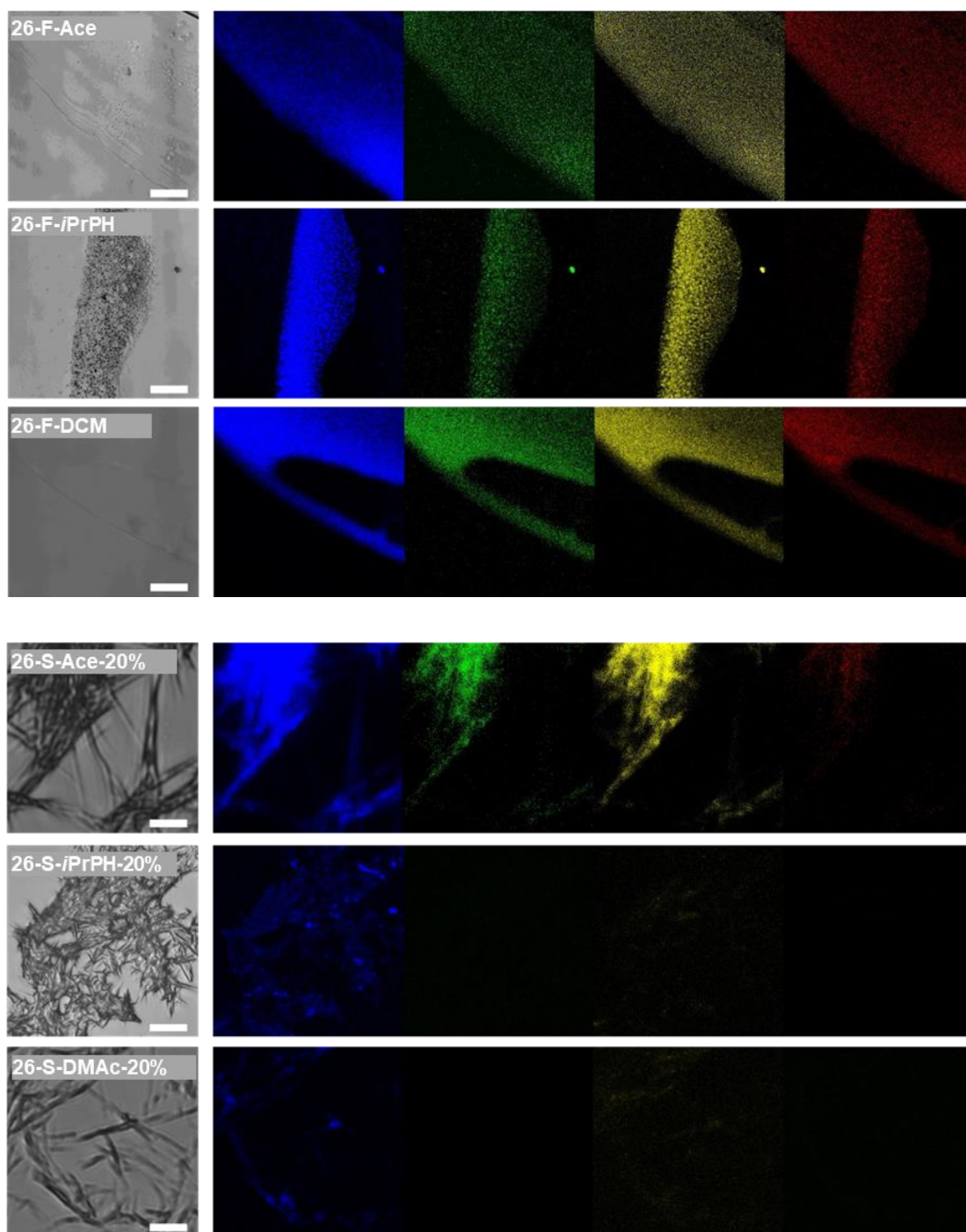


Figure 6-10. Confocal microscopy images of 26 prepared with different solvent with the film forming method F (top, scale bar: 100 μm) and the solvent-switch method S (bottom, scale bar: 10 μm) in four different channels (blue(ex/em): 405/451 nm, green: 488/529 nm, yellow: 561/597 nm, nd red: 633/709 nm).

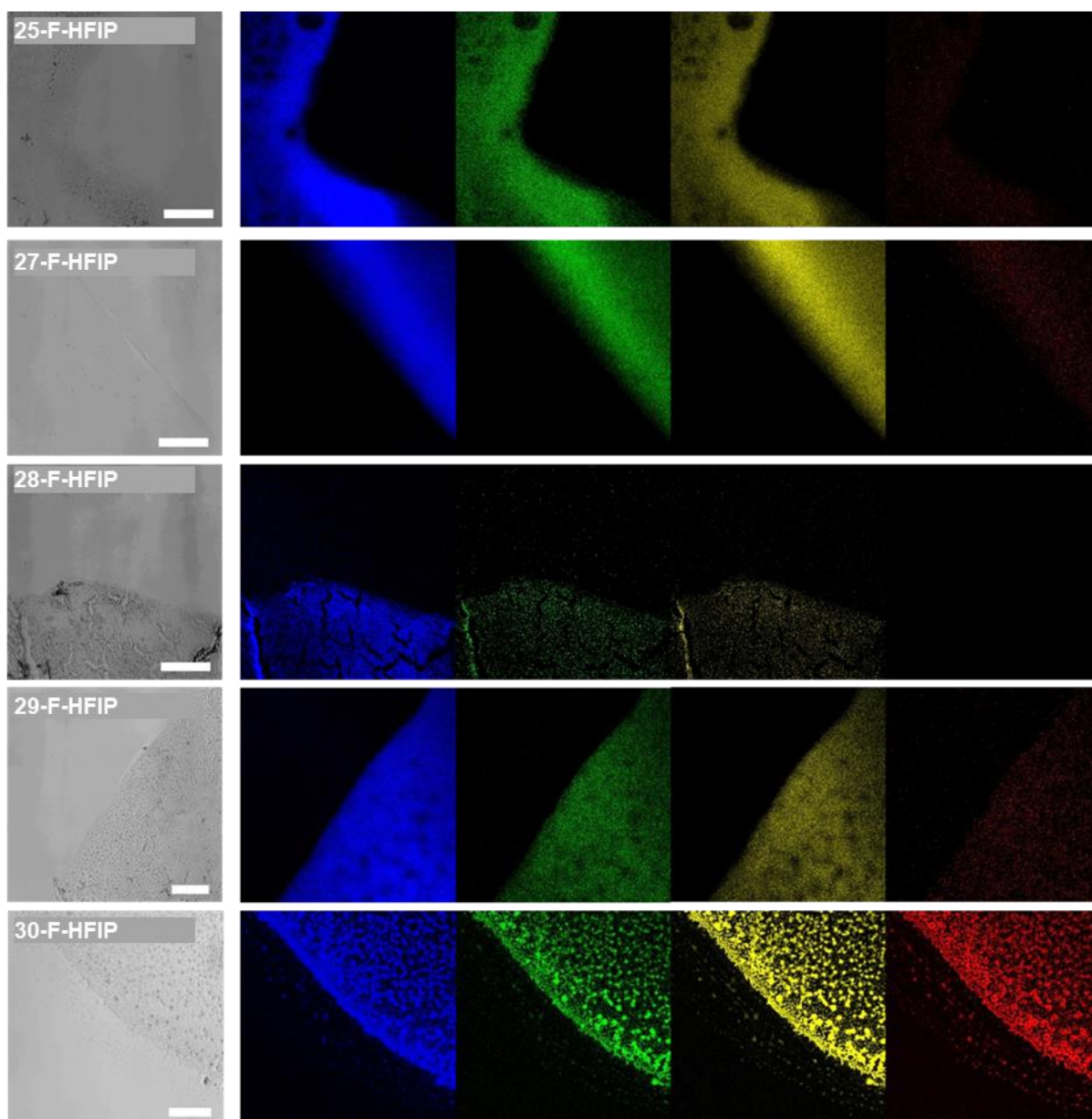


Figure 6-11. Confocal microscopy images of the five oligosaccharides prepared by film forming method F in four different channels (blue(ex/em): 405/451 nm, green: 488/529 nm, yellow: 561/597 nm, and red: 633/709 nm) (Scale bar: 100 μ m).

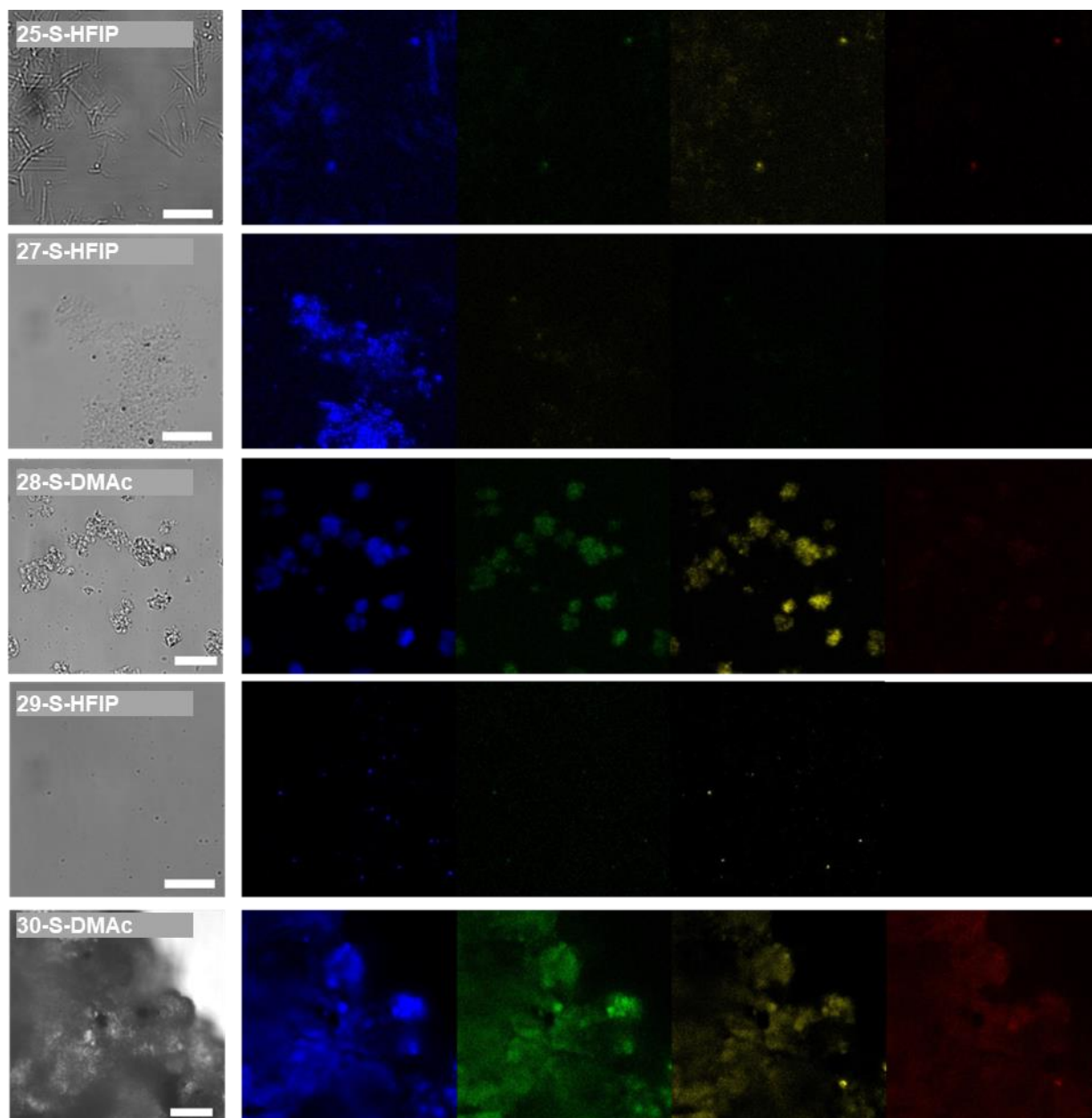


Figure 6-12. Confocal microscopy images of the five oligosaccharides prepared by solvent-switch method S in four different channels (blue(ex/em): 405/451 nm, green: 488/529 nm, yellow: 561/597 nm, and red: 633/709 nm). (Scale bar: 10 μ m).

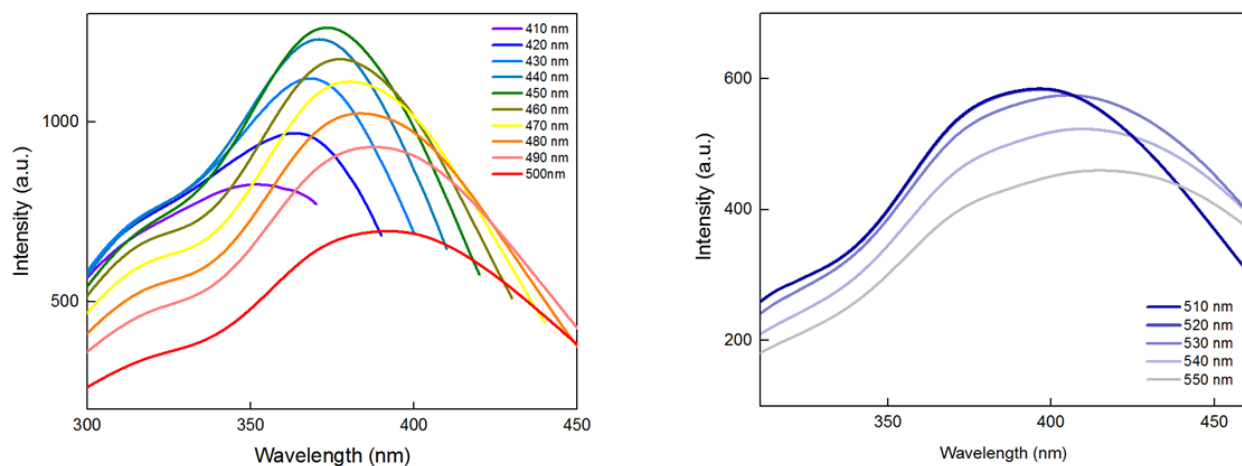


Figure 6-13. Excitation spectra for 26-F-HFIP at emission wavelengths of 410, 420, 430, 440, 450, 460, 470, 480, 490, 500, 510, 520, 530, 540 and 550 nm.

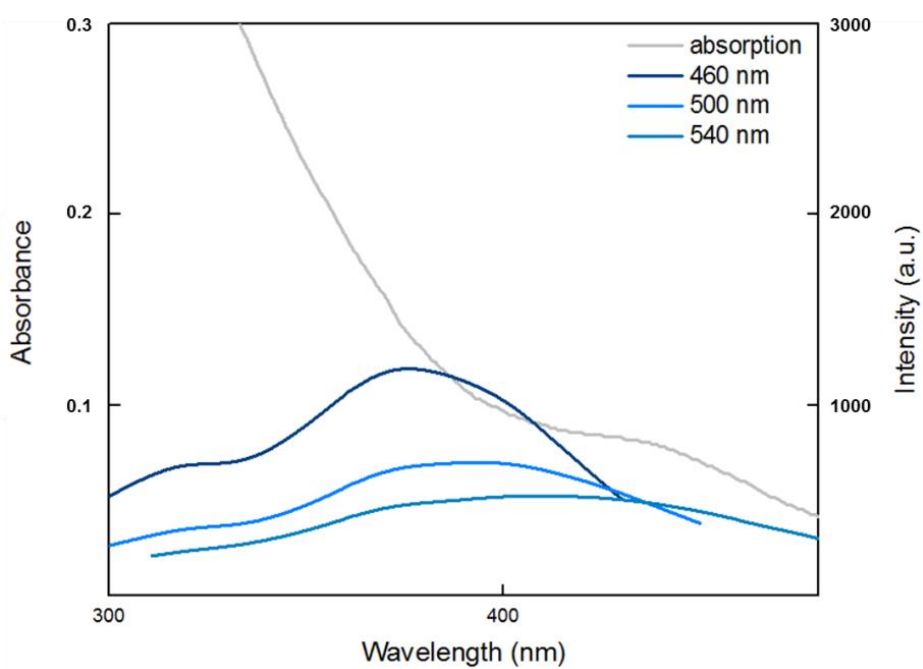


Figure 6-14. Absorption (grey) and excitation (scale of blue) spectra for 26-F-HFIP. Excitation spectra were recorded for emission wavelengths of 460, 500, and 540 nm.

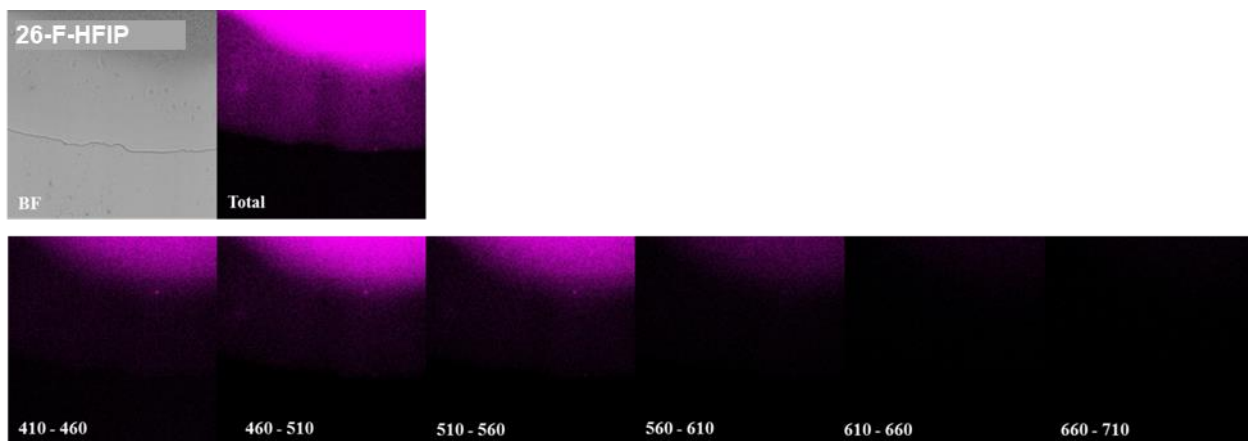


Figure 6-15. Fluorescence emission images of 26-F-HFIP collected at different spectral windows with excitation wavelength at 405 nm.

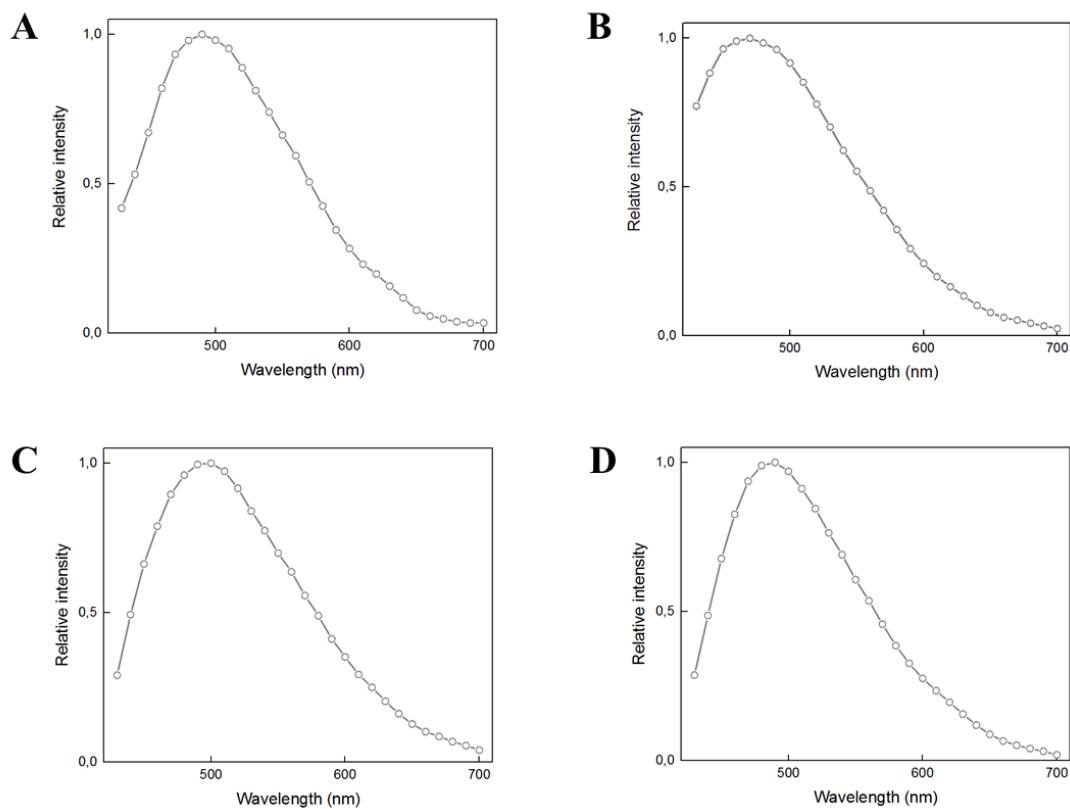


Figure 6-16. Emission spectra of (A) 26-F-HFIP, (B) 31-F-HFIP, (C) 32-F-HFIP, and (D) 33-F-HFIP from confocal microscopy with excitation wavelength at 405 nm.

7. References

1. Varki, Ajit, Richard D. Cummings, Jeffrey D. Esko, Pamela Stanley, Gerald W. Hart, Markus Aebi, and others, eds., *Essentials of Glycobiology, Third Edition*, 3rd edn (La Jolla, California: Cold Spring Harbor Laboratory Press, 2017)
2. Bertozzi, C. R.; Kiessling; L., L., Chemical Glycobiology. *Science* **2001**, *291* (5512), 2357-2364.
3. Feizi, T., Oligosaccharides that mediate mammalian cell-cell adhesion. *Curr. Opin. Struct. Biol.* **1993**, *3* (5), 701-710.
4. Schenkel-Brunner, H., *Human Blood Groups*. Springer-Verlag Wien: Vienna, 2000.
5. Dennis, J. W.; Laferte, S., Tumor cell surface carbohydrate and the metastatic phenotype. *Cancer Metastasis Rev.* **1987**, *5* (3), 185-204.
6. Wertz, J.-L.; Mercier, J. P.; Bédué, O., *Cellulose Science and Technology*. EPFL Press: Lausanne, **2010**.
7. Esa, F.; Tasirin, S. M.; Rahman, N. A., Overview of Bacterial Cellulose Production and Application. *Agric. Agric. Sci. Procedia.* **2014**, *2*, 113-119.
8. Dhingra, D.; Michael, M.; Rajput, H.; Patil, R. T., Dietary fibre in foods: a review. *J. Food Sci. Technol.* **2012**, *49* (3), 255-266.
9. Nishiyama, Y.; Langan, P.; Chanzy, H., Crystal Structure and Hydrogen-Bonding System in Cellulose I β from Synchrotron X-ray and Neutron Fiber Diffraction. *J. Am. Chem. Soc.* **2002**, *124* (31), 9074-9082.
10. Atalla, R. H., Structures of Cellulose. In *The Structures of Cellulose*, American Chemical Society: **1987**; Vol. 340, pp 1-14.
11. Grover, J. A., Methylcellulose and its derivatives. In *Industrial Gums (Third Edition)*, Whistler, R. L.; Bemiller, J. N., Eds. Academic Press: London, **1993**; pp 475-504.
12. Structure and Properties of Cellulose Nanofibrils. In *Nanocellulose*, pp 53-80.
13. Thomas, B.; Raj, M. C.; Joy, J.; Moores, A.; Drisko, G. L.; Sanchez, C. m., Nanocellulose, a Versatile Green Platform: From Biosources to Materials and Their Applications. *Chem. Rev.* **2018**, *118* (24), 11575-11625.
14. Chau, M.; Sriskandha, S. E.; Pichugin, D.; Thérien-Aubin, H.; Nykypanchuk, D.; Chauve, G.; Méthot, M.; Bouchard, J.; Gang, O.; Kumacheva, E., Ion-Mediated Gelation of Aqueous Suspensions of Cellulose Nanocrystals. *Biomacromolecules* **2015**, *16* (8), 2455-2462.

15. Parker, R. M.; Guidetti, G.; Williams, C. A.; Zhao, T.; Narkevicius, A.; Vignolini, S.; Frka-Petecic, B., The Self-Assembly of Cellulose Nanocrystals: Hierarchical Design of Visual Appearance. *Adv. Mater.* **2018**, *30* (19), 1704477.
16. Nasatto, P. L.; Pignon, F.; Silveira, J. L. M.; Duarte, M. E. R.; Nosedá, M. D.; Rinaudo, M., Methylcellulose, a Cellulose Derivative with Original Physical Properties and Extended Applications. *Polymers* **2015**, *7* (5), 777.
17. Li, L., Thermal Gelation of Methylcellulose in Water: Scaling and Thermoreversibility. *Macromolecules* **2002**, *35* (15), 5990-5998.
18. Ke, H.; Zhou, J.; Zhang, L., Structure and physical properties of methylcellulose synthesized in NaOH/urea solution. *Polym. Bull.* **2006**, *56* (4), 349-357.
19. Hollabaugh, C. B.; Burt, L. H.; Walsh, A. P., Carboxymethylcellulose. Uses and Applications. *Ind. Eng. Chem.* **1945**, *37* (10), 943-947.
20. Arancibia, C.; Navarro-Lisboa, R.; Iga, R. N.; Matiacevich, S., Application of CMC as Thickener on Nanoemulsions Based on Olive Oil: Physical Properties and Stability. *Int. J. Polym. Sci.* **2016**, *2016*, 10.
21. Thongsomboon, W.; Serra, D. O.; Possling, A.; Hadjineophytou, C.; Hengge, R.; Cegelski, L., Phosphoethanolamine cellulose: A naturally produced chemically modified cellulose. *Science* **2018**, *359* (6373), 334-338.
22. Elieh-Ali-Komi, D.; Hamblin, M. R., Chitin and Chitosan: Production and Application of Versatile Biomedical Nanomaterials. *Int J Adv Res (Indore)* **2016**, *4* (3), 17.
23. Joye, I. J., Starch. In *Encyclopedia of Food Chemistry*, Melton, L.; Shahidi, F.; Varelis, P., Eds. Academic Press: Oxford, **2019**; pp 256-264.
24. Ai, Y.; Jane, J.-I., Chapter 3 - Understanding Starch Structure and Functionality. In *Starch in Food (Second Edition)*, Sjöö, M.; Nilsson, L., Eds. Woodhead Publishing: **2018**; pp 151-178.
25. Partain, E. M., INDUSTRIALLY IMPORTANT POLYSACCHARIDES. In *Applied Polymer Science: 21st Century*, Craver, C. D.; Carraher, C. E., Eds. Pergamon: Oxford, **2000**; pp 303-323.
26. Xiao, R.; Grinstaff, M. W., Chemical synthesis of polysaccharides and polysaccharide mimetics. *Prog. Polym. Sci.* **2017**, *74*, 78-116.
27. Pérez, S., 2.11 - Molecular Modeling in Glycoscience. In *Comprehensive Glycoscience*, Kamerling, H., Ed. Elsevier: Oxford, **2007**; pp 347-388.
28. Guo, Q.; Ai, L.; Cui, S., *Methodology for Structural Analysis of Polysaccharides*. Springer International Publishing: Germany, **2018**.
29. Liu, H.; Sale, K. L.; Simmons, B. A.; Singh, S., Molecular Dynamics Study of Polysaccharides in Binary Solvent Mixtures of an Ionic Liquid and Water. *J. Phys. Chem. B* **2011**, *115* (34), 10251-10258.

30. Schmalhorst, P. S.; Deluweit, F.; Scherrers, R.; Heisenberg, C.-P.; Sikora, M., Overcoming the Limitations of the MARTINI Force Field in Simulations of Polysaccharides. *J. Chem. Theory Comput.* **2017**, *13* (10), 5039-5053.
31. Yao, D.; Liu, Y.; Yan, S.; Li, Y.; Hu, C.; Ding, N., Evidence of robust participation by an equatorial 4-O group in glycosylation on a 2-azido-2-deoxy-glucopyranosyl donor. *Chem. Commun.* **2017**, *53* (20), 2986-2989.
32. Hahm, H. S.; Hurevich, M.; Seeberger, P. H., Automated assembly of oligosaccharides containing multiple cis-glycosidic linkages. *Nat. Commun.* **2016**, *7* (1), 12482.
33. Ishiwata, A.; Akao, H.; Ito, Y., Stereoselective Synthesis of a Fragment of Mycobacterial Arabinan. *Org. Lett.* **2006**, *8* (24), 5525-5528.
34. Wu, Y.; Xiong, D.-C.; Chen, S.-C.; Wang, Y.-S.; Ye, X.-S., Total synthesis of mycobacterial arabinogalactan containing 92 monosaccharide units. *Nat. Commun.* **2017**, *8* (1), 14851.
35. Nokami, T.; Hayashi, R.; Saigusa, Y.; Shimizu, A.; Liu, C.-Y.; Mong, K.-K. T.; Yoshida, J.-i., Automated Solution-Phase Synthesis of Oligosaccharides via Iterative Electrochemical Assembly of Thioglycosides. *Org. Lett.* **2013**, *15* (17), 4520-4523.
36. Tang, S.-L.; Linz, L. B.; Bonning, B. C.; Pohl, N. L. B., Automated Solution-Phase Synthesis of Insect Glycans to Probe the Binding Affinity of Pea Enation Mosaic Virus. *J. Org. Chem.* **2015**, *80* (21), 10482-10489.
37. Ganesh, N. V.; Fujikawa, K.; Tan, Y. H.; Stine, K. J.; Demchenko, A. V., HPLC-Assisted Automated Oligosaccharide Synthesis. *Org. Lett.* **2012**, *14* (12), 3036-3039.
38. Schuerch, C.; Frechet, J. M., Solid-phase synthesis of oligosaccharides. I. Preparation of the solid support. Poly[p-(1-propen-3-ol-1-yl)styrene]. *J. Am. Chem. Soc.* **1971**, *93* (2), 492-496.
39. Kaplan, B. E., The automated synthesis of oligodeoxyribonucleotides. *Trends Biotechnol.* **1985**, *3* (10), 253-256.
40. Merrifield, R. B.; Stewart, J. M., Automated Peptide Synthesis. *Nature* **1965**, *207* (4996), 522-523.
41. Merrifield, R. B., Automated Synthesis of Peptides. *Science* **1965**, *150* (3693), 178-185.
42. Plante, O. J.; Palmacci, E. R.; Seeberger, P. H., Automated Solid-Phase Synthesis of Oligosaccharides. *Science* **2001**, *291* (5508), 1523-1527.
43. Guberman, M.; Seeberger, P. H., Automated Glycan Assembly: A Perspective. *J. Am. Chem. Soc.* **2019**, *141* (14), 5581-5592.
44. Pardo-Vargas, A.; Delbianco, M.; Seeberger, P. H., Automated glycan assembly as an enabling technology. *Curr. Opin. Chem. Biol.* **2018**, *46*, 48-55.

45. Le Mai Hoang, K.; Pardo-Vargas, A.; Zhu, Y.; Yu, Y.; Loria, M.; Delbianco, M.; Seeberger, P. H., Traceless Photolabile Linker Expedites the Chemical Synthesis of Complex Oligosaccharides by Automated Glycan Assembly. *J. Am. Chem. Soc.* **2019**, *141* (22), 9079-9086.
46. Eller, S.; Collot, M.; Yin, J.; Hahm, H. S.; Seeberger, P. H., Automated Solid-Phase Synthesis of Chondroitin Sulfate Glycosaminoglycans. *Angew. Chem. Int. Ed.* **2013**, *52* (22), 5858-5861.
47. Calin, O.; Eller, S.; Seeberger, P. H., Automated Polysaccharide Synthesis: Assembly of a 30mer Mannoside. *Angew. Chem. Int. Ed.* **2013**, *52* (22), 5862-5865.
48. Naresh, K.; Schumacher, F.; Hahm, H. S.; Seeberger, P. H., Pushing the limits of automated glycan assembly: synthesis of a 50mer polymannoside. *Chem. Commun.* **2017**, *53* (65), 9085-9088.
49. Delbianco, M.; Kononov, A.; Poveda, A.; Yu, Y.; Diercks, T.; Jiménez-Barbero, J.; Seeberger, P. H., Well-Defined Oligo- and Polysaccharides as Ideal Probes for Structural Studies. *J. Am. Chem. Soc.* **2018**, *140* (16), 5421-5426.
50. Valverde, P.; Quintana, J. I.; Santos, J. I.; Ardá, A.; Jiménez-Barbero, J., Novel NMR Avenues to Explore the Conformation and Interactions of Glycans. *ACS Omega* **2019**, *4* (9), 13618-13630.
51. Zierke, M.; Smieško, M.; Rabbani, S.; Aeschbacher, T.; Cutting, B.; Allain, F. H. T.; Schubert, M.; Ernst, B., Stabilization of Branched Oligosaccharides: LewisX Benefits from a Nonconventional C–H...O Hydrogen Bond. *J. Am. Chem. Soc.* **2013**, *135* (36), 13464-13472.
52. Battistel, M. D.; Azurmendi, H. F.; Frank, M.; Freedberg, D. I., Uncovering Nonconventional and Conventional Hydrogen Bonds in Oligosaccharides through NMR Experiments and Molecular Modeling: Application to Sialyl Lewis-X. *J. Am. Chem. Soc.* **2015**, *137* (42), 13444-13447.
53. Zhang, Q.; Gimeno, A.; Santana, D.; Wang, Z.; Valdés-Balbin, Y.; Rodríguez-Noda, L. M.; Hansen, T.; Kong, L.; Shen, M.; Overkleeft, H. S.; Vérez-Bencomo, V.; van der Marel, G. A.; Jiménez-Barbero, J.; Chiodo, F.; Codée, J. D. C., Synthetic, Zwitterionic Sp1 Oligosaccharides Adopt a Helical Structure Crucial for Antibody Interaction. *ACS Cent. Sci.* **2019**, *5* (8), 1407-1416.
54. Rothmund, P. W. K., Folding DNA to create nanoscale shapes and patterns. *Nature* **2006**, *440* (7082), 297-302.
55. Wang, P.; Meyer, T. A.; Pan, V.; Dutta, P. K.; Ke, Y., The Beauty and Utility of DNA Origami. *Chem* **2017**, *2* (3), 359-382.
56. Hendricks, M. P.; Sato, K.; Palmer, L. C.; Stupp, S. I., Supramolecular Assembly of Peptide Amphiphiles. *Acc. Chem. Res.* **2017**, *50* (10), 2440-2448.

57. Hartgerink, J. D.; Beniash, E.; Stupp, S. I., Self-Assembly and Mineralization of Peptide-Amphiphile Nanofibers. *Science* **2001**, *294* (5547), 1684-1688.
58. Choe, S.; Kalmanek, E.; Bond, C.; Harrington, D. A.; Stupp, S. I.; McVary, K. T.; Podlasek, C. A., Optimization of Sonic Hedgehog Delivery to the Penis from Self-Assembling Nanofiber Hydrogels to Preserve Penile Morphology after Cavernous Nerve Injury. *Nanomedicine: Nanotechnology, Biol. Med.* **2019**, *20*, 102033.
59. Zhou, S.; Hokugo, A.; McClendon, M.; Zhang, Z.; Bakshi, R.; Wang, L.; Segovia, L. A.; Rezzadeh, K.; Stupp, S. I.; Jarrahy, R., Bioactive peptide amphiphile nanofiber gels enhance burn wound healing. *Burns* **2019**, *45* (5), 1112-1121.
60. Zha, R. H.; Sur, S.; Stupp, S. I., Self-assembly of Cytotoxic Peptide Amphiphiles into Supramolecular Membranes for Cancer Therapy. *Adv. Healthc. Mater.* **2013**, *2* (1), 126-133.
61. Mansukhani, N. A.; Peters, E. B.; So, M. M.; Albaghdadi, M. S.; Wang, Z.; Karver, M. R.; Clemons, T. D.; Laux, J. P.; Tsihlis, N. D.; Stupp, S. I.; Kibbe, M. R., Peptide Amphiphile Supramolecular Nanostructures as a Targeted Therapy for Atherosclerosis. *Macromol. Biosci.* **2019**, *19* (6), 1900066.
62. Gazit, E., Self Assembly of Short Aromatic Peptides into Amyloid Fibrils and Related Nanostructures. *Prion* **2007**, *1* (1), 32-35.
63. Rochet, J.-C.; Lansbury, P. T., Amyloid fibrillogenesis: themes and variations. *Curr. Opin. Struct. Biol.* **2000**, *10* (1), 60-68.
64. Tao, K.; Makam, P.; Aizen, R.; Gazit, E., Self-assembling peptide semiconductors. *Science* **2017**, *358* (6365), eaam9756.
65. Schnaider, L.; Brahmachari, S.; Schmidt, N. W.; Mensa, B.; Shaham-Niv, S.; Bychenko, D.; Adler-Abramovich, L.; Shimon, L. J. W.; Kolusheva, S.; DeGrado, W. F.; Gazit, E., Self-assembling dipeptide antibacterial nanostructures with membrane disrupting activity. *Nat. Commun.* **2017**, *8* (1), 1365.
66. Rechtes, M.; Gazit, E., Casting Metal Nanowires Within Discrete Self-Assembled Peptide Nanotubes. *Science* **2003**, *300* (5619), 625-627.
67. Tao, K.; Fan, Z.; Sun, L.; Makam, P.; Tian, Z.; Ruegsegger, M.; Shaham-Niv, S.; Hansford, D.; Aizen, R.; Pan, Z.; Galster, S.; Ma, J.; Yuan, F.; Si, M.; Qu, S.; Zhang, M.; Gazit, E.; Li, J., Quantum confined peptide assemblies with tunable visible to near-infrared spectral range. *Nat. Commun.* **2018**, *9* (1), 3217.
68. Berger, O.; Adler-Abramovich, L.; Levy-Sakin, M.; Grunwald, A.; Liebes-Peer, Y.; Bachar, M.; Buzhansky, L.; Mossou, E.; Forsyth, V. T.; Schwartz, T.; Ebenstein, Y.; Frolow, F.; Shimon, L. J. W.; Patolsky, F.; Gazit, E., Light-emitting self-assembled peptide nucleic acids exhibit both stacking interactions and Watson–Crick base pairing. *Nat. Nanotechnol.* **2015**, *10* (4), 353-360.

69. Lee, S. S.; Fyrner, T.; Chen, F.; Álvarez, Z.; Sleep, E.; Chun, D. S.; Weiner, J. A.; Cook, R. W.; Freshman, R. D.; Schallmo, M. S.; Katchko, K. M.; Schneider, A. D.; Smith, J. T.; Yun, C.; Singh, G.; Hashmi, S. Z.; McClendon, M. T.; Yu, Z.; Stock, S. R.; Hsu, W. K.; Hsu, E. L.; Stupp, S. I., Sulfated glycopeptide nanostructures for multipotent protein activation. *Nat. Nanotechnol.* **2017**, *12* (8), 821-829.
70. Hendrikse, S. I. S.; Su, L.; Hogervorst, T. P.; Lafleur, R. P. M.; Lou, X.; van der Marel, G. A.; Codee, J. D. C.; Meijer, E. W., Elucidating the Ordering in Self-Assembled Glycocalyx Mimicking Supramolecular Copolymers in Water. *J. Am. Chem. Soc.* **2019**, *141* (35), 13877-13886.
71. Caruthers, M., Gene synthesis machines: DNA chemistry and its uses. *Science* **1985**, *230* (4723), 281-285.
72. Procopiou, P. A.; Baugh, S. P. D.; Flack, S. S.; Inglis, G. G. A., An Extremely Powerful Acylation Reaction of Alcohols with Acid Anhydrides Catalyzed by Trimethylsilyl Trifluoromethanesulfonate. *J. Org. Chem.* **1998**, *63* (7), 2342-2347.
73. Hyenne, V.; Labouesse, M., Making sense of glycosphingolipids in epithelial polarity. *Nat. Cell Biol.* **2011**, *13* (10), 1185-1187.
74. Hakomori, S., *Biochim. Biophys. Acta, Gen. Subj.* **2008**, *1780*, 325.
75. Zhang, X.; Kiechle, F. L., *Ann. Clin. Lab. Sci.* **2004**, *34*, 3.
76. Hahm, H. S.; Liang, C.-F.; Lai, C.-H.; Fair, R. J.; Schuhmacher, F.; Seeberger, P. H., Automated Glycan Assembly of Complex Oligosaccharides Related to Blood Group Determinants. *J. Org. Chem.* **2016**, *81* (14), 5866-5877.
77. French, A. D.; Pérez, S.; Bulone, V.; Rosenau, T.; Gray, D., Cellulose. In *Encyclopedia of Polymer Science and Technology*, **2019**, Wiley & Sons.
78. Bergenstråhle, M.; Wohler, J.; Himmel, M. E.; Brady, J. W., Simulation studies of the insolubility of cellulose. *Carbohydr. Res.* **2010**, *345* (14), 2060-2066.
79. Kroon-Batenburg, L. M. J.; Kroon, J., The crystal and molecular structures of cellulose I and II. *Glycoconjugate J.* **1997**, *14* (5), 677-690.
80. Kolpak, F. J.; Blackwell, J., Determination of the Structure of Cellulose II. *Macromolecules* **1976**, *9* (2), 273-278.
81. Kostag, M.; Gericke, M.; Heinze, T.; El Seoud, O. A., Twenty-five years of cellulose chemistry: innovations in the dissolution of the biopolymer and its transformation into esters and ethers. *Cellulose* **2019**, *26* (1), 139-184.
82. Fox, S. C.; Li, B.; Xu, D.; Edgar, K. J., Regioselective Esterification and Etherification of Cellulose: A Review. *Biomacromolecules* **2011**, *12* (6), 1956-1972.
83. Arca, H. C.; Mosquera-Giraldo, L. I.; Bi, V.; Xu, D.; Taylor, L. S.; Edgar, K. J., Pharmaceutical Applications of Cellulose Ethers and Cellulose Ether Esters. *Biomacromolecules* **2018**, *19* (7), 2351-2376.

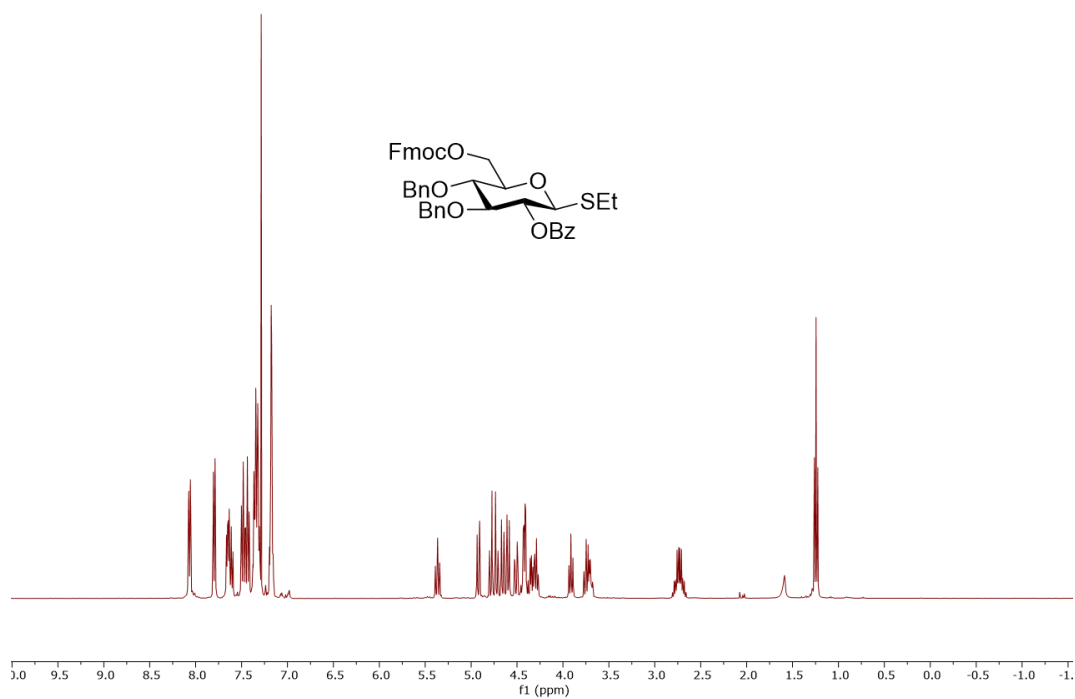
84. Woods, R. J., Predicting the Structures of Glycans, Glycoproteins, and Their Complexes. *Chem. Rev.* **2018**, *118* (17), 8005-8024.
85. Xiong, X.; Chen, Z.; Cossins, B. P.; Xu, Z.; Shao, Q.; Ding, K.; Zhu, W.; Shi, J., Force fields and scoring functions for carbohydrate simulation. *Carbohydr. Res.* **2015**, *401*, 73-81.
86. Sauter, J. r.; Grafmüller, A., Solution properties of hemicellulose polysaccharides with four common carbohydrate force fields. *J. Chem. Theory Comput.* **2015**, *11* (4), 1765-1774.
87. Marianski, M.; Supady, A.; Ingram, T.; Schneider, M.; Baldauf, C., Assessing the Accuracy of Across-the-Scale Methods for Predicting Carbohydrate Conformational Energies for the Examples of Glucose and α -Maltose. *J. Chem. Theory Comput.* **2016**, *12* (12), 6157-6168.
88. Le Mai Hoang, K.; Pardo-Vargas, A.; Zhu, Y.; Yu, Y.; Loria, M.; Delbianco, M.; Seeberger, P. H., Traceless Photolabile Linker Expedites Chemical Synthesis of Complex Oligosaccharides by Automated Glycan Assembly. *J. Am. Chem. Soc.* **2019**, *141* (22), 9079-9086.
89. Synthesis of Peptides and Peptidomimetics, Houben Weyl, Eds. M. Goodman, A. Felix, L. Moroder, C. Toniolo, Georg Thieme Verlag Stuttgart, New York, (2002) Volume 22, p 676.
90. Kirschner, K. N.; Yongye, A. B.; Tschampel, S. M.; González-Outeiriño, J.; Daniels, C. R.; Foley, B. L.; Woods, R. J., GLYCAM06: A generalizable biomolecular force field. *Carbohydrates. J. Comput. Chem.* **2008**, *29* (4), 622-655.
91. Sauter, J. r.; Grafmüller, A., Predicting the Chemical Potential and Osmotic Pressure of Polysaccharide Solutions by Molecular Simulations. *J. Chem. Theory Comput.* **2016**, *12* (9), 4375-4384.
92. Yu, Y.; Tyrikos-Ergas, T.; Zhu, Y.; Fittolani, G.; Bordoni, V.; Singhal, A.; Fair, R. J.; Grafmüller, A.; Seeberger, P. H.; Delbianco, M., Systematic Hydrogen-Bond Manipulations To Establish Polysaccharide Structure–Property Correlations. *Angew. Chem. Int. Ed.* **2019**, *58* (37), 13127-13132.
93. Ghadiri, M. R.; Granja, J. R.; Milligan, R. A.; McRee, D. E.; Khazanovich, N., Self-assembling organic nanotubes based on a cyclic peptide architecture. *Nature* **1993**, *366*, 324.
94. Bera, S.; Mondal, S.; Rencus-Lazar, S.; Gazit, E., Organization of Amino Acids into Layered Supramolecular Secondary Structures. *Acc. Chem. Res.* **2018**.
95. Tao, K.; Makam, P.; Aizen, R.; Gazit, E., Self-assembling peptide semiconductors. *Science* **2017**, *358* (6365).
96. Rothmund, P. W. K., Folding DNA to create nanoscale shapes and patterns. *Nature* **2006**, *440*, 297.

97. Dietz, H.; Douglas, S. M.; Shih, W. M., Folding DNA into Twisted and Curved Nanoscale Shapes. *Science* **2009**, *325* (5941), 725-730.
98. Ke, Y.; Ong, L. L.; Shih, W. M.; Yin, P., Three-Dimensional Structures Self-Assembled from DNA Bricks. *Science* **2012**, *338* (6111), 1177-1183.
99. Adler-Abramovich, L.; Vaks, L.; Carny, O.; Trudler, D.; Magno, A.; Caflich, A.; Frenkel, D.; Gazit, E., Phenylalanine assembly into toxic fibrils suggests amyloid etiology in phenylketonuria. *Nat. Chem. Biol.* **2012**, *8* (8), 701-706.
100. Webber, M. J.; Appel, E. A.; Meijer, E. W.; Langer, R., Supramolecular biomaterials. *Nat. Mater.* **2016**, *15* (1), 13-26.
101. Hu, Q.; Li, H.; Wang, L.; Gu, H.; Fan, C., DNA Nanotechnology-Enabled Drug Delivery Systems. *Chem. Rev.* **2018**, 10.1021/acs.chemrev.7b00663.
102. Lan, X.; Wang, Q., DNA-programmed self-assembly of photonic nanoarchitectures. *NPG Asia Mater.* **2014**, *6*, e97.
103. Almeida, I. F.; Pereira, T.; Silva, N. H. C. S.; Gomes, F. P.; Silvestre, A. J. D.; Freire, C. S. R.; Sousa Lobo, J. M.; Costa, P. C., Bacterial cellulose membranes as drug delivery systems: An in vivo skin compatibility study. *European Eur. J. Pharm. Biopharm.* **2014**, *86* (3), 332-336.
104. Hassanzadeh, P.; Kharaziha, M.; Nikkiah, M.; Shin, S. R.; Jin, J.; He, S.; Sun, W.; Zhong, C.; Dokmeci, M. R.; Khademhosseini, A.; Rolandi, M., Chitin nanofiber micropatterned flexible substrates for tissue engineering. *J. Mater. Chem. B* **2013**, *1* (34), 4217-4224.
105. Colomer, I.; Chamberlain, A. E. R.; Haughey, M. B.; Donohoe, T. J., Hexafluoroisopropanol as a highly versatile solvent. *Nat. Rev. Chem.* **2017**, *1*, 0088.
106. Andersen, N. H.; Dyer, R. B.; Fesinmeyer, R. M.; Gai, F.; Liu, Z.; Neidigh, J. W.; Tong, H., Effect of Hexafluoroisopropanol on the Thermodynamics of Peptide Secondary Structure Formation. *J. Am. Chem. Soc.* **1999**, *121* (42), 9879-9880.
107. Pinotsi, D.; Buell, A. K.; Dobson, C. M.; Kaminski Schierle, G. S.; Kaminski, C. F., A Label-Free, Quantitative Assay of Amyloid Fibril Growth Based on Intrinsic Fluorescence. *ChemBioChem* **2013**, *14* (7), 846-850.
108. Berger, O.; Adler-Abramovich, L.; Levy-Sakin, M.; Grunwald, A.; Liebes-Peer, Y.; Bachar, M.; Buzhansky, L.; Mossou, E.; Forsyth, V. T.; Schwartz, T.; Ebenstein, Y.; Frolov, F.; Shimon, L. J. W.; Patolsky, F.; Gazit, E., Light-emitting self-assembled peptide nucleic acids exhibit both stacking interactions and Watson–Crick base pairing. *Nat. Nanotechnol.* **2015**, *10*, 353.
109. Pinotsi, D.; Grisanti, L.; Mahou, P.; Gebauer, R.; Kaminski, C. F.; Hassanali, A.; Kaminski Schierle, G. S., Proton Transfer and Structure-Specific Fluorescence in Hydrogen Bond-Rich Protein Structures. *J. Am. Chem. Soc.* **2016**, *138* (9), 3046-3057.

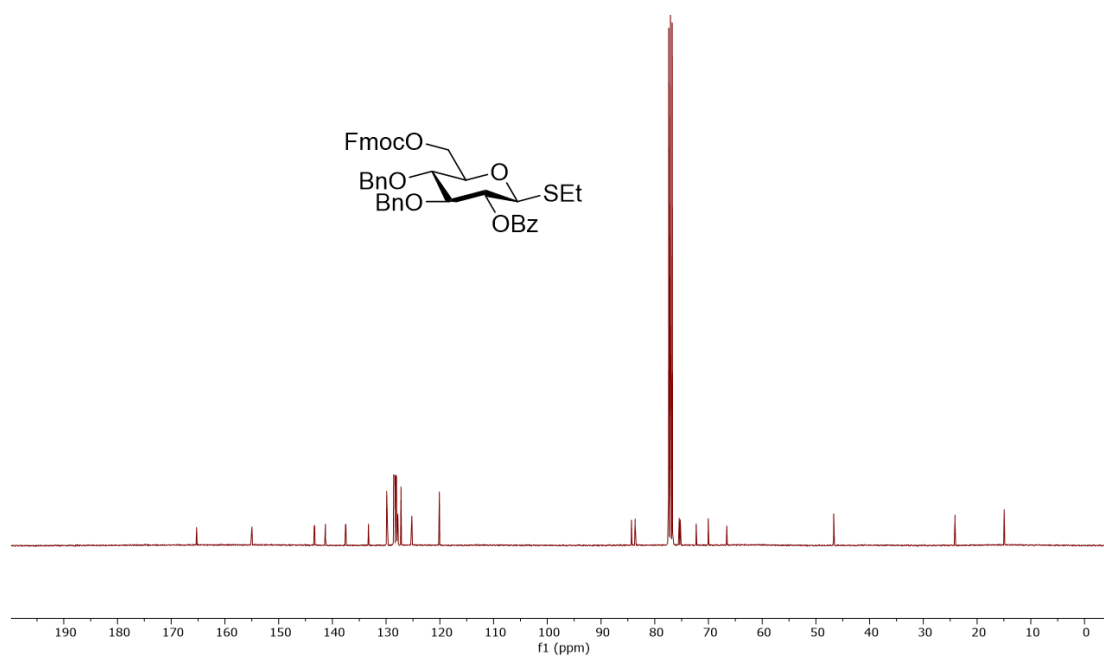
110. Shang, J.; Ma, L.; Li, J.; Ai, W.; Yu, T.; Gurzadyan, G. G., The Origin of Fluorescence from Graphene Oxide. *Sci. Rep.* **2012**, *2*, 792.
111. Samanta, A., Dynamic Stokes Shift and Excitation Wavelength Dependent Fluorescence of Dipolar Molecules in Room Temperature Ionic Liquids. *J. Phys. Chem. B* **2006**, *110* (28), 13704-13716.
112. Tyrikos-Ergas, T.; Fittolani, G.; Seeberger, P. H.; Delbianco, M., Structural Studies Using Unnatural Oligosaccharides: Toward Sugar Foldamers. *Biomacromolecules* **2019**.
113. Valone, M. C. Effect of humidity on the creep response of cellulose nanocrystals films. Thesis, Purdue University, **2016**.
114. Adelizzi, B.; Rösch, A. T.; van Rijen, D. J.; Martire, R. S.; Esiner, S.; Lutz, M.; Palmans, A. R. A.; Meijer, E. W., Chiral Aggregates of Triphenylamine-Based Dyes for Depleting the Production of Hydrogen Peroxide in the Photochemical Water-Splitting Process. *Helv. Chim. Acta* **2019**, *102* (5), e1900065.
115. Sai, H.; Erbas, A.; Dannenhoffer, A.; Huang, D.; Weingarten, A.; Siismets, E.; Jang, K.; Qu, K.; Palmer, L. C.; Olvera de la Cruz, M.; Stupp, S. I., Chromophore amphiphile–polyelectrolyte hybrid hydrogels for photocatalytic hydrogen production. *J. Mater. Chem. A* **2020**, *8* (1), 158-168.
116. Moyer, T. J.; Chen, F.; Toft, D. J.; Ruff, Y.; Cryns, V. L.; Stupp, S. I., Self-Assembled Peptide Nanostructures Targeting Death Receptor 5 and Encapsulating Paclitaxel As a Multifunctional Cancer Therapy. *ACS Biomater. Sci. Eng.* **2019**, *5* (11), 6046-6053.
117. Daragics, K.; Fügedi, P., Synthesis of glycosaminoglycan oligosaccharides. Part 5: Synthesis of a putative heparan sulfate tetrasaccharide antigen involved in prion diseases. *Tetrahedron* **2010**, *66* (40), 8036-8046.
118. Kröck, L.; Esposito, D.; Castagner, B.; Wang, C.-C.; Bindschädler, P.; Seeberger, P. H., Streamlined access to conjugation-ready glycans by automated synthesis. *Chem. Sci.* **2012**, *3* (5), 1617-1622.

Appendix 1: NMR spectra

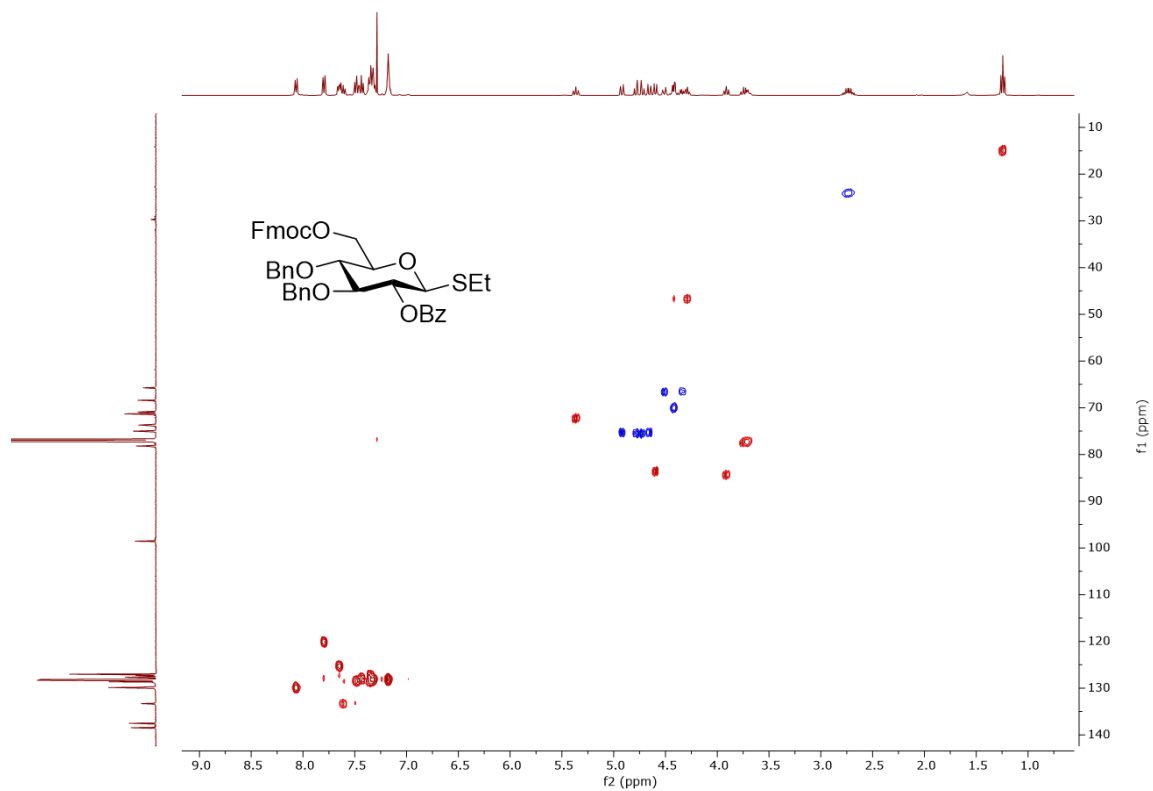
¹H NMR of BB-6a (400 MHz, CDCl₃)



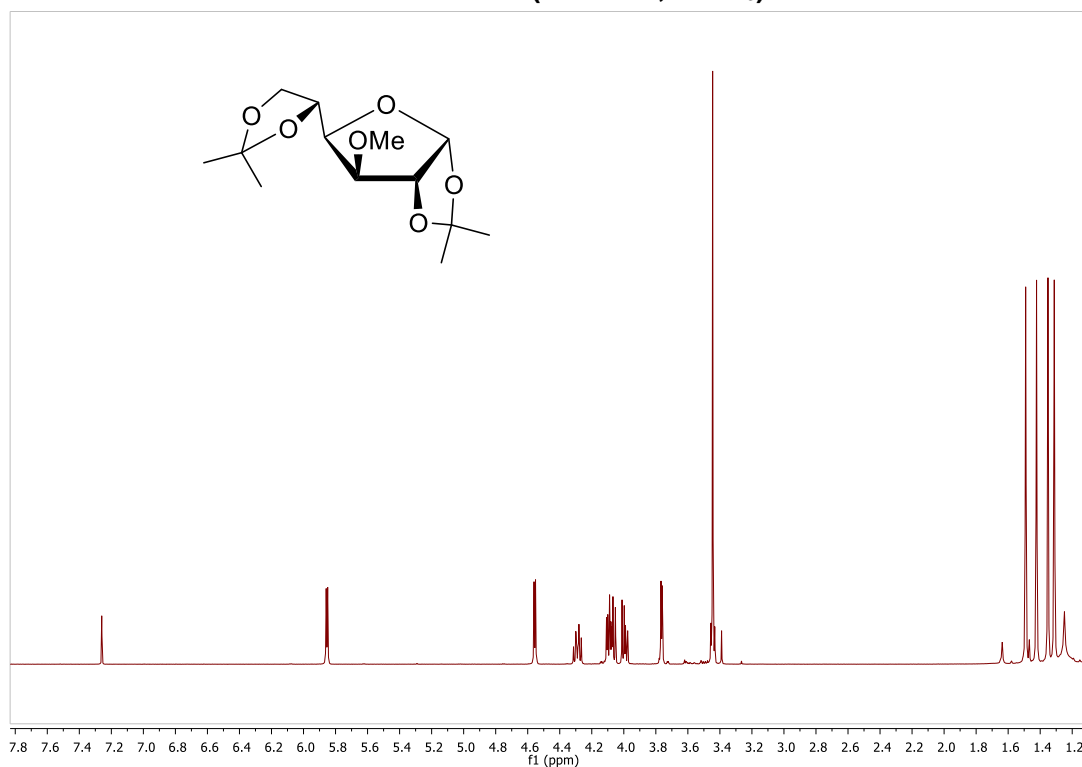
¹³C NMR of BB-6a (101 MHz, CDCl₃)



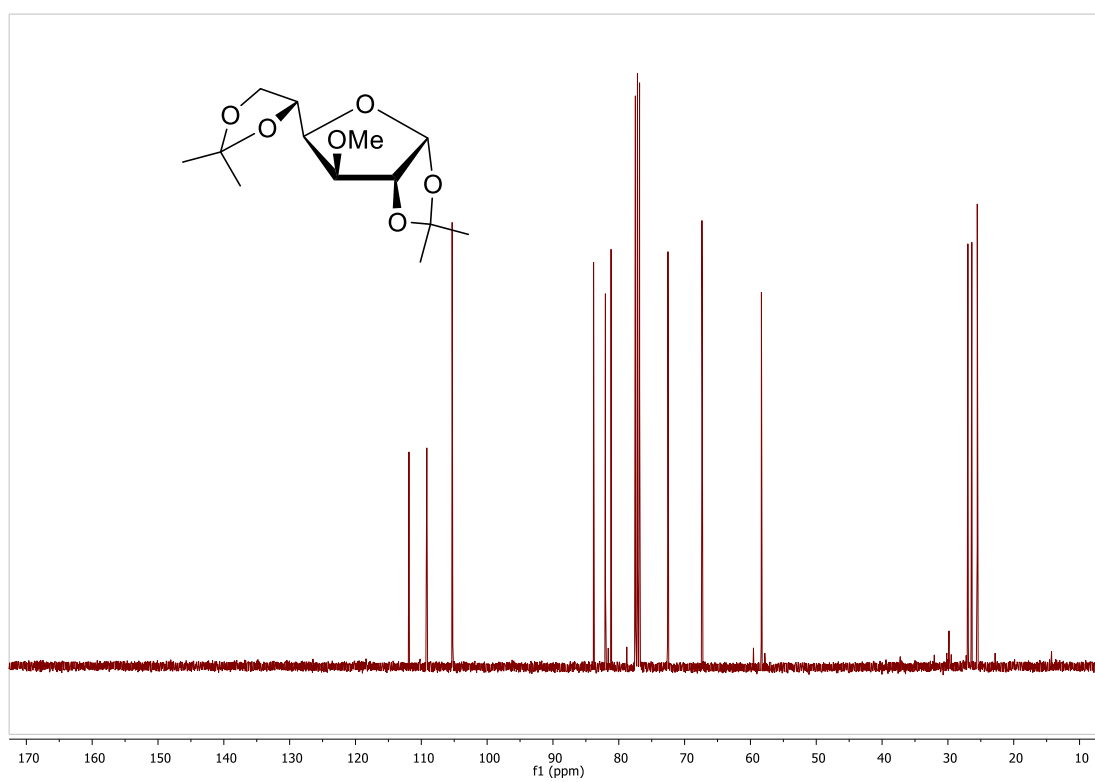
HSQC NMR of BB-6a (CDCl₃)



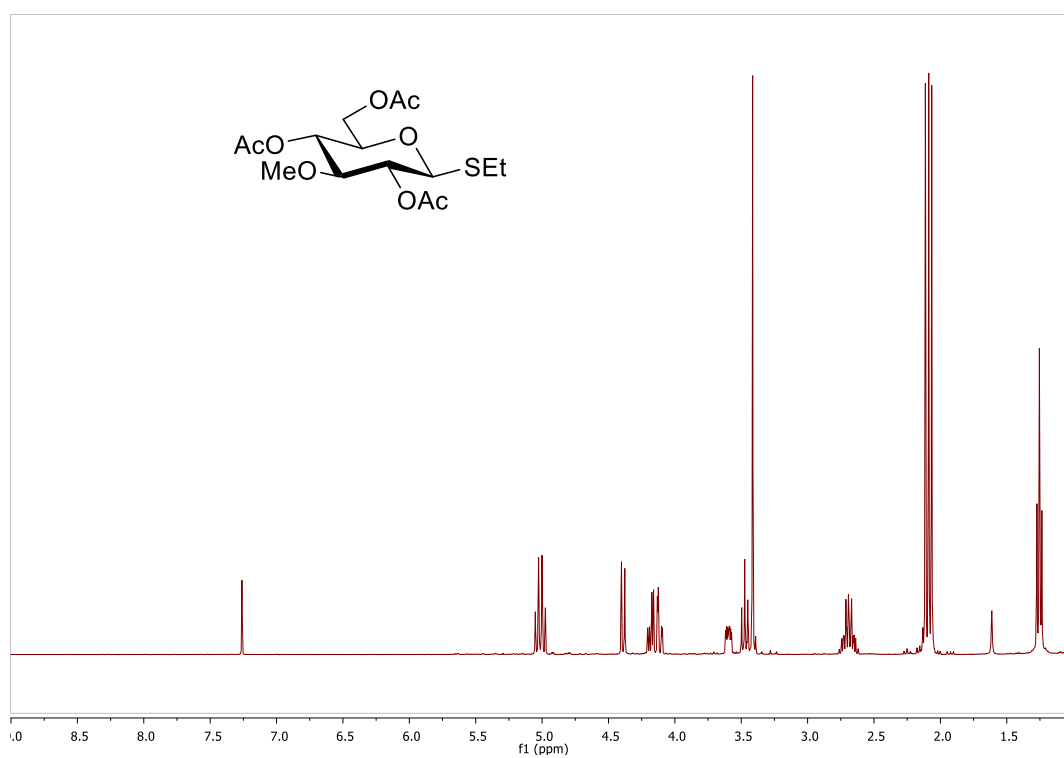
¹H NMR of S3 (400 MHz, CDCl₃)



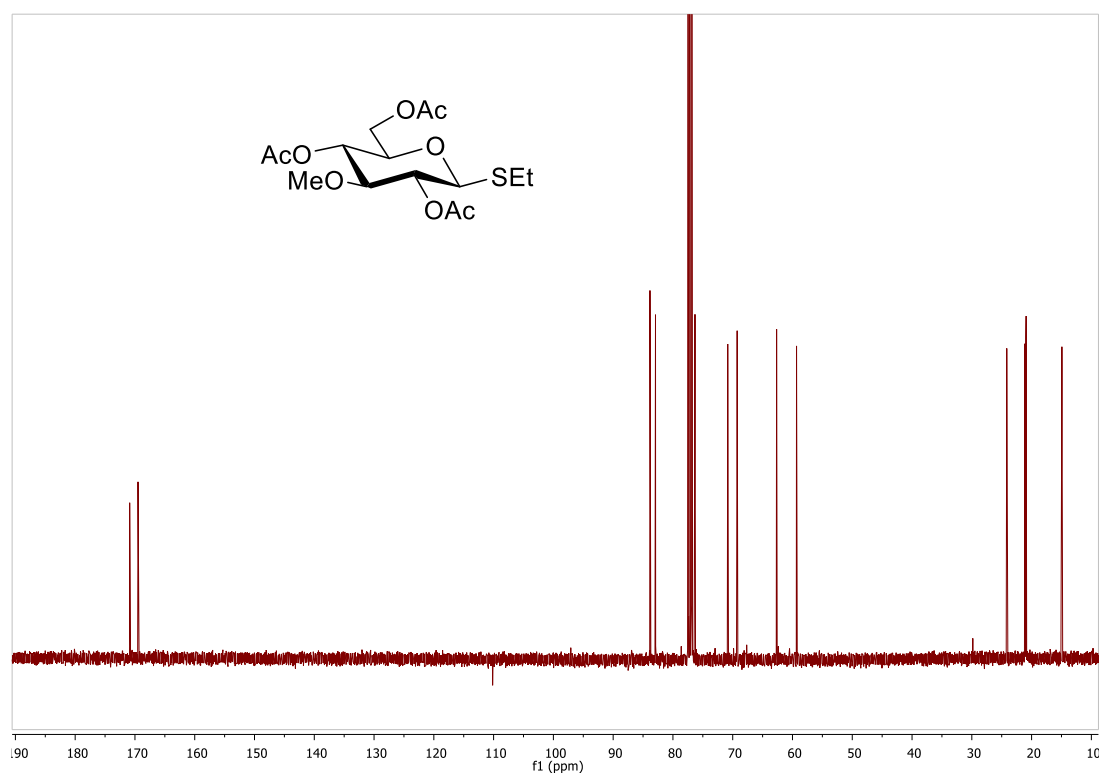
¹³C NMR of S3 (101 MHz, CDCl₃)



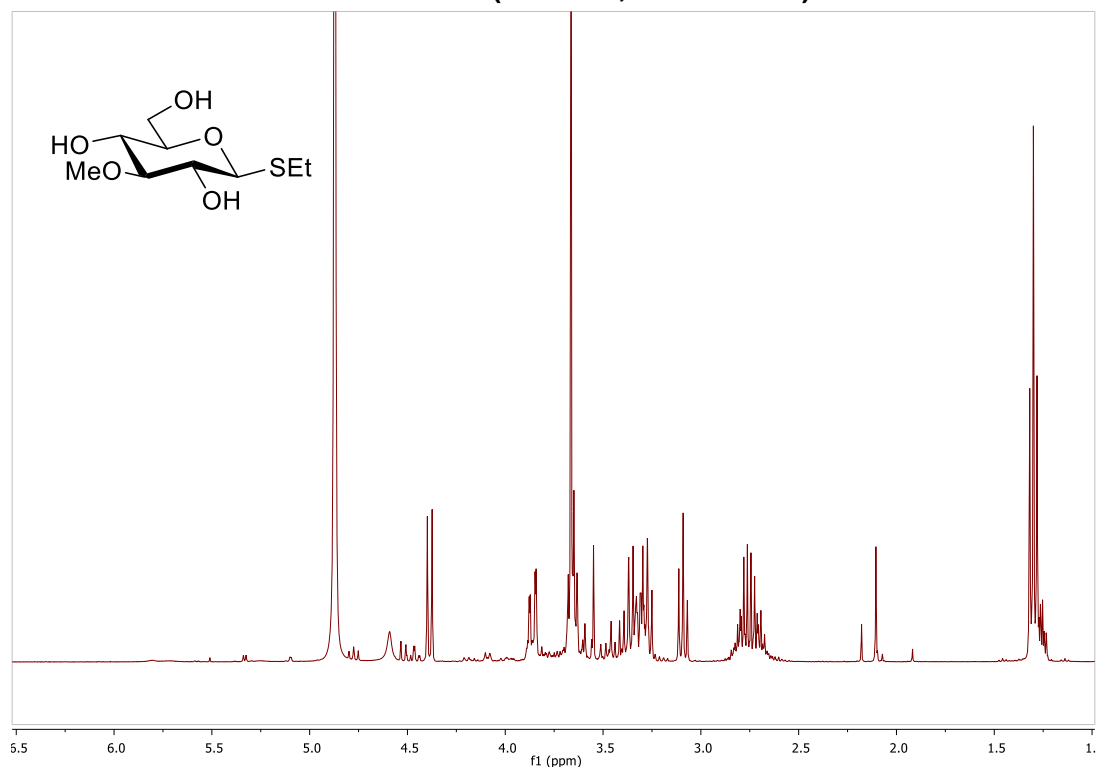
¹H NMR of S4 (400 MHz, CDCl₃)



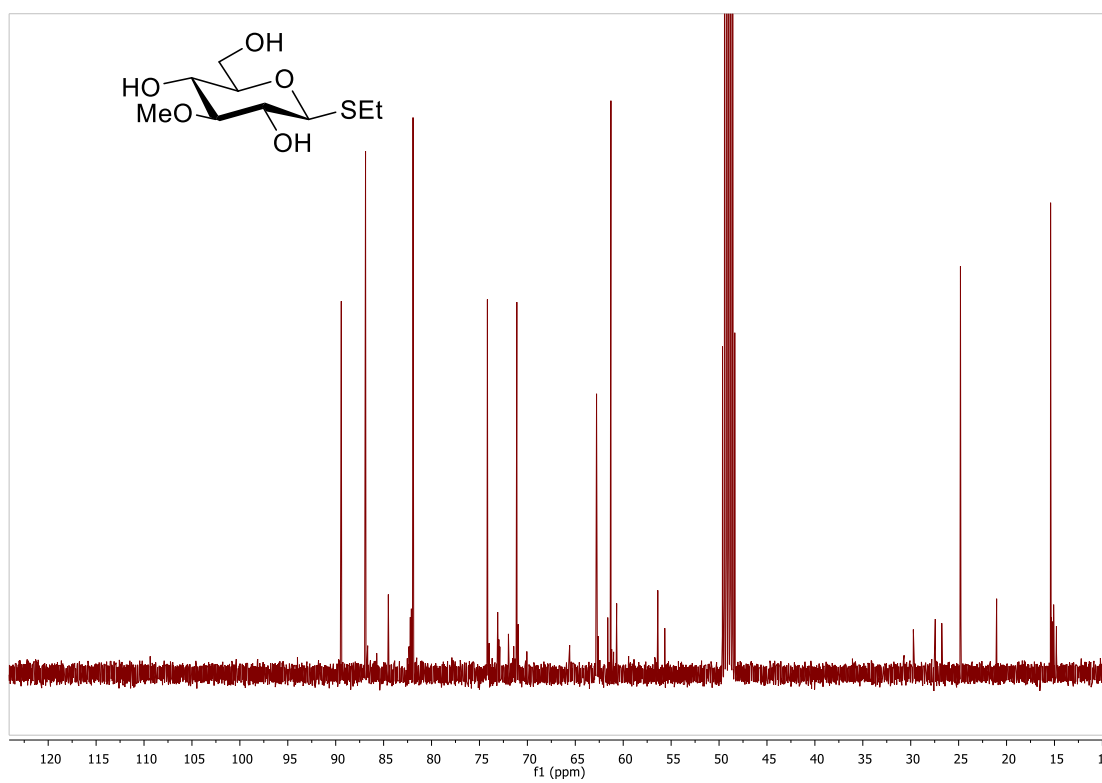
¹³C NMR of S4 (101 MHz, CDCl₃)



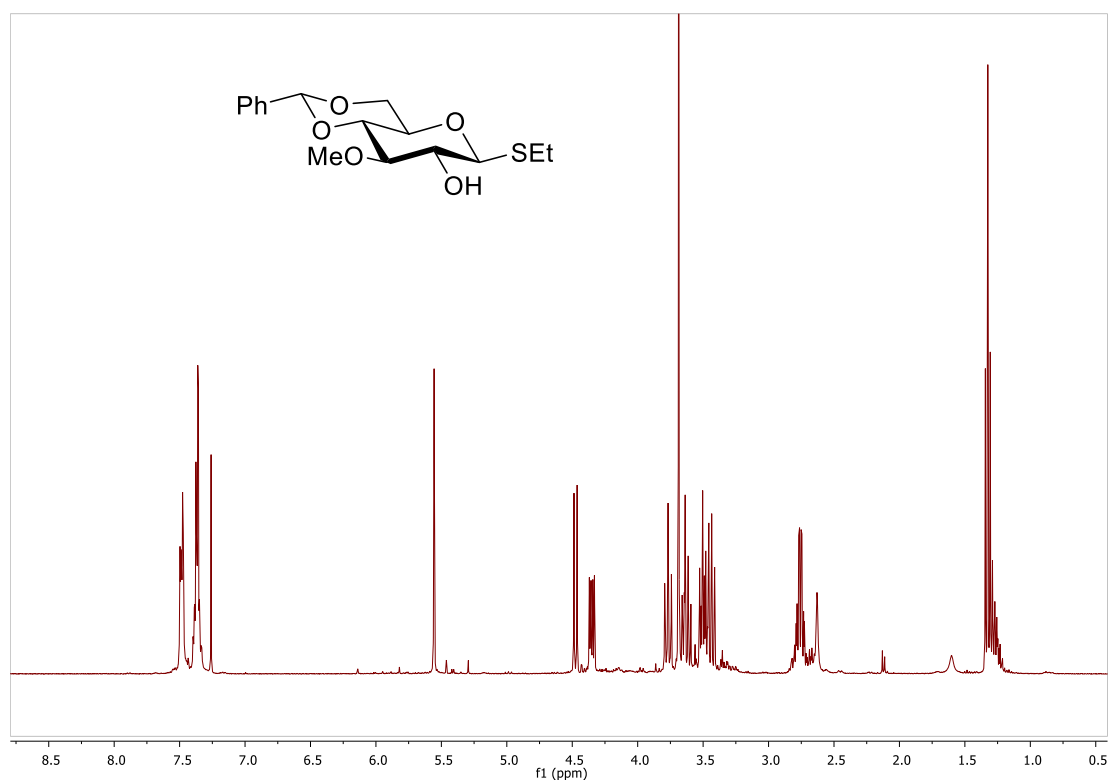
¹H NMR of S5 (400 MHz, Methanol-d₄)



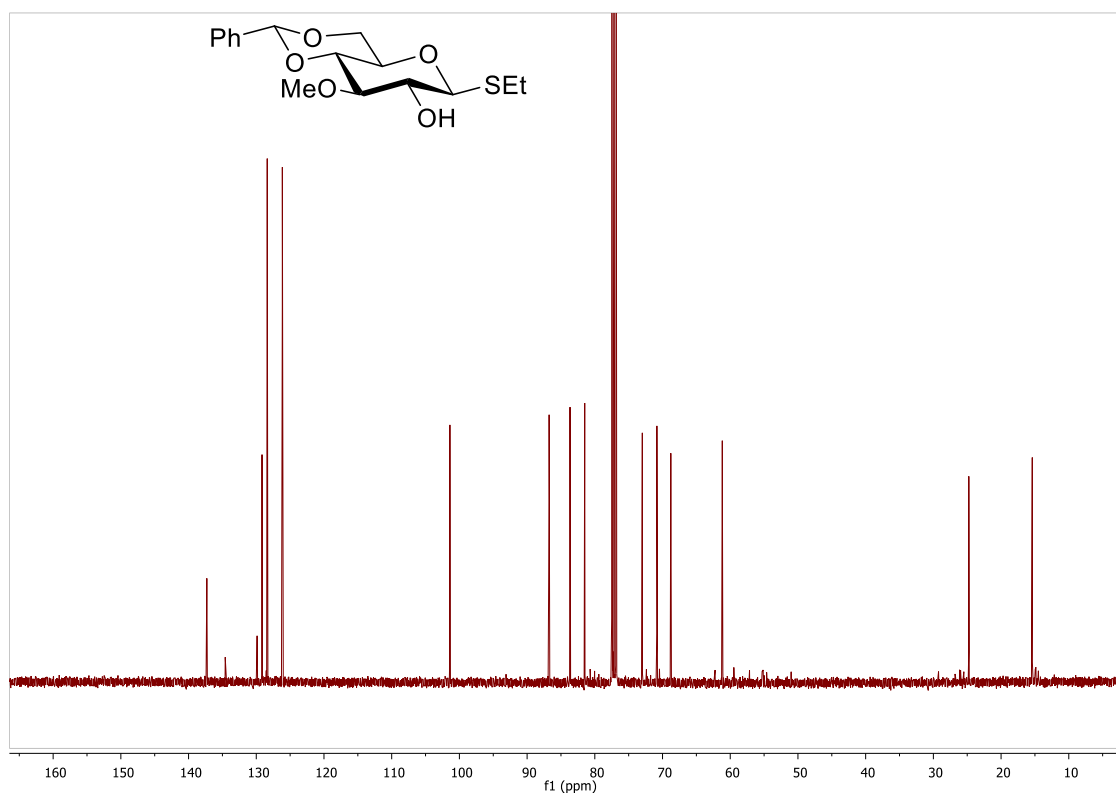
¹³C NMR of S5 (101 MHz, Methanol-d₄)



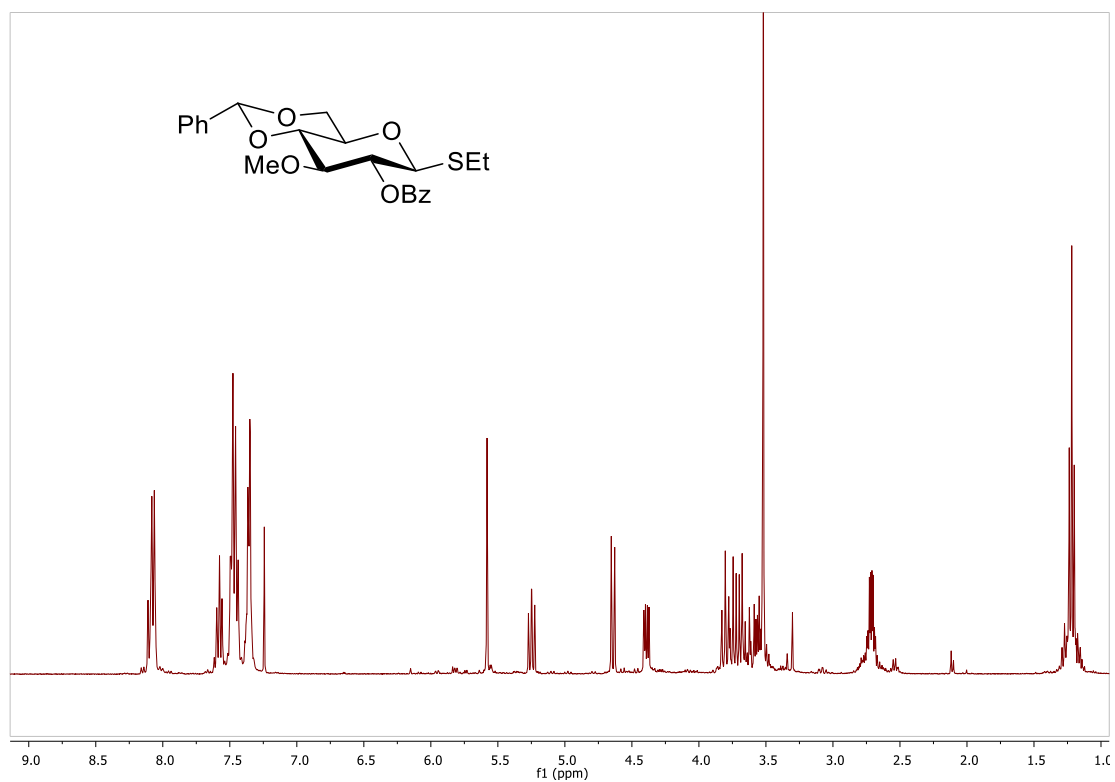
¹H NMR of S6 (400 MHz, CDCl₃)



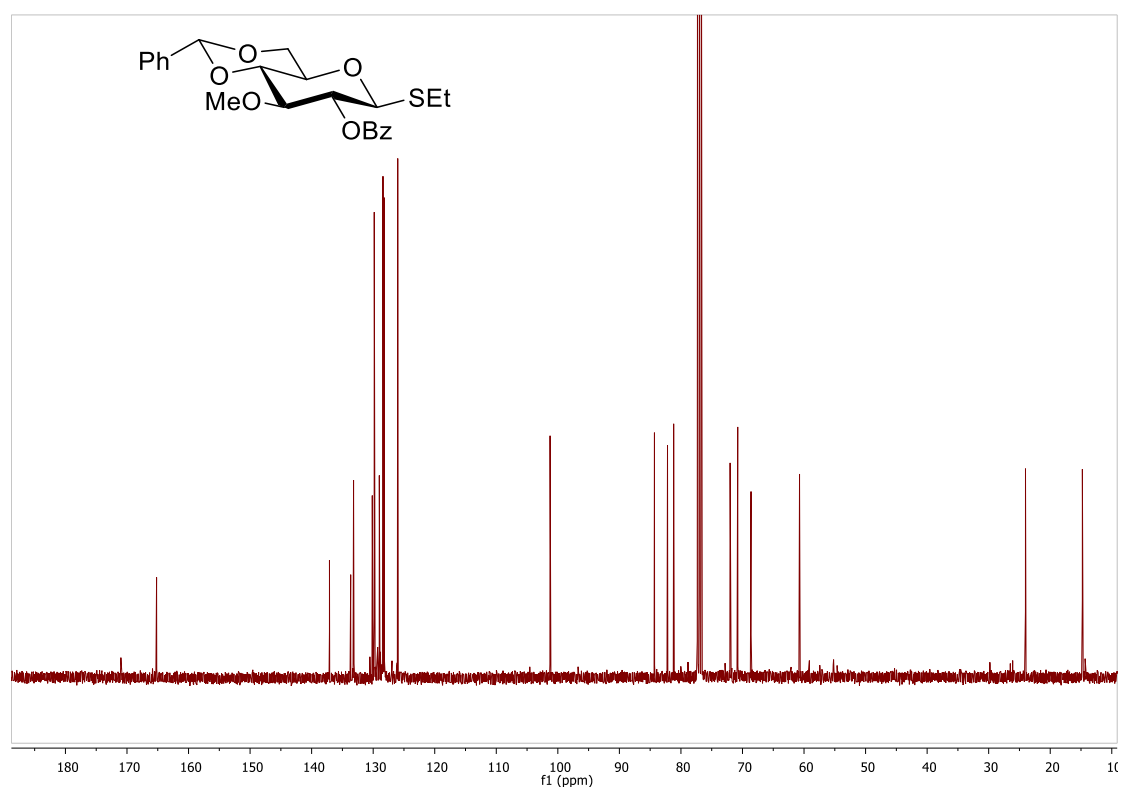
¹³C NMR of S6 (101 MHz, CDCl₃)



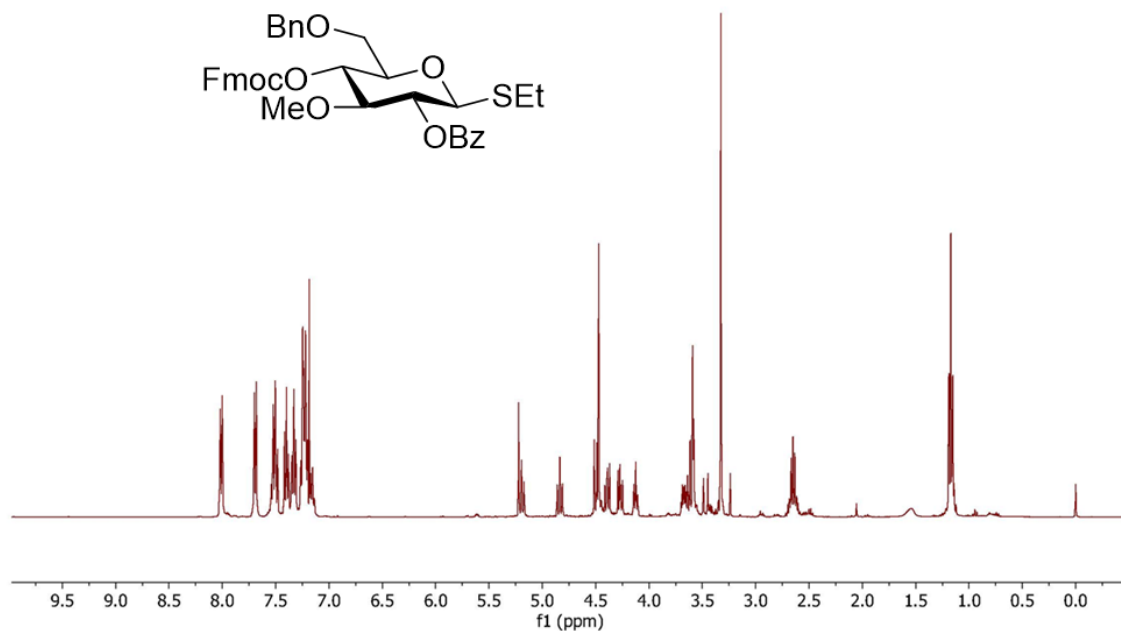
¹H NMR of S7 (400 MHz, CDCl₃)



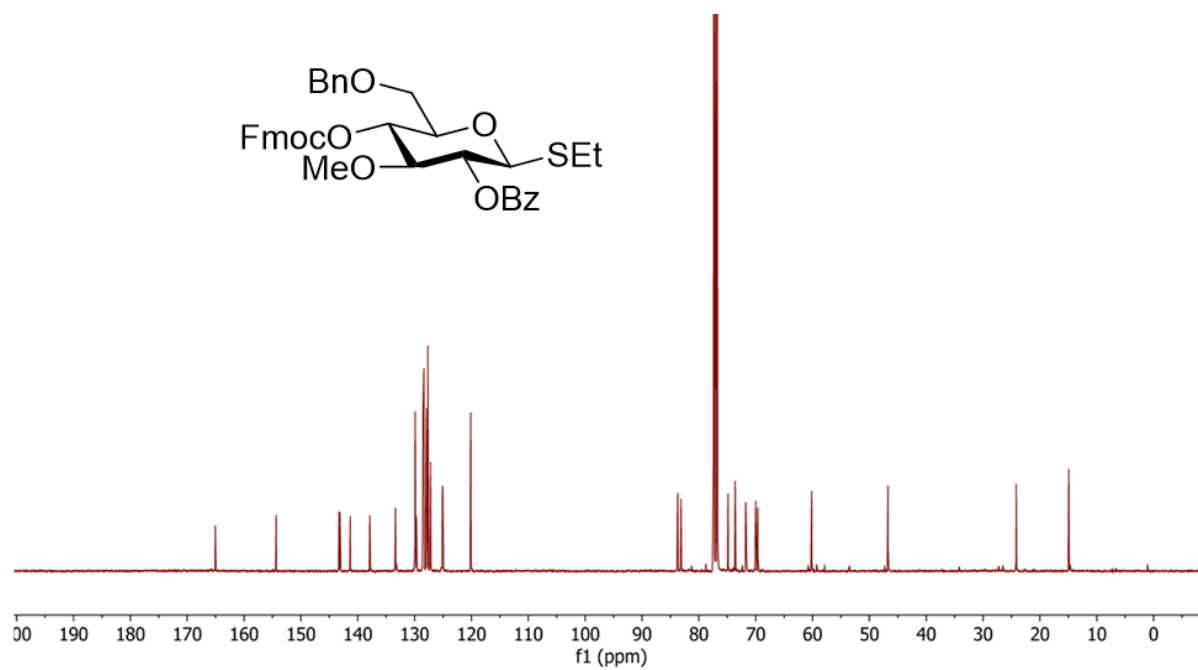
¹³C NMR of S7 (101 MHz, CDCl₃)



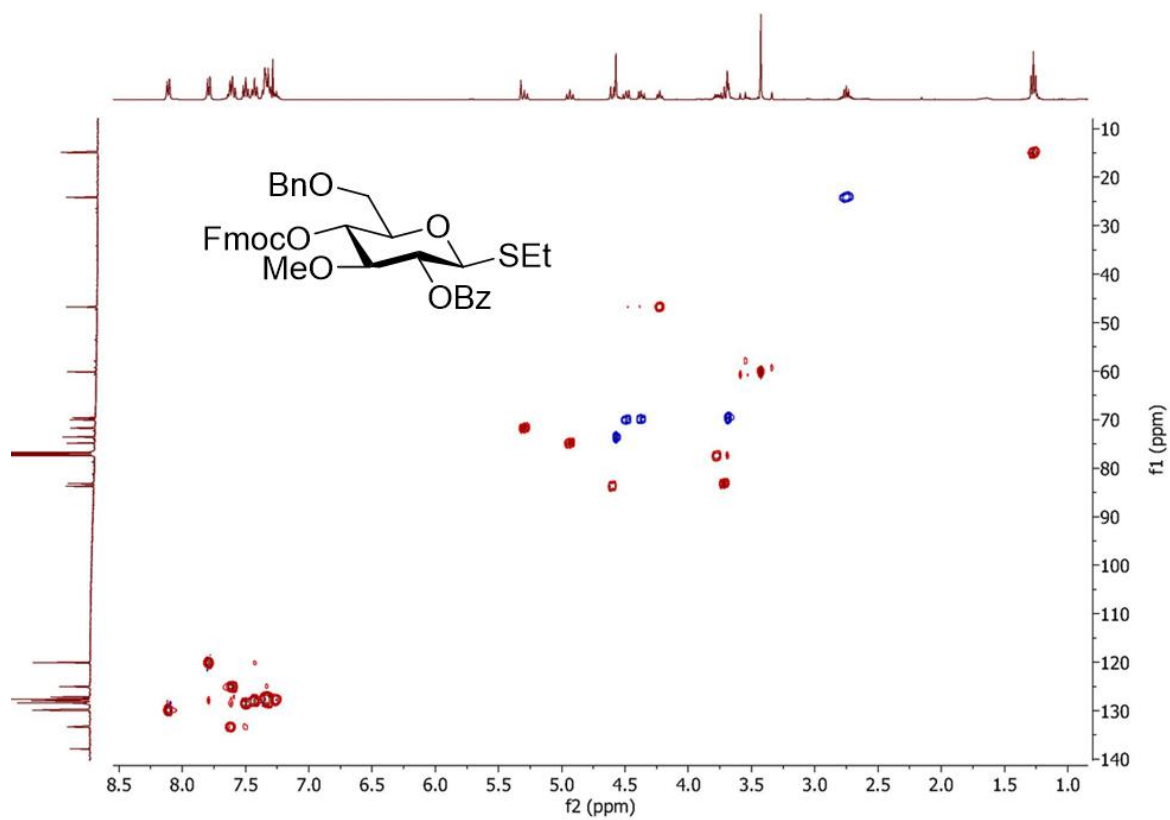
¹H NMR of BB-11 (400 MHz, CDCl₃)



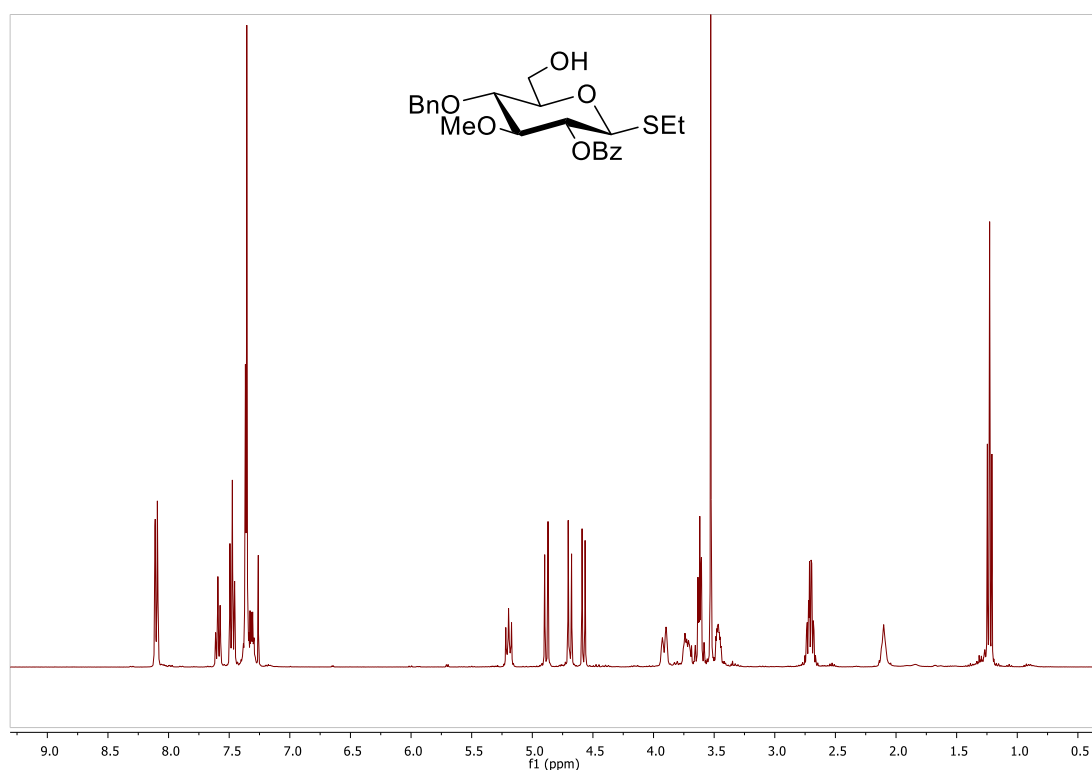
¹³C NMR of BB-11 (101 MHz, CDCl₃)



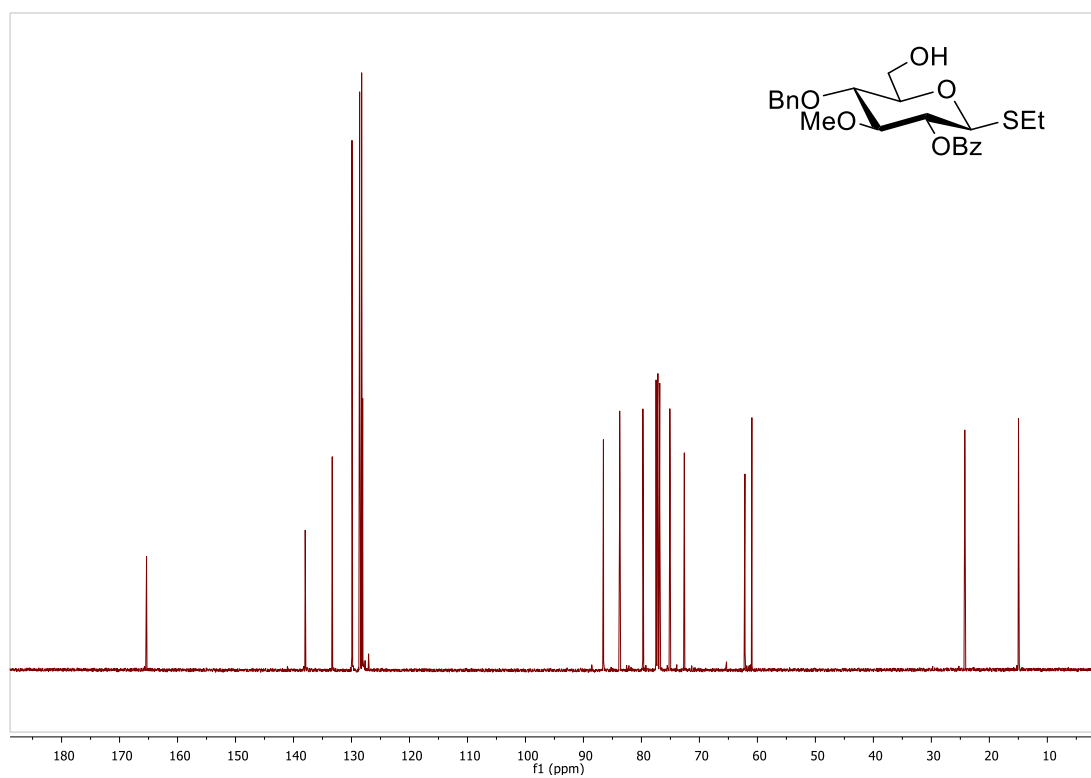
HSQC NMR of BB-11 (CDCl₃)



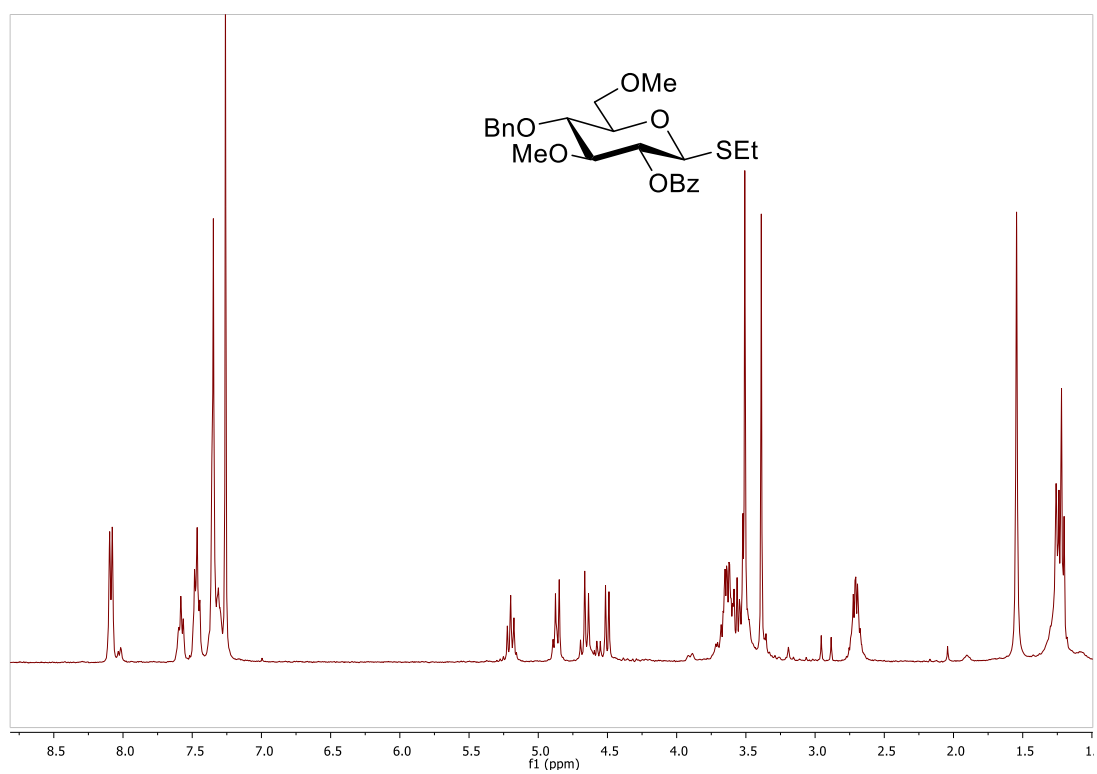
¹H NMR of S8 (400 MHz, CDCl₃)



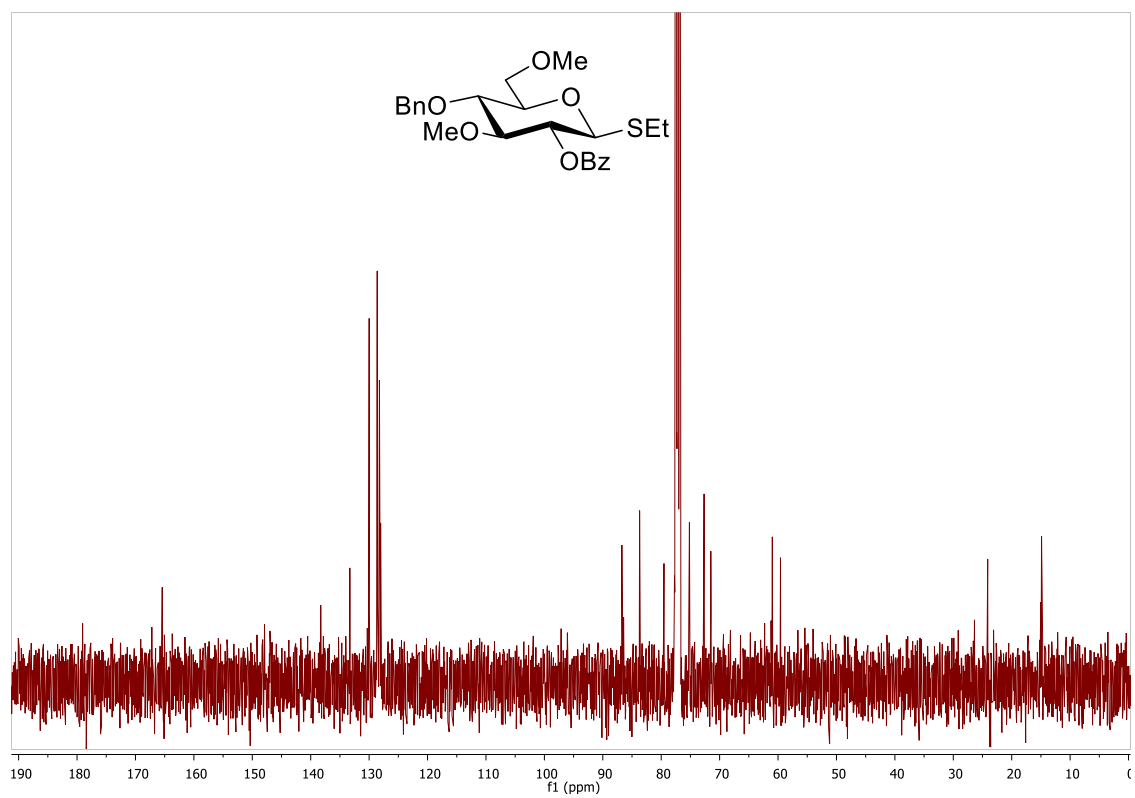
¹³C NMR of S8 (101 MHz, CDCl₃)



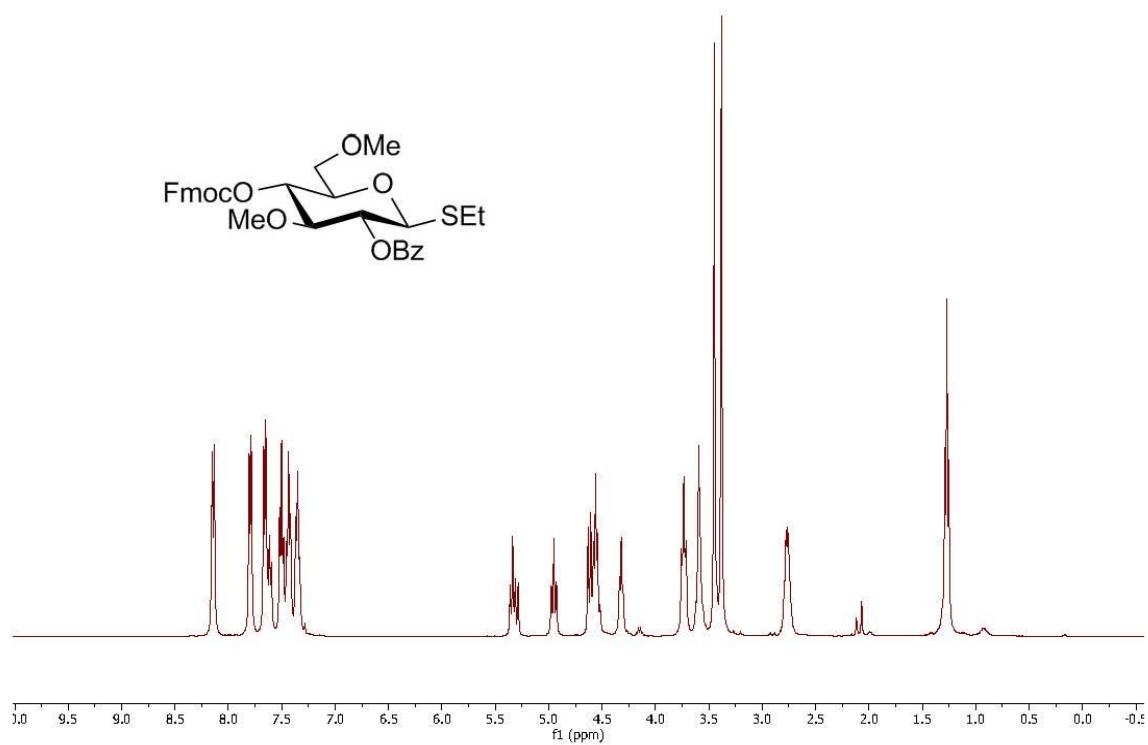
¹H NMR of S9 (400 MHz, CDCl₃)



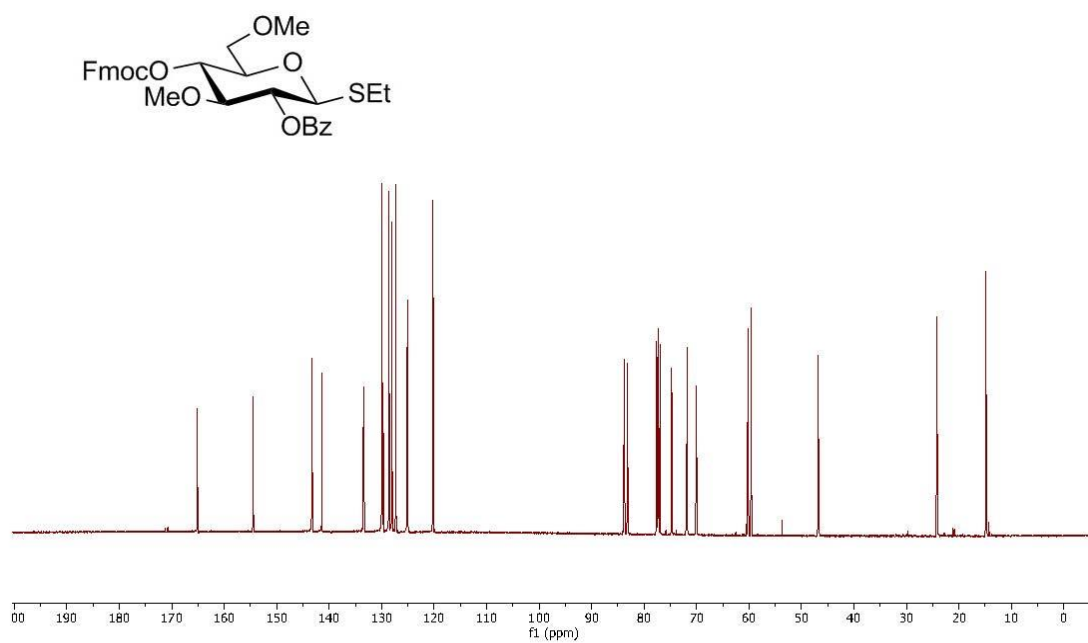
¹³C NMR of S9 (101 MHz, CDCl₃)



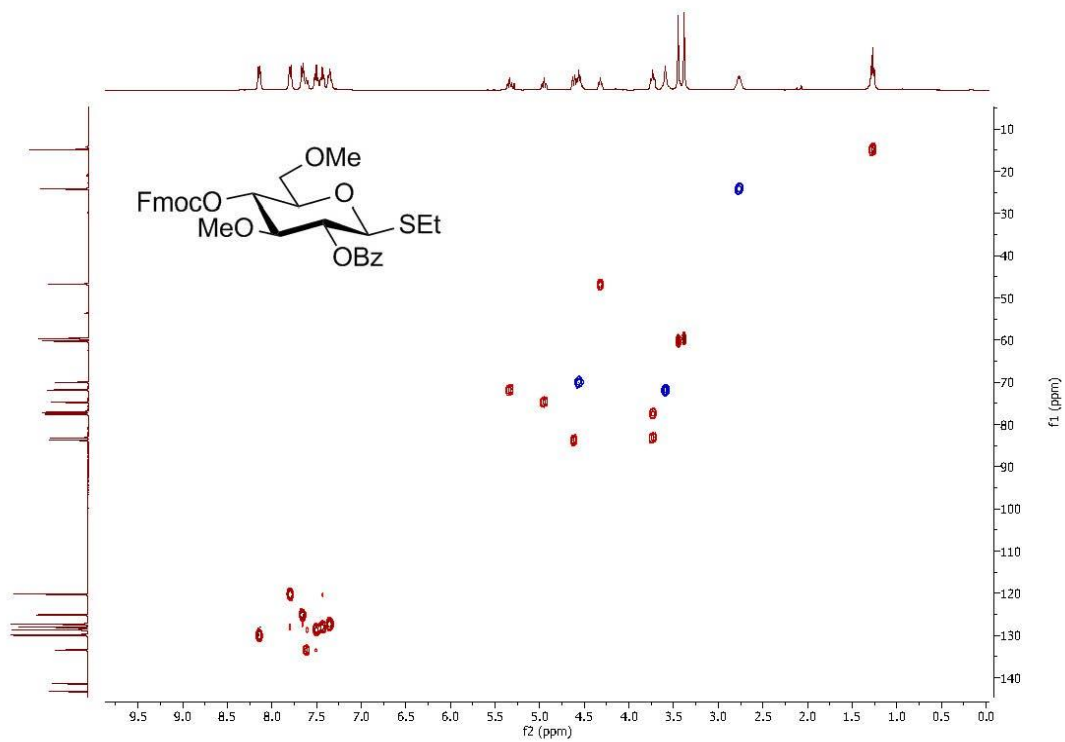
¹H NMR of BB-12 (400 MHz, CDCl₃)



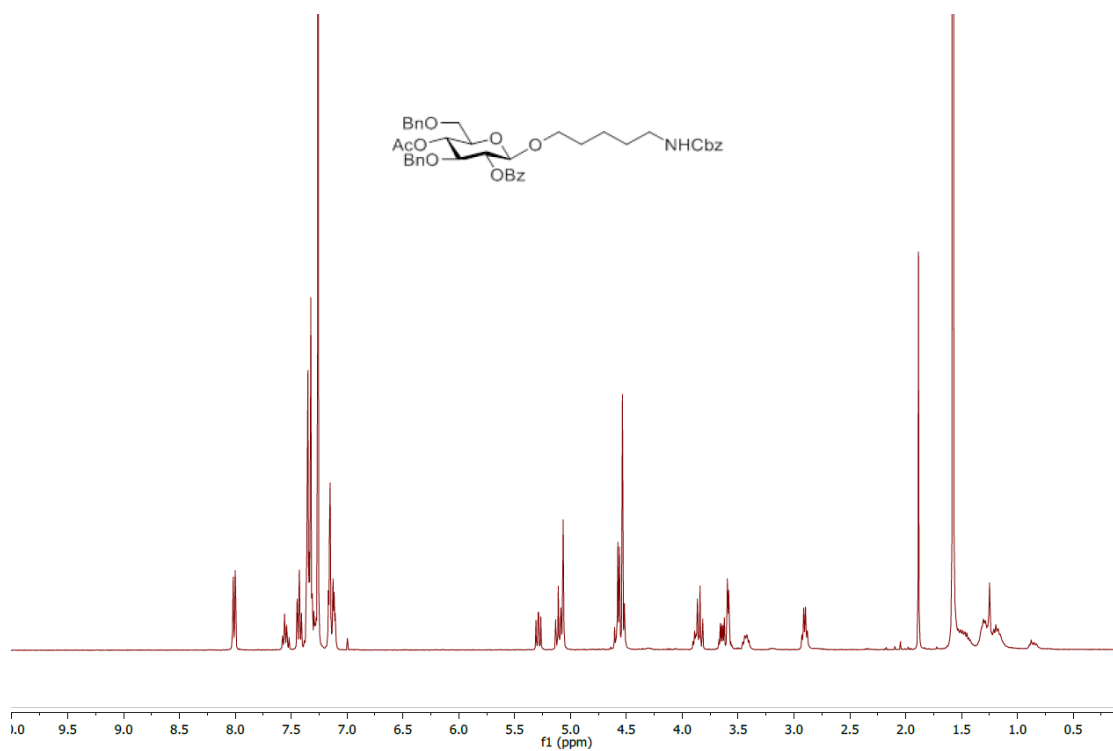
¹³C NMR of BB-12 (101 MHz, CDCl₃)



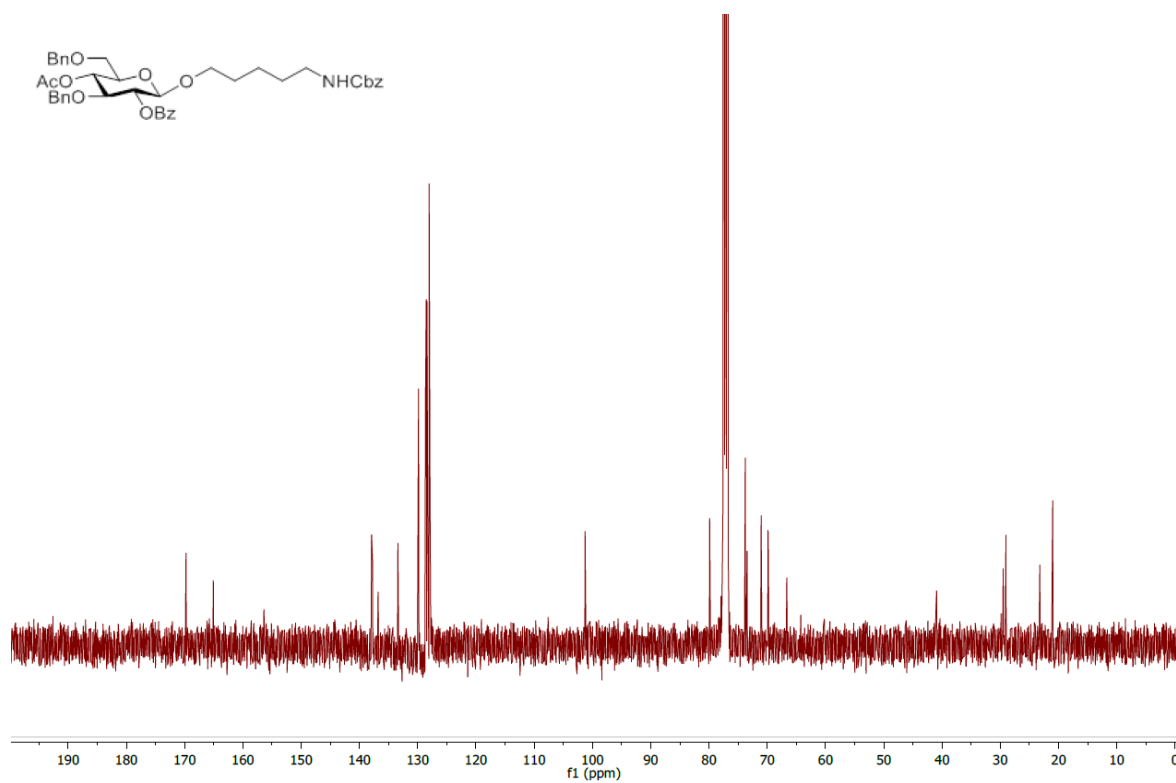
HSQC NMR of BB-12 (CDCl₃)



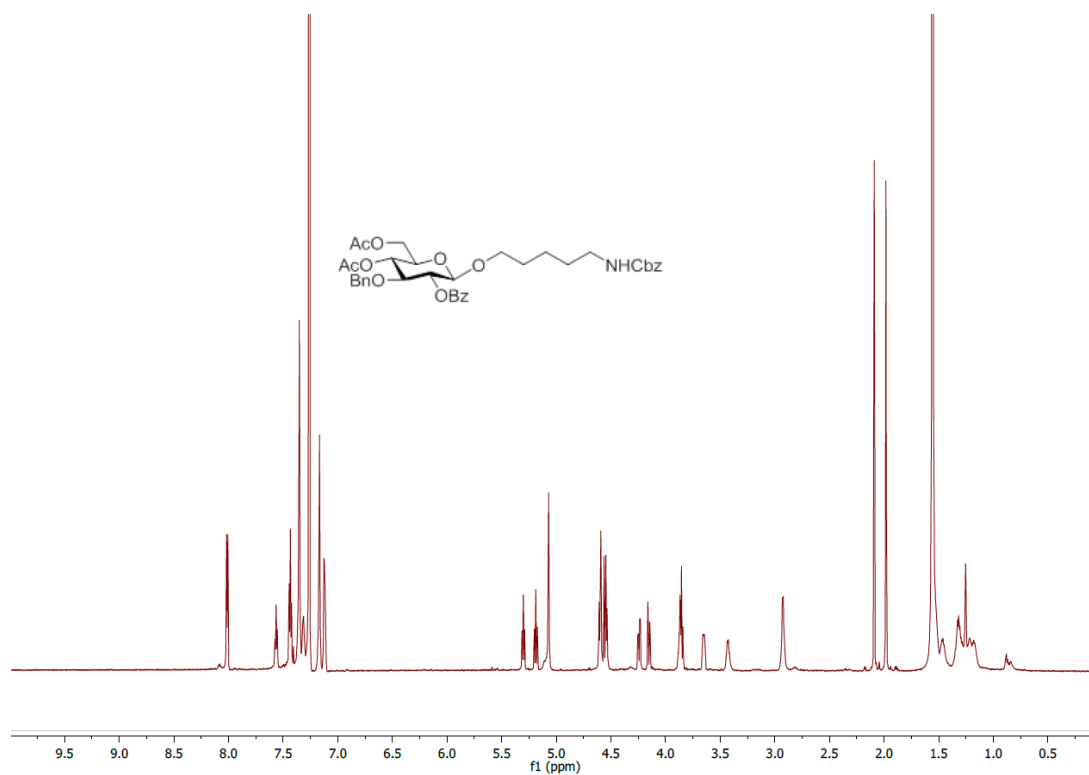
¹H NMR of 14 (400 MHz, CDCl₃)



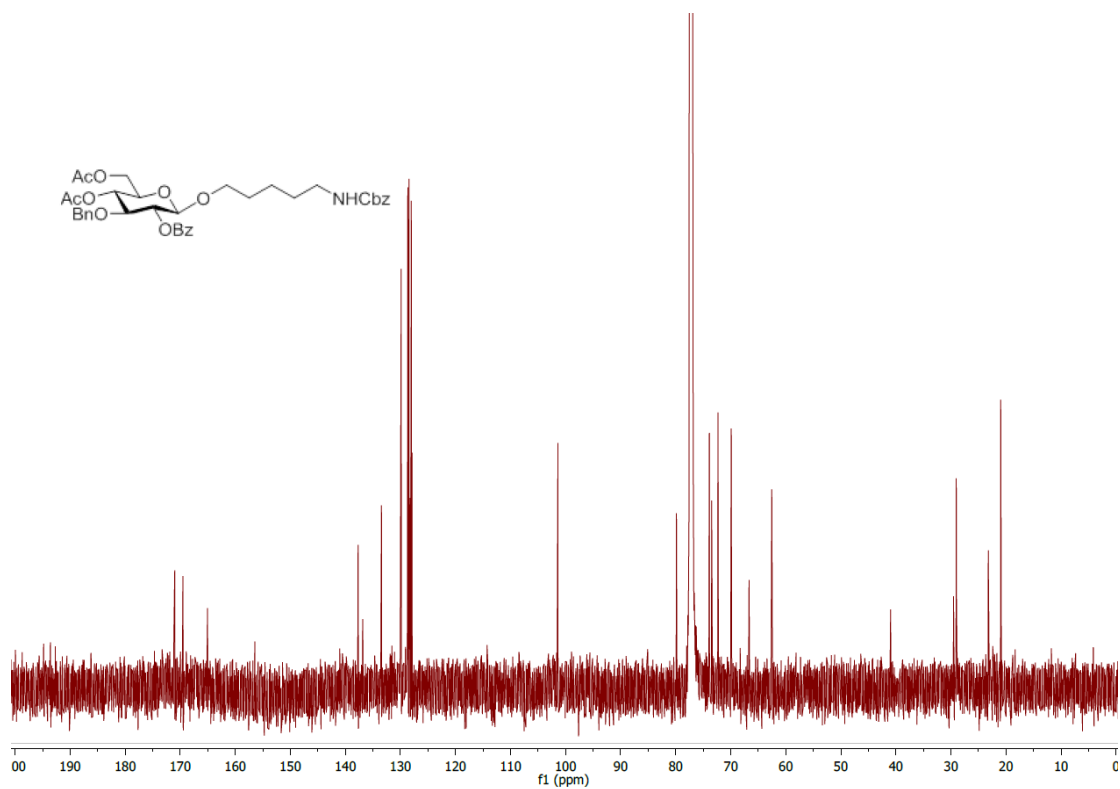
¹³C NMR of 14 (101 MHz, CDCl₃)



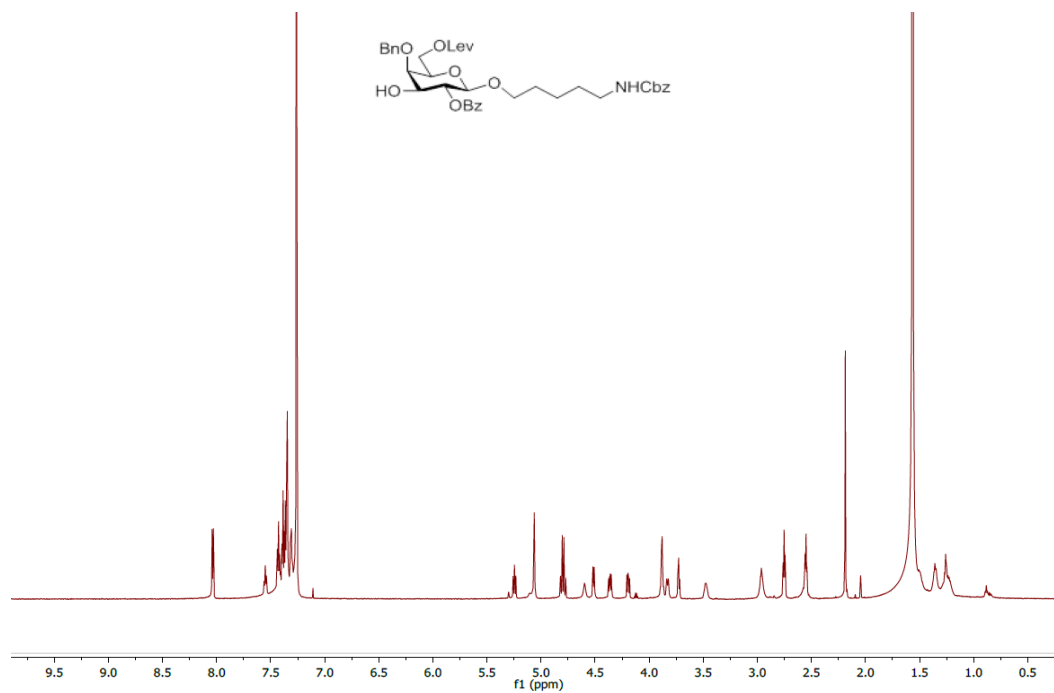
¹H NMR of 15 (400 MHz, CDCl₃)



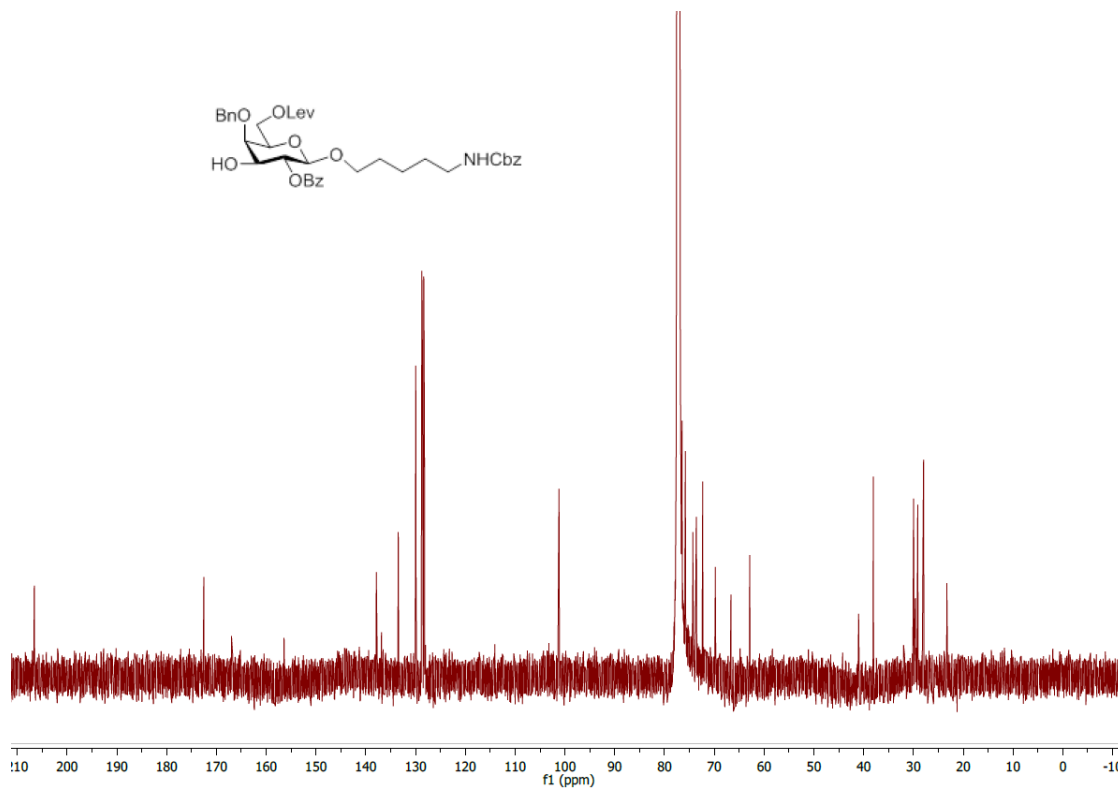
¹³C NMR of 15 (101 MHz, CDCl₃)



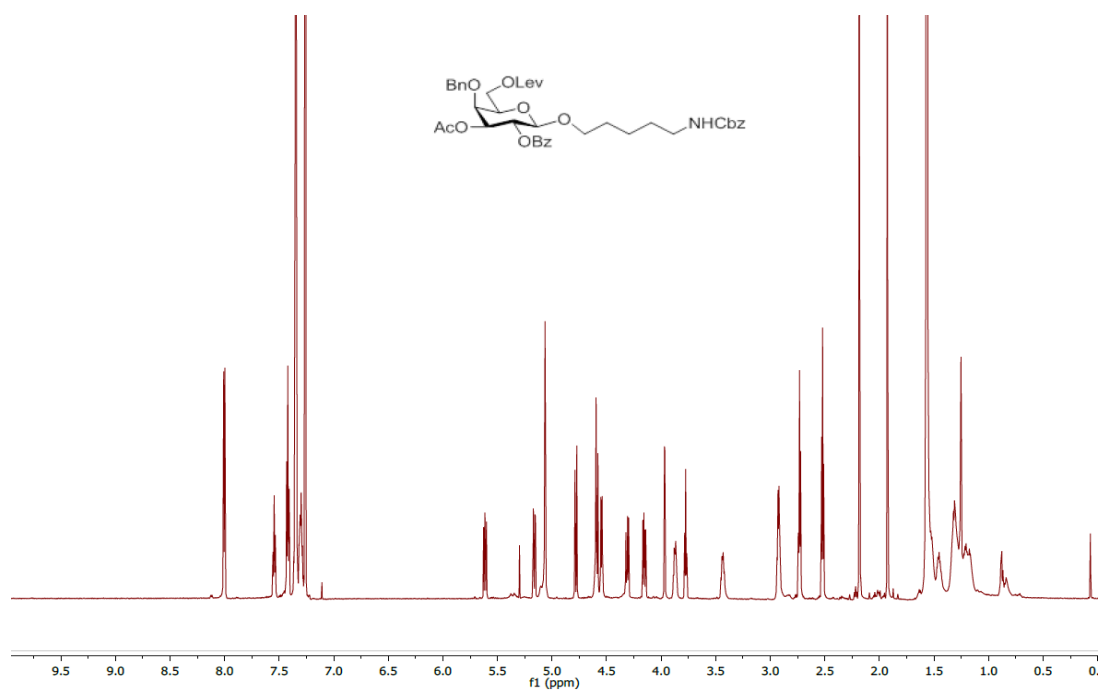
¹H NMR of S12 (400 MHz, CDCl₃)



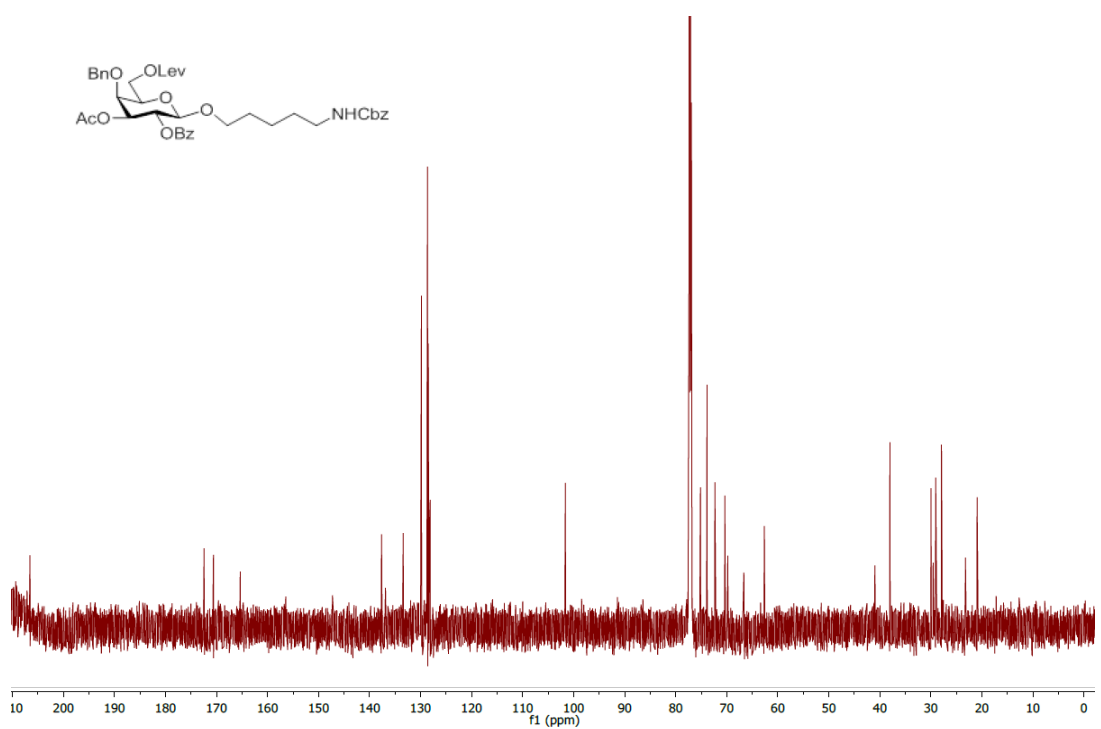
¹³C NMR of S12 (101 MHz, CDCl₃)



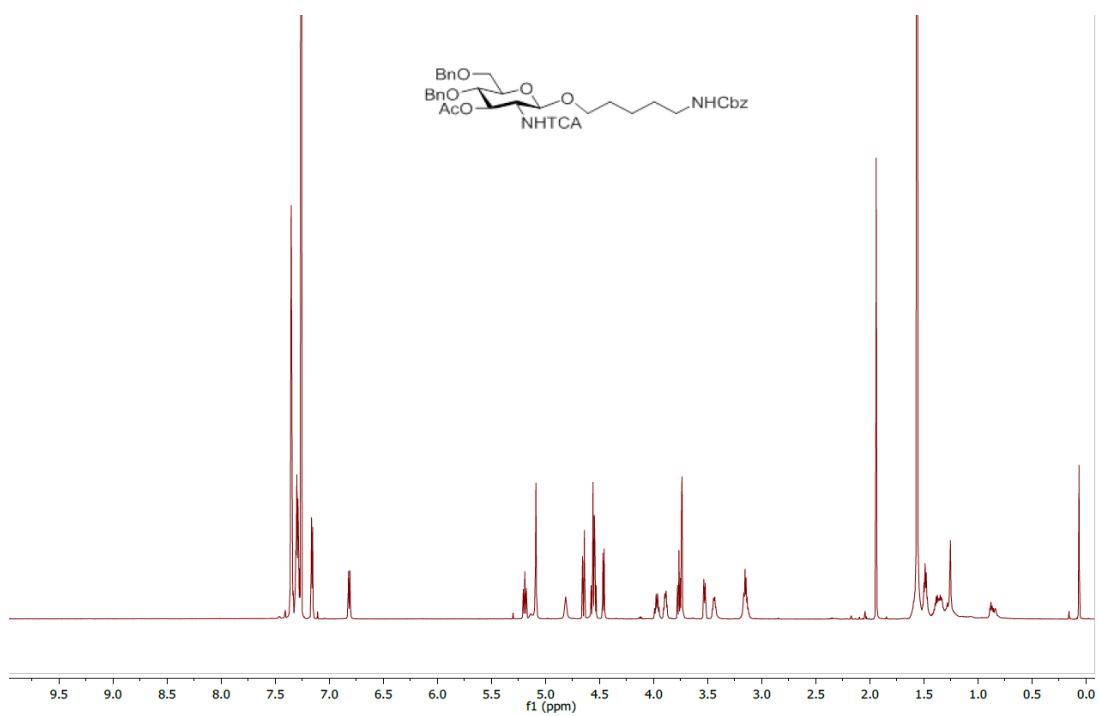
¹H NMR of S13 (400 MHz, CDCl₃)



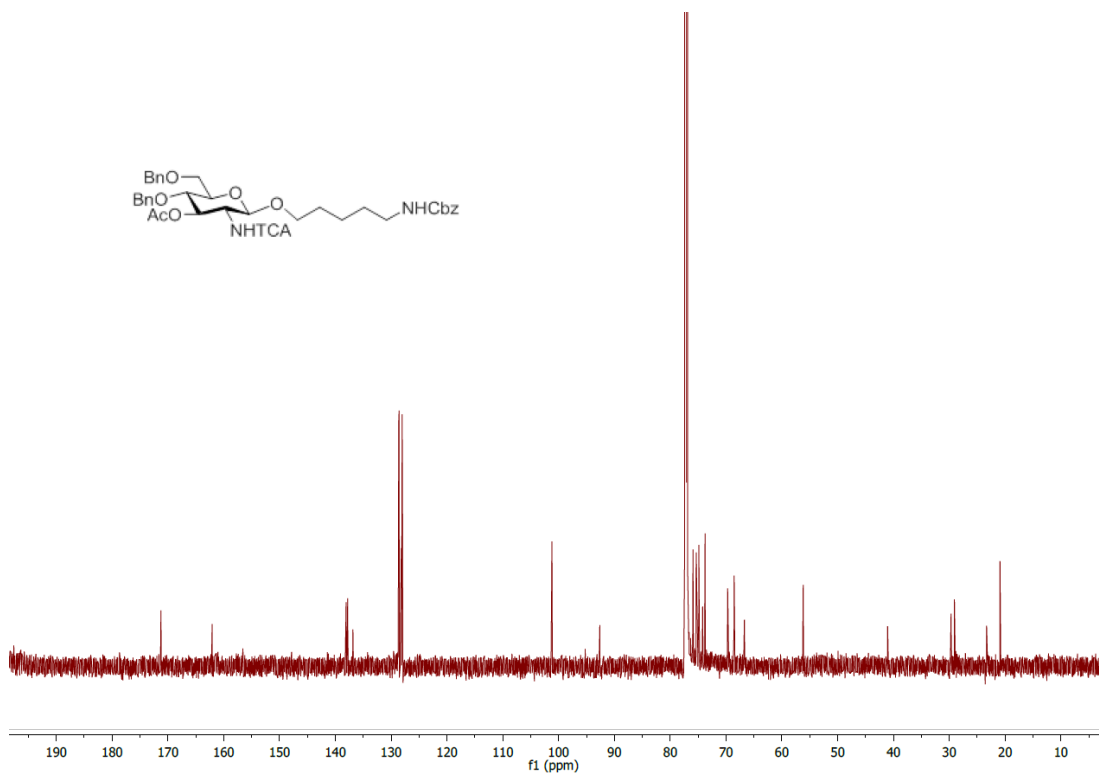
¹³C NMR of S13 (101 MHz, CDCl₃)



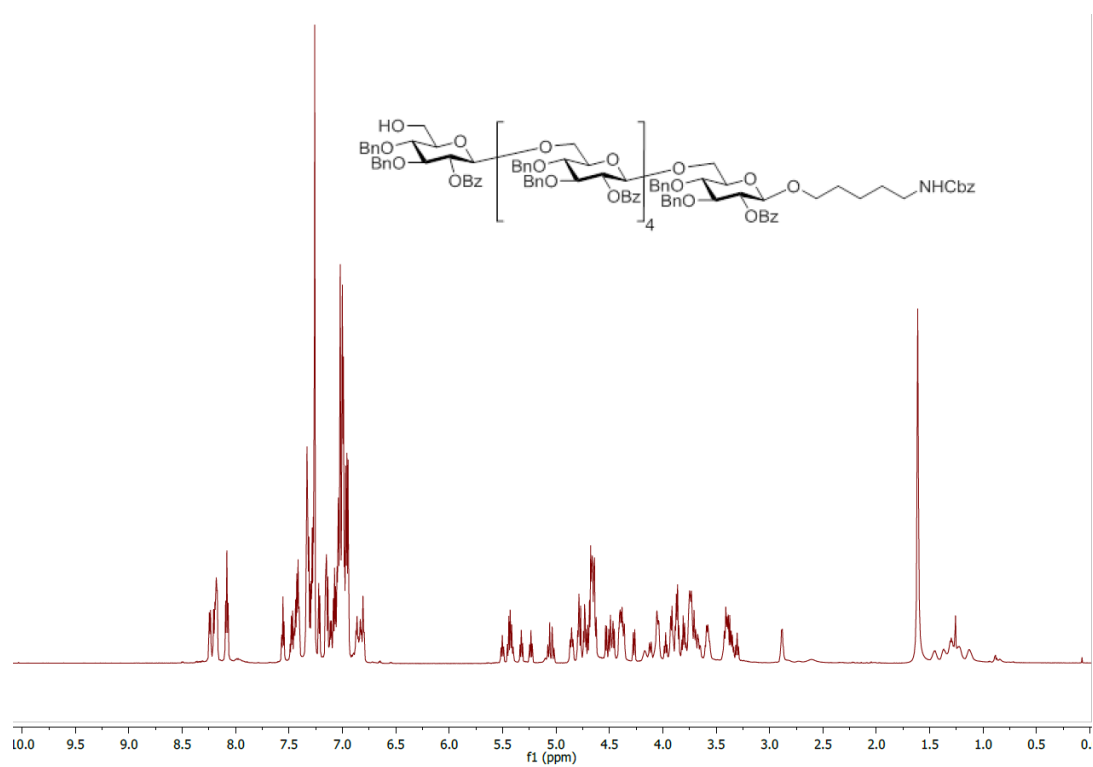
¹H NMR of S15 (400 MHz, CDCl₃)



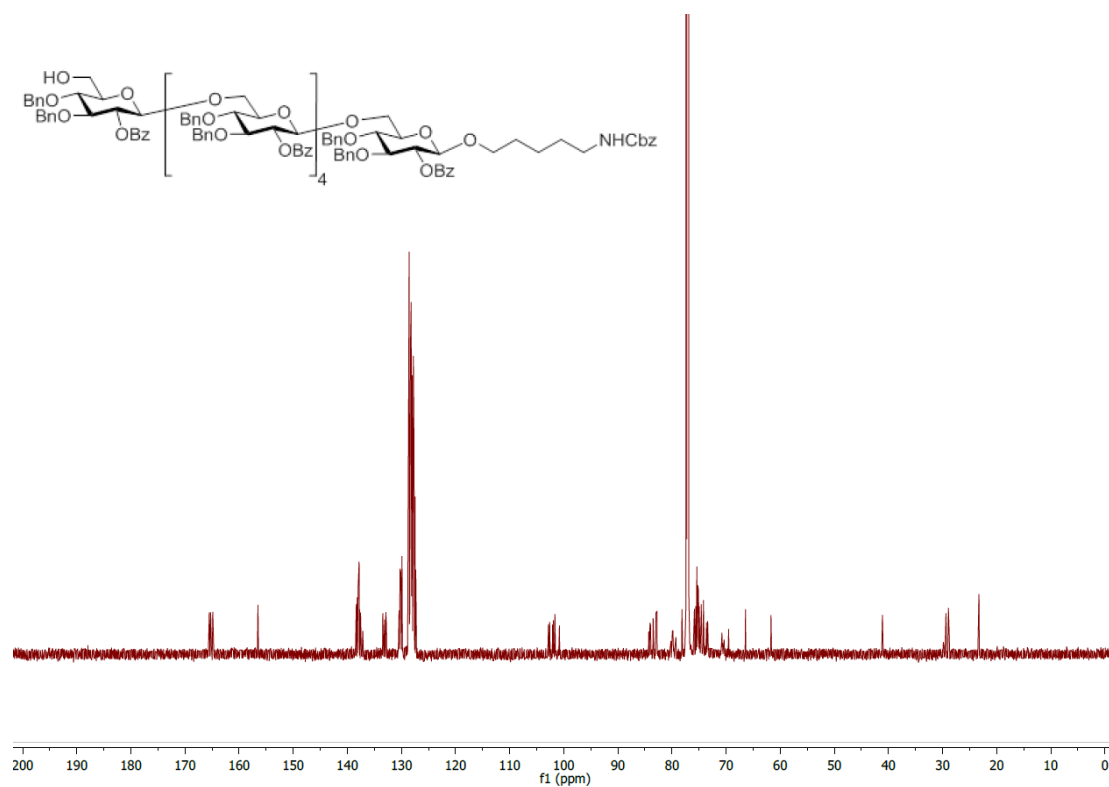
¹³C NMR of S15 (101 MHz, CDCl₃)



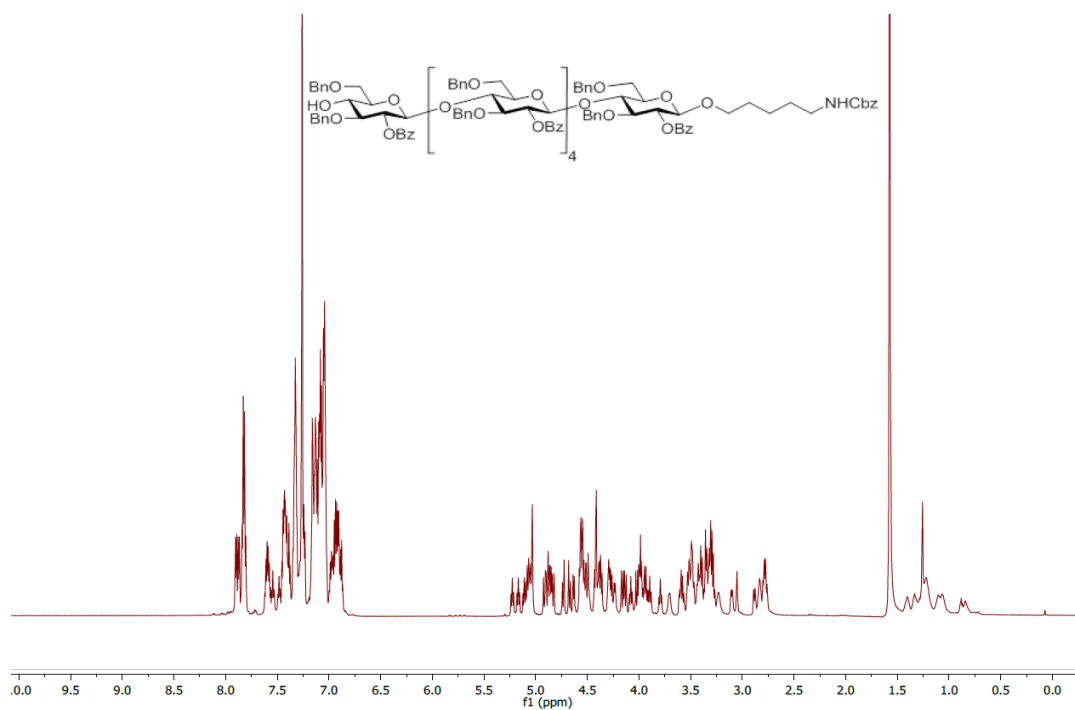
¹H NMR of 16a (700 MHz, CDCl₃)



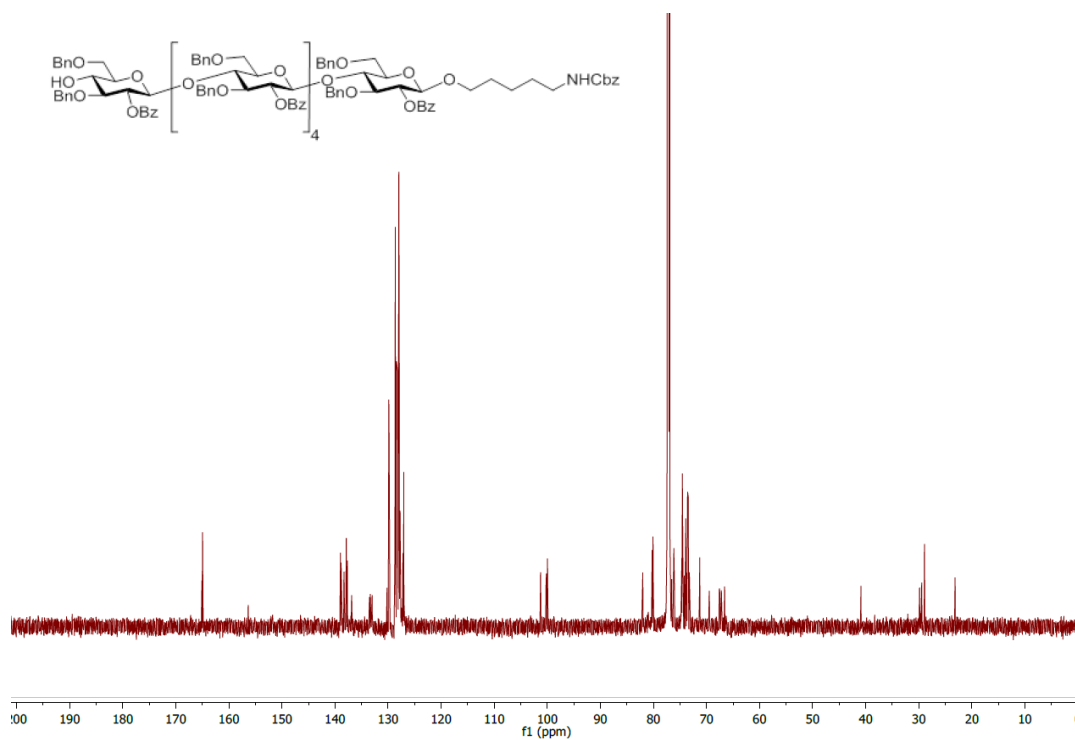
¹³C NMR of 16a (176 MHz, CDCl₃)



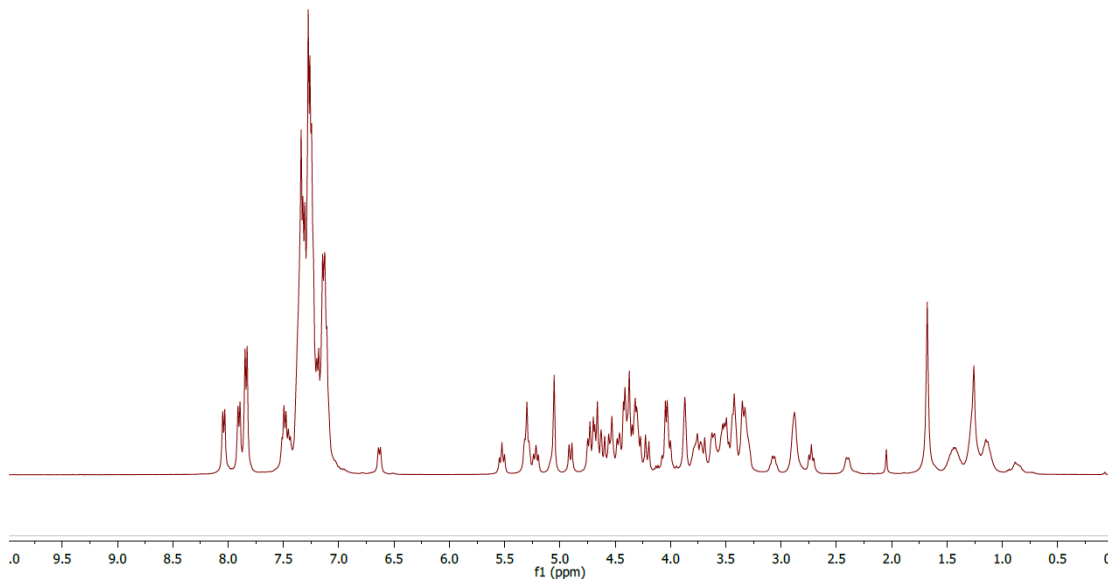
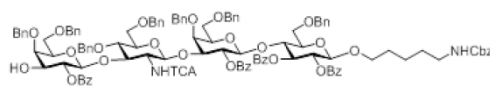
¹H NMR of 16b (700 MHz, CDCl₃)



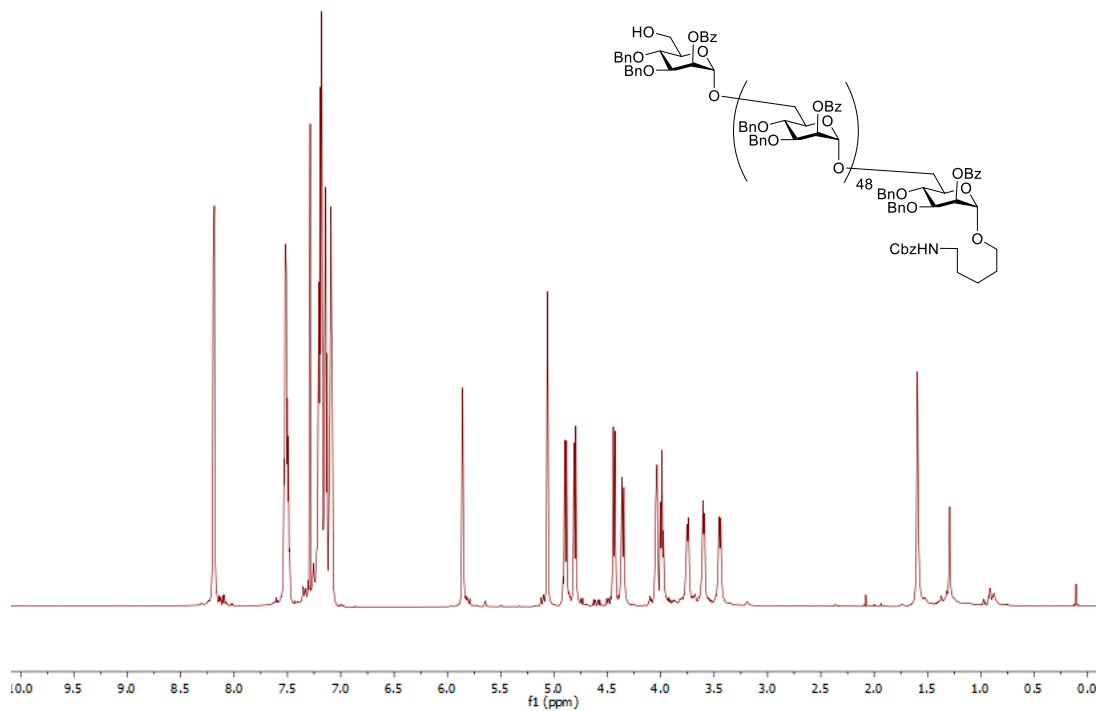
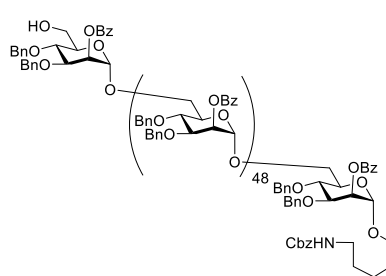
¹³C NMR of 16b (176 MHz, CDCl₃)



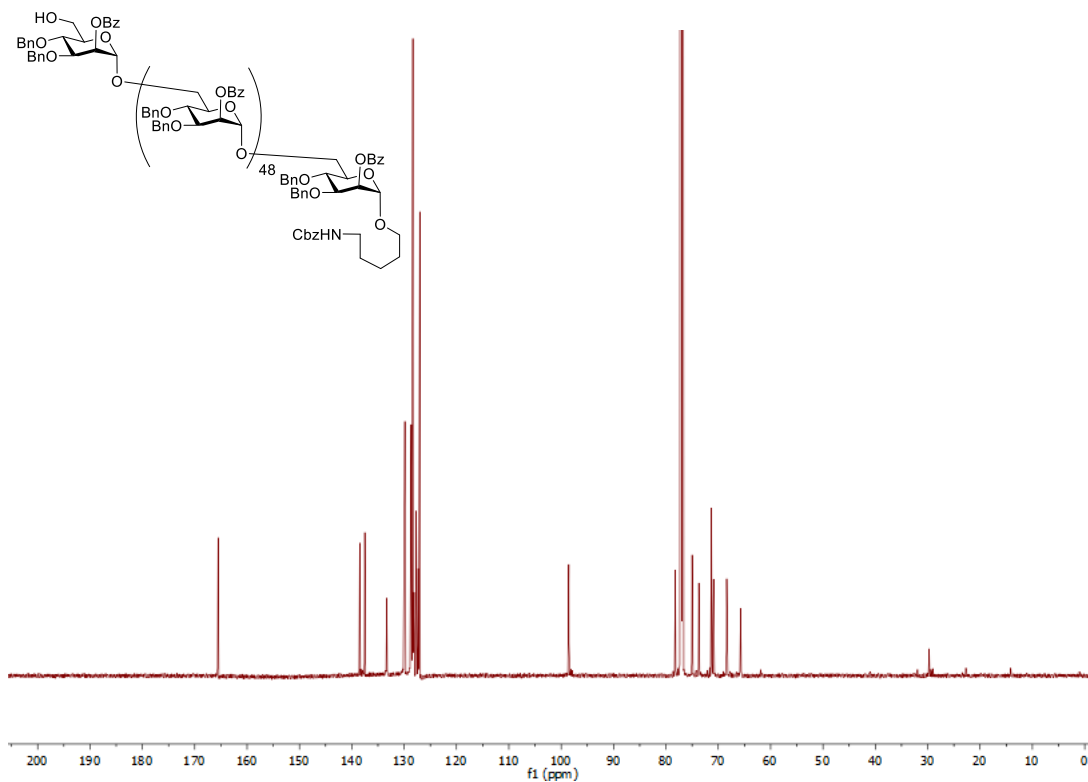
¹H NMR of 17 (400 MHz, CDCl₃)



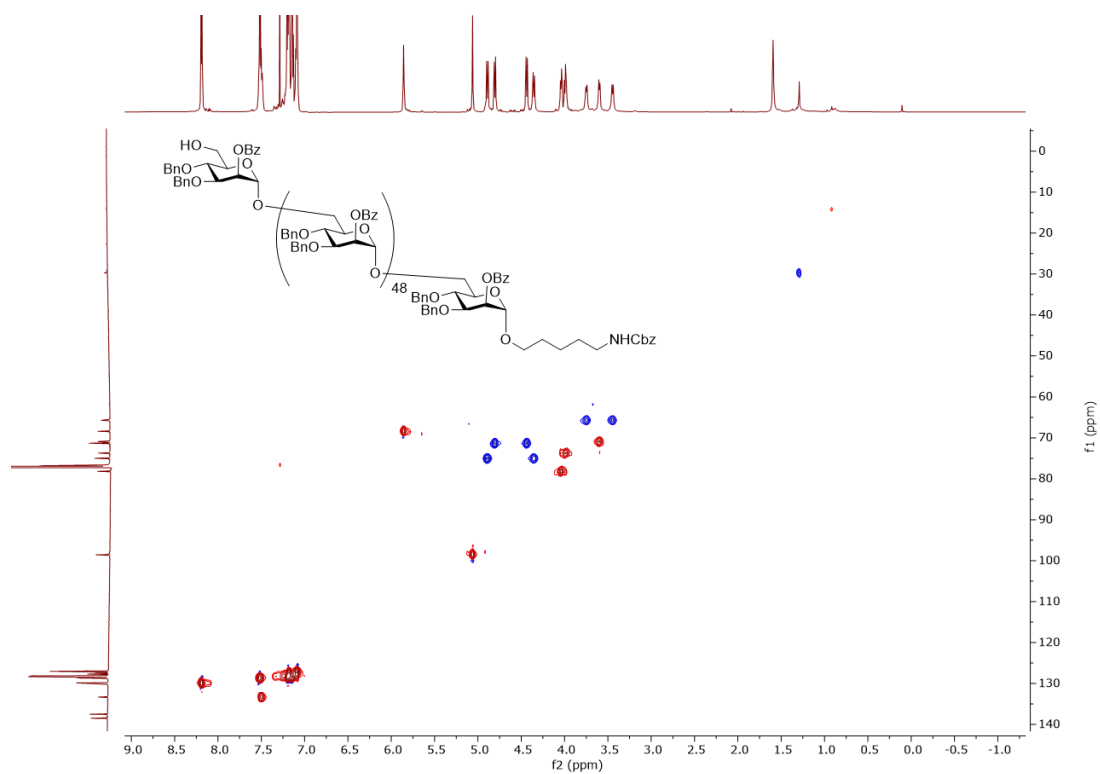
¹H NMR of 6 (700 MHz, CDCl₃)



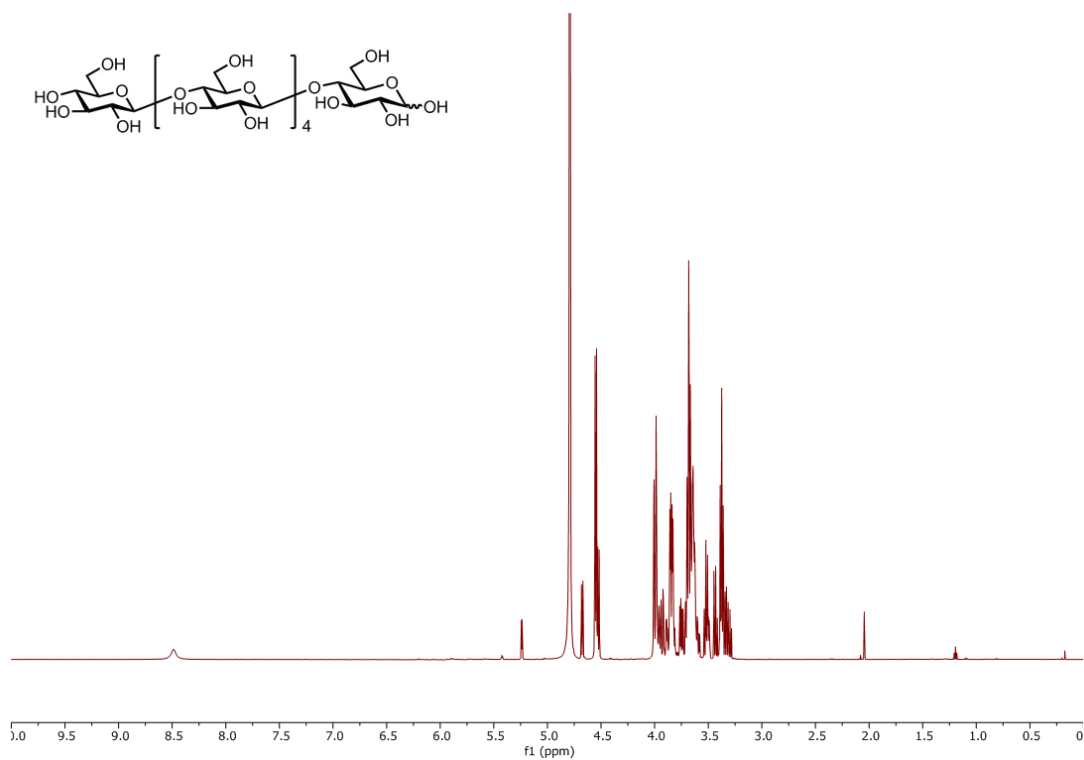
^{13}C NMR of 6 (176 MHz, CDCl_3)



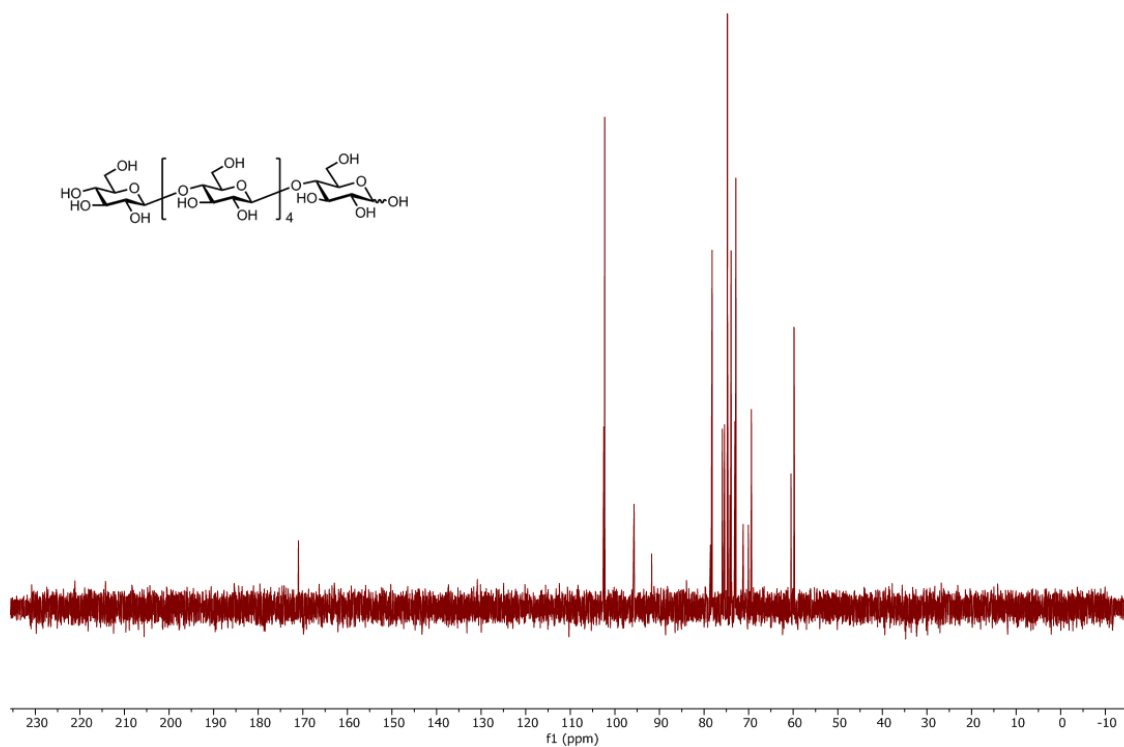
HSQC NMR of 6 (CDCl_3)



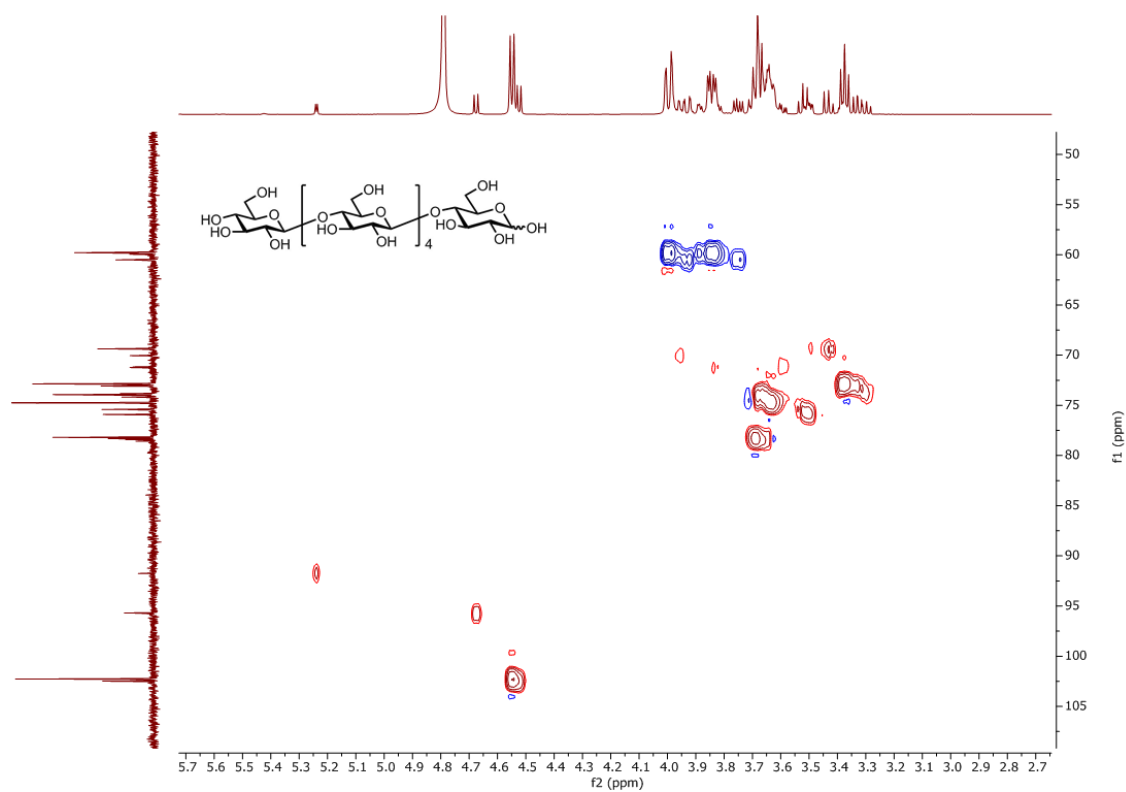
¹H NMR of AAAAAA-OH (600 MHz, D₂O)



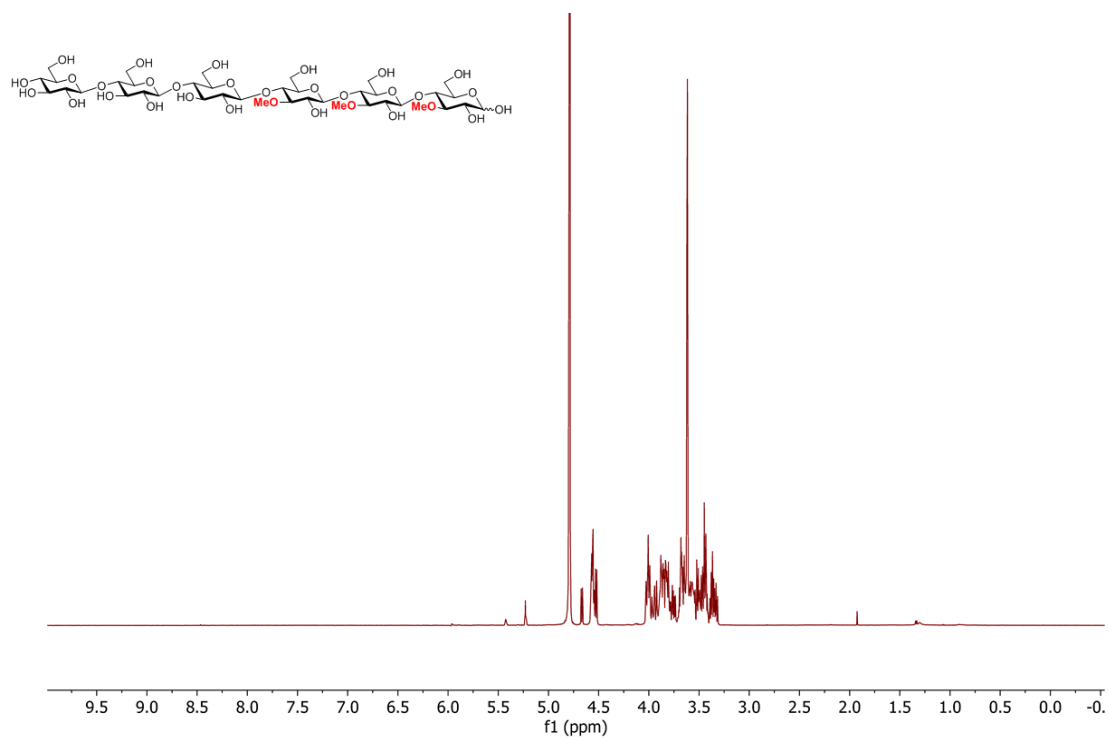
¹³C NMR of AAAAAA-OH (151 MHz, D₂O)



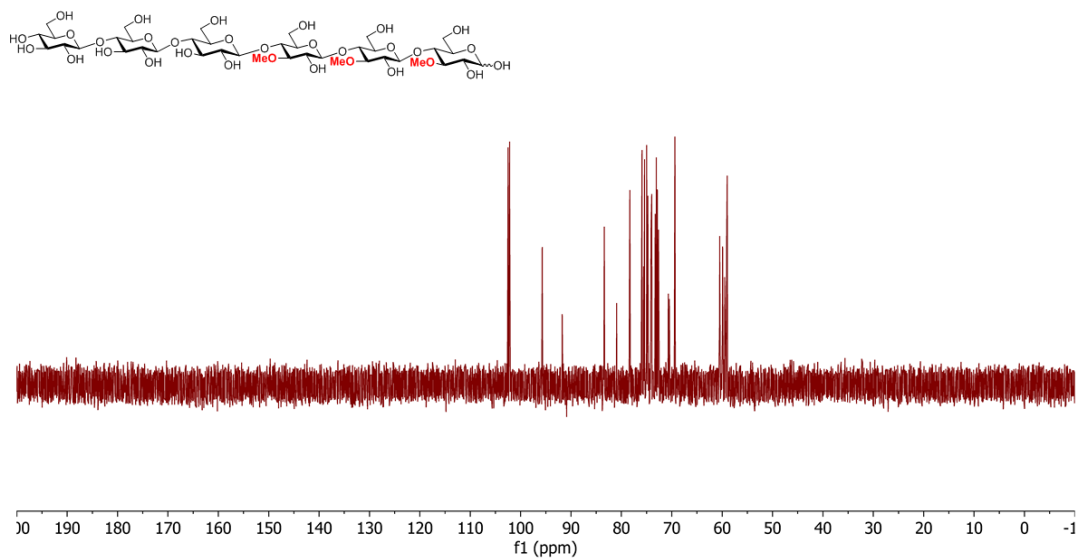
HSQC NMR of AAAAAA-OH (D₂O)



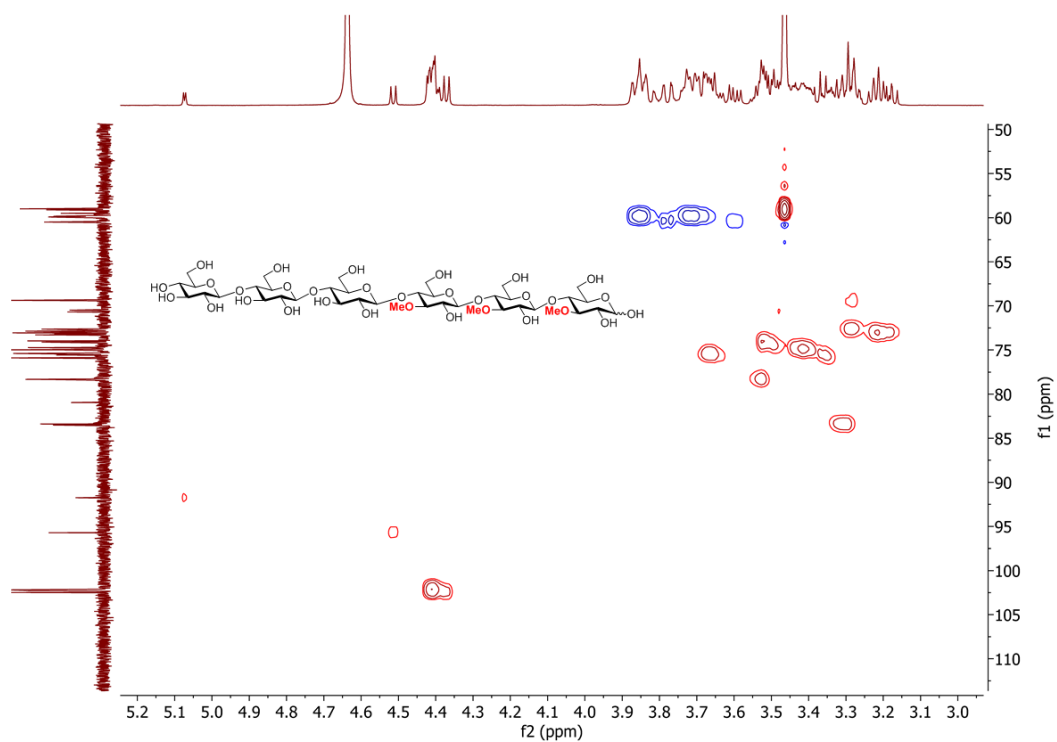
¹H NMR of AAABBB-OH (600 MHz, D₂O)



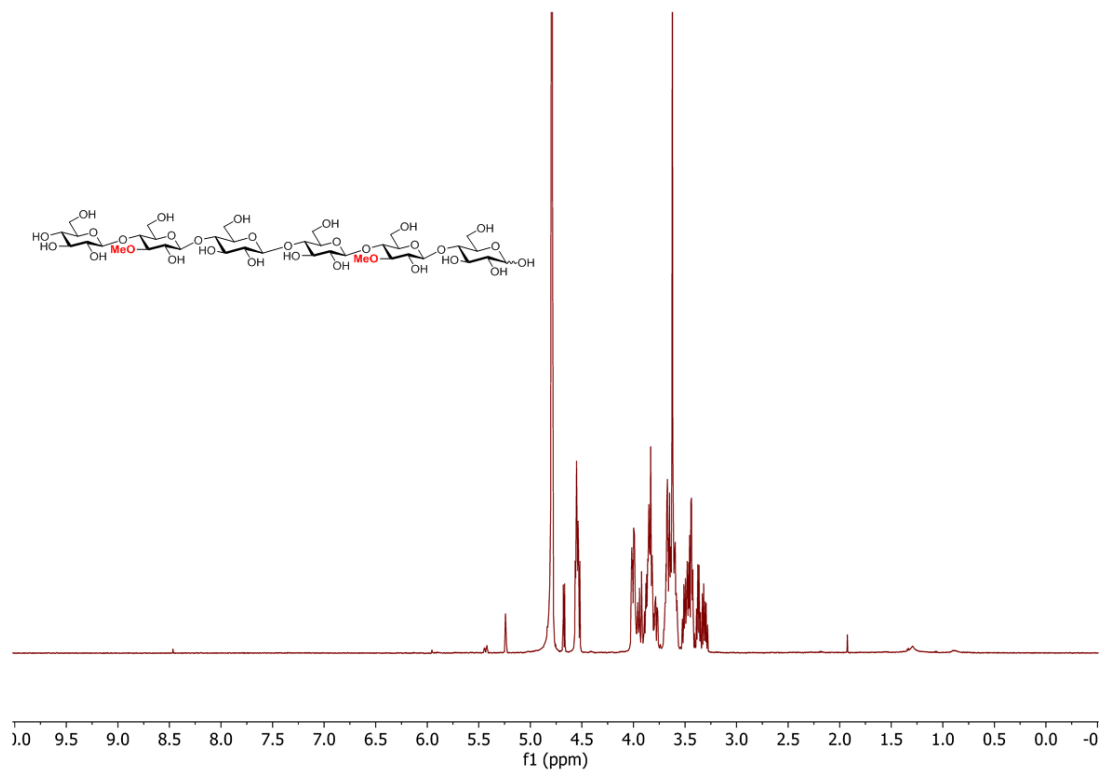
¹³C NMR of AAABBB-OH (151 MHz, D₂O)



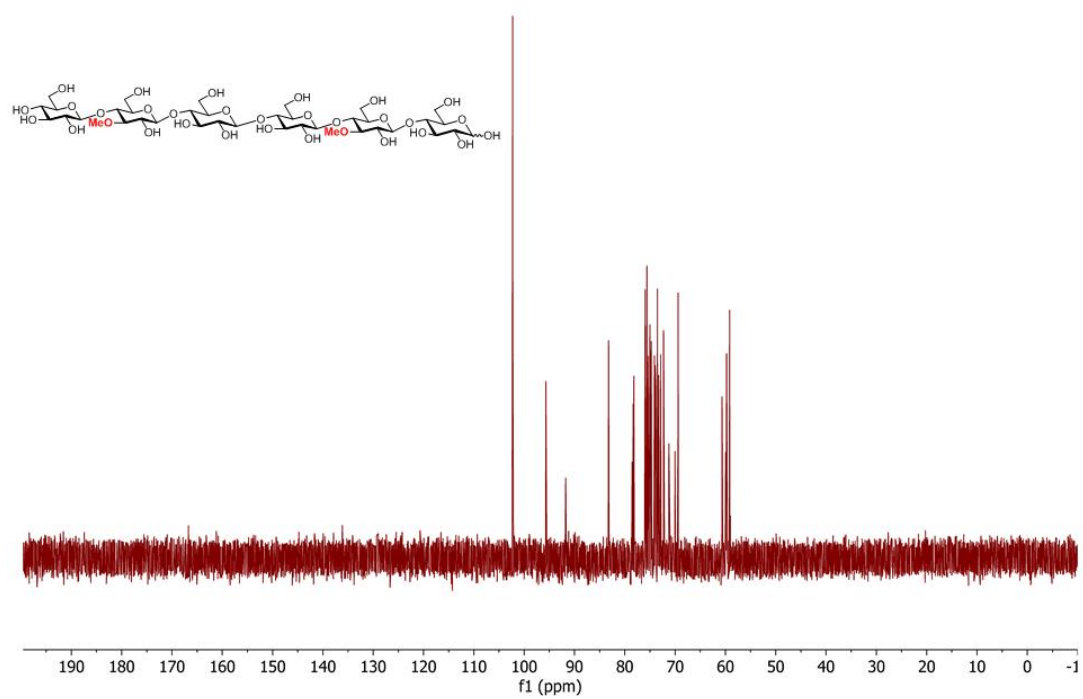
HSQC NMR of AAABBB-OH (D₂O)



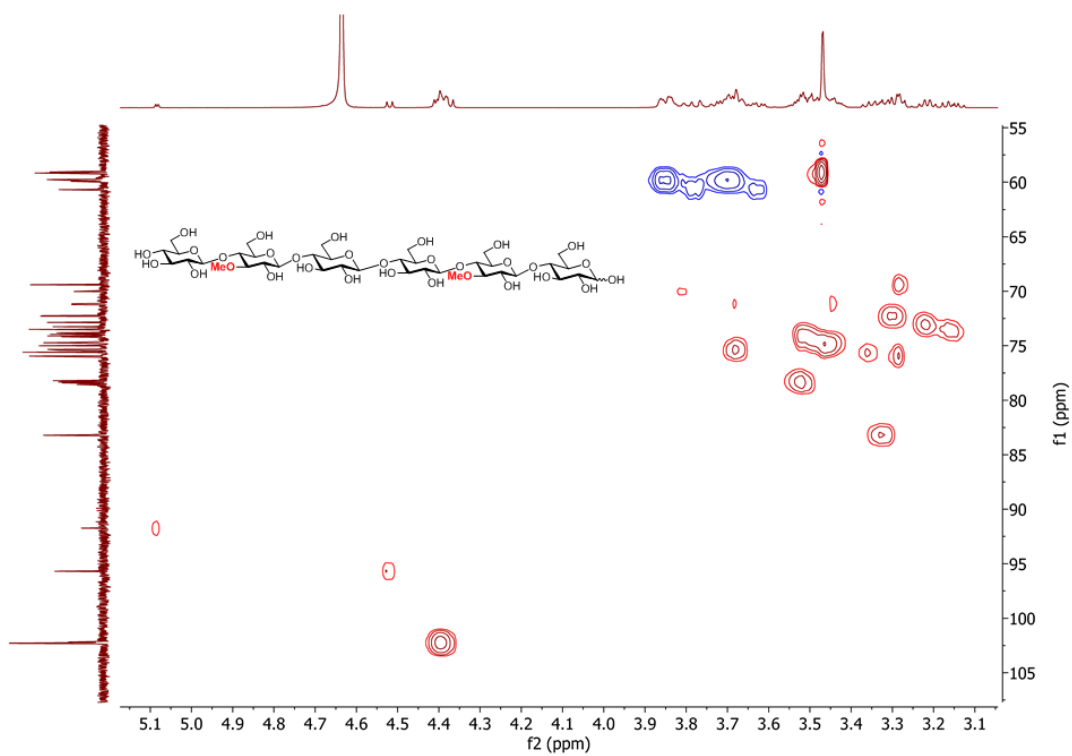
¹H NMR of ABAABA-OH (600 MHz, D₂O)



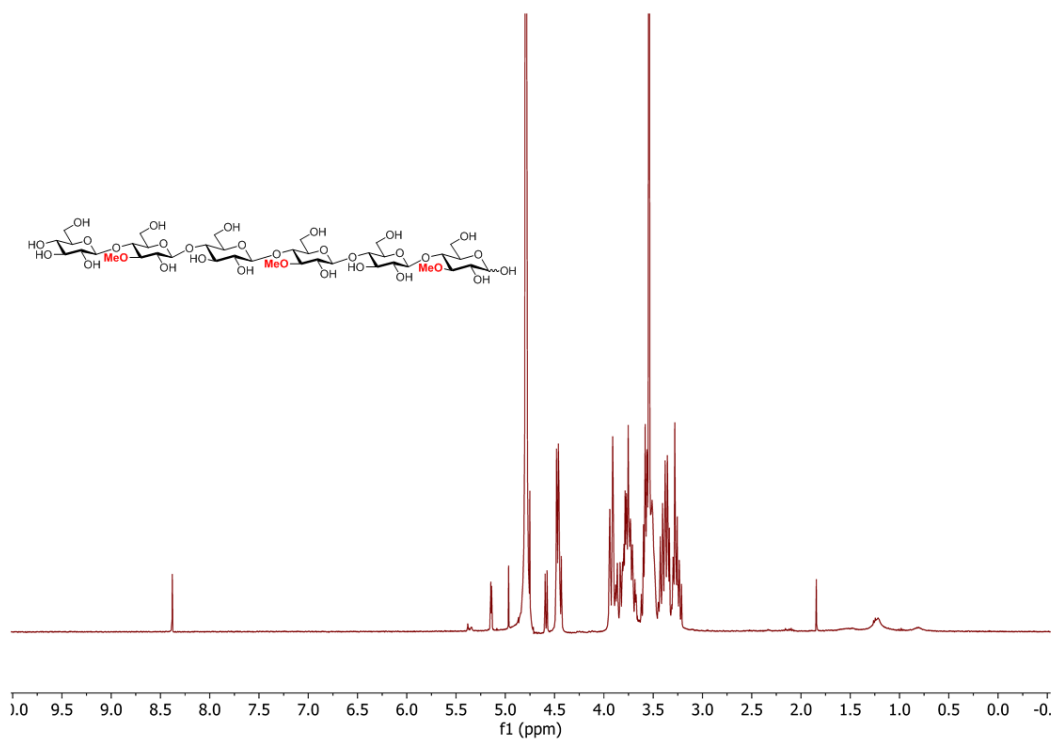
¹³C NMR of ABAABA-OH (151 MHz, D₂O)



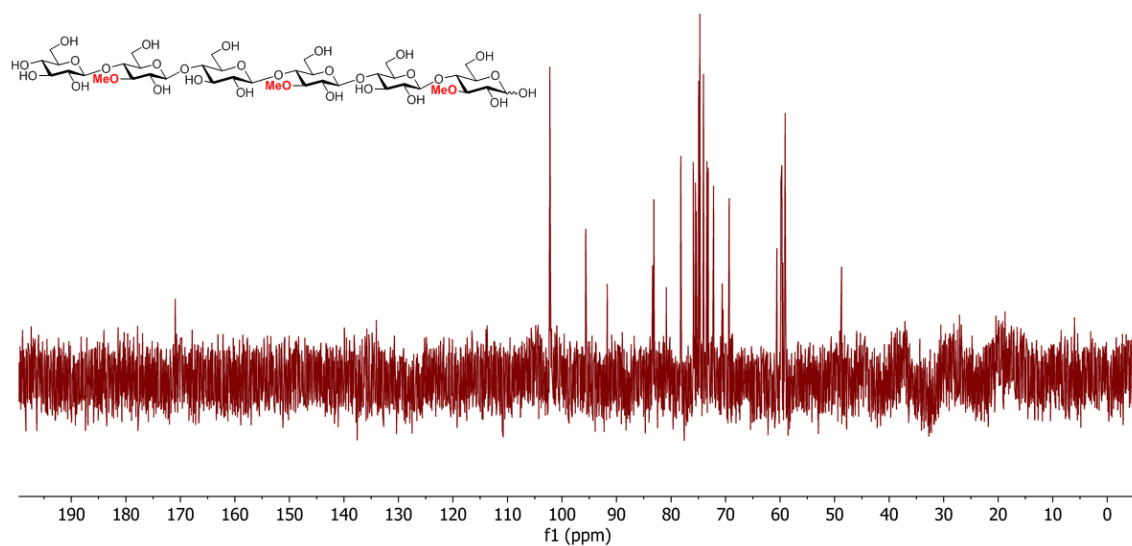
HSQC NMR of ABAABA-OH (D₂O)



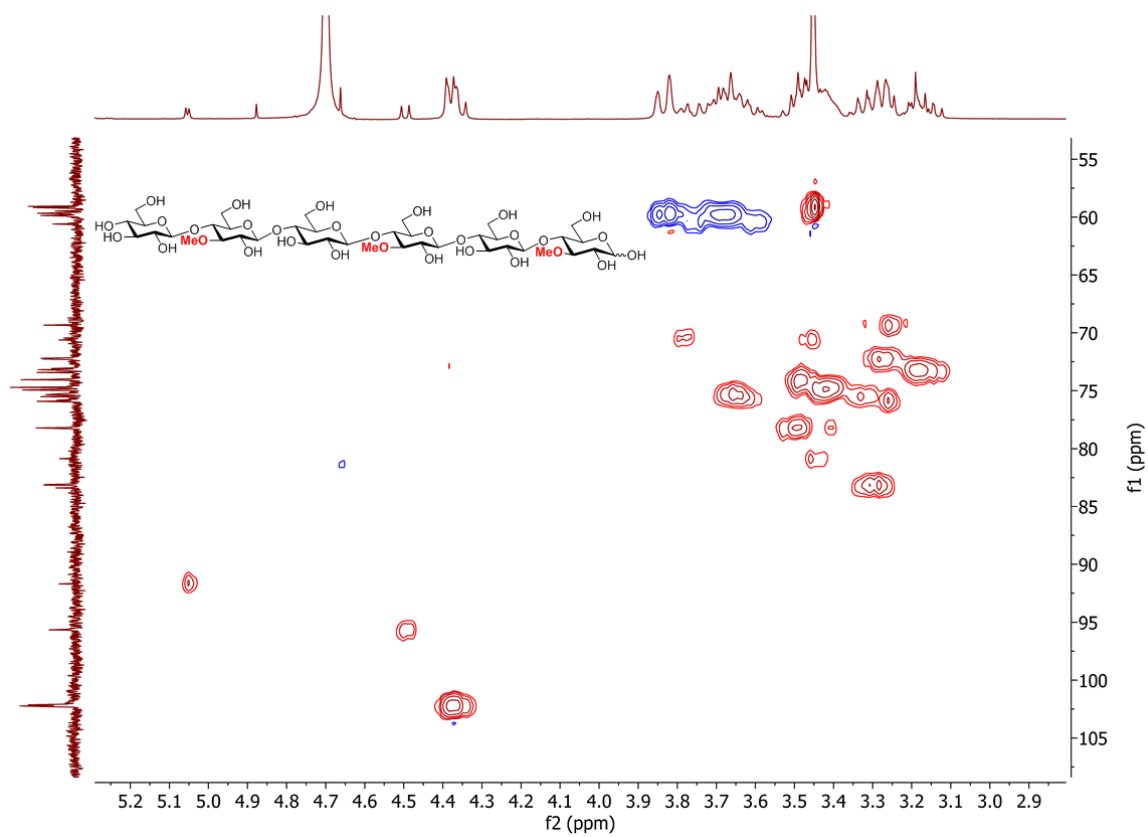
¹H NMR of ABABAB-OH (400 MHz, D₂O)



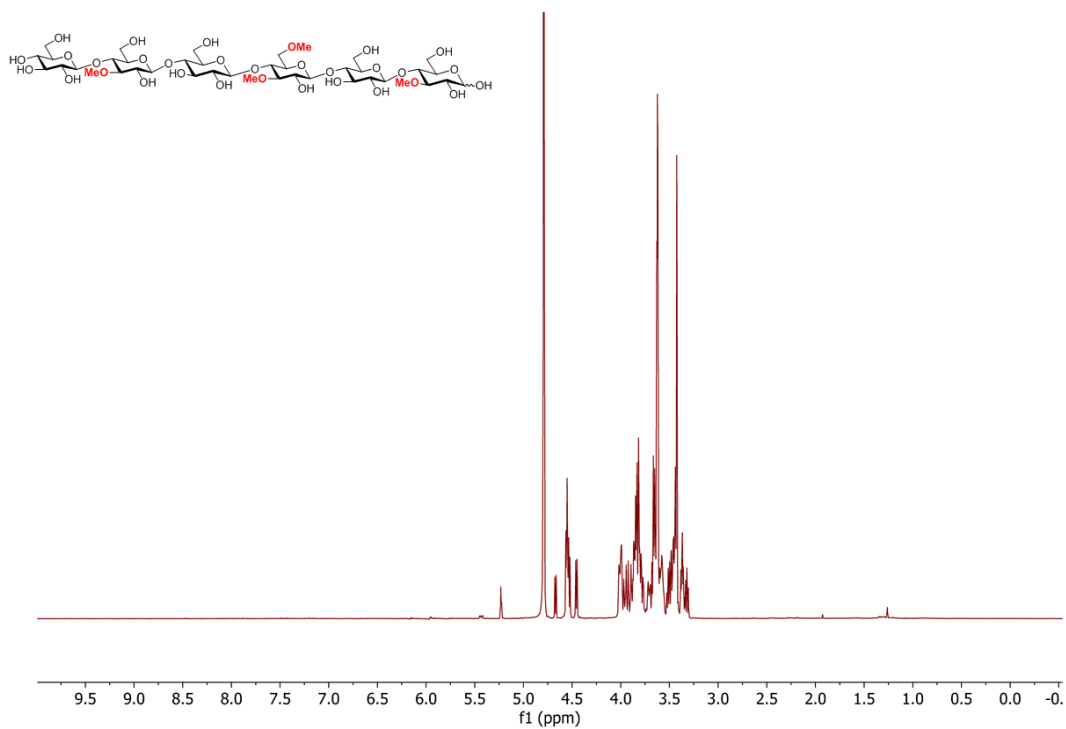
¹³C NMR of ABABAB-OH (101 MHz, D₂O)



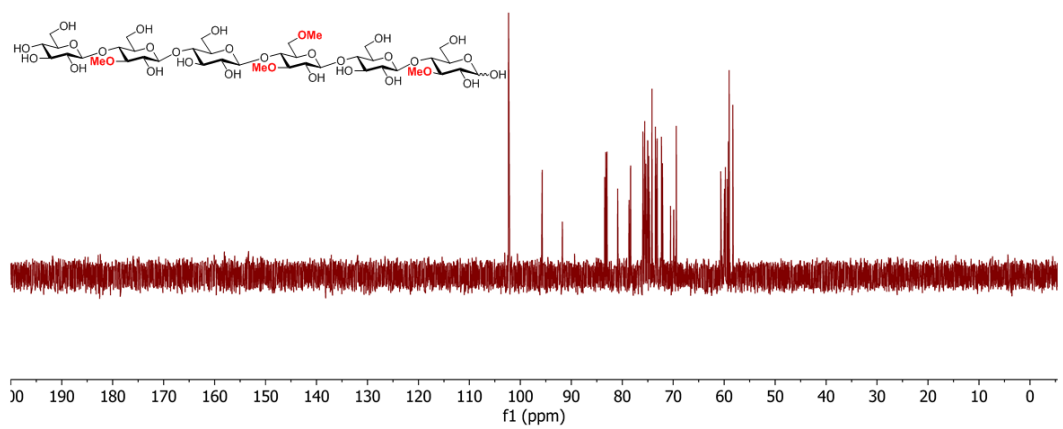
HSQC NMR of ABABAB-OH (D₂O)



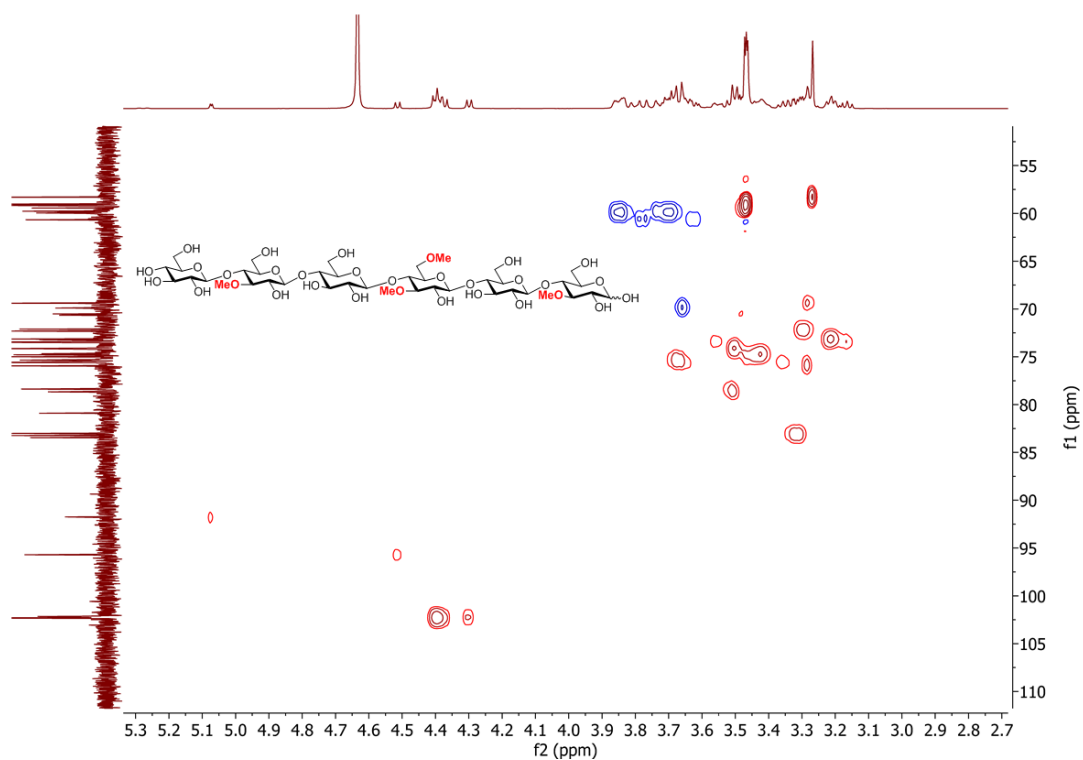
¹H NMR of ABACAB-OH (600 MHz, D₂O)



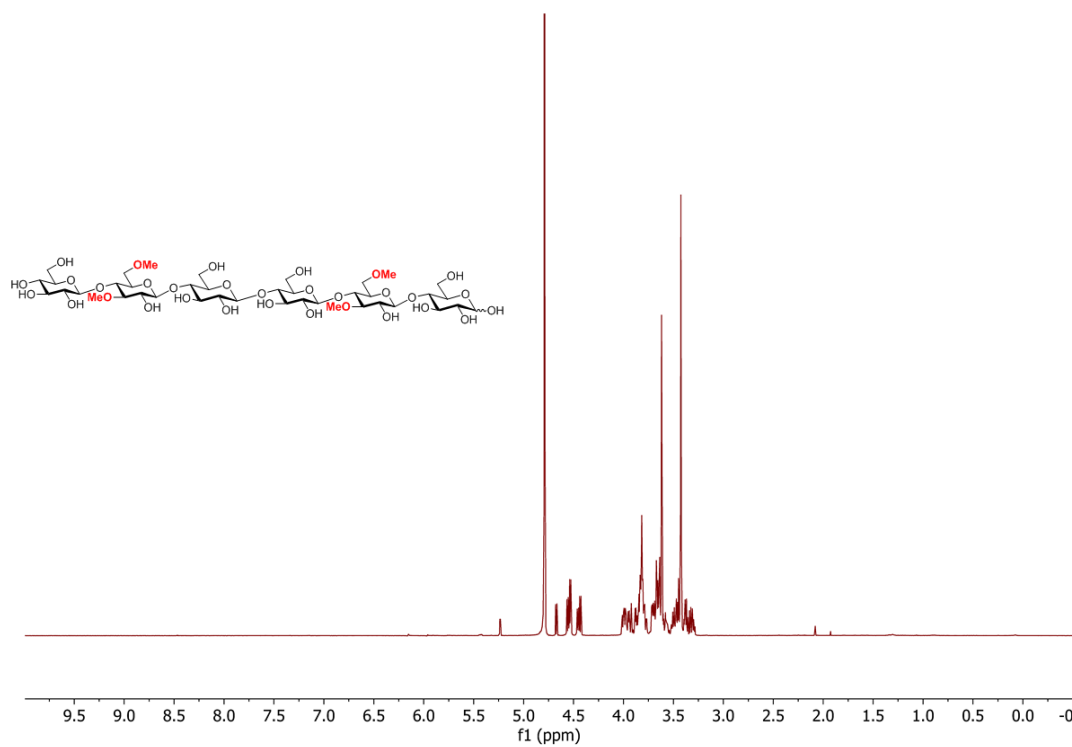
¹³C NMR of ABACAB-OH (151 MHz, D₂O)



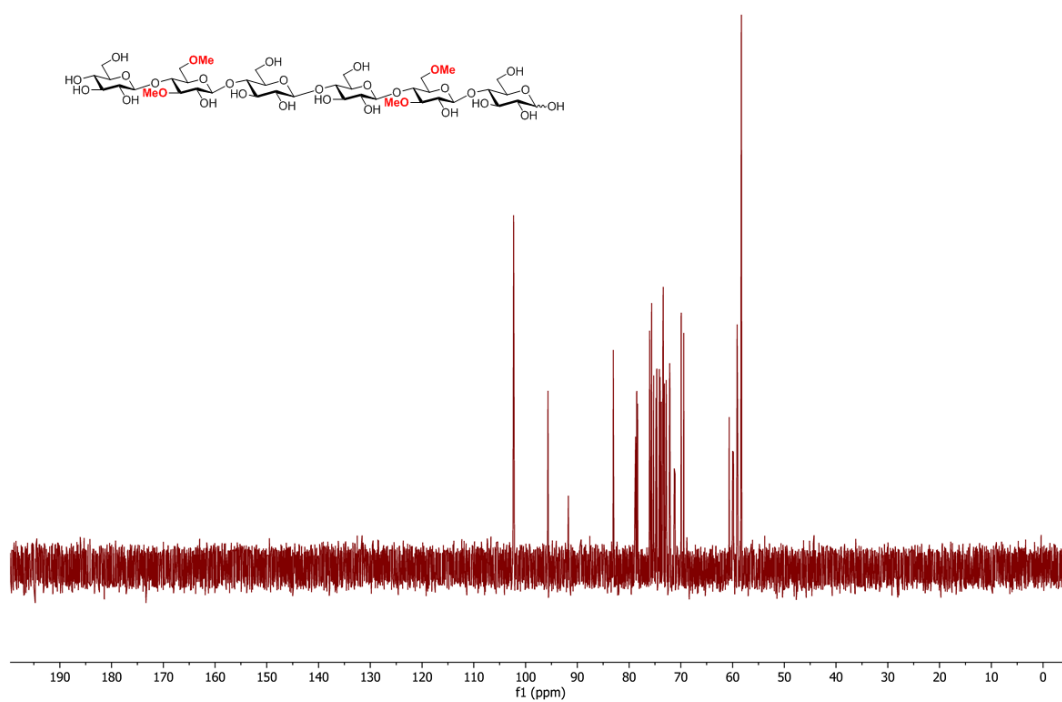
HSQC NMR of ABACAB-OH (D₂O)



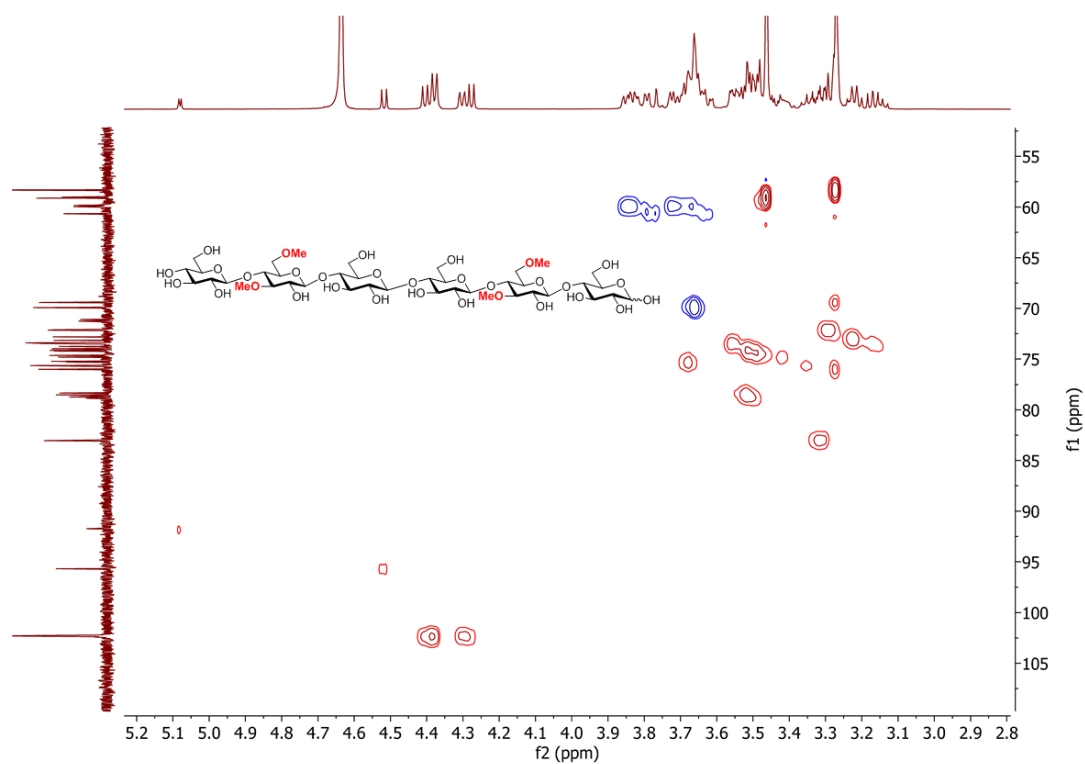
¹H NMR of ACAACA-OH (600 MHz, D₂O)



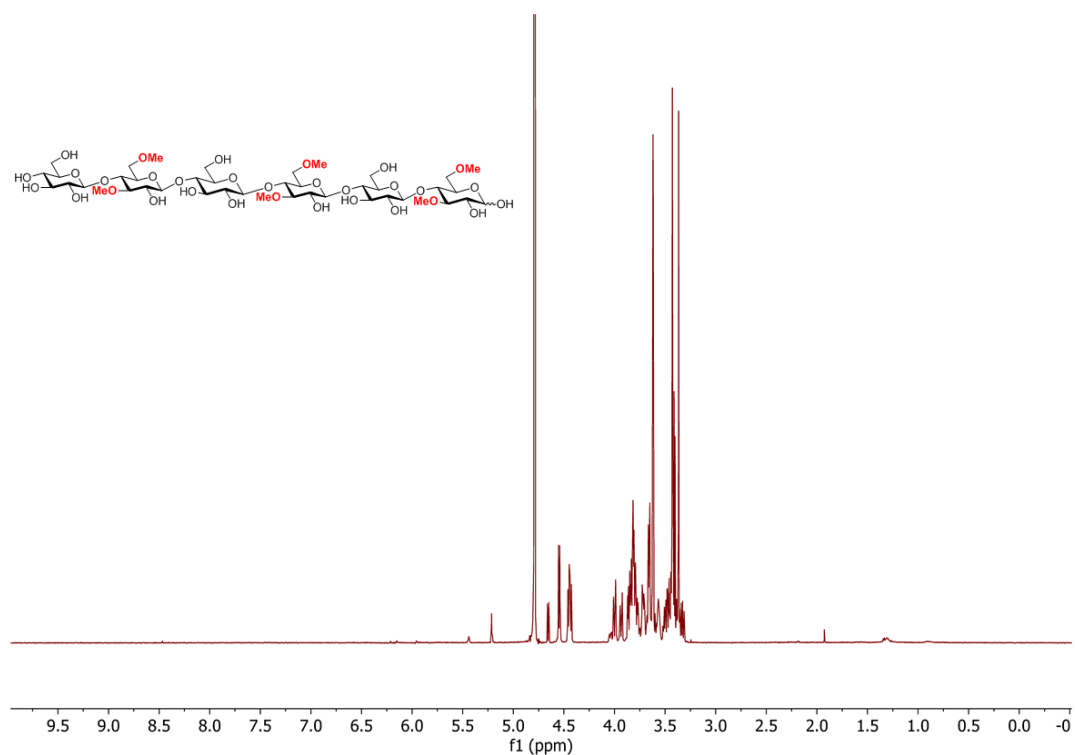
¹³C NMR of ACAACA-OH (151 MHz, D₂O)



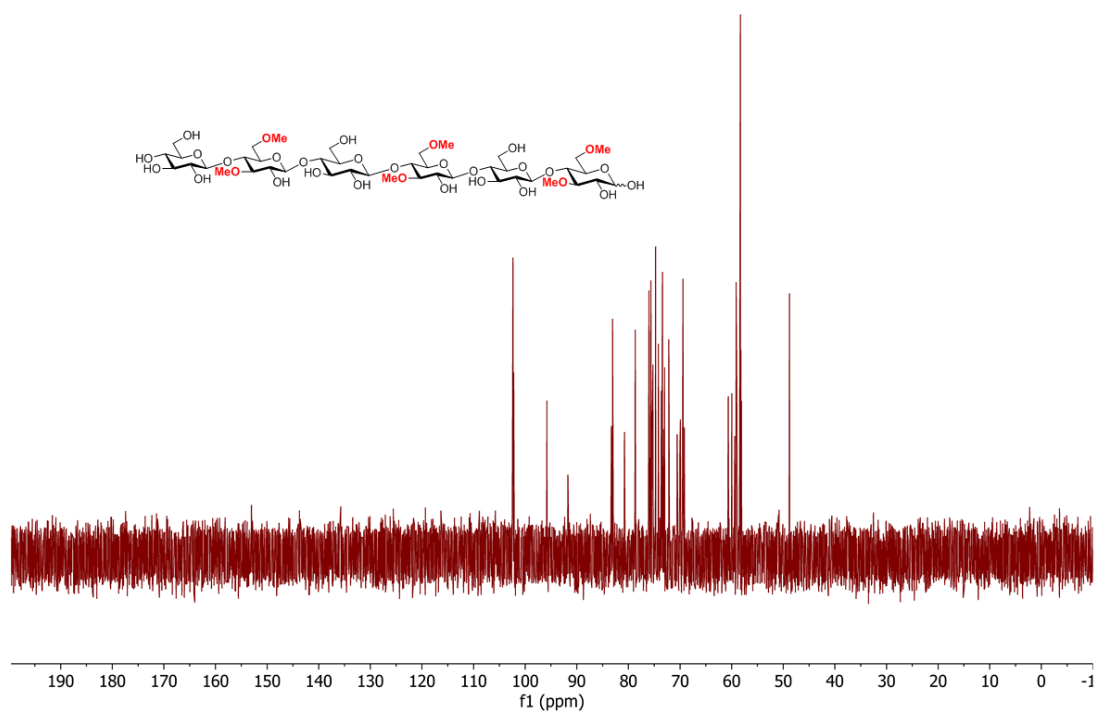
HSQC NMR of ACAACA-OH (D₂O)



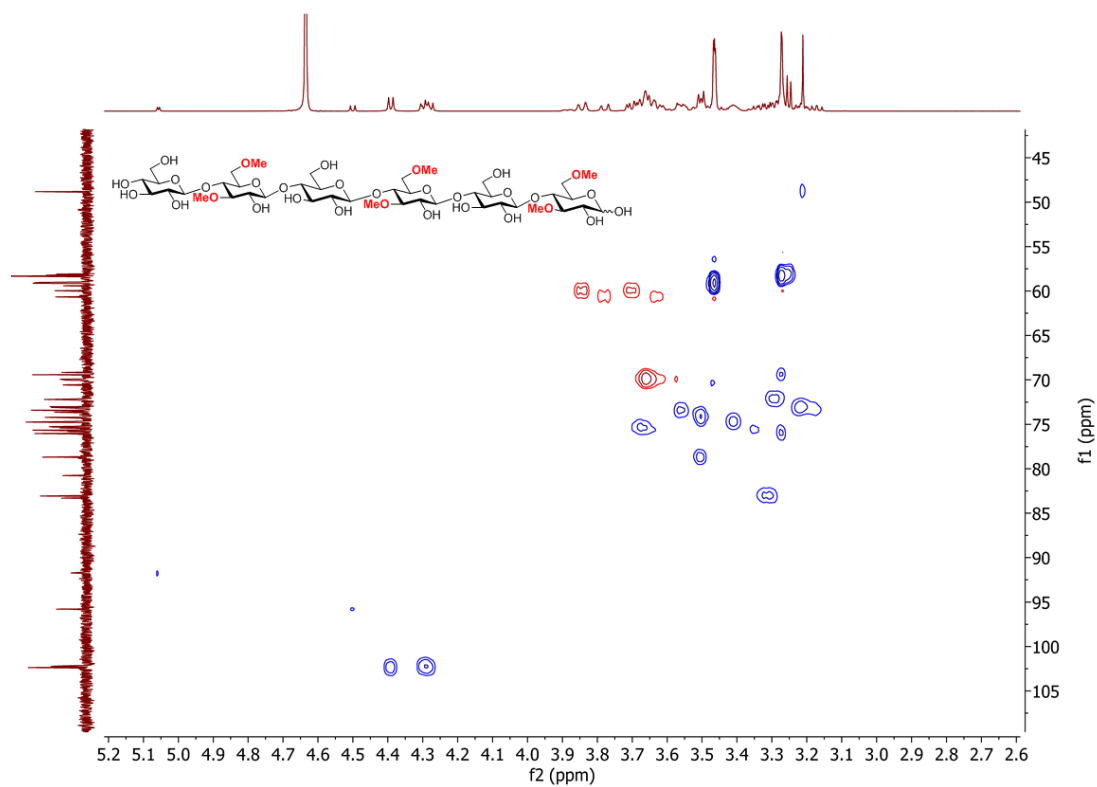
¹H NMR of ACACAC-OH (600 MHz, D₂O)



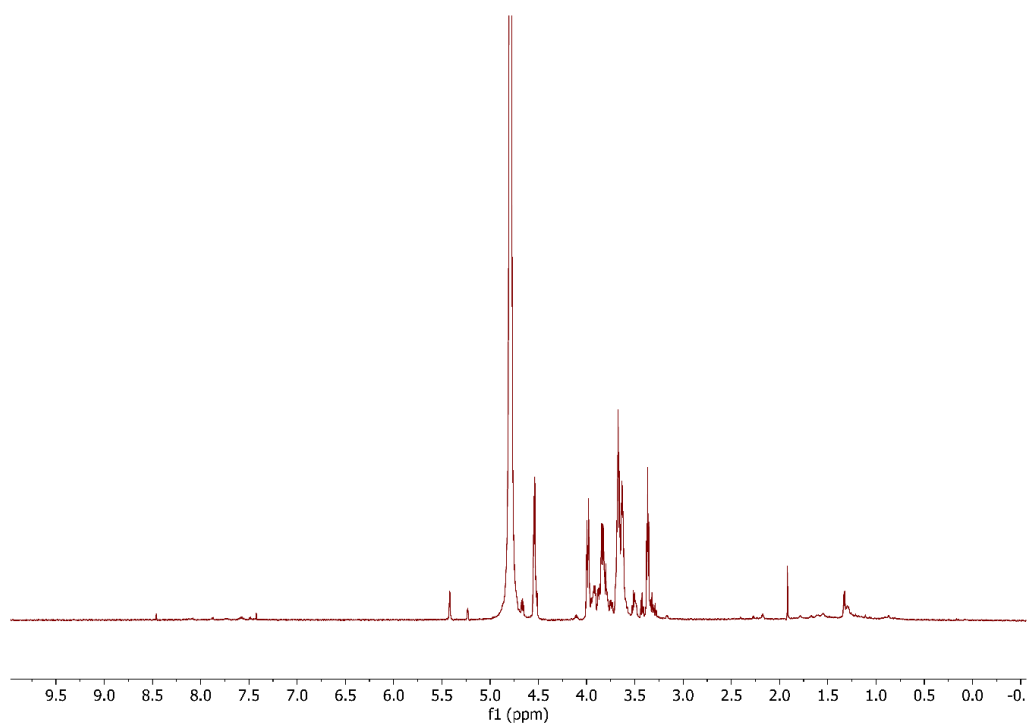
¹³C NMR of ACACAC-OH (151 MHz, D₂O)



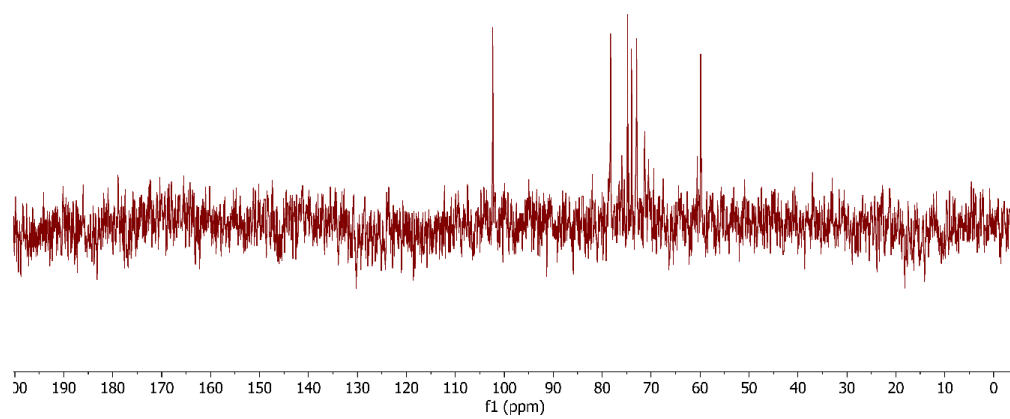
HSQC NMR of ACACAC-OH (D₂O)



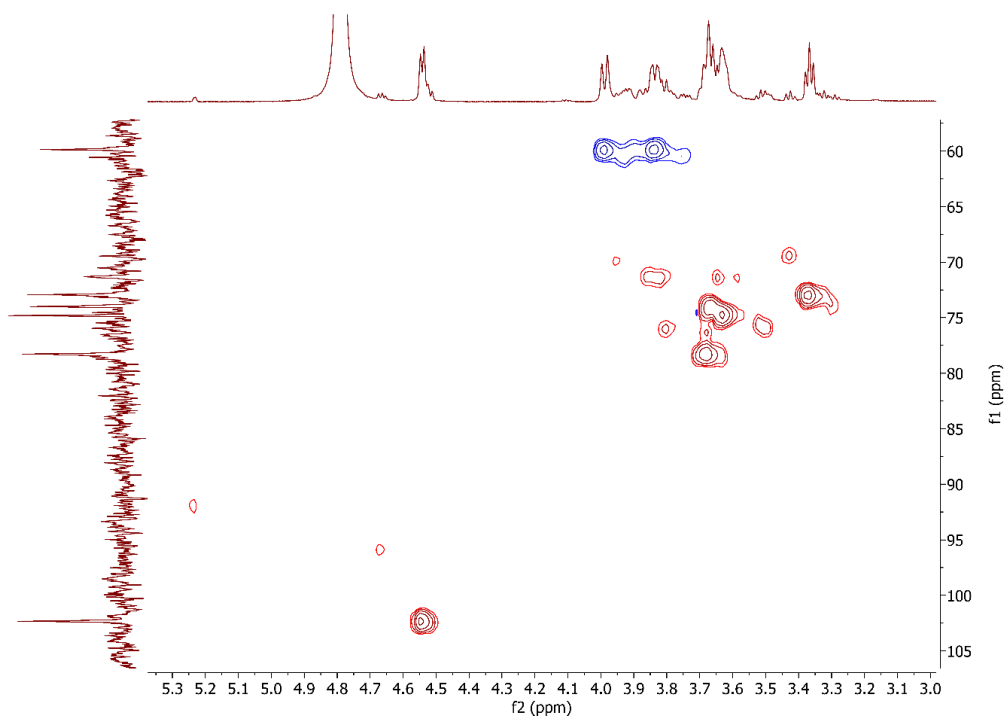
^1H NMR of AAAAAAAAAA-OH (700 MHz, D₂O)



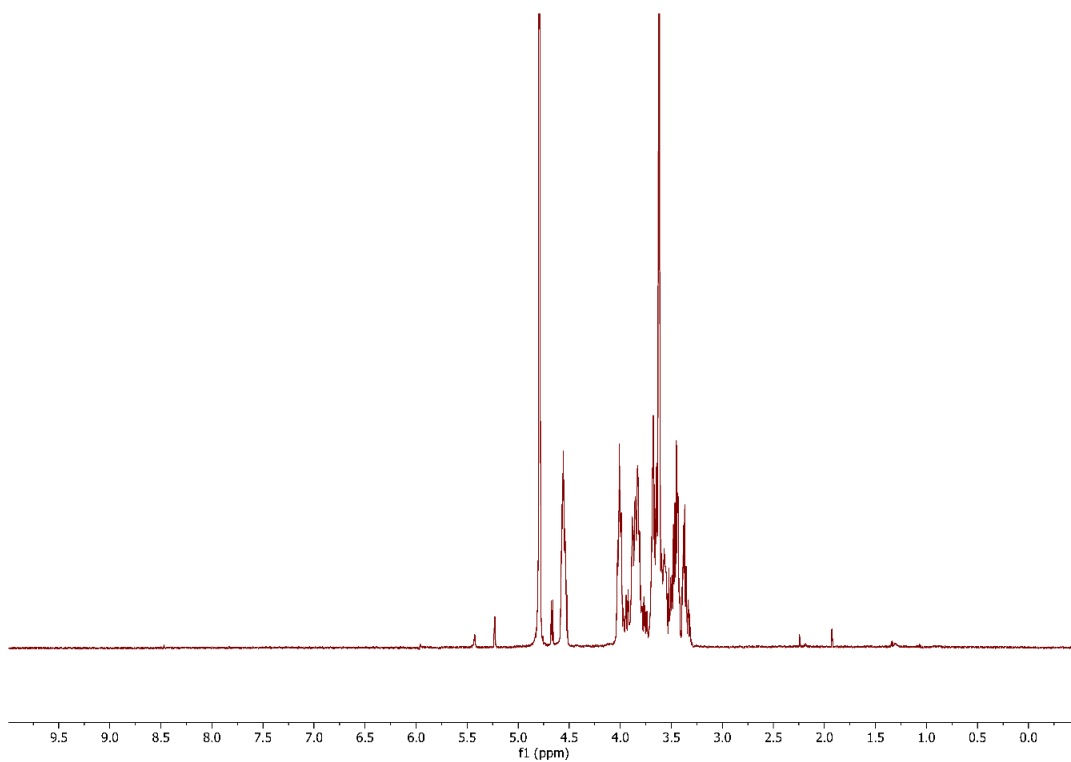
^{13}C NMR of AAAAAAAAAA-OH (176 MHz, D_2O)



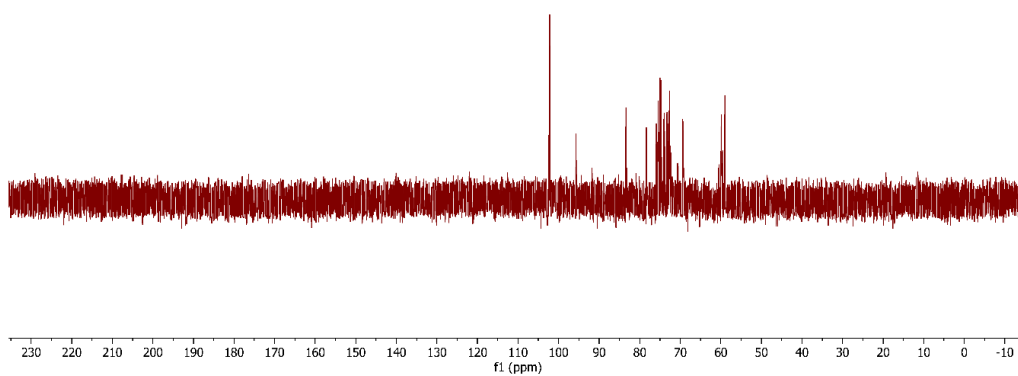
HSQC NMR of AAAAAAAAAA-OH (D_2O)



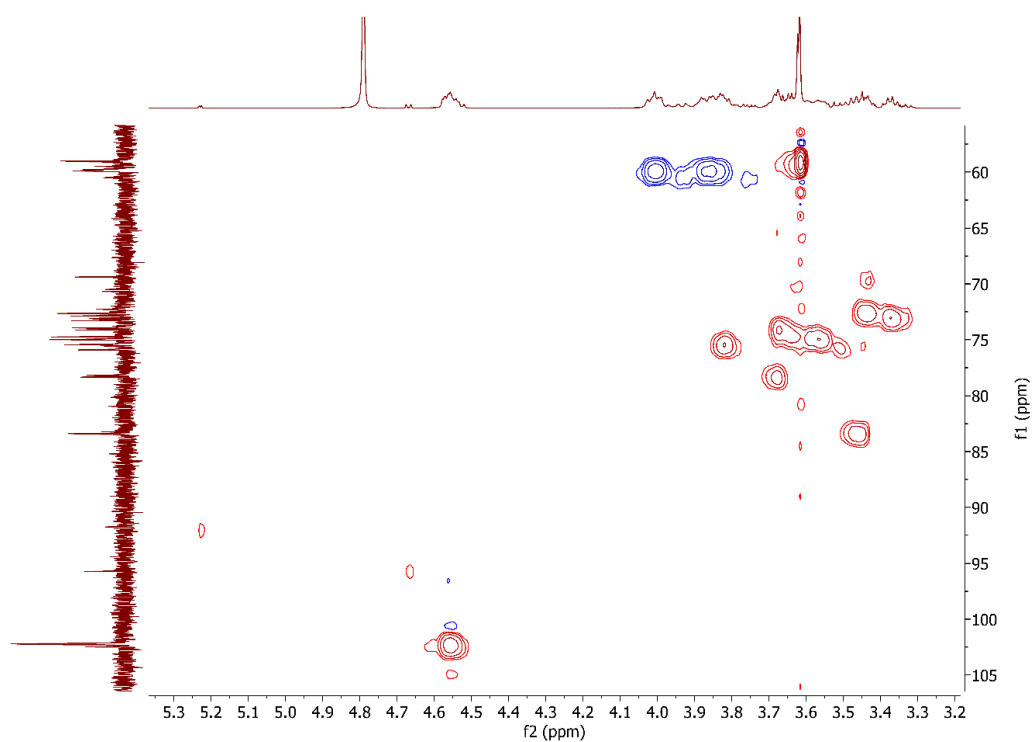
¹H NMR of AAABBBAAABBB-OH (600 MHz, D₂O)



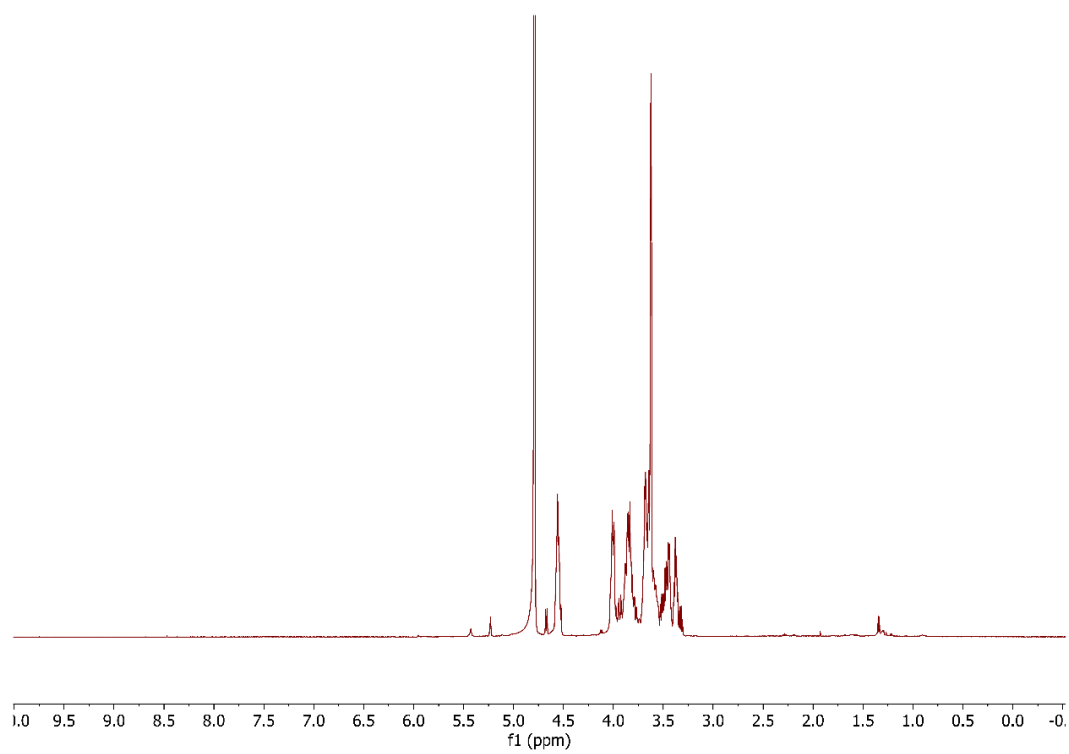
¹³C NMR AAABBBAAABBB-OH (151 MHz, D₂O)



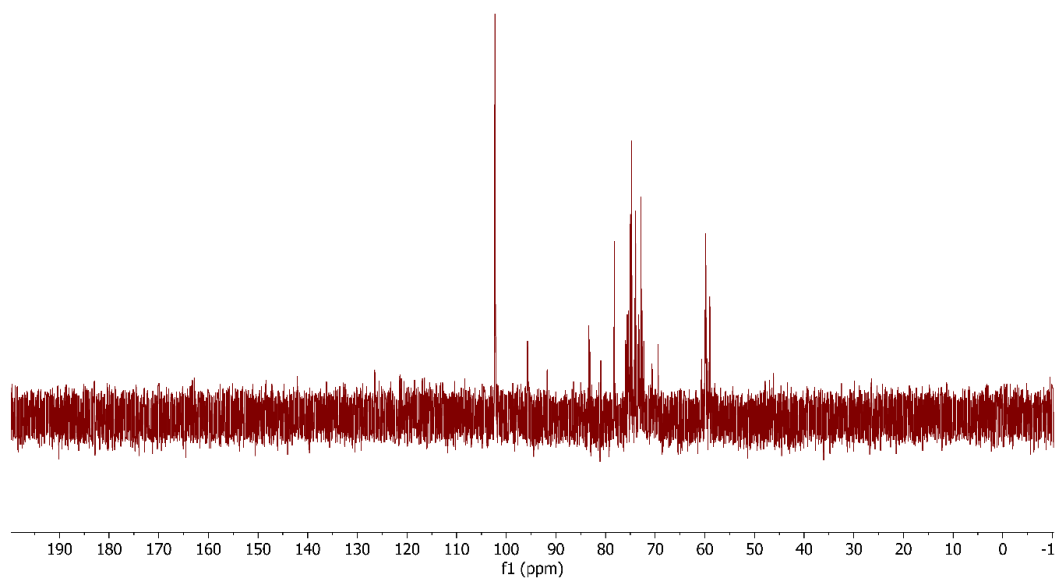
HSQC NMR of AAABBBAAABBB-OH (D₂O)



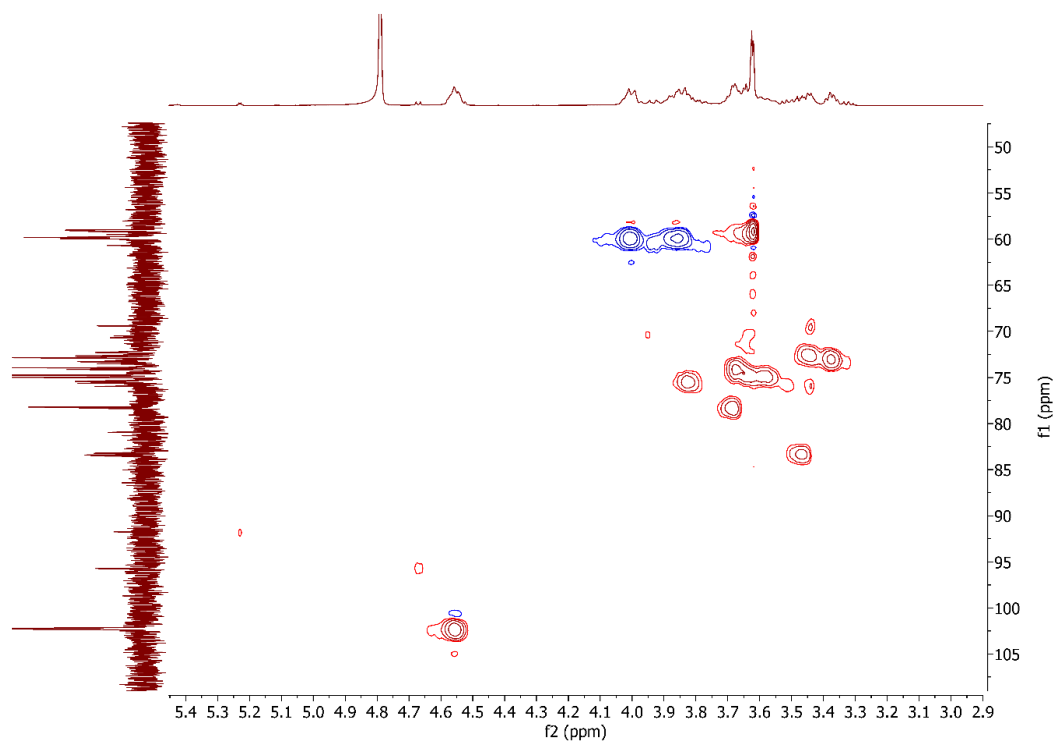
¹H NMR of ABAABAAAABBB-OH (600 MHz, D₂O)



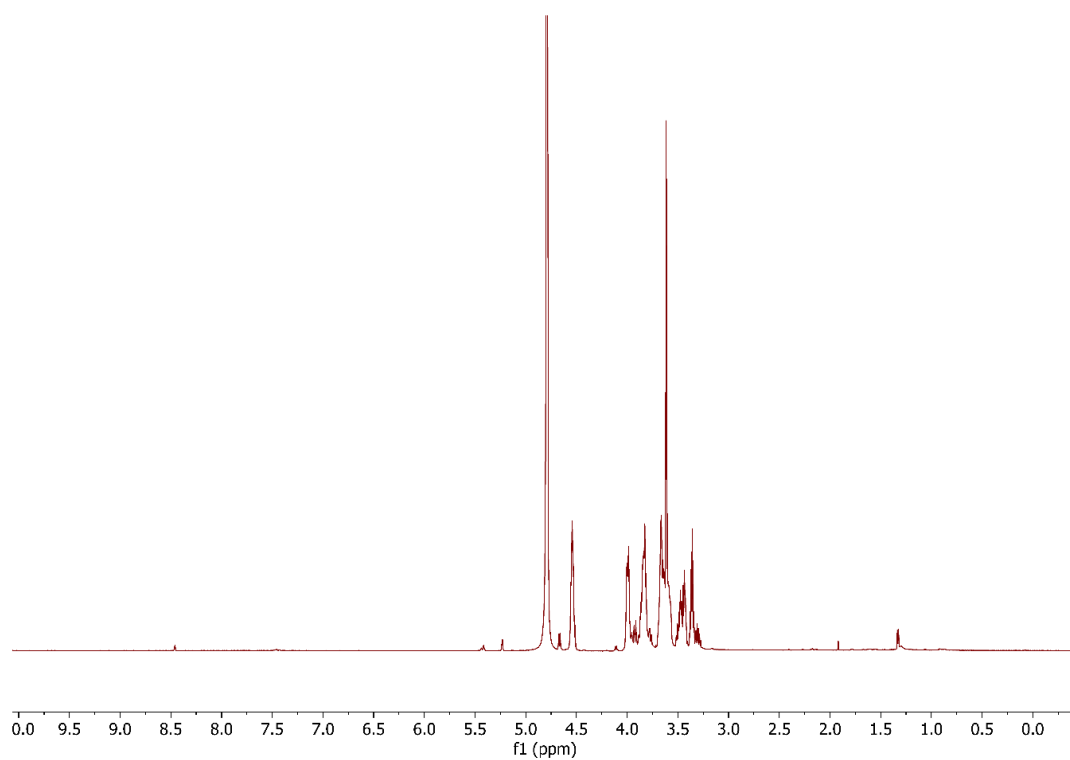
^{13}C NMR of ABAABAAAABBB-OH (151 MHz, D_2O)



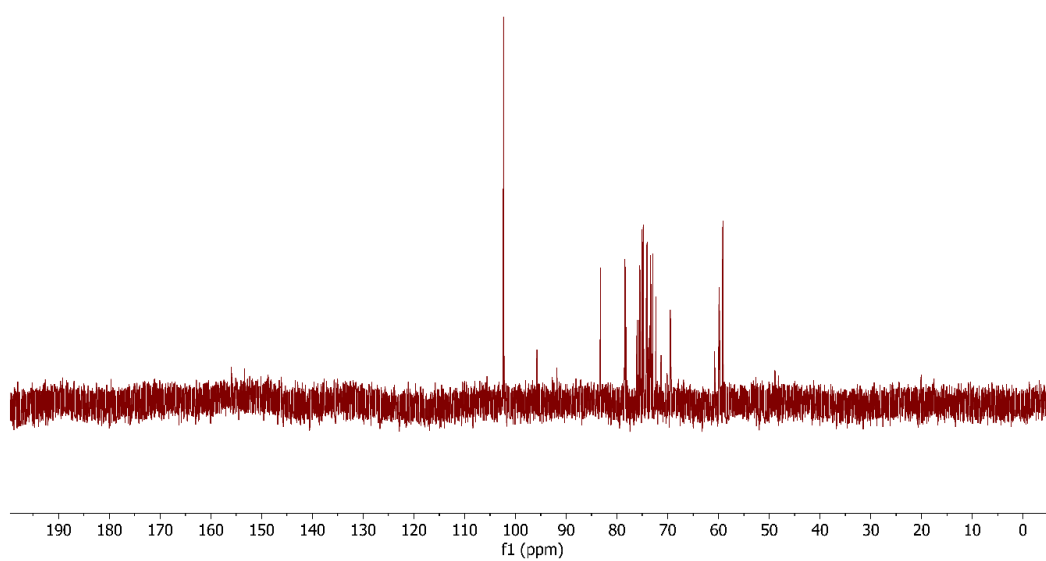
HSQC NMR of ABAABAAAABBB-OH (D_2O)



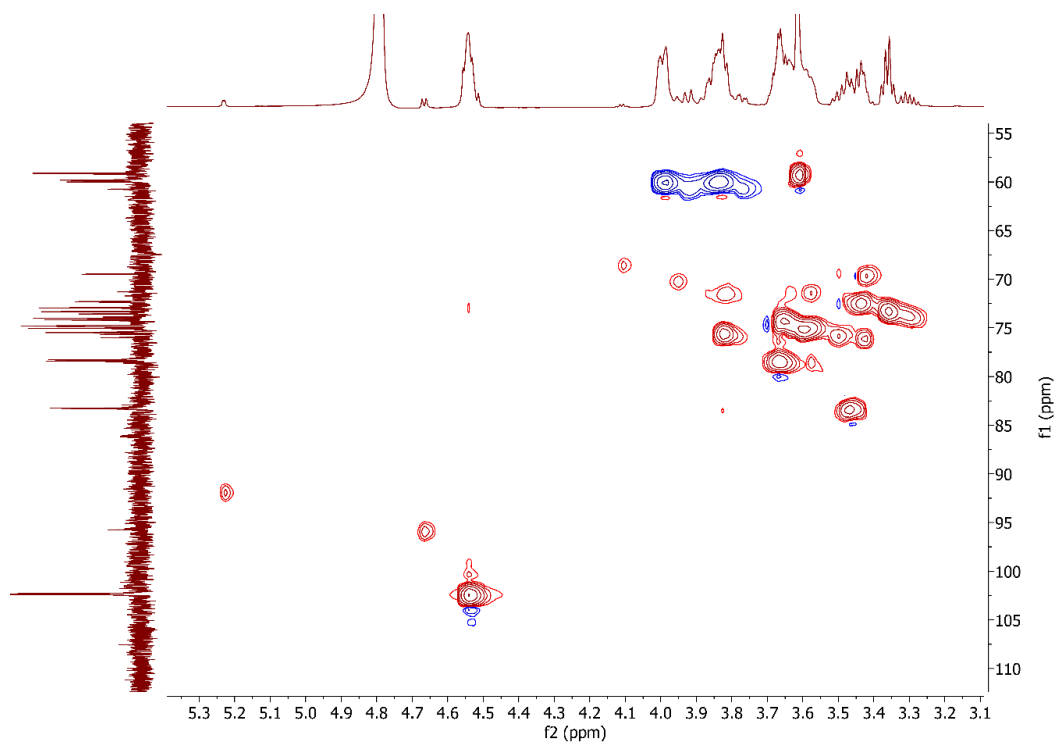
¹H NMR of ABAABAABAABA-OH (700 MHz, D₂O)



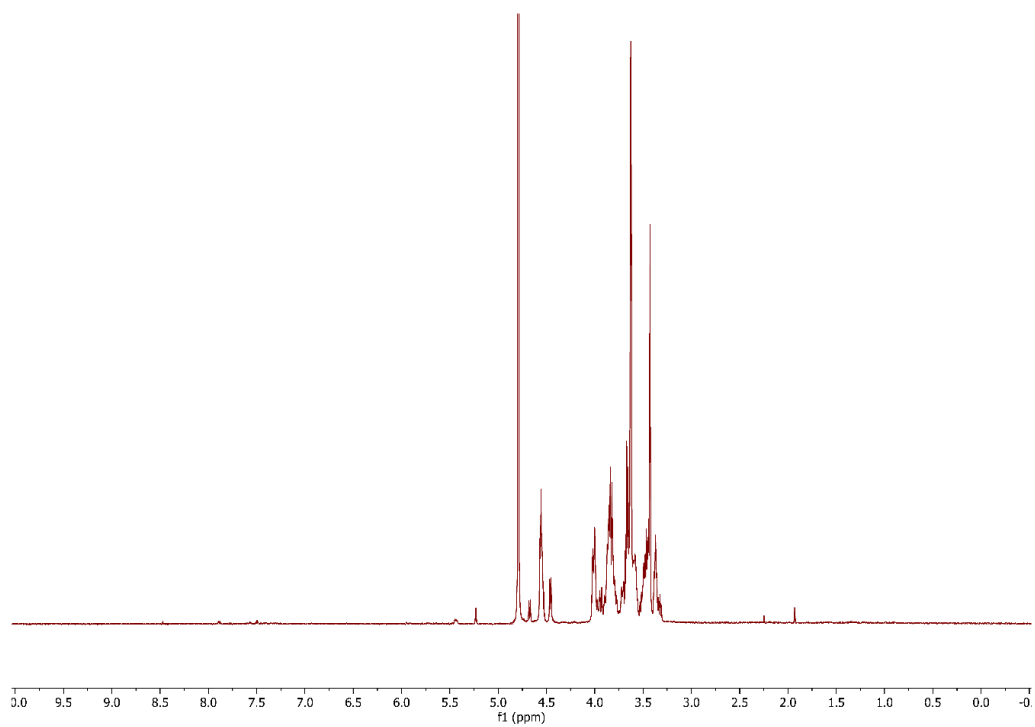
¹³C NMR of ABAABAABAABA-OH (176 MHz, D₂O)



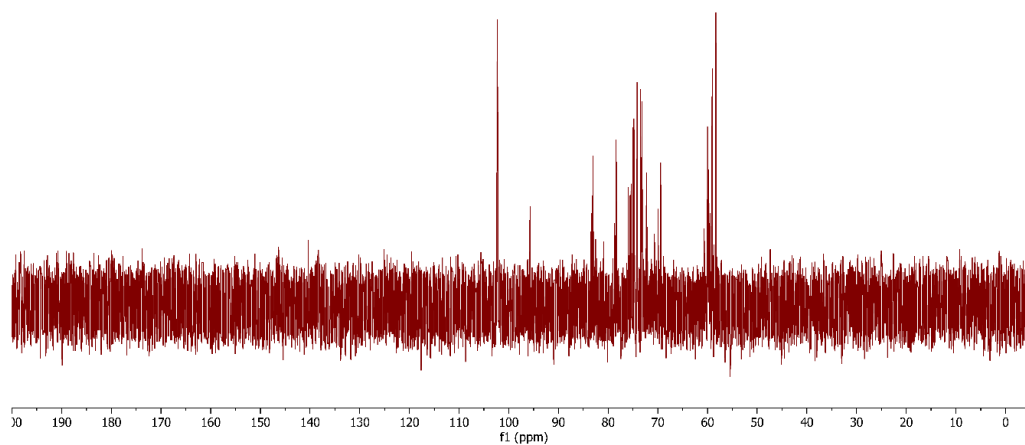
HSQC NMR of ABAABAABAABA-OH (D₂O)



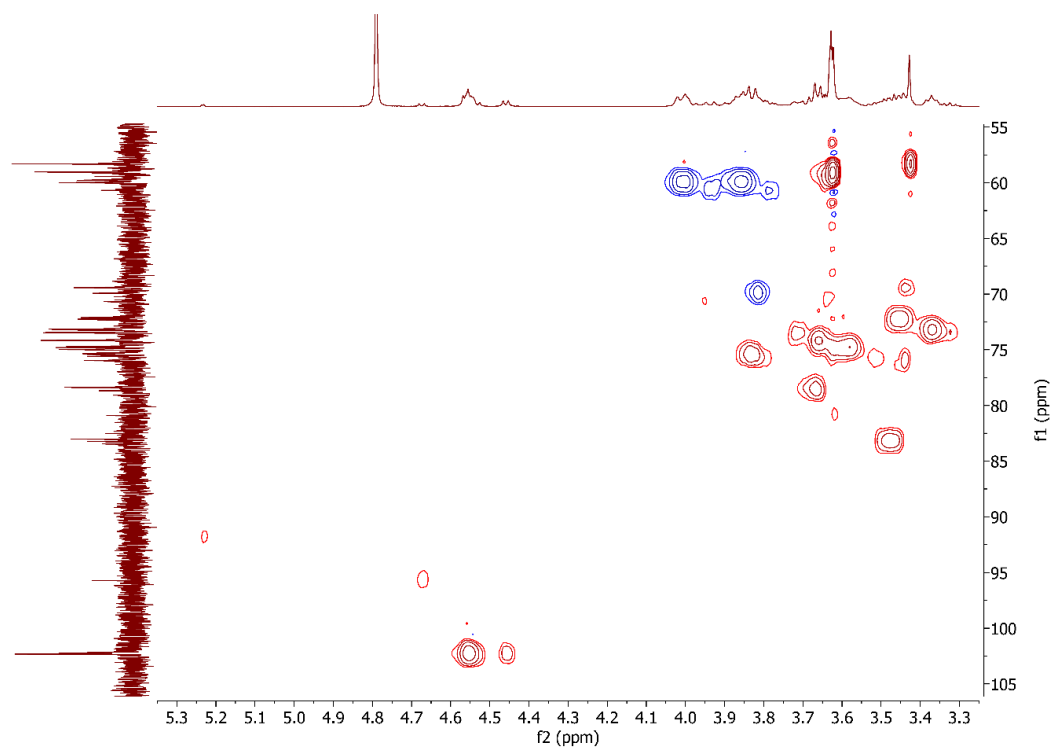
¹H NMR of ABACABABACAB-OH (600 MHz, D₂O)



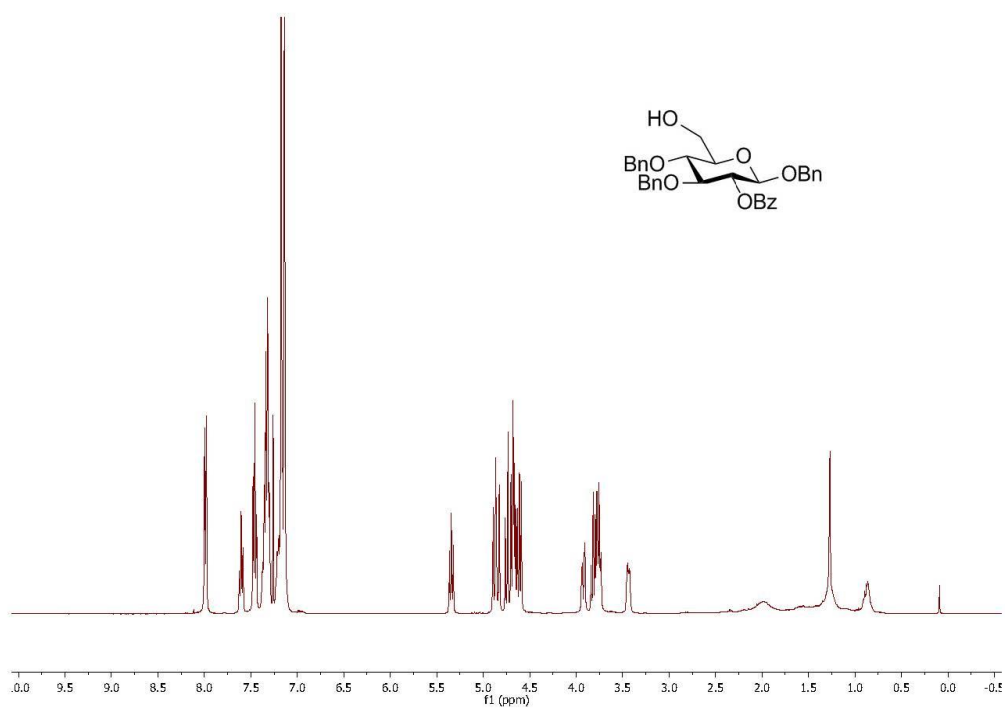
¹³C NMR of ABACABABACAB-OH (151 MHz, D₂O)



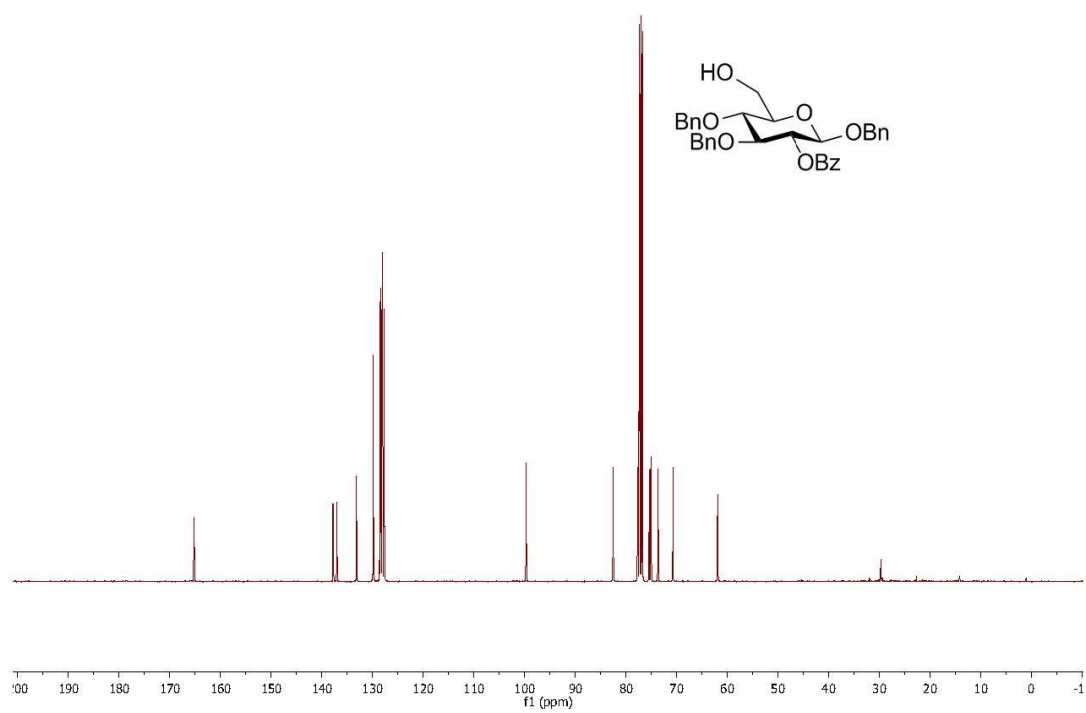
HSQC NMR of ABACABABACAB-OH (D₂O)



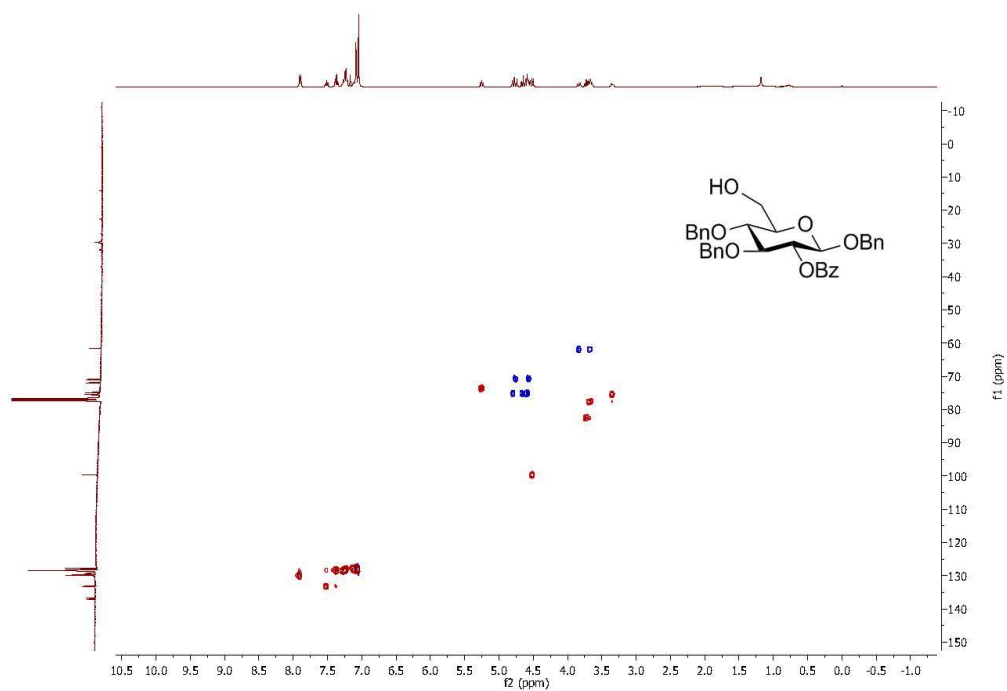
¹H NMR of S16 (400 MHz, CDCl₃)



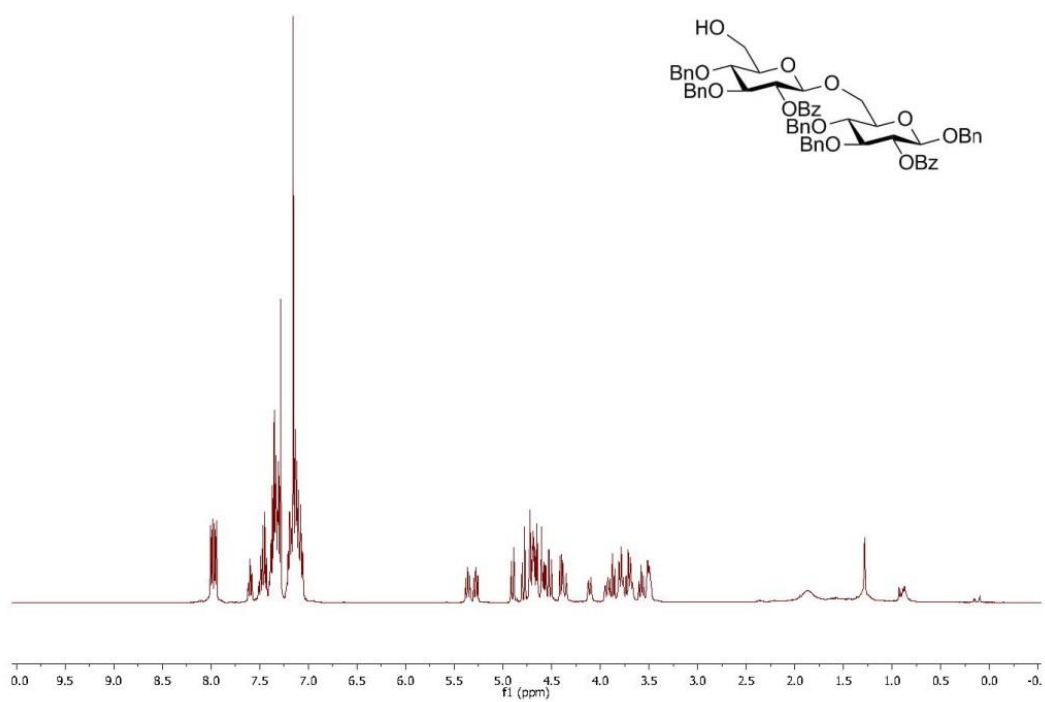
¹³C NMR of S16 (101 MHz, CDCl₃)



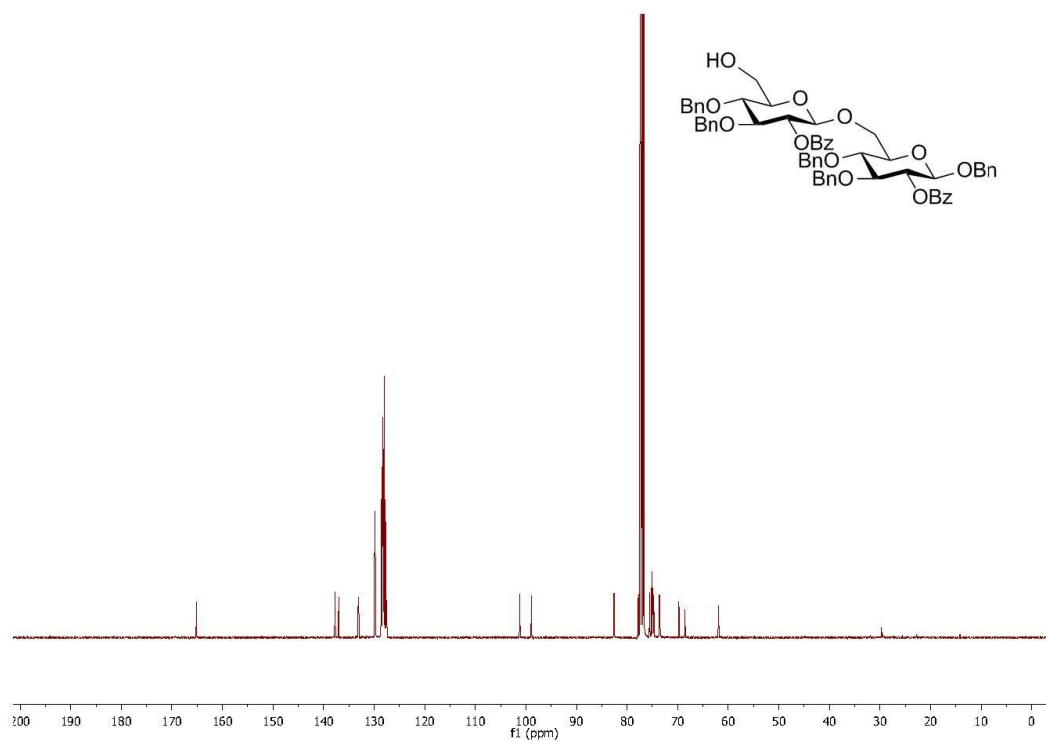
HSQC NMR of S16 (CDCl₃)



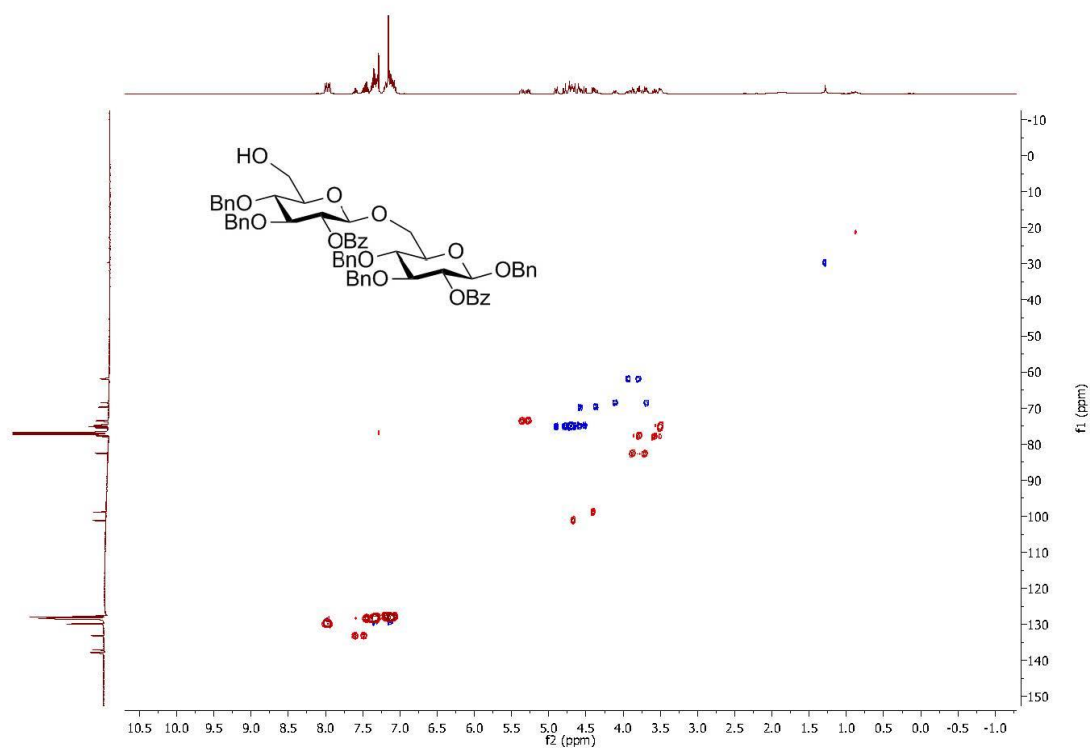
¹H NMR of S17 (400 MHz, CDCl₃)



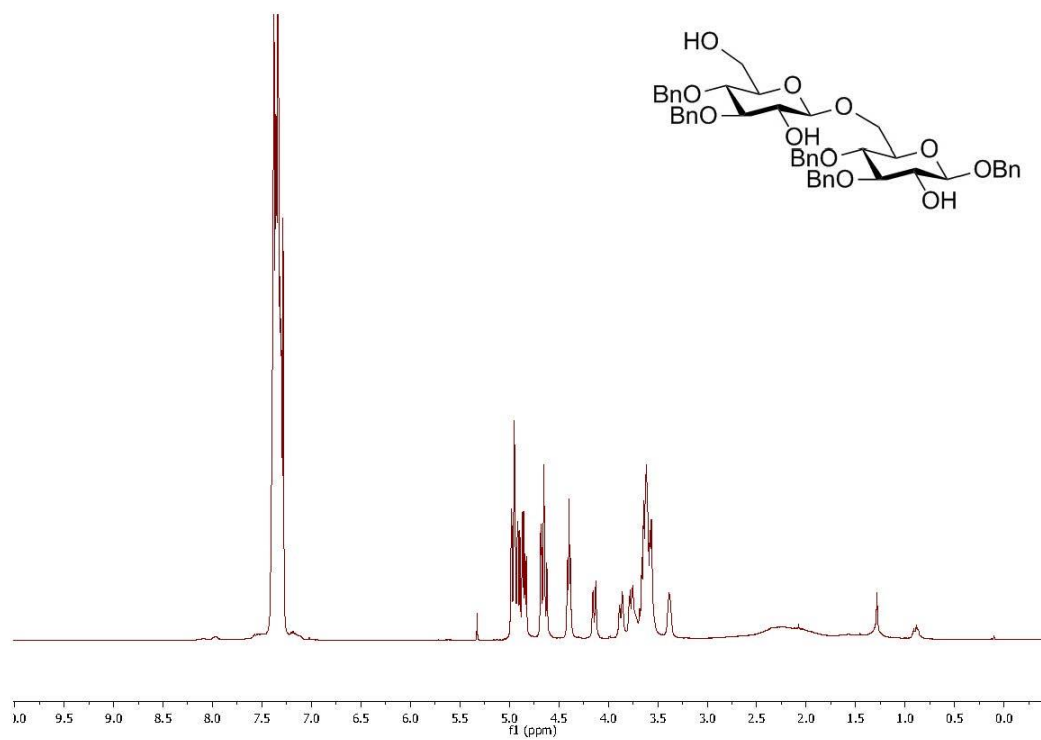
^{13}C NMR of S17 (101 MHz, CDCl_3)



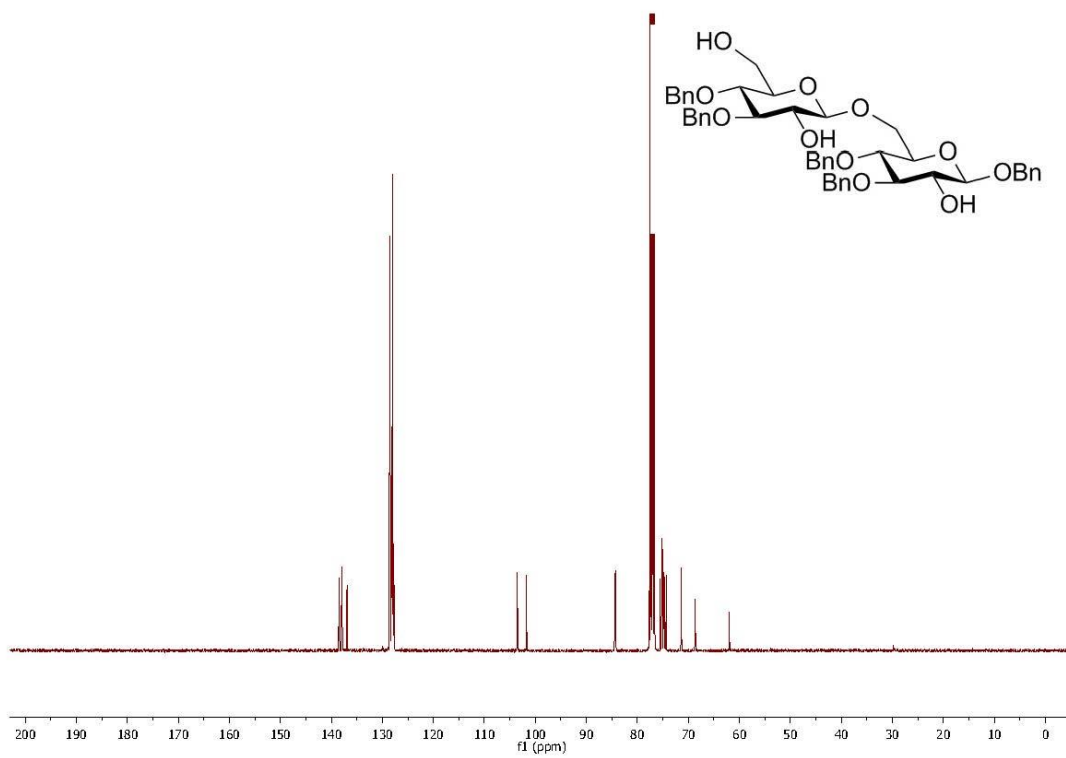
HSQC NMR of S17 (CDCl_3)



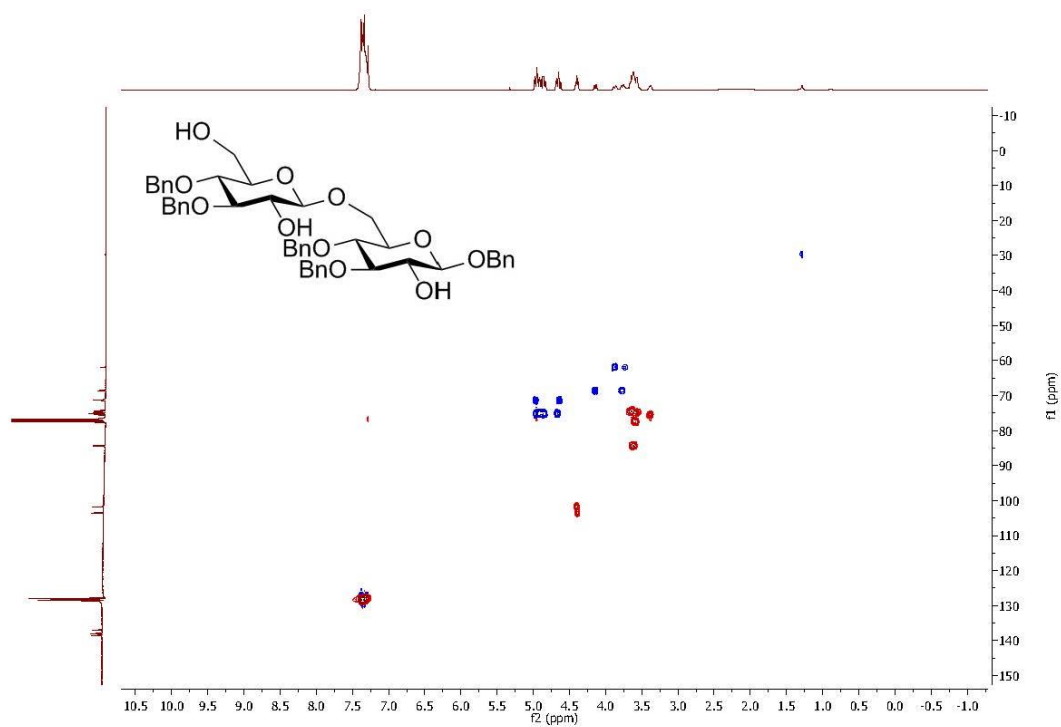
¹H NMR of 25 (400 MHz, CDCl₃)



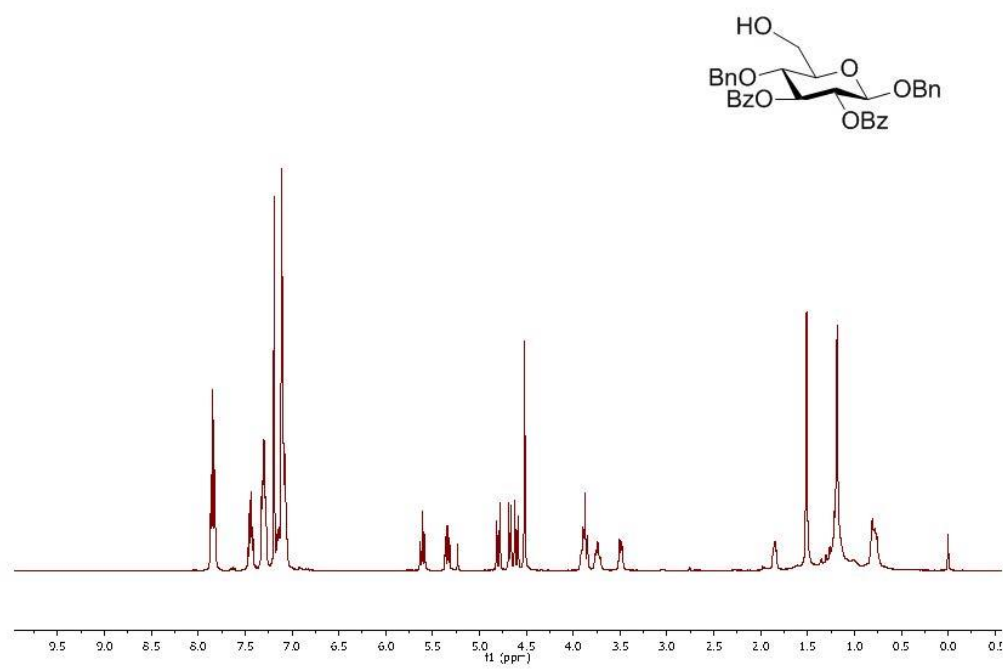
¹³C NMR of 25 (101 MHz, CDCl₃)



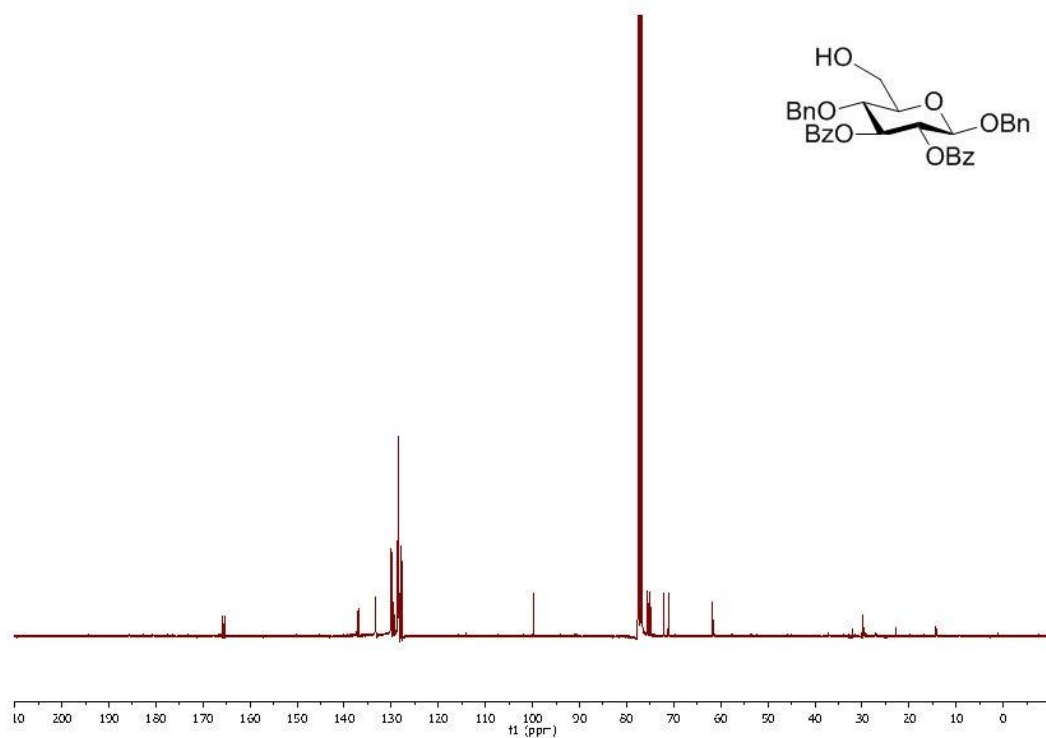
HSQC NMR of 25 (CDCl₃)



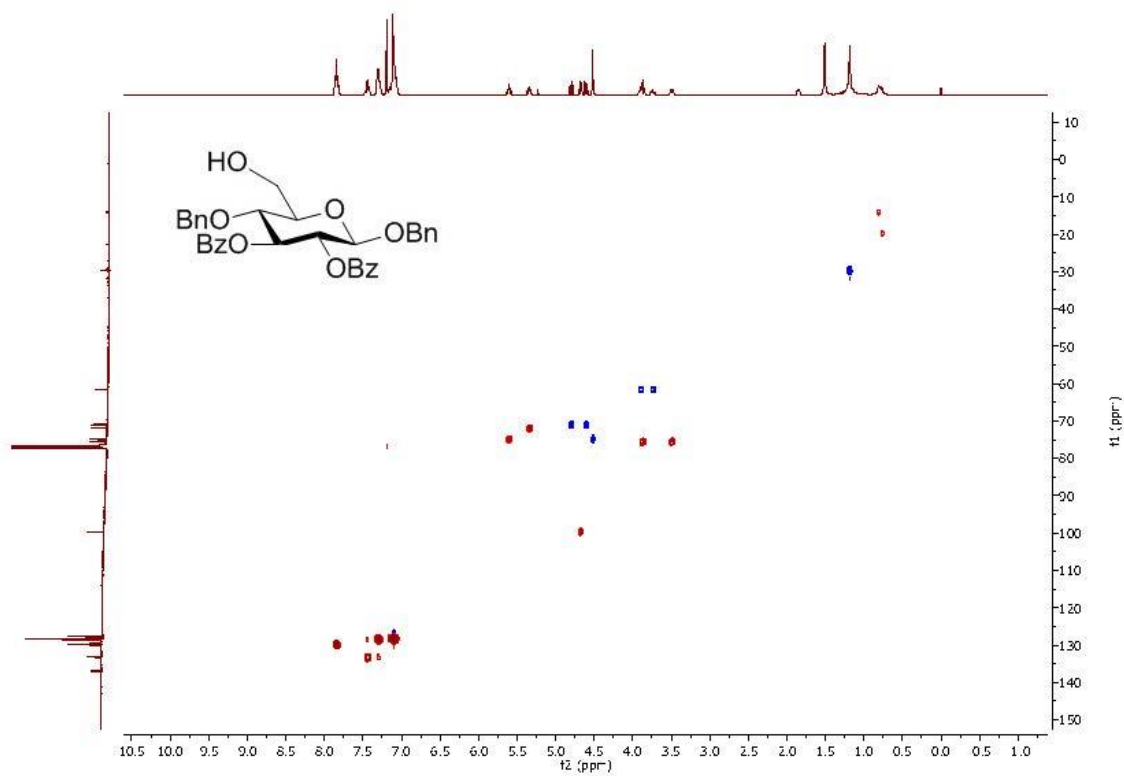
¹H NMR of S19 (400 MHz, CDCl₃)



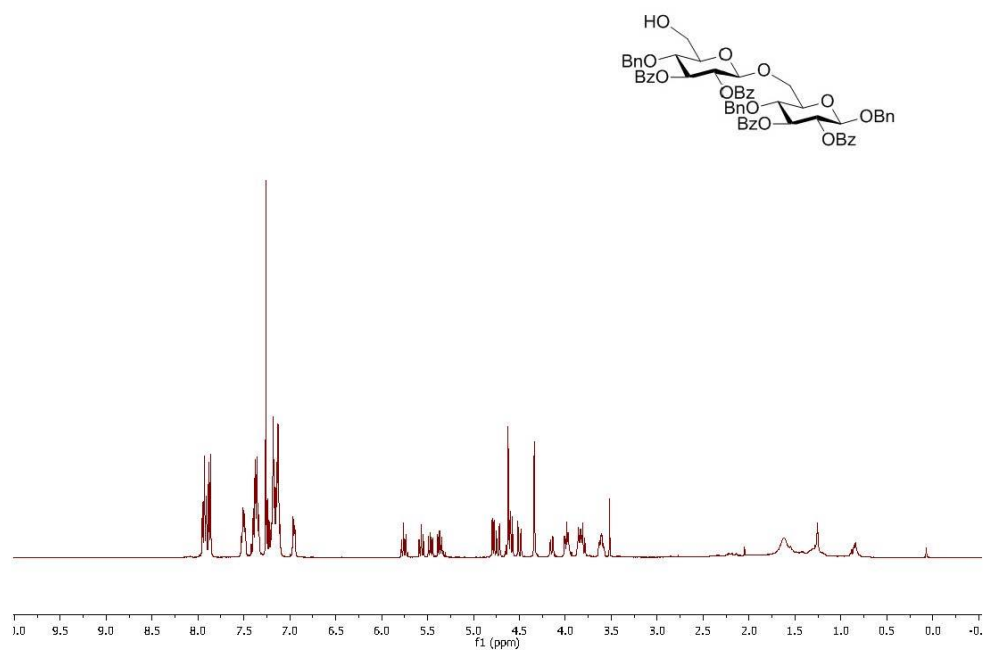
¹³C NMR of S19 (101 MHz, CDCl₃)



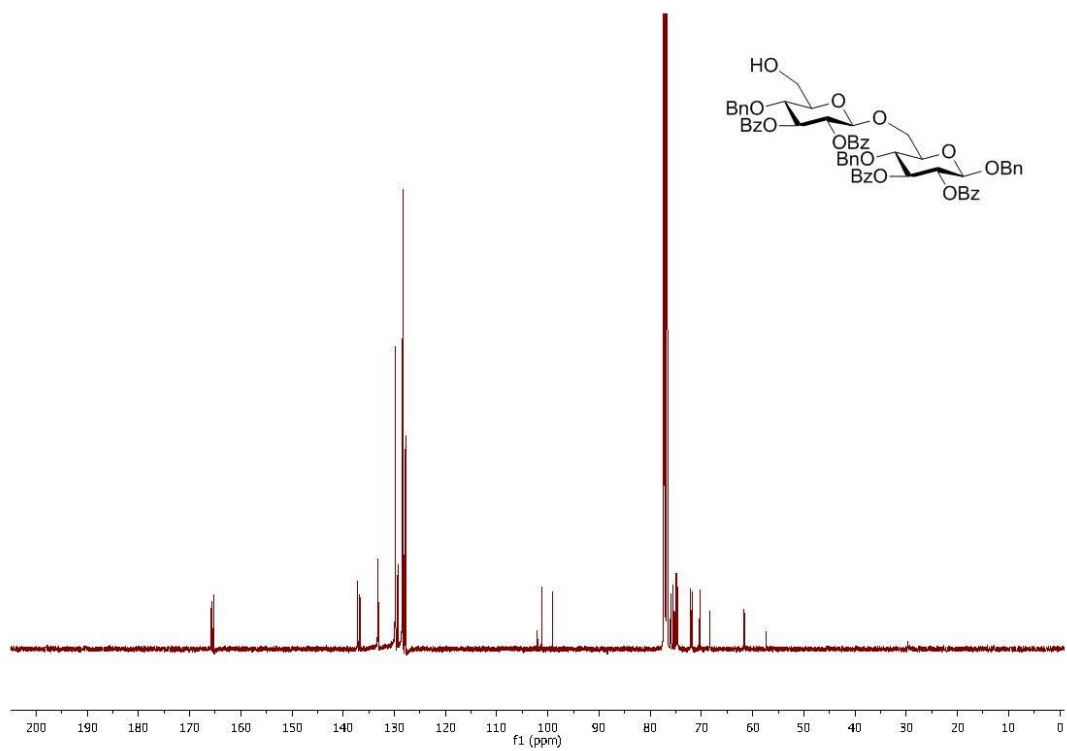
HSQC NMR of S19 (CDCl₃)



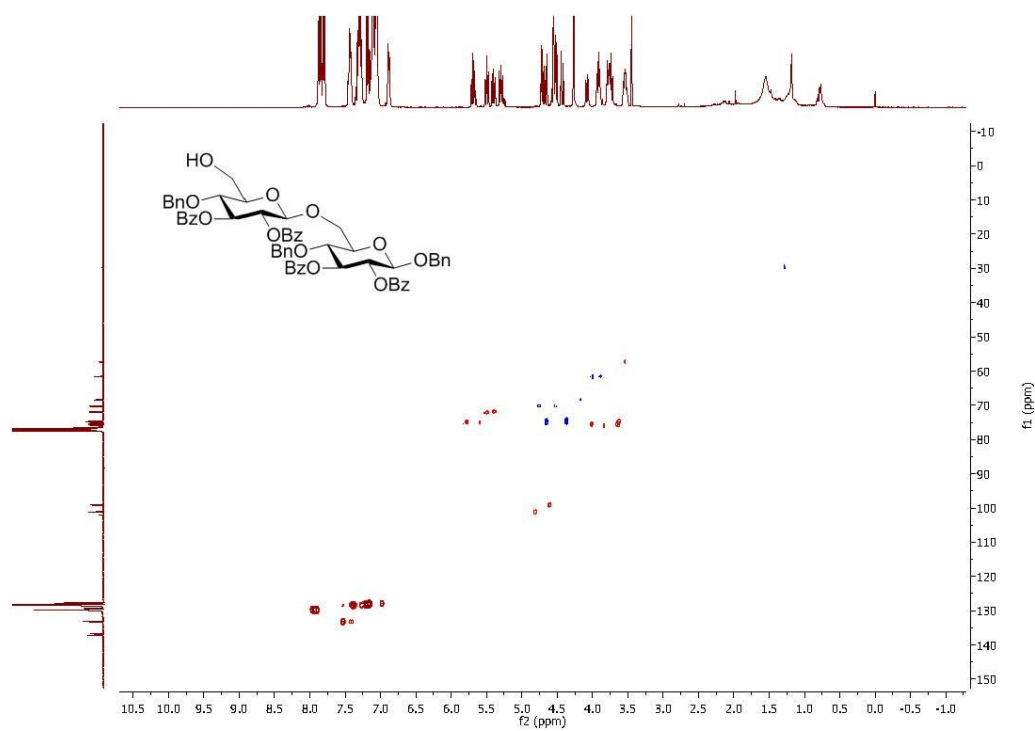
¹H NMR of S20 (400 MHz, CDCl₃)



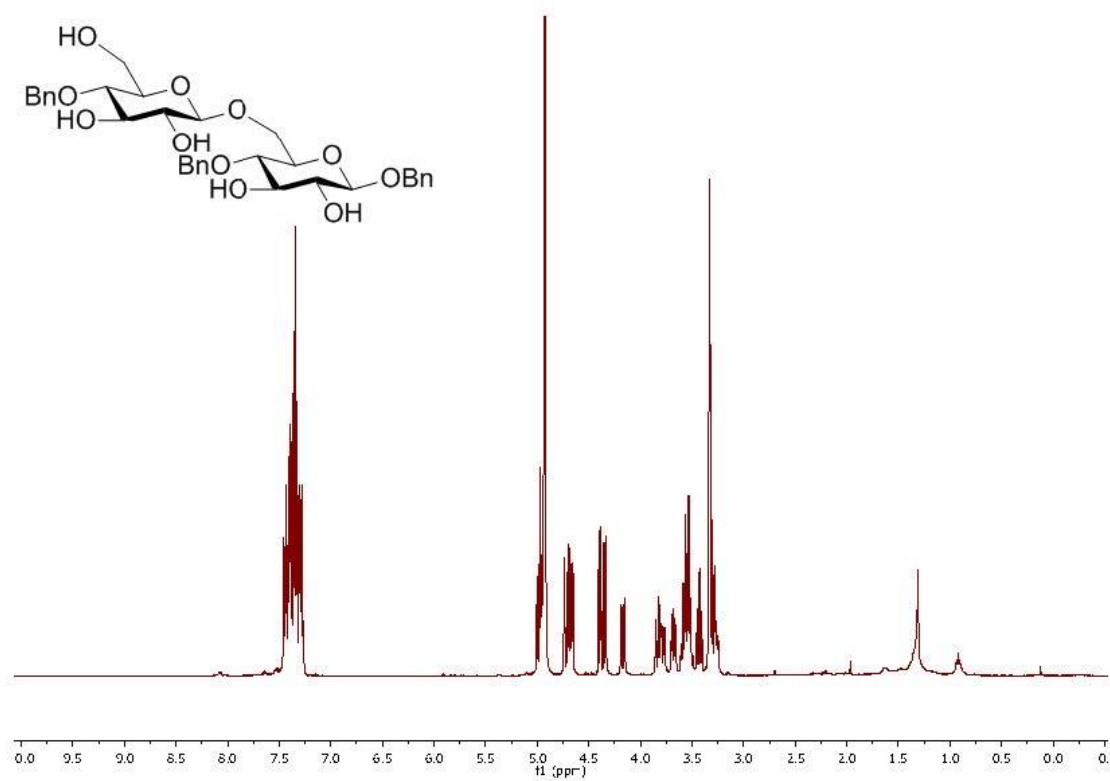
¹³C NMR of S20 (101 MHz, CDCl₃)



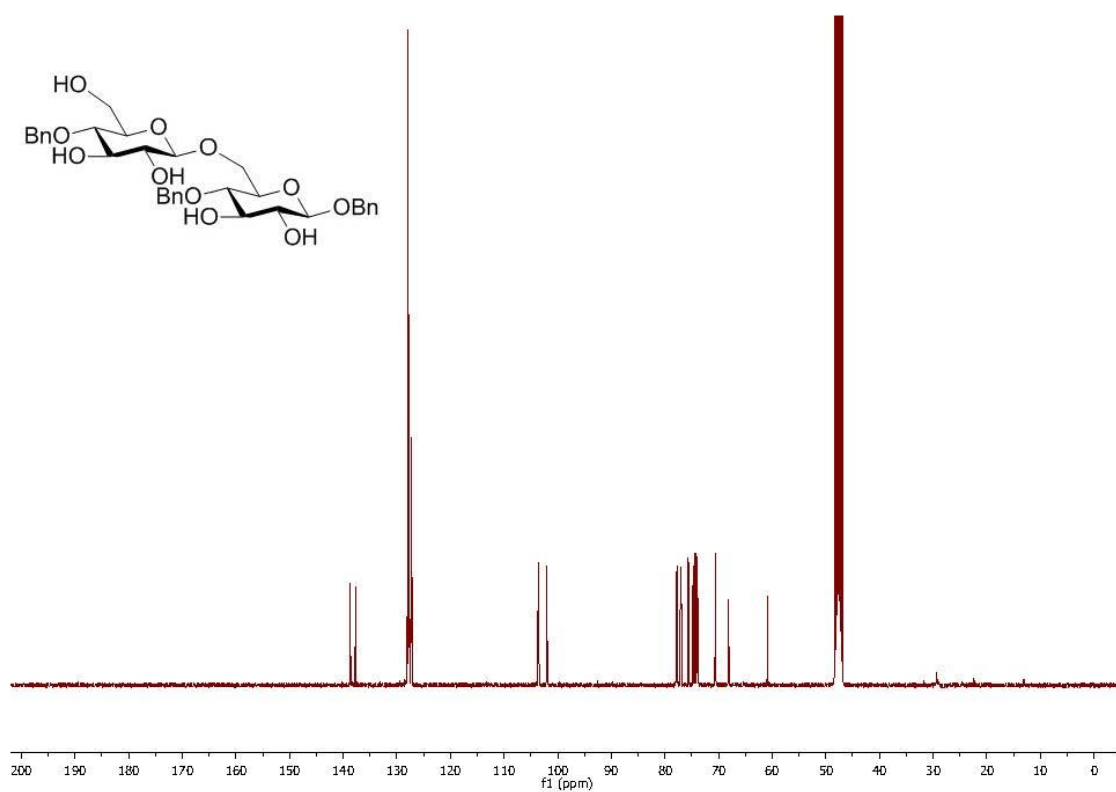
HSQC NMR of S20 (CDCl₃)



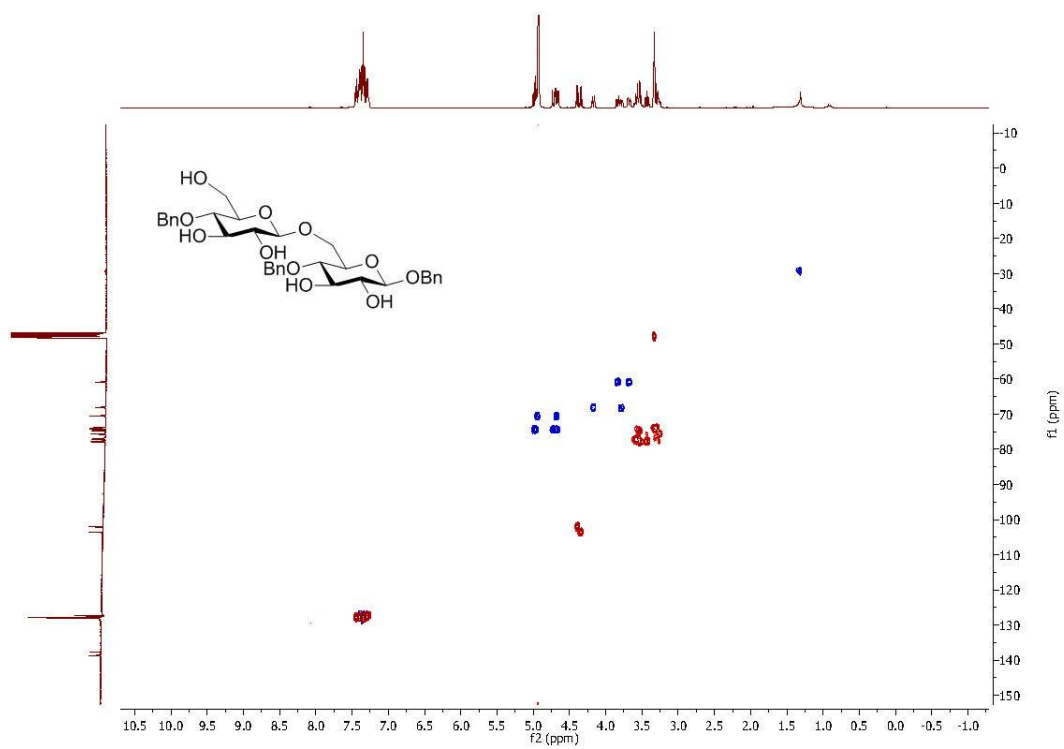
¹H NMR of 26 (400 MHz, Methanol-d₄)



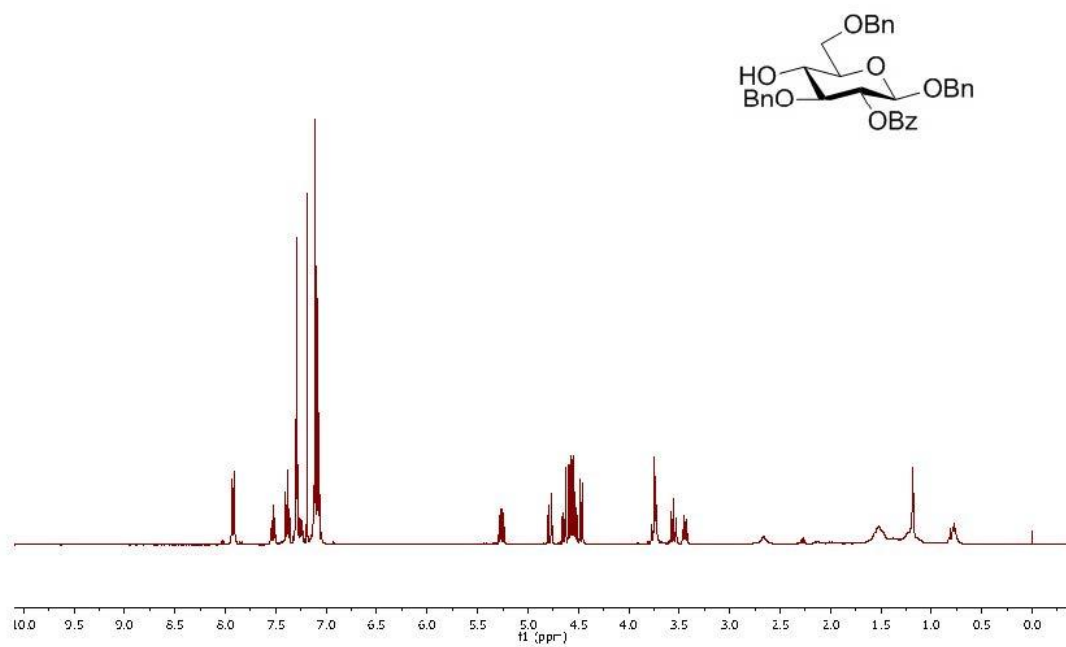
¹³C NMR of 26 (101 MHz, Methanol-d₄)



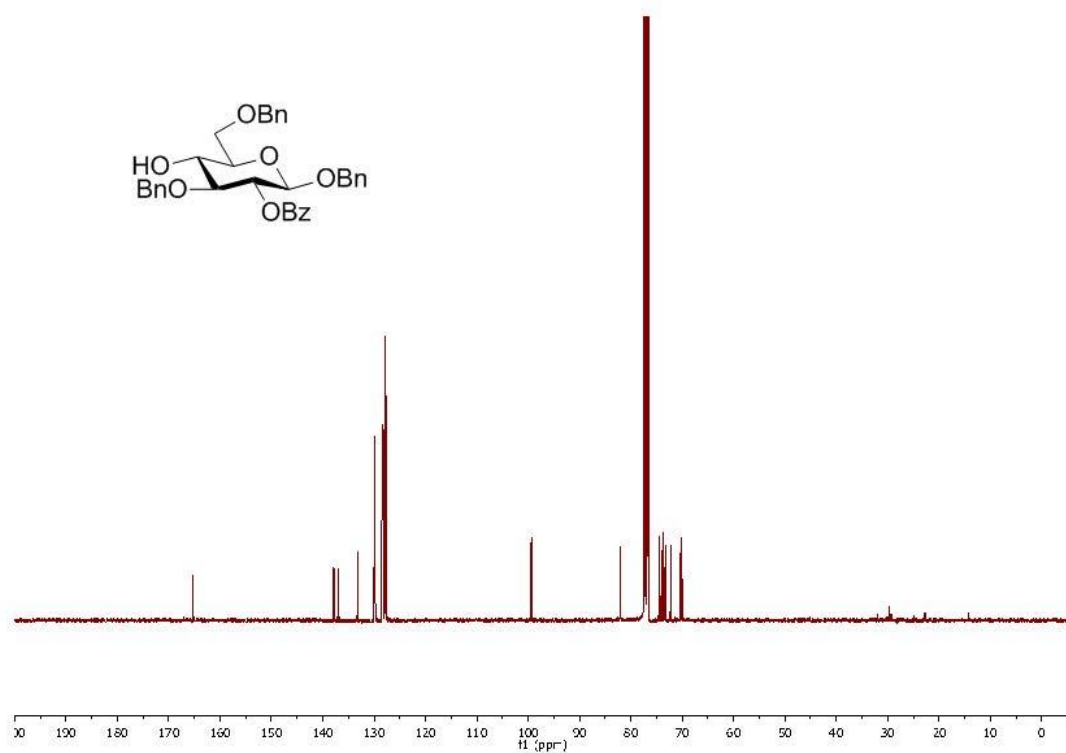
HSQC NMR of 26 (Methanol-d₄)



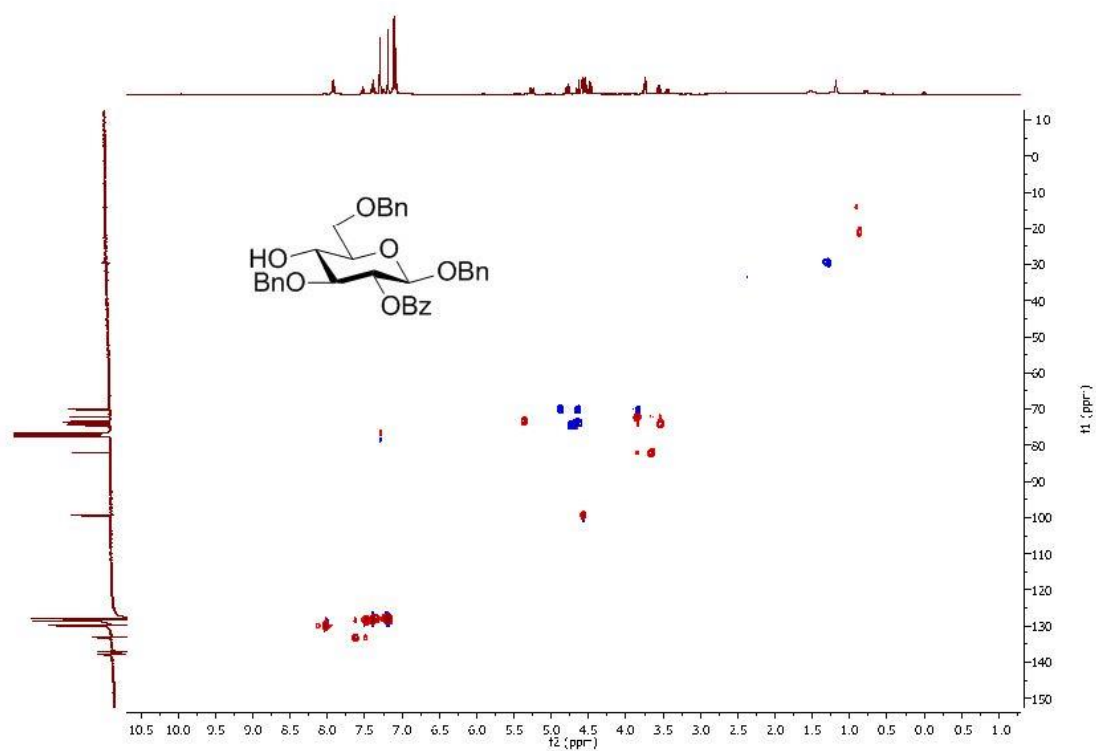
¹H NMR of S22 (400 MHz, CDCl₃)



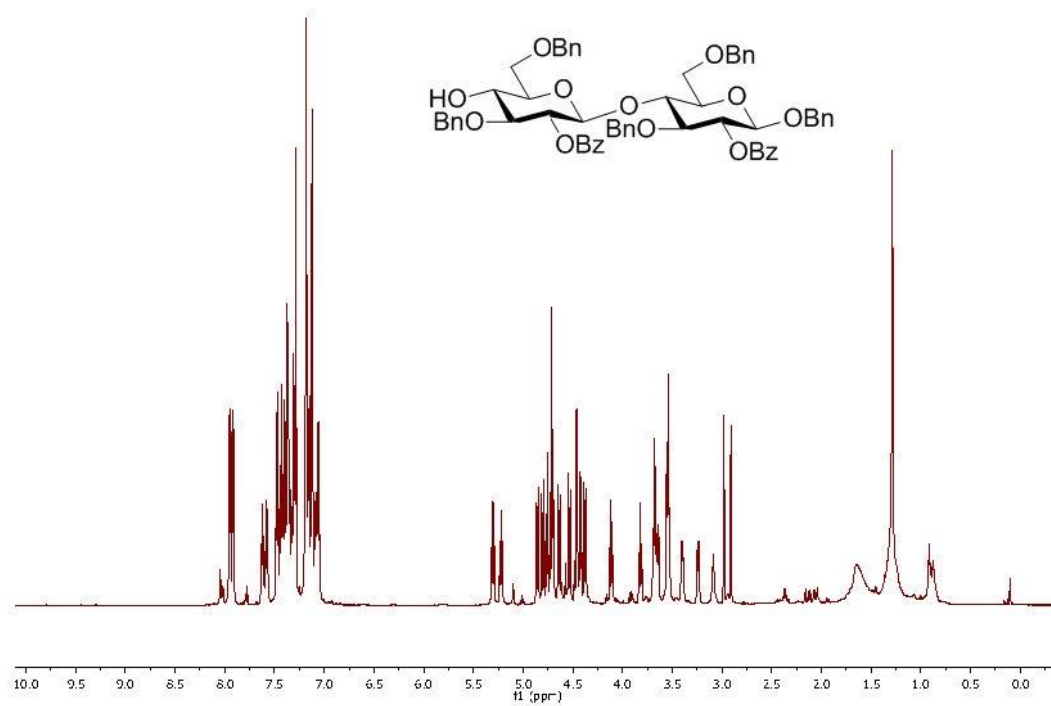
¹³C NMR of S22 (101 MHz, CDCl₃)



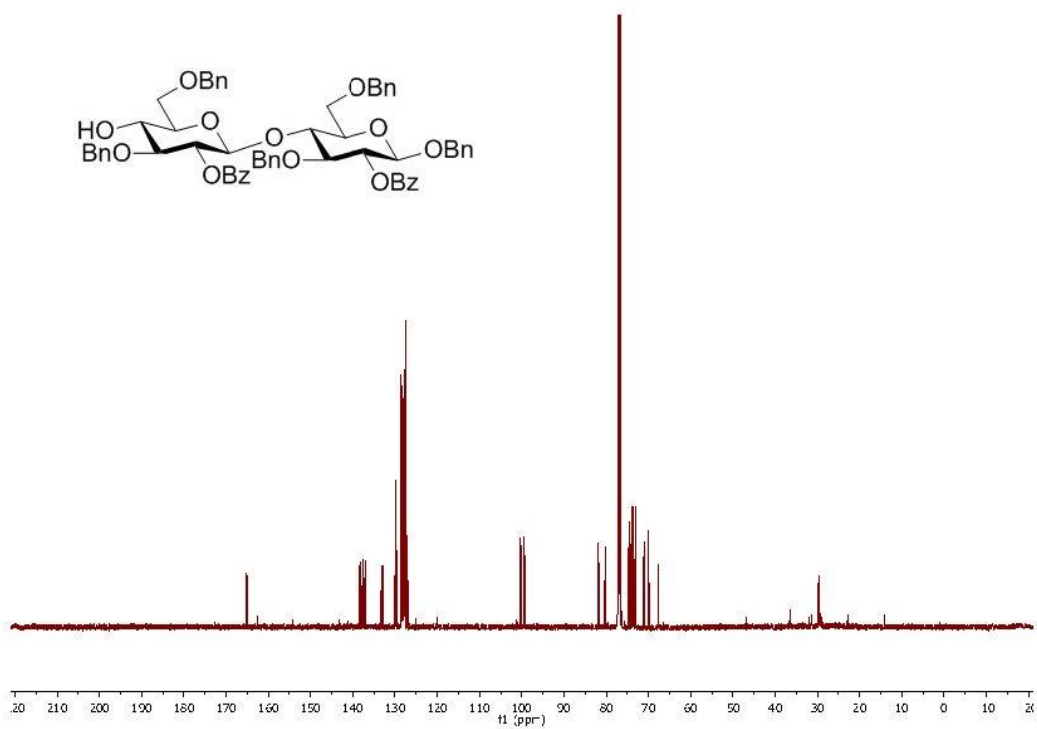
HSQC NMR of S22 (CDCl₃)



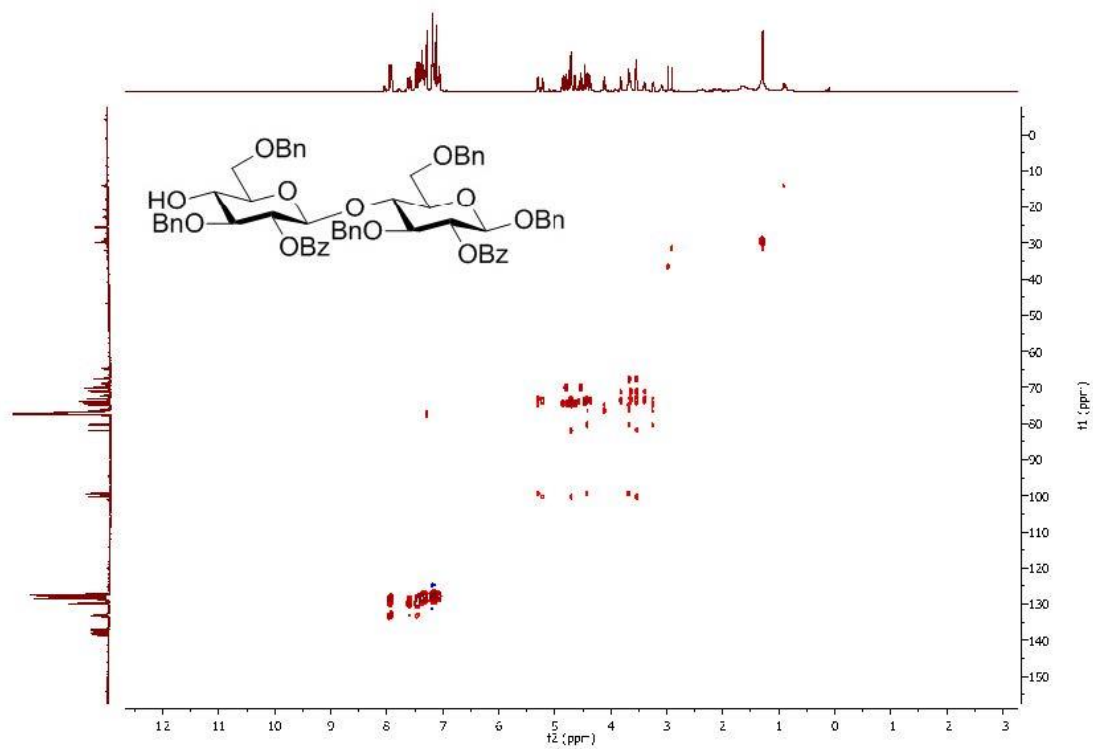
¹H NMR of S23 (400 MHz, CDCl₃)



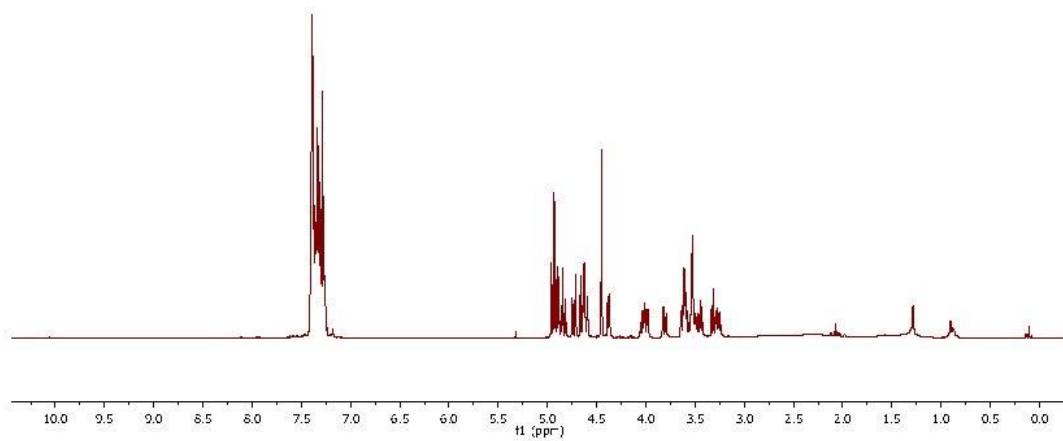
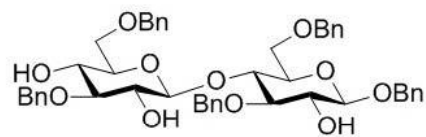
^{13}C NMR of S23 (101 MHz, CDCl_3)



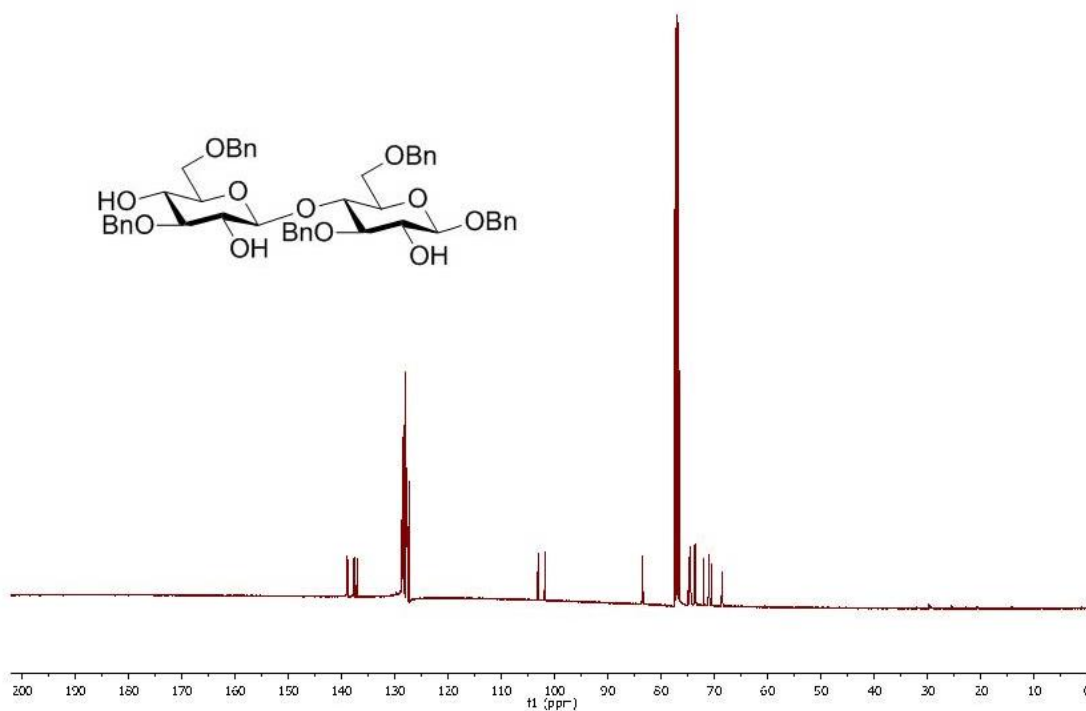
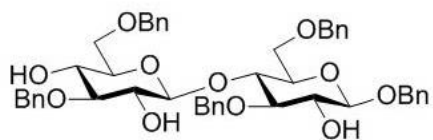
HSQC NMR of S23 (CDCl_3)



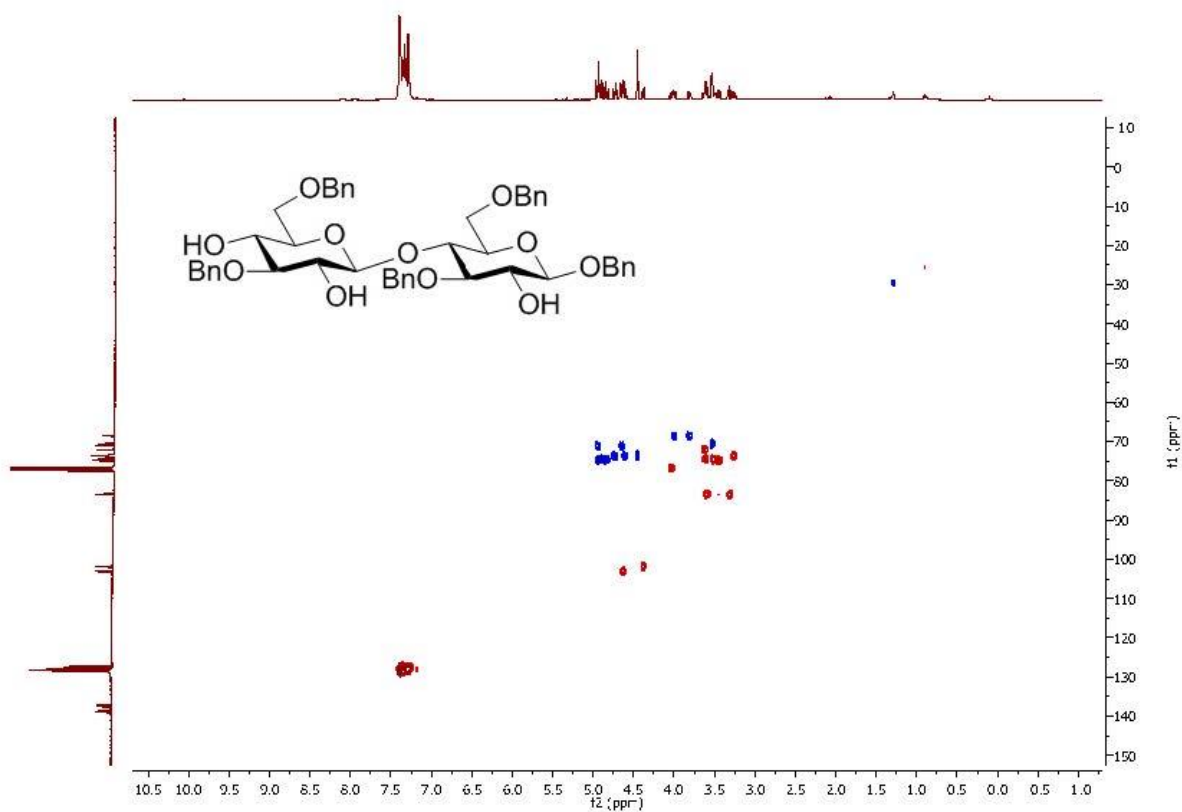
¹H NMR of 27 (400 MHz, CDCl₃)



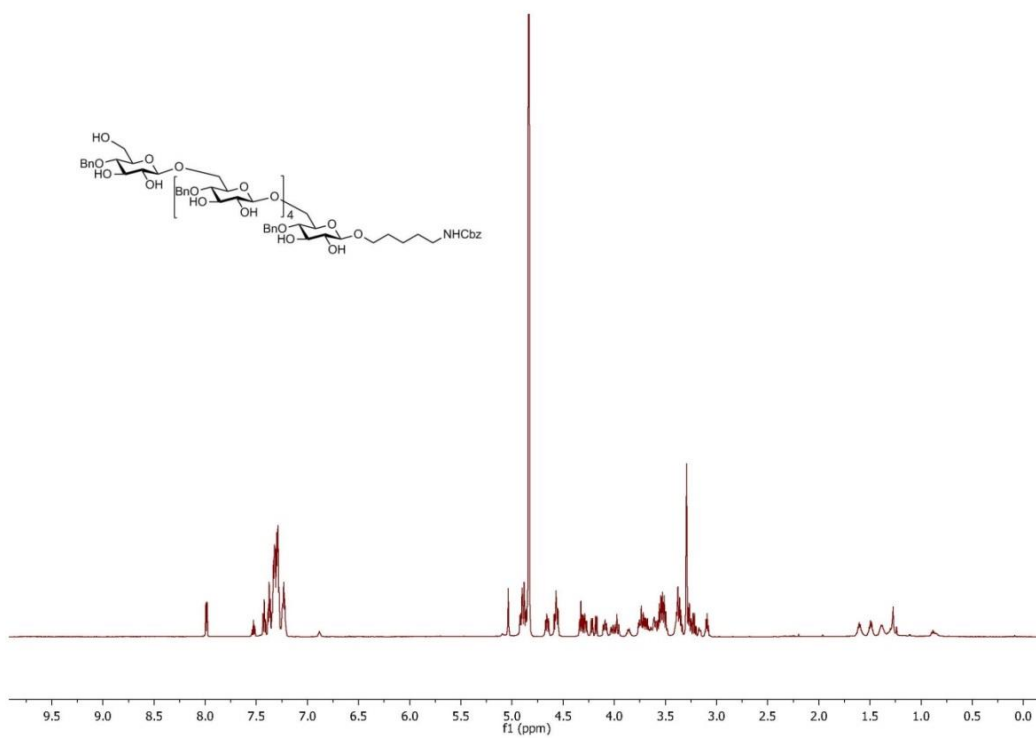
¹³C NMR of 27 (101 MHz, CDCl₃)



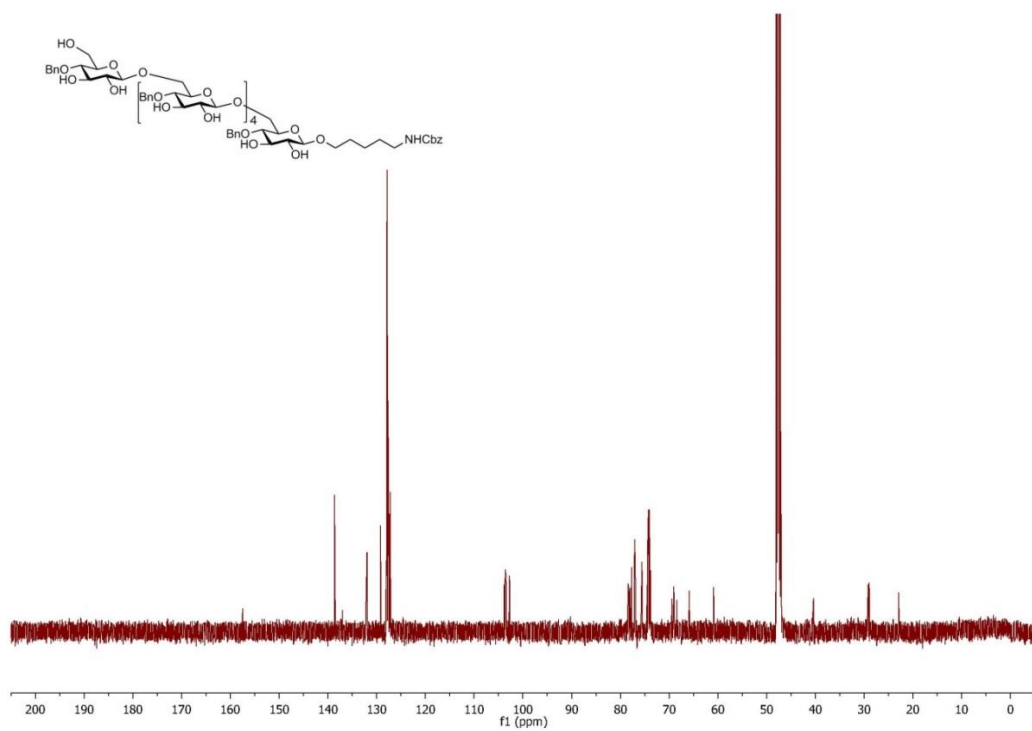
HSQC NMR of 27 (CDCl₃)



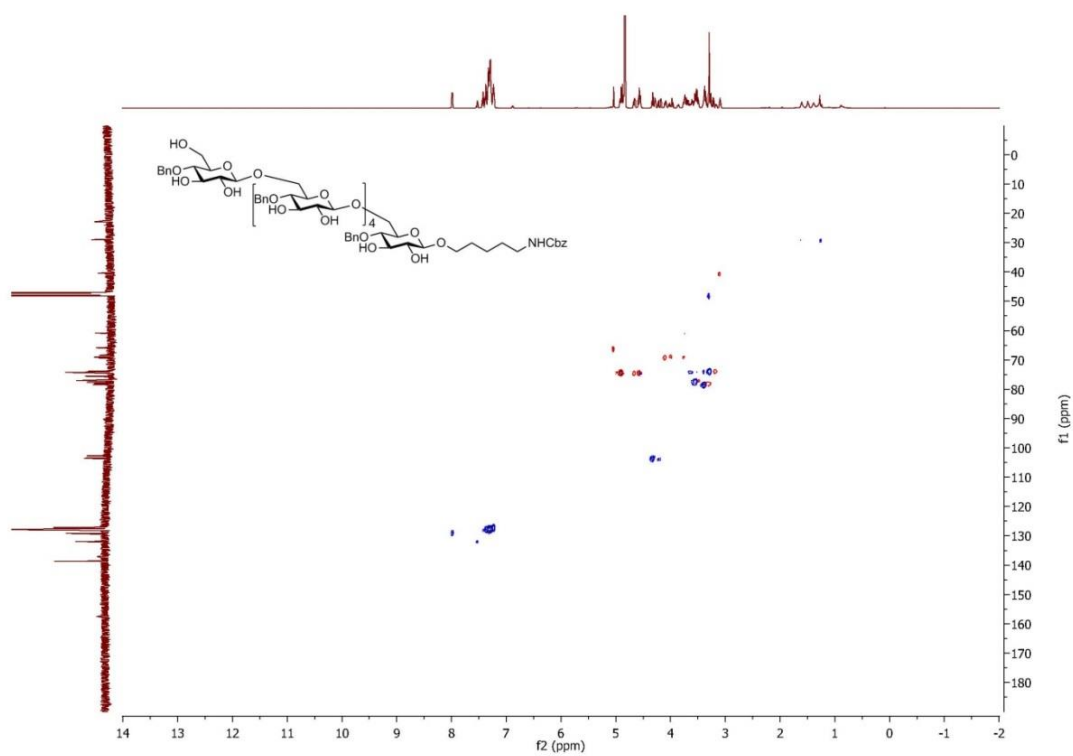
¹H NMR of 29 (400 MHz, Methanol-d₄)



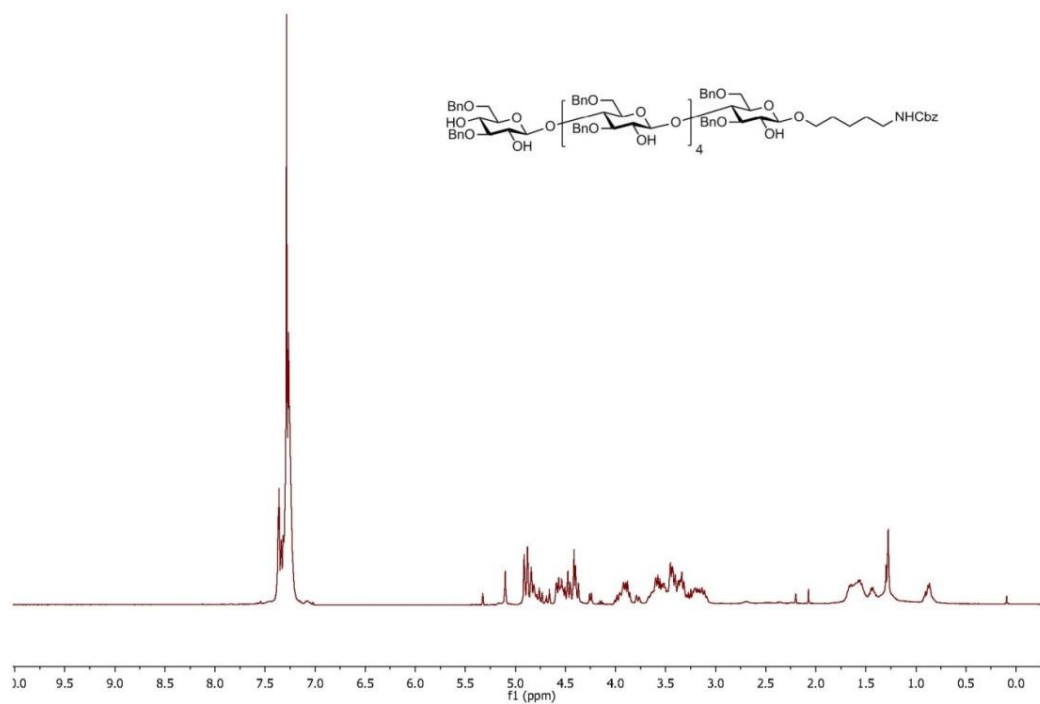
¹³C NMR of 29 (101 MHz, Methanol-d₄)



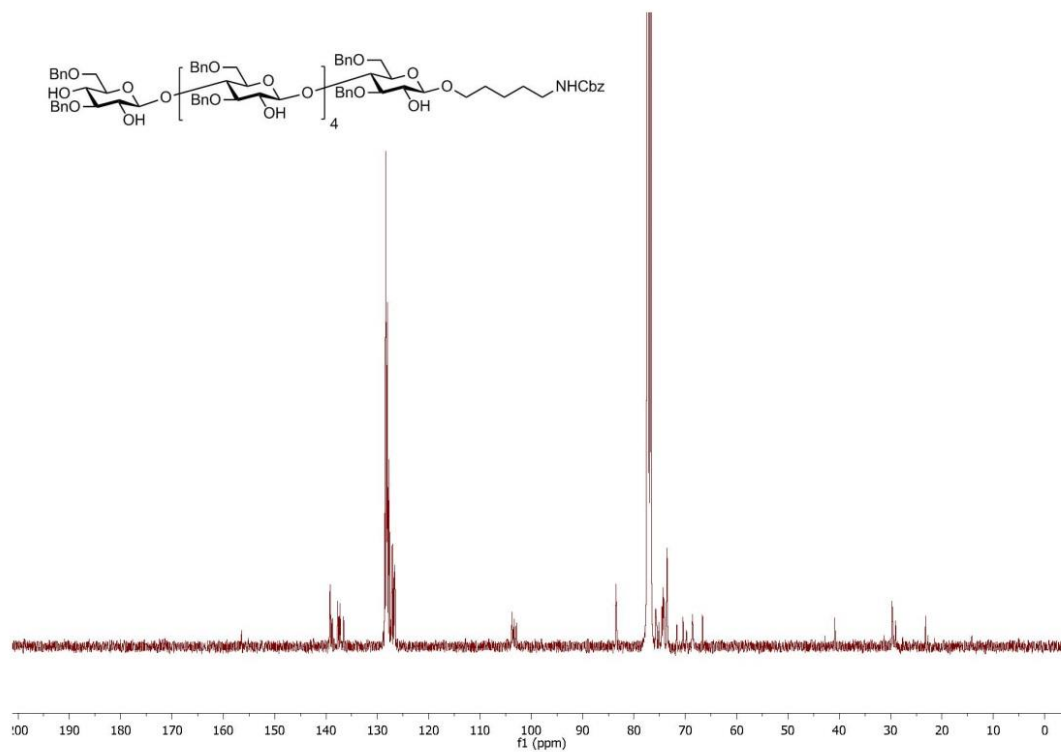
HSQC NMR of 29 (Methanol-d₄)



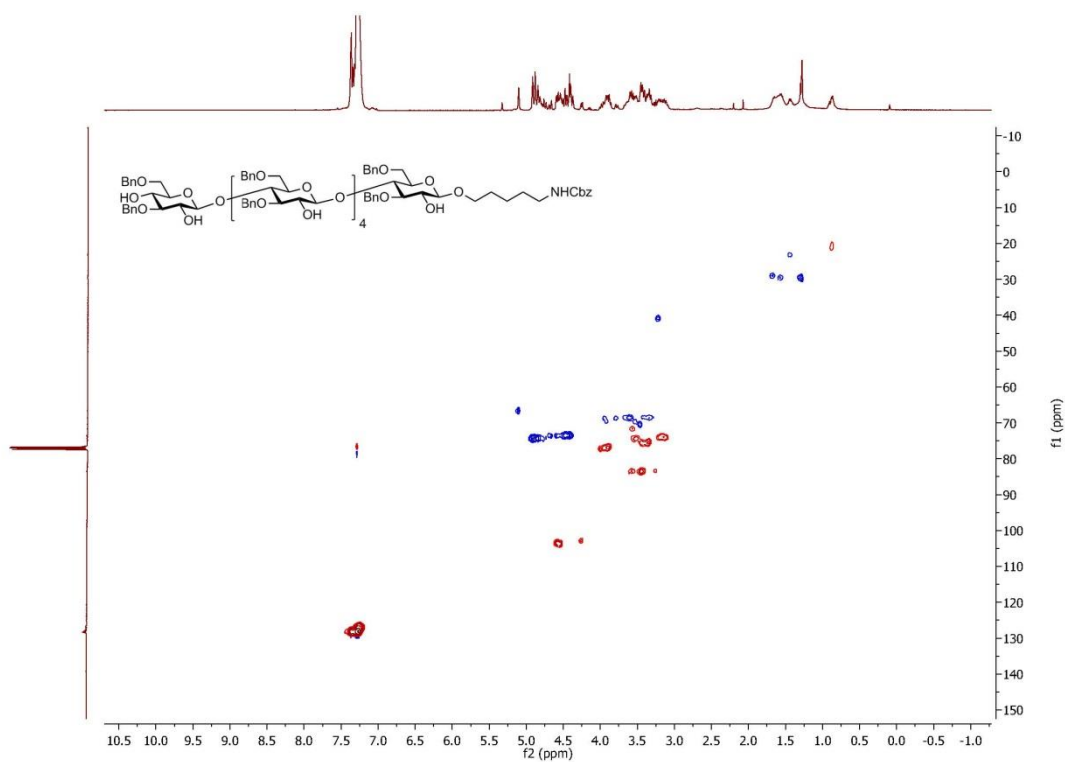
¹H NMR of 30 (400 MHz, CDCl₃)



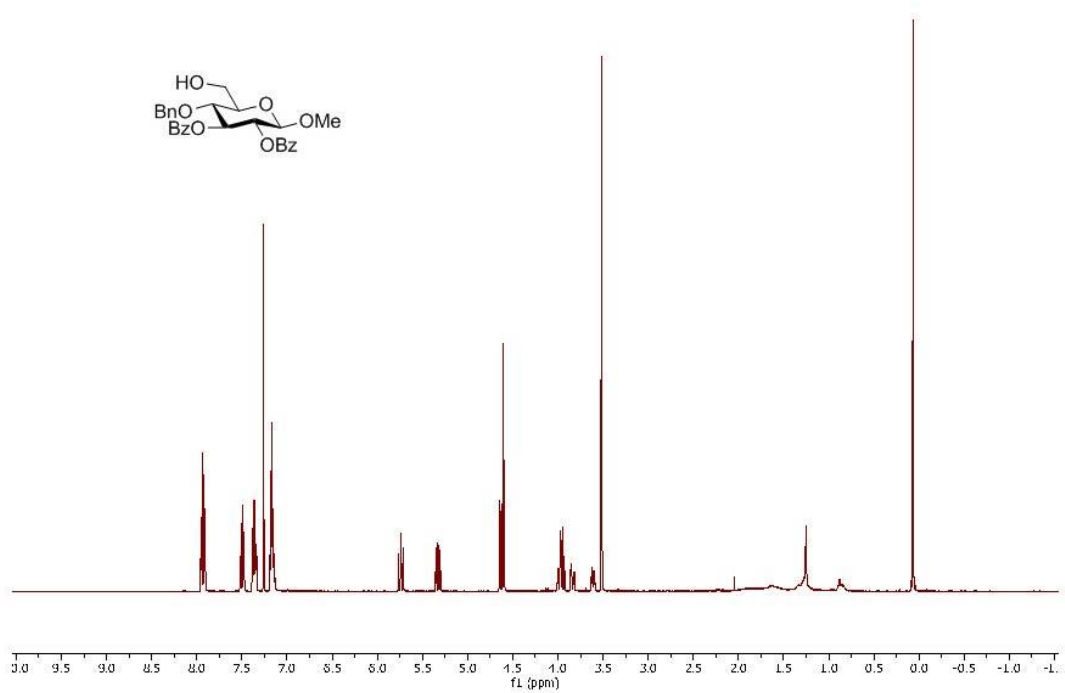
¹³C NMR of 30 (101 MHz, CDCl₃)



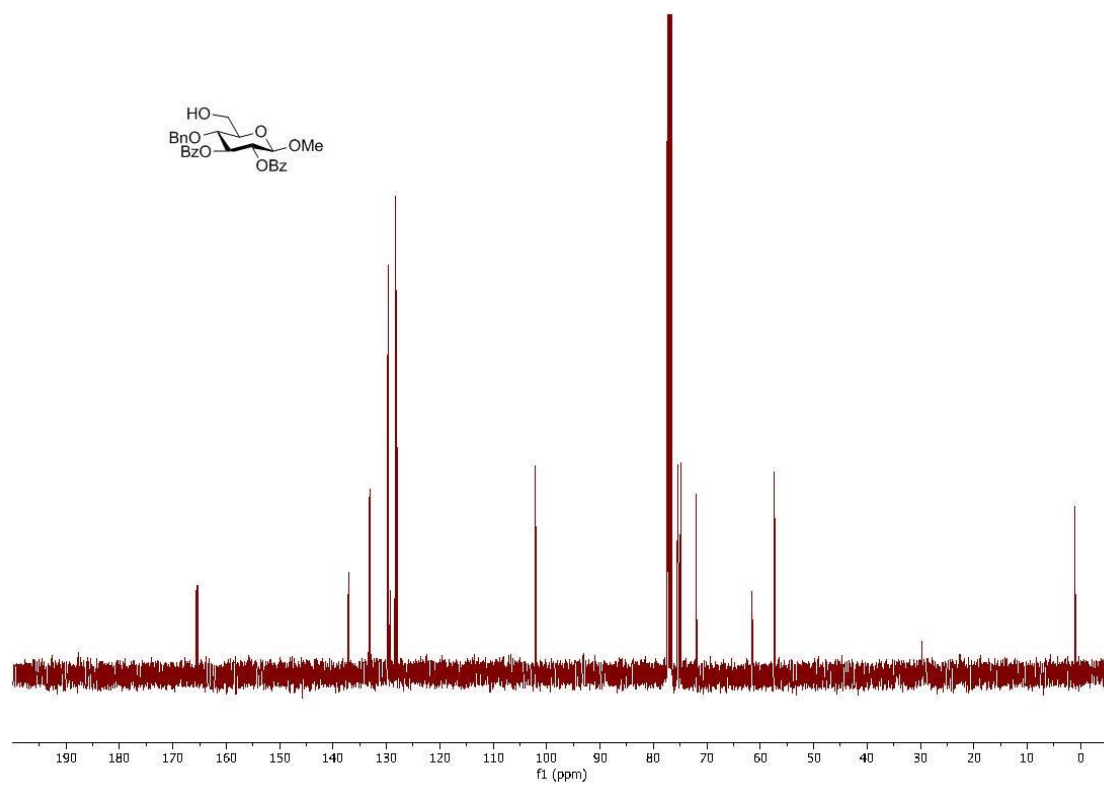
HSQC NMR of 30 (CDCl₃)



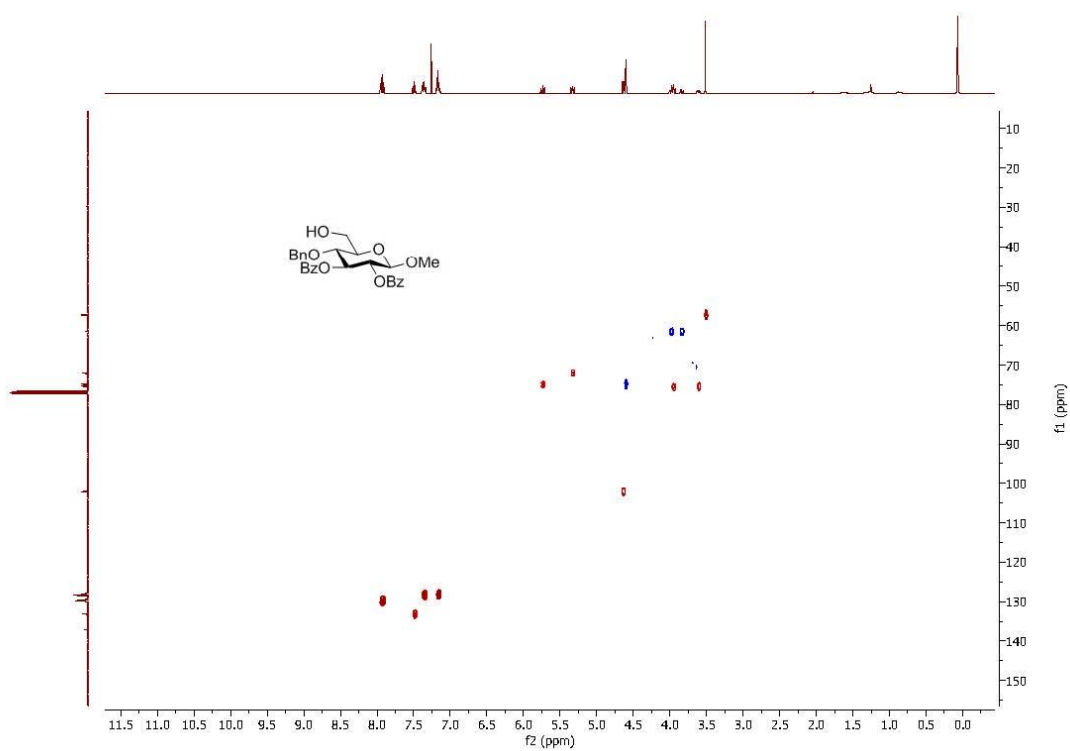
¹H NMR of S24 (400 MHz, CDCl₃)



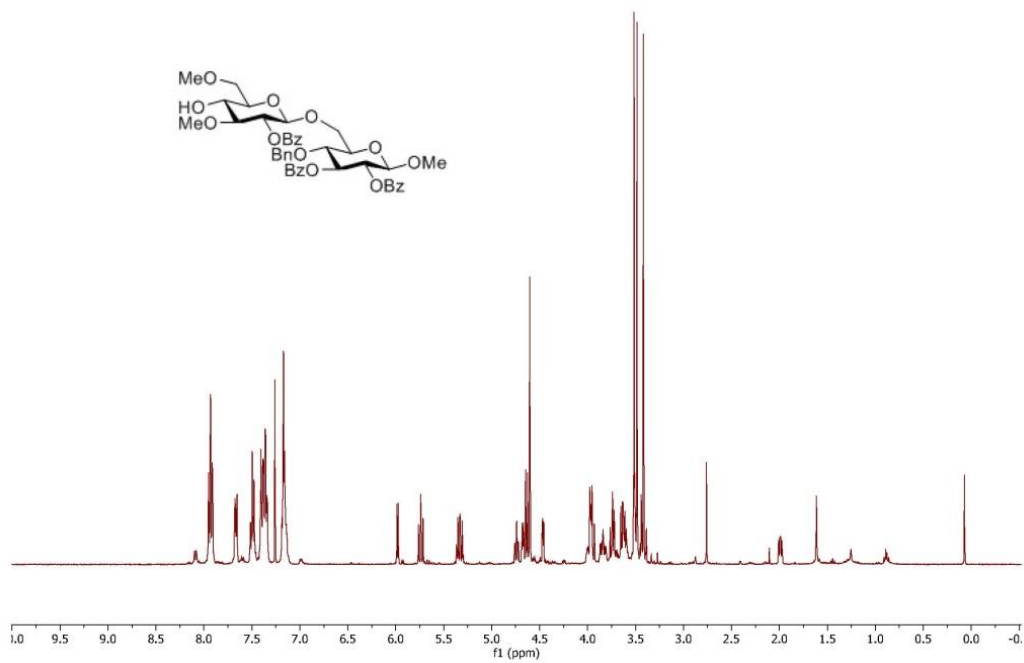
¹³C NMR of S24 (101 MHz, CDCl₃)



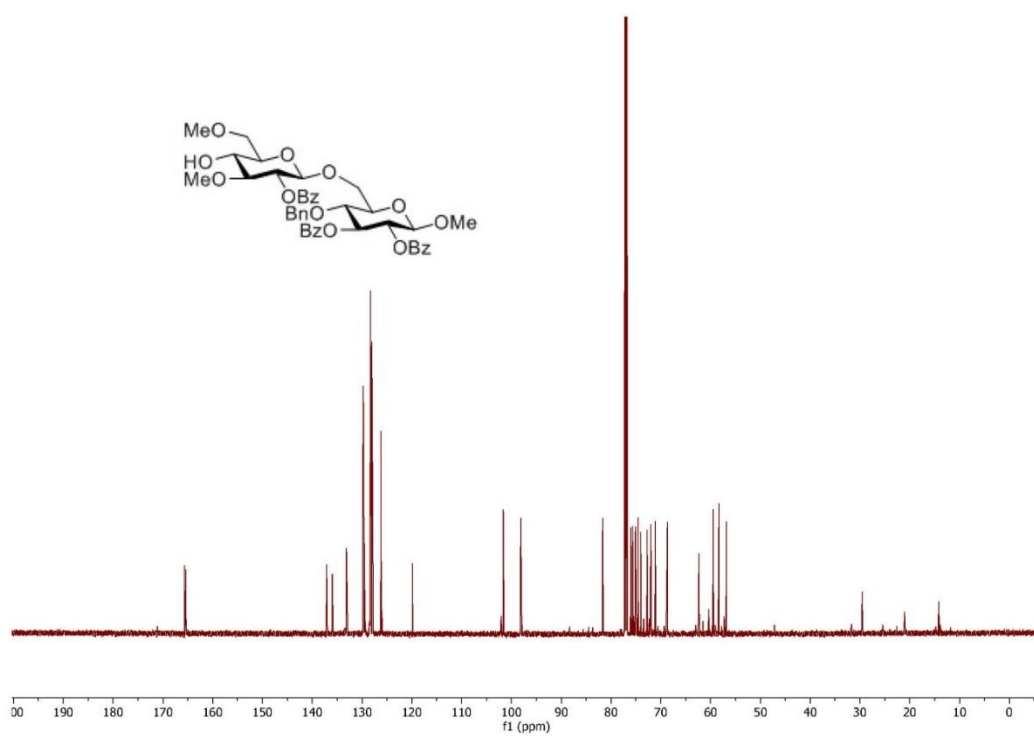
HSQC NMR of S24 (CDCl₃)



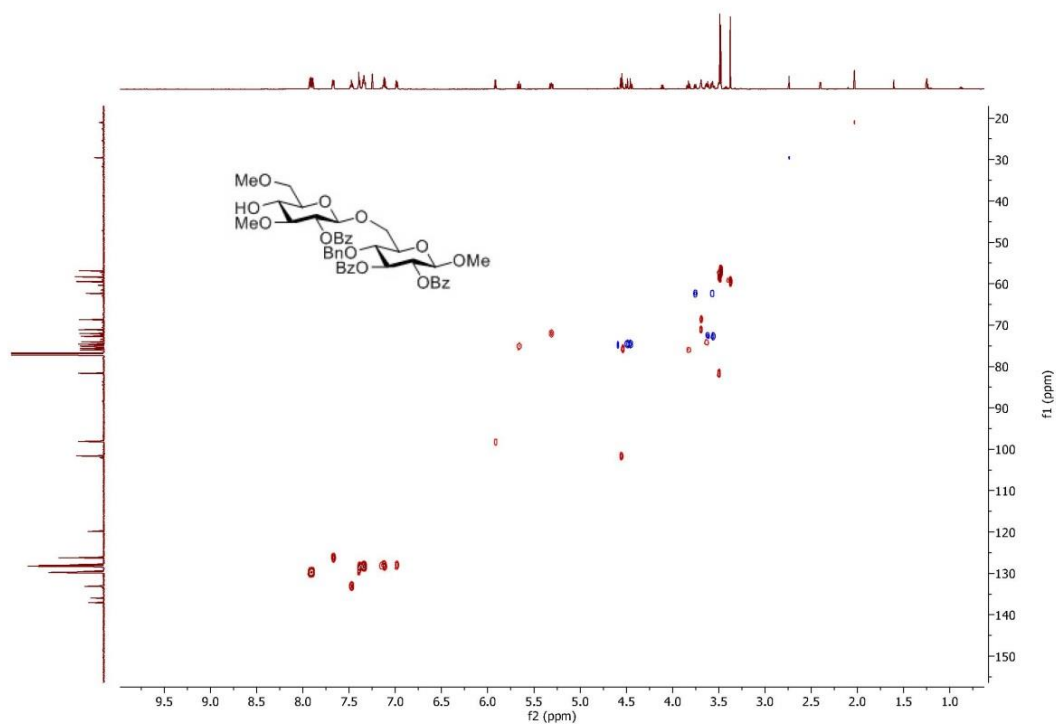
¹H NMR of S25 (400 MHz, CDCl₃)



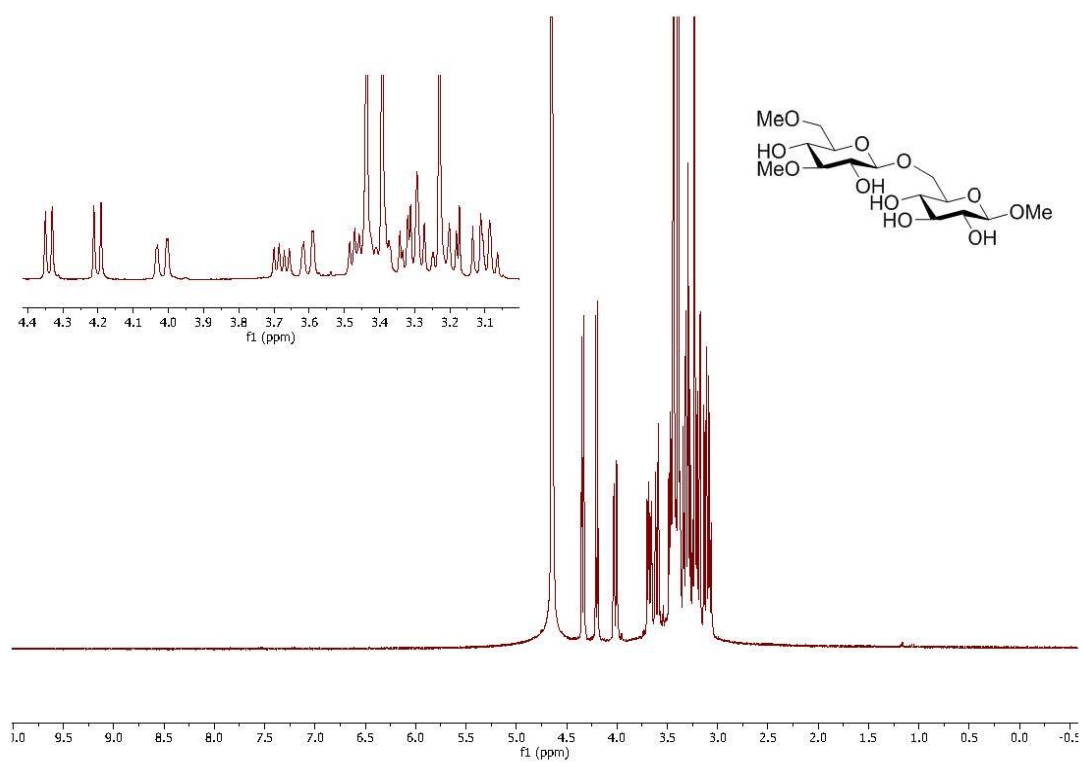
¹³C NMR of S25 (101 MHz, CDCl₃)



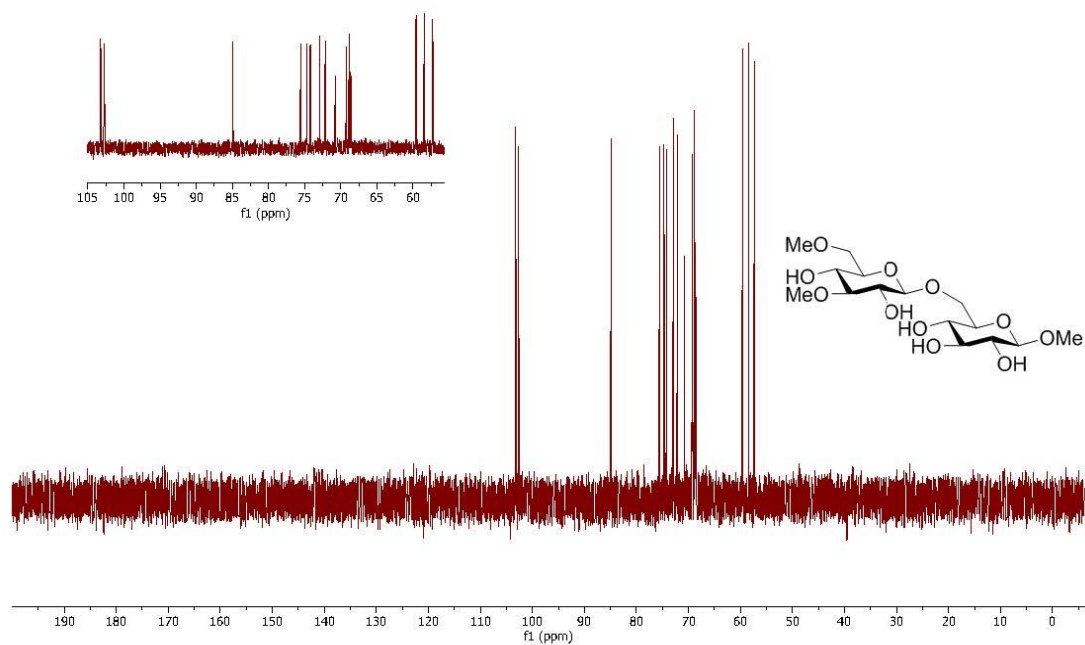
HSQC NMR of S25 (CDCl₃)



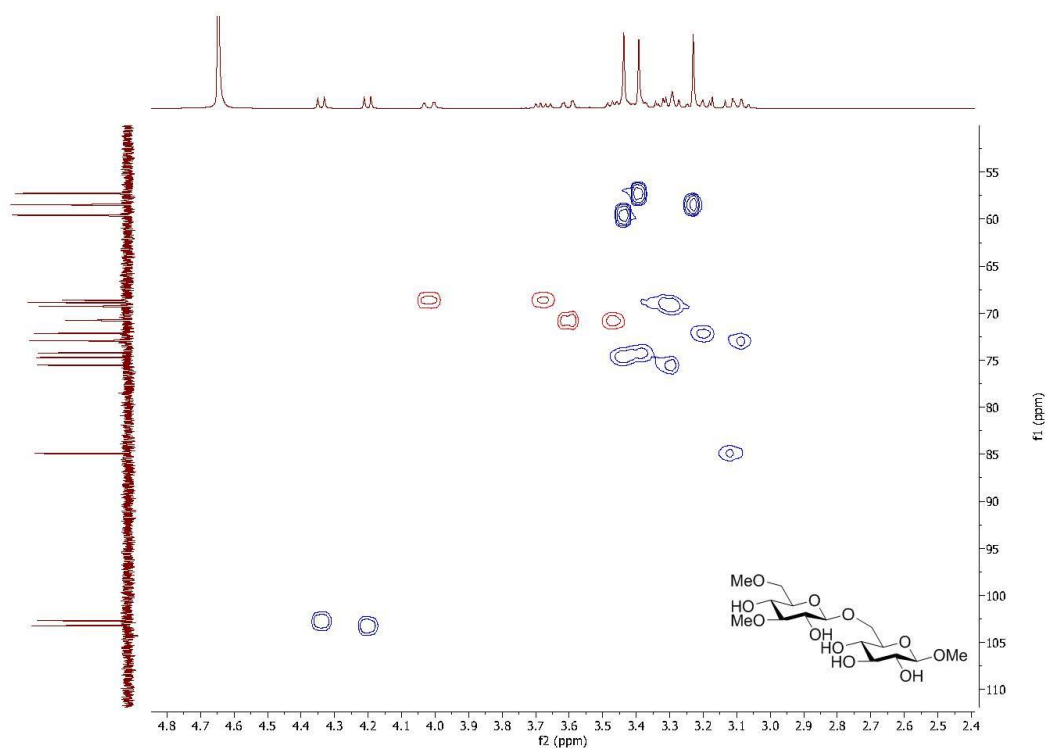
¹H NMR of 31 (400 MHz, D₂O)



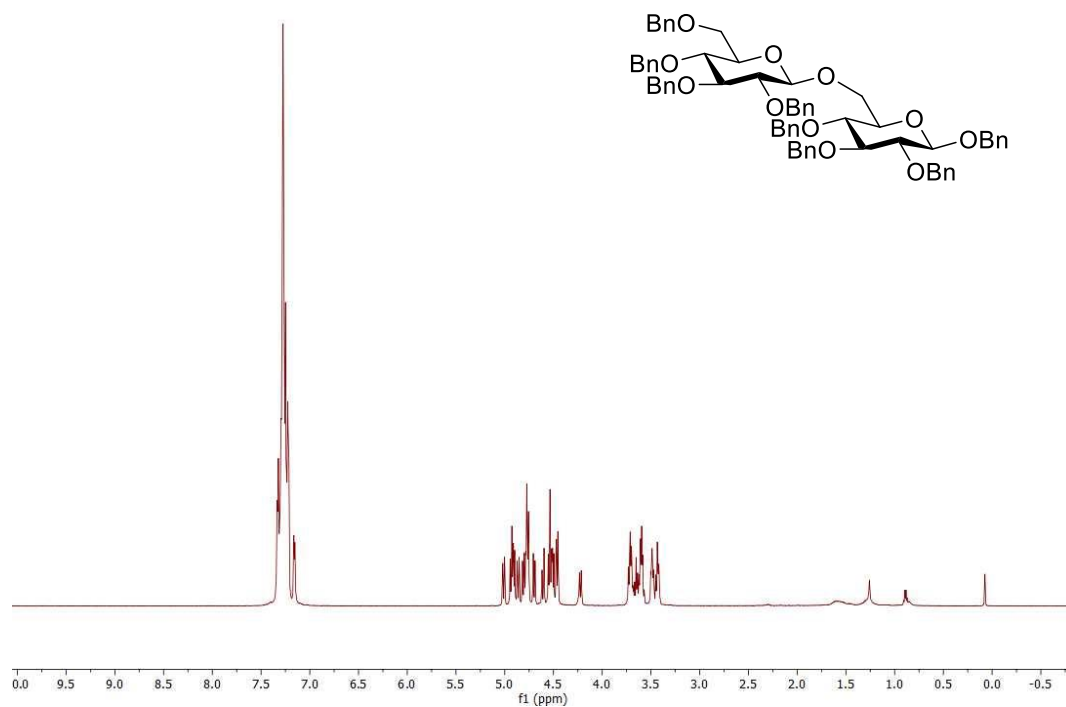
¹³C NMR of 31 (101 MHz, D₂O)



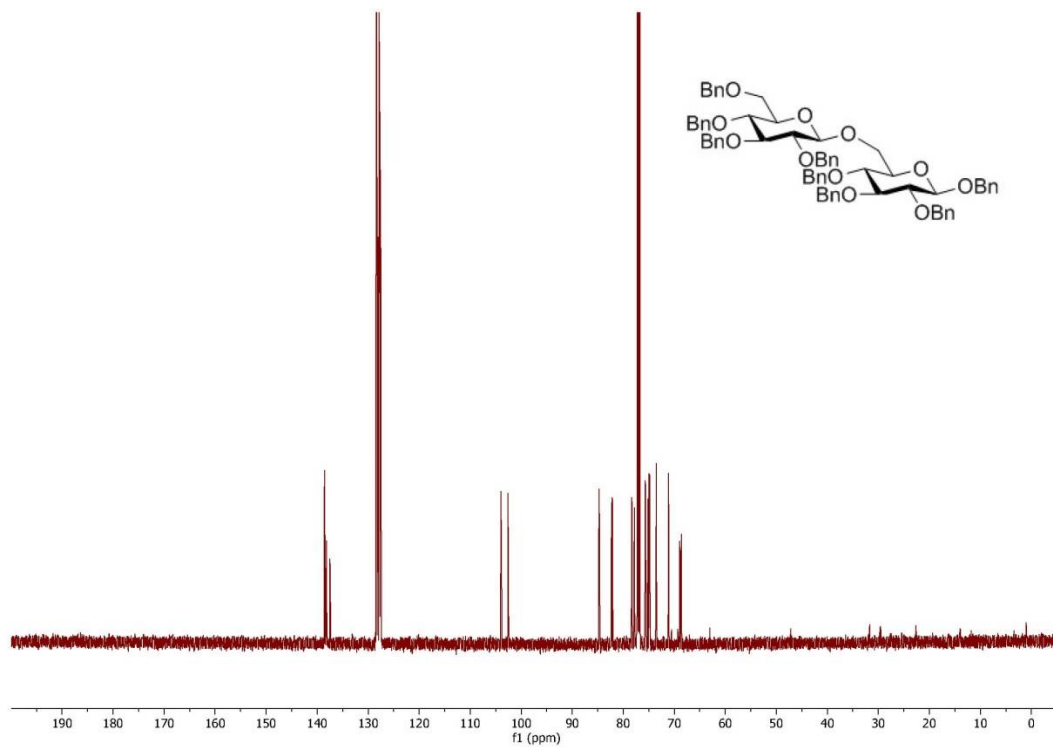
HSQC NMR of 31 (D₂O)



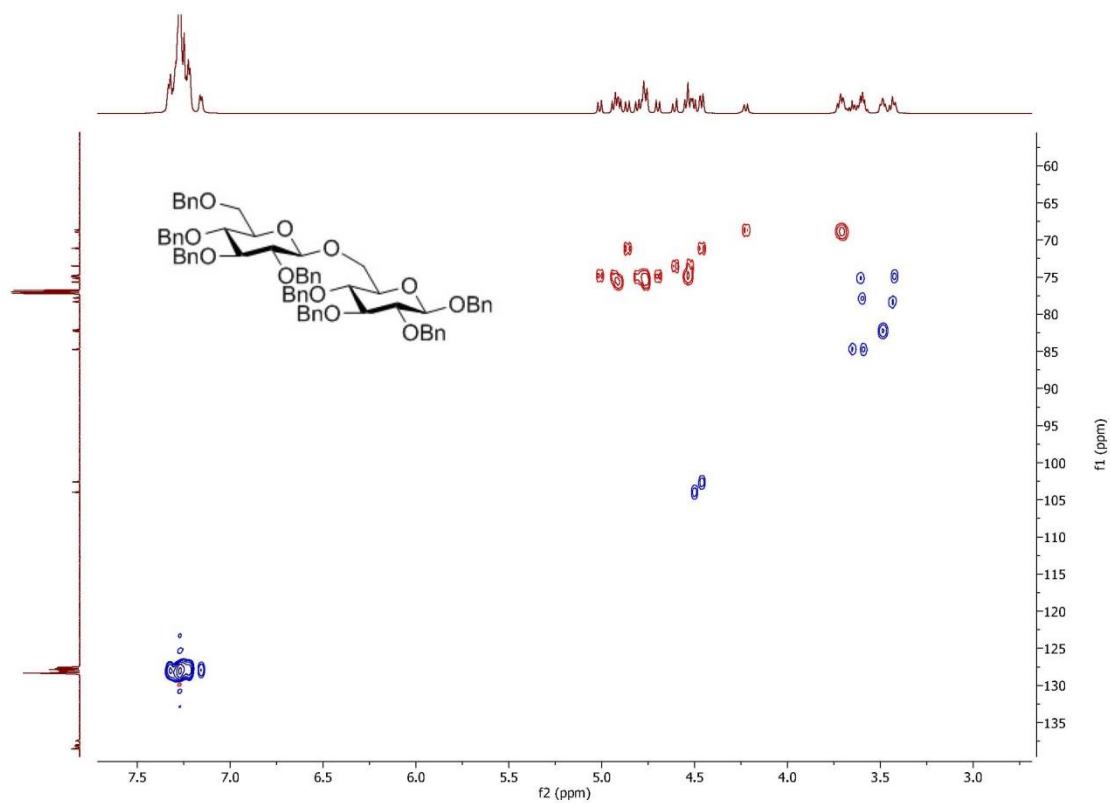
¹H NMR of 32 (400 MHz, CDCl₃)



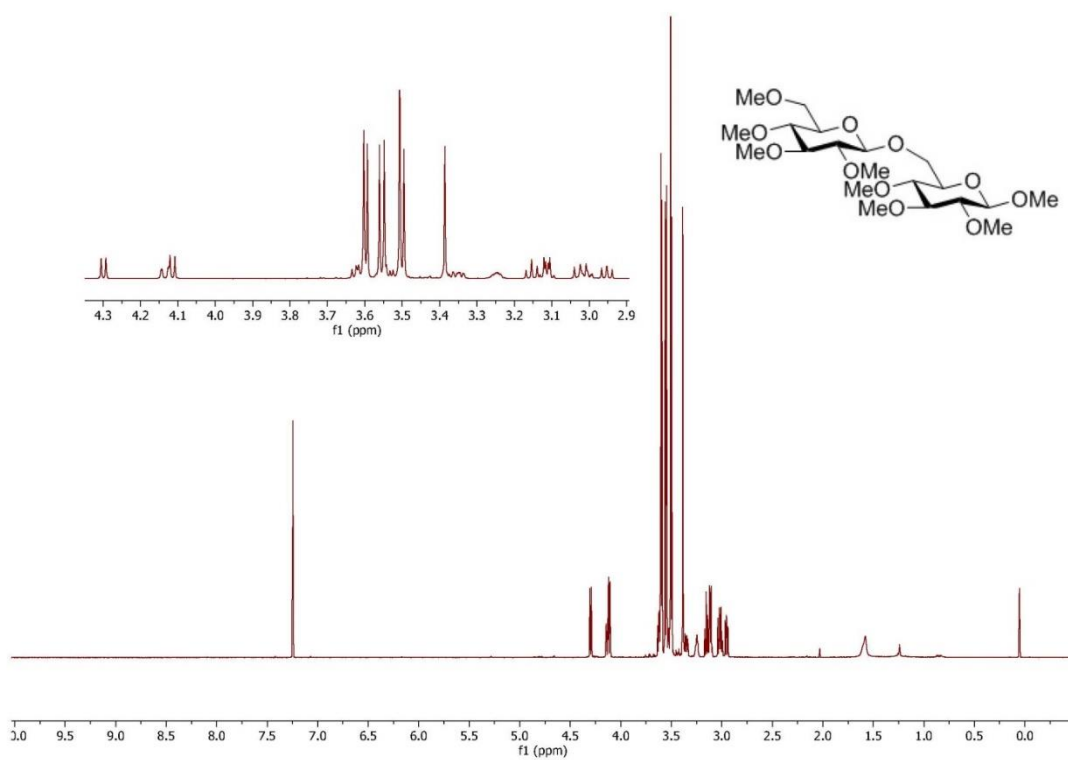
¹³C NMR of 32 (101 MHz, CDCl₃)



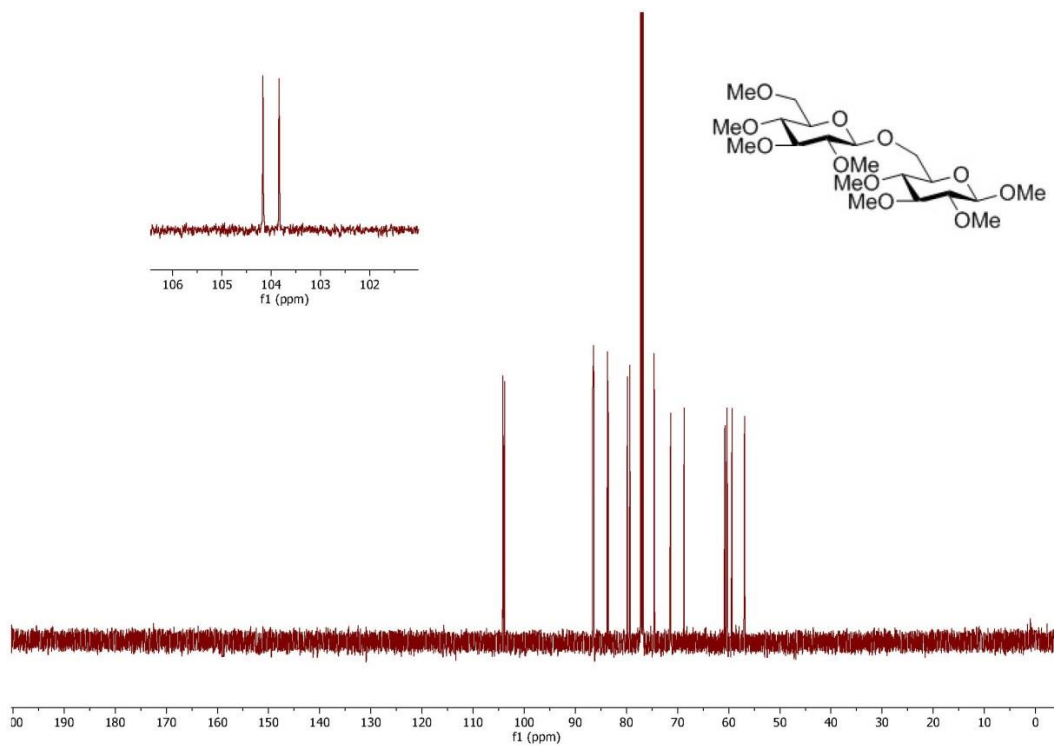
HSQC NMR of 32 (CDCl₃)



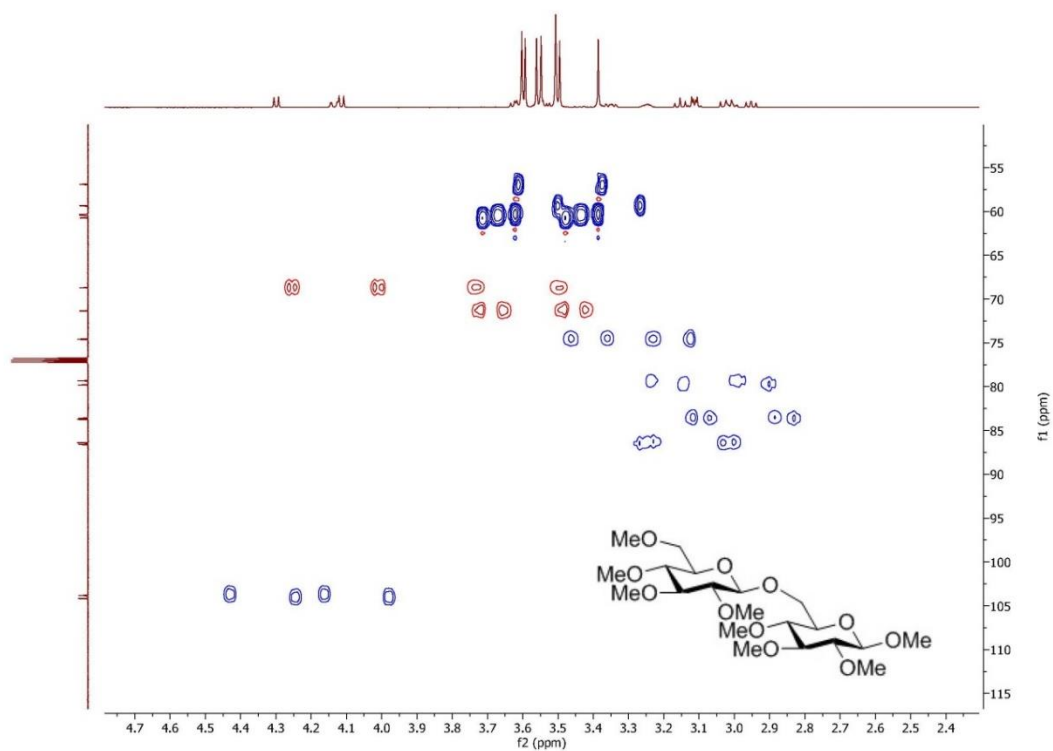
¹H NMR of 33 (400 MHz, CDCl₃)



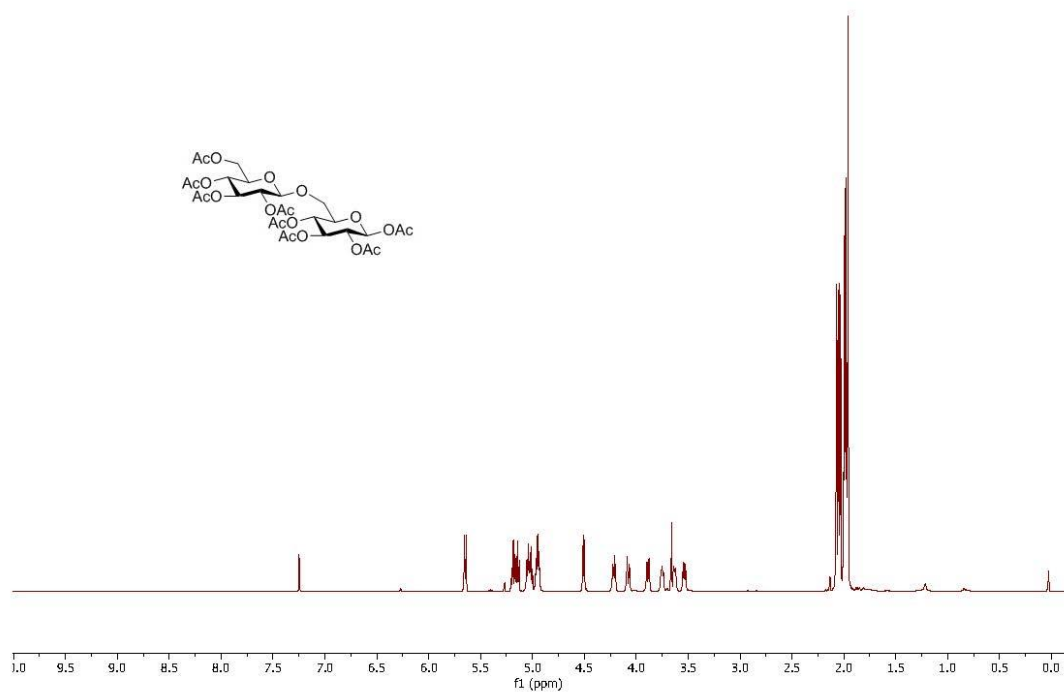
^{13}C NMR of 33 (101 MHz, CDCl_3)



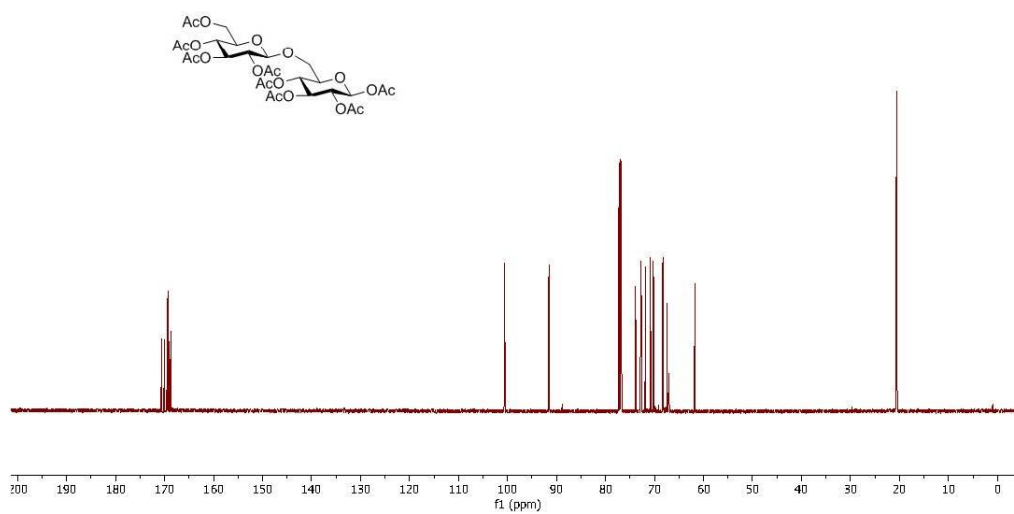
Coupled HSQC NMR of 33 (CDCl_3)



¹H NMR of 34 (400 MHz, CDCl₃)



¹³C NMR of 34 (101 MHz, CDCl₃)



HSQC NMR of 34 (CDCl₃)

